Significant factors affecting the forced-air cooling process of polylined horticultural produce

A thesis presented in partial fulfilment of the requirements for the degree of

Doctor of Philosophy

in

Food Technology

at Massey University, Palmerston North, New Zealand

Justin O'Sullivan

2016

Abstract

New Zealand is the world's third biggest producer of kiwifruit, with 94 % of the kiwifruit produced exported (NZ $ 1.0 bn in 2014). Forced-air cooling of the produce (from the harvest temperature of about 20 ℃ to near storage temperature of 0 ℃) immediately after harvest improves storage potential and maintains produce quality before transportation to market. The design of the kiwifruit packaging system influences the rate of cooling and temperature achieved, mainly by affecting the airflow within and throughout the package.

The typical kiwifruit package contains 10.5 kg of fruit and consists of a cardboard box and polyliner bag to prevent the loss of moisture and fruit shrivelling. Individual boxes are assembled onto pallets (10 boxes to a pallet layer, 10 layers high) Open areas or vents (in the box) facilitate cooling by allowing cool air to enter and circulate throughout the package. In forced-air cooling pallets are assembled into double rows with an aisle between the rows. Cool air is sucked through the pallets by a fan in the aisle, cooling the fruit and warming the air. The air is then either blown or ducted to the refrigeration system to be re-cooled. The polyliner keeps the local humidity high near the fruit, preventing weight loss due to evaporative cooling, but, as a barrier to direct fruit to air contact, slows the cooling rate. This project investigated the impact of operating conditions and package design on the cooling performance in such systems.

A numerical model was developed (a CFD model implemented using the Fluent CFD software) that describes and predicts the temperature profiles of palletised kiwifruit packages undergoing forced-air cooling. The capability of the model to predict the fruit

temperatures in each package was quantitatively validated against experimental data. The numerical model was able to predict temperature profiles within experimental error bars over 14 h of cooling.

The numerical model was used to determine the operating point (in terms of pressure drop and flowrate across the pallet) to ensure rapid cooling of the produce without incurring excessive operational costs due to the power requirements. Results from both experimental work and the numerical model informed that there was an effective limit to the volumetric flowrate of 0.243 L kg^{-1} s^{-1}: flowrates in excess of the limit had no or little effective benefit. This threshold flowrate is below the typical range recommended in industry for the forced-air cooling of non-polylined horticultural produce, which is 0.5 – 2.0 L kg^{-1} s^{-1}.

The numerical model demonstrated that the overall cooling performance (cooling rate, uniformity, power consumption and pallet throughput per week) can be improved by controlling the airflow distribution between the fastest and slowest cooling kiwifruit packages. An alternative design that channels cool air through the pallet towards the slowest cooling packages, located at the back of the pallet, by using two package designs in the same pallet, was presented.

At 0.243 L kg^{-1} s^{-1} it was found that the pressure drop and power required to achieve equivalent cooling rates with the new design was reduced (by 24 % each) compared to the conventional design. Additionally, at the half-cooling time the cooling uniformity was improved by 19 %. The key features of the new design can be expected to be applicable for the cooling of horticultural produce involving an inner packaging liner.

Acknowledgements

I would like to thank a number of people who assisted me over the course of this project.

At Massey University Dr. Andrew East (principle supervisor) Dr. Maria J. Ferrua (co-supervisor) and Dr. Richard Love (co-supervisor) provided invaluable advice and guidance, which I am truly grateful for. I am also thankful for the technical assistance provided by Peter Jeffery, Sue Nicholson and Gary Radford, who made all the experiments carried out in the laboratory possible.

As part of this project I spent six months at KU Leuven, Belgium, where I would like to thank Dr. Pieter Verboven (co-supervisor) and Dr Bart M. Nicolaï (co-supervisor) who taught me about numerical modelling.

I would also to thank Dr Patricia Kieran and Professor Brian Glennon of UCD, Ireland who gave me a research internship when I was an undergraduate and inspired me to pursue a doctorate.

I would like to thank Zespri International Ltd for their financial support.

I would like to take the opportunity to appreciate my parents, brothers and sister for their support and encouragement.

Table of Contents

List of Figures

List of Tables

Nomenclature

English Symbols

A – area, m^2

B – ratio of outer to inner diameter, dimensionless

C_D – discharge coefficient

C_p – specific heat at constant pressure, J kg^{-1} K^{-1}

d – inner diameter, m

D – outer diameter, m

D_H – hydraulic diameter (m)

E – energy per unit mass, J kg^{-1}

g – gravity, m s^{-2}

G – generation of turbulent kinetic energy, kg m^{-1} s^{-3}

Gr – Grashof number, dimensionless

h – specific enthalpy, J kg^{-1}

I – unit tensor

J – diffusion flux, kg m^{-2} s^{-1}

k – thermal conductivity, W m^{-1} K^{-1}

l – length scale, m

L – characteristic length, m

m – mass, kg

n – number of replicates

p – pressure, Pa

P – power, W

Pr – Prandtl number, dimensionless

q – heat flow rate, W

Q – volumetric flowrate, m^3 s^{-1}

Re – Reynolds number, dimensionless

RH – Relative Humidity, %

t – time, s

T – temperature, K

u, v, w –velocity magnitude, m s^{-1}

$\vec{v}$ – overall velocity vector, m s^{-1}

x, y, z – Cartesian coordinates, m

X – mass fraction, dimensionless

Y – Fractional Unaccomplished Temperature Change, dimensionless

Greek Symbols

β – thermal expansion coefficient, K^{-1}

ε – turbulent dissipation rate, m^2 s^{-3}

κ – turbulent kinetic energy, m^2 s^{-2}

λ – latent heat, kJ kg^{-1}

ρ – density, kg m^{-3}

τ – stress sensor, N m^{-2}

μ – viscosity, kg m^{-1} s^{-1}

υ – kinematic viscosity, m^2 s^{-1}

σ – Stefan Boltzmann constant, 5.67 x10^{-8} J m^{-2} s^{-1} K^{-4}

σ_ε – turbulent Prandtl number for ε, dimensionless

σ_κ – turbulent Prandtl number for κ, dimensionless

ω – turbulent specific dissipation rate, s^{-1}

Miscellaneous Symbols

ϵ - emissivity, dimensionless

Mathematical operators

d – total derivative

Δ – difference (i.e. change in variable)

δ_{ij} – Kronecker delta function

∂ – partial derivative

∇ – partial derivative with respect to all directions in Cartesian space

Subscripts

a – species "a"

b – buoyancy

f – fruit

i, j, k – vector directions in Cartesian coordinates

t – turbulent

eff – effective

w – water

Constants

C_{μ}, $C_{1\varepsilon}$, $C_{2\varepsilon}$, $C_{3\varepsilon}$ – constants for κ-ε turbulent model

Abbreviations

CAT– Computerized Axial Tomography

FUTC – Fractional Unaccomplished Temperature Change, -

h.t.c – heat transfer coefficient, W m^{-2} K^{-1}

HCT – Half Cooling Time, h

LSD – Least Squares Difference

MBP – Modular Bulk Pack

rpm – revolutions per minute (min^{-1})

rps – revolutions per second (s^{-1})

SECT – Seven Eights Cooling Time, h

TCR – Temperature Control Room

VSD – Variable Speed Drive

Chapter 1

Introduction

1.1. Kiwifruit industry in New Zealand

The primary sector accounts for 7.5 % of the GDP of New Zealand and contributes approximately 50 % of New Zealand's total export earnings (The Treasury, 2015). In 2014 the export value of horticultural produce was over NZ $ 3.9 bn, accounting for 7.6 % of New Zealand's total merchandise exports (Fresh Facts, 2014). New Zealand is the world's third biggest producer of kiwifruit (Bano & Scrimgeour, 2012). In 2014 kiwifruit exports had a value of almost NZ $ 1.0 bn, approximately 25 % of New Zealand's total horticultural export (Fresh Facts, 2014).

Within the food industry (which includes the New Zealand kiwifruit industry) the "supply chain" is the system used to move a steady supply of fresh horticultural produce from farm to consumer. It becomes the "cold chain" when cooling or freezing of the produce is included. This cold chain incorporates all phases, from harvest, through transport and retail, to the home refrigerator (Figure 1.1).

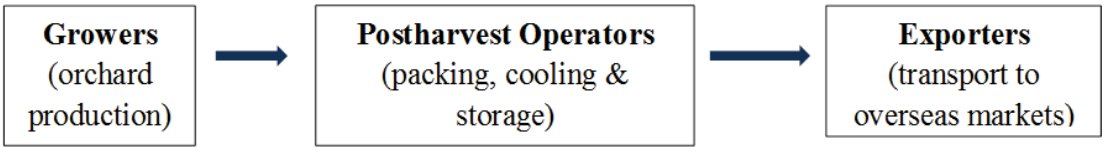

Figure 1.1. Summary of the cold chain in New Zealand for horticultural produce

Growers are responsible for producing kiwifruit of specific quality and size. Grading, packing, cooling and storage of kiwifruit are managed by postharvest operators.

Kiwifruit can be damaged by rough handling or the overhead weight of other kiwifruit packages. The temperature and humidity of the environment can adversely affect the kiwifruit quality, while the shelf life can be extended by efficiently cooling the kiwifruit after harvest. Kiwifruit are exported globally, with destinations like Europe as far as 19,000 km from New Zealand (typically a 6 week journey by ship). In addition the kiwifruit harvest season is relatively short (approximately mid-April to mid-May) so rather than flooding the market with fruit in season, large numbers of fruit are stored and subsequently sent to market over a period of months. The aim is to maximise the period that kiwifruit are available to consumers, and thus maximise the return to growers. Hence, the kiwifruit packaging system must ensure that the product is kept safe from external forces it could be exposed to during transport, facilitate controlled, uniform cooling and maintain the product at the storage conditions for long periods of time.

1.2. Role of packaging and forced-air cooling

It is the role of the kiwifruit package and refrigeration systems to maintain the produce at optimal environmental conditions as it travels through the cold chain from orchard to retail, which can include long storage periods. The packaging needs to have sufficient mechanical strength to withstand and protect the fruit from the rigors of the transportation system whilst still being cheap to manufacture; be easy to dispose of, once the fruit is sold or consumed; allow the product to be initially cooled, as uniformly as possible and commonly through forced-air cooling; and maintain a low storage temperature (possibly also under a modified atmosphere) to extend the fruit's shelf life. The main package element is a cardboard box, but in addition a polyliner bag (within

the box) encases the kiwifruit to prevent the loss of moisture to the surrounding air. The facilitation of cooling through the cardboard package is achieved with the use of openings (i.e. hand vents or end vents) which do compromise the structural integrity of the package, to an extent. However, these openings allow for cold air to enter and circulate throughout the package, enabling rapid and uniform postharvest cooling. The polyliner around the kiwifruit acts against rapid cooling as it is a barrier to direct fruit to air contact, but by ensuring a high humidity within the polyliner envelope (near the fruit) it reduces moisture loss, which is detrimental to fruit quality and appearance. The design of all these elements of the kiwifruit packaging system influences the airflow and temperature control within the package, thus influencing the storage life and maintenance of the kiwifruit quality until retail and domestic consumption.

1.3. Numerical model

There are multiple permutations that can be considered for an alternate kiwifruit package design (including dimensions of the package, size and location of the openings). Experimental prototyping is time consuming and costly, not least because it is the performance of the whole industrial-scale system that matters. That is, meaningful prototyping must involve batches of pallets and tonnes of fruit. To reduce this cost and time a numerical model can allow any potential design modifications to be evaluated cheaply and rapidly. Advances and availability in computational power over the past two decades allow for complicated airflow and heat transfer problems, such as refrigerated air pulled through the complex geometry of a package containing warm horticultural produce, to be solved with the resources available to a small design office.

1.4. Project aim

This research project aims to find the optimal operating conditions and to propose an alternative package design for the forced-air cooling of palletised kiwifruit, through experiments (in laboratory set-ups and in industry) and numerical modelling techniques, with a particular focus on the impact of the polyliner. Currently, there is a lack of information around the optimal operating conditions (air flowrate and pressure drop across the pallet) and whether existing package designs are the optimal to promote efficient cooling times and uniformity in polylined horticultural packaging systems.

Chapter 2

Literature review

2.1 Introduction

This literature review begins with a review of postharvest operations, the current package design and associated constraints. It is important to have an understanding of not just the forced-air cooling process but also the entire cold chain, as any new package has to successfully function from harvest to retail. The potential numerical models and strategies were evaluated with an emphasis on the advantages and disadvantages of each and what versions have been most commonly successfully employed for similar work involving the postharvest cooling of horticultural produce. Finally, the literature review describes the potential transport phenomenon to be considered and the numerical schemes used to solve the equations.

2.2 Postharvest operations

Postharvest cooling is essential to ensure that product quality is maintained from harvest to retail. For kiwifruit, the maximum storage potential is achieved when the fruit are cooled to near 0 ℃ efficiently, shortly after harvest (Ashby, 1995). Kiwifruit, kept at 0 ℃ and 90 - 95 % relative humidity can have a storage period of 3 – 5 months (Simson & Straus, 2010). This affords market flexibility and eliminates the need for kiwifruit producers to market immediately after harvest.

*Material from this chapter is included in journal paper: O'Sullivan, J.L., Ferrua, M.J., Love, R.J., Verboven, P., Nicolaï, B.M., & East, A.R. (2014). Airflow measurement techniques for the improvement of forced-air cooling, refrigeration and drying operations, Journal of Food Engineering, 143(0), 90-101. Figures 2.1, 2.2 and 2.4 and associated descriptions are included

Improper cooling can lead to hot or cold spots, within the package or pallet, and consequently quality loss in horticulture produce during storage (Verboven et al., 2003). It is critical to avoid storing the kiwifruit at temperatures ≤ – 0.5 ℃ as this induces low-temperature breakdown (a post-storage disorder) and product quality loss (Gerasopoulos et al., 2006). The most common industrial practice is to efficiently cool the horticultural produce immediately after harvest and then store it in a refrigerated room before transport to market.

2.2.1. Forced-air cooling

Horticultural produce is typically cooled via a forced-air application after sorting, grading and packing. Forced-air cooling involves forcing refrigerated air through packed fresh produce stacked upon pallets by generating a pressure difference across the pallets. Of the different air flow systems available the tunnel cooler is the most common (Brosnan & Sun, 2001; Figure 2.1).

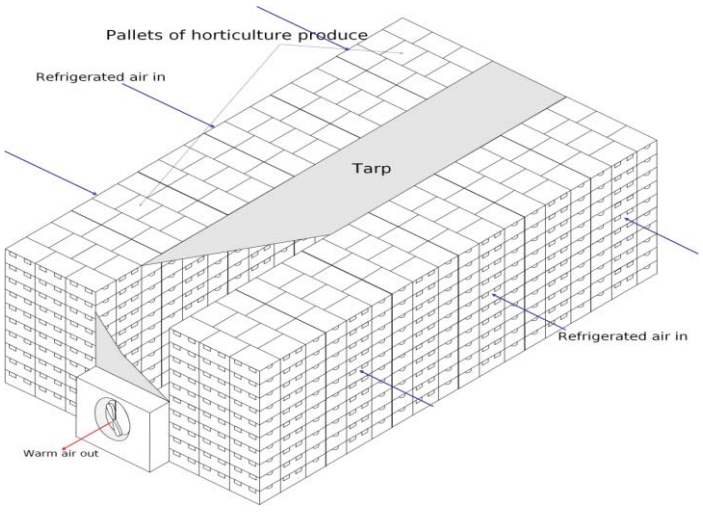

Figure 2.1. Tunnel cooler: the most common forced-air cooling device. The fan creates a vacuum which draws refrigerated air through two palletized rows of horticulture produce. The warm air is then blown or ducted towards the refrigeration system where it is cooled and returned to be subsequently drawn through the pallets again.

A variety of factors can affect the cooling times of the produce inside the package. For example, strawberries (a relatively small fruit and packed in individual clamshells within trays) can cool to near 0 °C in as little as 2 h (Ferrua & Singh, 2009c). Conversely, palletized boxes of apples can take up to 12 h to cool (East et al., 2003). Introducing a barrier between the produce and cooling air (as in the case of polylined packaging or fruit wrapped in paper) can extend the cooling period even further. For example, pears stacked in boxes and wrapped in paper can take up to 24 h to cool (Thompson & Chen, 1988).

In addition, the rate and uniformity of forced-air cooling is affected by the size and location of the openings of the ventilated packages (Delele et al., 2008; Ferrua & Singh, 2009a; van der Sman, 2002; Vigneault et al., 2006). These openings determine how much air can come in contact with the product and how it is distributed inside the package. Hence, cooling heterogeneity within packages is often a result of uneven airflow distribution (Dehghannya et al., 2008, 2011, 2012). The configuration of the packages when stacked in a pallet, and when the pallets are assembled in the tunnel cooler, also determines which openings are available for airflow and consequently the temperature and distribution of the air that each package receives.

2.2.2. Room cooling/ refrigerated storage

Room cooling comprises of placing warm produce in an insulated room where an evaporator-fan(s) circulates and cools the air (Figure 2.2). Typically, cooling times of at least 24 hours (and often much longer) makes room cooling unsuitable for produce (like

kiwifruit) that require a rapid removal of field heat (Thompson, 2004). In general, cool rooms are used for the storage of already cooled produce. For this application the refrigerated air is constantly circulated to maintain the produce at a low temperature.

Room design and pallet stacking pattern are essential to ensure an air distribution that maintains uniform air temperatures throughout the room. When pallets are stacked high and closely together, pallets located at the centre and at the rear section of the room (away from the evaporator fans) will receive smaller volumetric flows of refrigerated air compared to the pallets at the front of the room (adjacent to the evaporator fans). These local differences in flowrate throughout the room may cause differences in the air temperature, with warm spots developing depending on pallet location (Verboven et al., 2003).

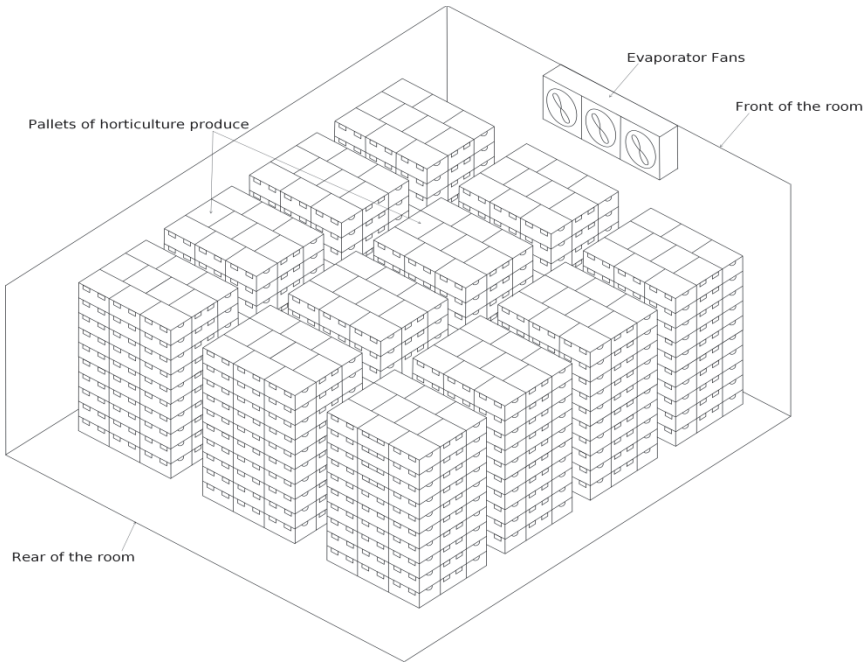

Figure 2.2. Refrigerated storage room for horticulture produce. Evaporator fans circulate refrigerated air through the room.

2.2.3. Refrigerated transportation

Horticultural produce is typically transported in refrigerated holds, of general cargo ocean vessels for marine transport and refrigerated trailer trucks for land transport. In both, shipping and truck transport, refrigerated air is delivered and returned to the same face of the refrigerated compartment (Figure 2.3 and 2.4). This universally used configuration has the practical advantage of all the refrigeration equipment being placed at one end of the transport unit (Smale, 2004). However, pallet compactness can lead to high airflow resistances and uneven airflow distribution, with the formation of stagnant zones with higher air temperatures in the rear of the compartment (Smale et al., 2006). The refrigeration systems used in transport are typically only sized to maintain temperature (Vigneault et al., 2009), as the product is not usually cooled during transport.

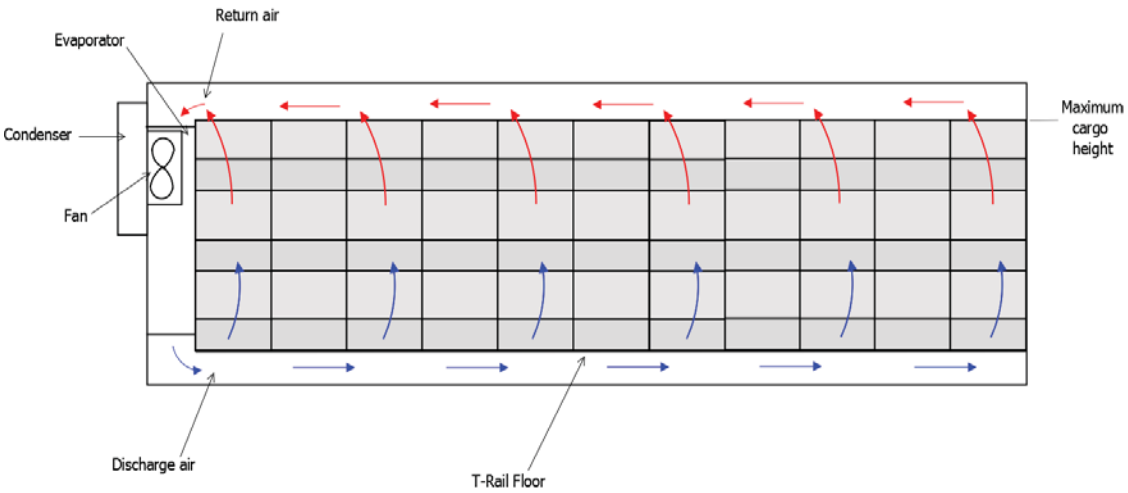

Figure 2.3. Pathways of air in a shipping container, for horticulture produce, featuring an integral unit with a bottom-air delivery system.

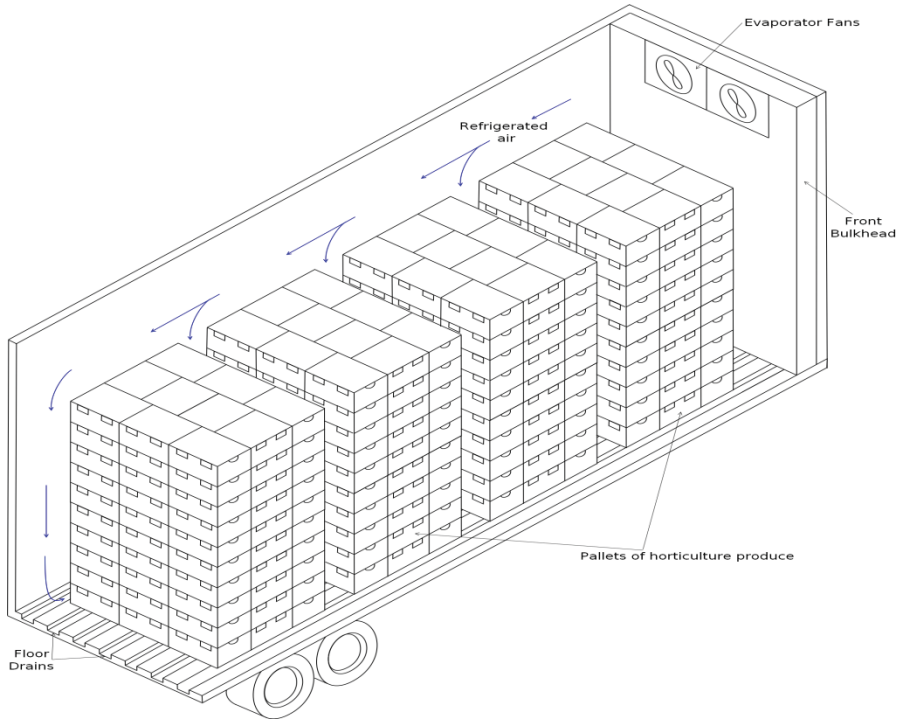

Figure 2.4. Refrigerated trailer truck with a top-air delivery system.

2.2.4. Horticulture package design

Horticulture packaging needs to facilitate a uniform airflow distribution among the product and have sufficient mechanical strength. This mechanical strength must be able to withstand compression from overhead containers; high humidity of cooling, transport and storage environments; impact and vibration during transportation; and handling during loading and unloading (Ezeike & Hung, 2009).

The packaging structure usually consists of a corrugated cardboard package that contains vents or hand holes to facilitate its handling and provide a means of contact between the refrigerated air and the produce. In addition, depending on the product, individual consumer produces (such as kiwifruit, grapes and berryfruit) are also contained within an internal package. In some situations this is used to separate consumer units of produce, in either bags or clamshells (e.g. strawberries are field

packed into individual clamshells (Ferrua & Singh, 2009a)). In other cases, including for kiwifruit and grapes (East et al., 2013) a polyliner bag is used, to assist in moisture retention for the fruit during the storage period. Following harvest, kiwifruit are at risk of shrivelling if more than 4 % of the total weight at harvest is lost due to water evaporation (Burdon & Lallu, 2011). This affects both its visual appearance and the selling weight at the end of the supply chain. Kiwifruit are encased within a polyliner to prevent excessive loss of product moisture and maintain product quality.

The most common package used for the forced-air cooling, storage and transport of Hayward green kiwifruit is the modular bulk pack (MBP). In order for the findings of this project to have the widest range of applicability the MBP will be the focus of this dissertation.

The MBP consists of a cardboard box with a lid that is folded at the top, with a 7 cm gap across the middle (Figure 2.5). The length, width and depth of the box are 40 cm, 30 cm and 19.5 cm, respectively. The box contains vents to enable handling and allow for cold air to pass through the package during cooling. Two rectangular vents (hand vents) are located at the top of the front and back face. Hemi-spherical end vents are located at each end face. Inside the box the kiwifruit are contained within a single polyliner bag, constructed of high density polyethylene and folded at the top. Each kiwifruit MBP holds approximately 10 kg of kiwifruit, with the exact number of fruit determined by the size grade of the fruit. For example, approximately 100 count 36 kiwifruit, weighing between 93 – 103 g, can be placed in one MBP.

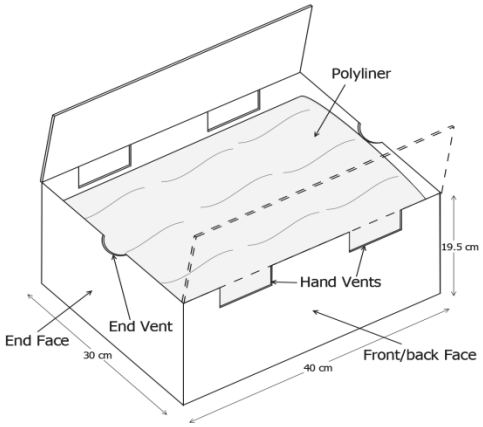

Figure 2.5. The modular bulk pack (MBP) for Hayward green kiwifruit

2.3. Numerical model approaches available for food processing

To date much research has been carried out into the improvement of forced-air cooling and refrigeration operations through experimental airflow measurement techniques (O'Sullivan et al., 2014). However, the experimental assessment of the cooling performance of different package systems is not only costly and time consuming, but also limited in scope. In experimental studies it is not only difficult to compare sets of data due to changes in operating conditions (ambient air temperature and produce temperature in particular), but also to gather detailed information of the airflow behaviour within the entire packed structure and subsequent impact on the temperature profile of the fruits.

The growth of computer power in recent years has led to an increased use of numerical models to the predict complicated airflow patterns and cooling profiles of horticultural packages during forced-air cooling (Defraeye et al., 2013b, 2014; Dehghannya et al., 2008, 2011, 2012; Delele et al., 2008, 2013a, 2013b, 2013c; and Ferrua & Singh, 2009a, 2009b, 2009c, 2009d, 2011). The use of numerical modelling facilitates an exact control of different operating conditions, while providing detailed information on the local

airflow behaviour and temperature profile within the system. This allows a more fundamental analysis of the design principles and mechanisms underpinning the overall performance of the cooling process.

In general, the airflow patterns and heat transfer that occur in horticultural packaging systems have been numerically simulated by means of three different modelling approaches; porous medium model, zonal model and direct numerical simulation (Zou et al., 2006a, 2006b). A brief description of each of these modelling approaches is given below.

2.3.1 Porous medium model

Converting a packaging system into a porous medium model simplifies the need to account for the complex configuration of the package structure when modelling the transport phenomenon within the system. The porous medium assumes the package structure as a homogeneous media (horticultural produce) of a solid matrix and interconnected void space, through which fluid (air) can flow. Variables, such as temperature, velocity and moisture content are then averaged over a representative elementary volume of this homogeneous media. The characteristic length of this representative volume needs to be much smaller than that of the package structure, but larger than the size of the voids/ products within it. The container-to-product equivalent diameter ratio must be higher than 10, for the averaging process to be valid (Whitaker, 1969). Pressure drop relationships, such as the Ergun and Darcy-Forchheimer models, are combined with coupled energy conservation equations for the solid (container material) and air phases to solve the relevant transport equations. A comprehensive

development of transport phenomena theory, relating to the porous media approach, in refrigerated food bulks, stacks and packages is given by Verboven et al. (2006).

The porous medium model avoids having to numerically compute the transport phenomena between the large number of solid-fluid interfaces present in a system (between the horticultural produce and surrounding air in a package). However, as the container-to-product equivalent diameter ratio must be higher than 10 it is unsuitable for packages containing relatively large horticulture produce. For count 36 Hayward kiwifruit, in a MBP, the container-to-product equivalent ratio is approximately 6.

The porous medium approach can assess airflow in large food plants with several hundreds or thousands of products. To overcome problems associated with the dissimilar scales of storage systems and flow paths around food products the porous medium approach can be utilised (Mirade & Daudin, 2011). Examples of the porous medium model in the heat transfer of food processing operations include Wang and Sun (2003), Chourasia and Goswami (2006a, 2006b, 2007a, 2007b), Delele et al. (2009a, 2009b, 2013a), Zou (2002) and Zou et al. (2006a, 2006b).

The porous medium model was rejected for this project due to the container-to-product diameter falling below the limit and the lack of detailed information that could be simulated about the transport phenomena within each individual MBP.

2.3.2. Zonal model

The zonal model divides a system into a series sub-models to allow for the problem to be simplified into manageable components. Energy and mass balances are then calculated for each zone while experimental data is used to define the velocity field. The model requires the development of appropriate interface models between the zones.

In developing a mathematical model to describe horticulture packaging Tanner et al. (2002a) employed a zonal model. Further examples include a zonal based heat transfer approach in order to optimise (changing insulation type and material thickness) an insulated box for the transport of perishables (East & Smale, 2008).

The zonal model approach requires the airflow pattern between the zones to be known. Typically, this is estimated via experimental measurements and this can be a major limitation to this approach; as the model is limited to the specific packages and package configurations associated with the data. Consequently, the zonal model approach is not suitable when one of the project objectives is to assess and predict the effect of changes to the package design which will impact upon the airflow patterns between zones.

2.3.3. Direct numerical simulation

Unlike the previous two model approaches discussed direct numerical simulation does not simplify the standard mass, momentum and energy conservation equations within the system. Computational Fluid Dynamic (CFD) tools have evolved over the years

from written-in-house codes to commercial codes which can cope with high levels of complexity, including iterative processes demanded by direct numerical simulation.

For direct numerical simulation property data for the horticulture produce and boundary conditions (density, thermal conductivity, initial temperature, air flowrate, etc...) are inputs for the model. Depending on the system or processes investigated simulations can require large amounts of CPU power and computer memory.

2.3.4 Alternative numerical models

Alternatives, to the porous medium, zonal and direct simulation models, such as the Lattice Boltzmann and network models, though less commonly employed in food operations, do exist.

2.3.4.1. Lattice Boltzmann method

Lattice Boltzmann method uses a particle description of matter where macroscopic properties, such as mass, momentum and energy, are carried by lattice gas particles within a regularly repeated lattice structure. Van der Sman (1999) used a Lattice Boltzmann scheme to predict heat and mass transfer in a container for seed potatoes and during the cooling of cut flowers. Guo and Zhao (2005) used a Lattice Boltzmann model to describe convective heat transfer in porous media.

2.3.4.2. Network models

Network models, in refrigerated food systems, break down the domain of interest into interconnected flow paths. A resistance is attributed to each flow path and the airflow will attempt to follow the path of least resistance. This model can only be applied to systems in which the flow paths can be predetermined, which is not the case for horticulture packages, and the solution accuracy is dependent on the channel resistance values. Advantages include the model simplicity and short computation times. Resistance network models are commonly employed by civil engineers in the design of water distribution systems (Smale et al., 2006).

2.4. Numerical schemes

Different numerical schemes are usually used to solve the relevant equations of CFD models, as they cannot actually be solved by any explicit analytical formulae. These schemes can be subdivided into finite difference, finite element, finite volume and discrete element methods.

2.4.1. Finite difference

The finite difference method replaces the derivatives in the governing equations with finite difference numerical approximations. For example, the derivative,

$$\frac{df}{dx} = \lim_{h \to 0} \frac{f(x+h) - f(x)}{h} \tag{2.1}$$

can be approximated by $(f(x+h)-f(x))/h$ where the resulting error is proportional to the value of *h* (the smaller the value of *h* the more accurate the solution).

The finite difference method can handle two or three-dimensional problems and is usually used for simple geometries (cylinder, sphere or slab). Applications include the mass and heat transfer models of the thermal process of cooking, frying and cooling. Disadvantages include limitations when predicting the surface temperatures of irregular shapes, due to its geometry simplification (Wang & Sun, 2003). To use the finite difference method to approximate the solution of a numerical model the system domain must be discretised into a uniform grid.

2.4.2 Finite element

In the finite element scheme the domain is divided into a large number of small elements within a finite area, forming a grid. Numerical approximations are then used to find a solution. The grid does not have to be structured or uniform, hence it can be applied to complex geometries (Dick, 2009). The finite element scheme has improvements over the finite difference method when dealing with irregular geometries, heterogeneous material and complex boundary conditions. Applications of the finite element method in mass and heat transfer models include cooking, drying and cooling. Disadvantages to the finite element method include the complexity and computation expense of it compared to the finite difference method (Wang & Sun, 2003).

Applications of the finite element numerical model for transient heat transfer simulations during food operations include a 3D model for the air blast cooling of cooked meats (Wang & Sun, 2002a, 2002b), 2D models of slow air, water immersion and air blast cooling of cooked meats, and investigating the influence of vent size and location in ventilated packages during forced-air cooling (Dehghannya et al., 2008, 2011, 2012).

2.4.3 Finite volume

The conservation equations of transport phenomena can be solved through the use of the finite volume method. This method subdivides the computational domain into multiple control volumes or elements to create a 'mesh'. The dimensions of the elements must be small enough to capture the main features of the process being modelled, particularly in areas of strong turbulence, or close to solid boundaries. The conservation equations are then applied and solved for each element. Taking Φ as a general fluid variable (i.e. density, velocity, enthalpy) the conservation equations, in each element, can be expressed as (Versteeg & Malalasekera, 1995),

$$\begin{bmatrix} Rate\ of\ change\ of \\ \Phi\ in\ the\ control \\ volume\ with \\ respect\ to\ time \end{bmatrix} + \begin{bmatrix} Net\ flux\ of\ \Phi \\ due\ to\ convection \\ out\ of\ the \\ control\ volume \end{bmatrix} = \begin{bmatrix} Net\ flux\ of\ \Phi \\ due\ to\ diffusion \\ into\ the \\ control\ volume \end{bmatrix} + \begin{bmatrix} Net\ rate\ of \\ creation\ of\ \Phi \\ inside\ the \\ control\ volume \end{bmatrix}$$

Convection describes changes due to fluid flow, while diffusion describes changes due to a difference in Φ between two points in an element. The final terms accounts for the change in Φ due to additional sources, e.g. gravity, radiation. CFD codes in Fluent contain discretisation techniques to apply to the transport phenomena. This results in complex, non-linear equations, which require an iterative process to solve. Currently,

many CFD software packages, such as Fluent (which was used in this project), are based on the finite volume method.

Multiple examples of the finite volume method in numerical models in the food industry exist: Delele et al. (2009a, 2009b) and Nahor et al. (2005) in refrigerated rooms; Ferrua and Singh (2009d, 2011) and Tutar et al. (2009) in ventilated packaging during forced-air cooling; Moureh et al. (2009a, 2009b, 2009c) in refrigerated trailer transport; António and Alfonso (2011) and Laguerre et al. (2010) in domestic refrigeration; Delele et al. (2007) and Endalew et al. (2009a, 2009b, 2010a, 2010b, 2010c) in orchard spraying. Relevant examples are expanded upon in section 2.7.

2.5. Transport equations in the finite volume numerical scheme

For each of the transport phenomena one of the following underlying physical principles is applied and the resulting conservation equations in each control volume solved (Versteeg & Malalasekera, 1995),

- Mass is conserved
- The rate of momentum change is equal to sum of forces acting on the fluid
- Energy is conserved

To reduce the length of the written equations the divergence of the overall velocity vector, $\vec{v}$ (m s^{-1}), in conservation form in Cartesian space is denoted by $\nabla \cdot \vec{v}$,

$$\nabla \cdot \vec{v} = \frac{\partial u}{\partial x} + \frac{\partial v}{\partial y} + \frac{\partial z}{\partial z} \tag{2.2}$$

2.5.1 Mass transport

For certain types of horticultural produce mass transfer can become significant. Moisture loss can result in produce shrinkage (Ngcobo et al., 2012) and impact the heat transfer process (Ferrua & Singh, 2009a). The mass conservation equation can be expressed as (Fluent-Theory, 2010),

$$\underbrace{\frac{\partial}{\partial t}(\rho)}_{\substack{Local\ change \\ with\ time}} + \underbrace{\nabla \cdot (\rho \vec{v})}_{\substack{Convective \\ term}} = 0 \tag{2.3}$$

where ρ (kg m^{-3}) is the fluid density.

2.5.2 Momentum transport,

Momentum equations describe how the fluid (refrigerated air) passes through the MBPs of produce and calculates the fluid velocity and flowrate at different points in the system. Fluent-Theory (2010) expresses the conservation of momentum as,

$$\underbrace{\frac{\partial}{\partial t}(\rho \vec{v})}_{\substack{Local \\ change \\ with \\ time}} + \underbrace{\nabla \cdot (\rho \vec{v} \vec{v})}_{\substack{Convection \\ term}} = \underbrace{-\nabla p + \nabla \cdot (\bar{\bar{\tau}})}_{\substack{Diffusion \\ term}} + \underbrace{\underbrace{\rho \vec{g}}_{\substack{Gravitational \\ body\ force}}}_{Soure\ terms} \tag{2.4}$$

where p (Pa) is the pressure, $\bar{\bar{\tau}}$ (N m^{-2}) is the stress tensor, g (m s^{-2}) is gravity.

The stress tensor, which accounts for the effect of viscous and shear stresses on the fluid, is given by,

$$\bar{\bar{\tau}} = \mu\left[(\nabla\vec{v} + \nabla\vec{v}^{T}) - \frac{2}{3}\nabla\cdot\vec{v}\mathrm{I}\right] \tag{2.5}$$

Where μ (kg m^{-1} s^{-1}) is the viscosity and I is the unit tensor.

2.5.2.1 Turbulence models

Typically the fluid flow in packaging systems will be at moderate to high Reynolds numbers, due to either to the small space between the polyliner and the box/tray or the narrow gaps between individual products if no polyliner is present. Consequently, turbulence, defined as the three-dimensional unstable motion in fluids, is often present in the fluid flow. The velocity fluctuations cause additional stresses to the fluid, termed Reynolds stresses (Versteeg & Malalasekera, 1995). Turbulent flows cause the velocity and all other flow properties to adopt random behaviour. However, it is too computational expensive to calculate each of these unsteady, time-dependent flow changes caused by turbulence. A turbulence model is required to calculate the mean fluid flow without first resolving all the unstable fluid flow fluctuations. In Reynolds averaging the solution variables are decomposed into the mean and fluctuating components. For the velocity magnitude, *u* (m s^{-1});

$$u_i = \bar{u}_i + u_i^{'} \tag{2.6}$$

The turbulent flow can then be described by the mean value of the flow properties (i.e. $\bar{\rho}_i, \bar{v}_i$) and the statistical properties of their fluctuations (i.e. ρ_i', v_i'). A turbulence model provides a computational procedure to close a system of mean flow equations (Versteeg

& Malalasekera, 1995). In this case "close" refers to introducing additional transport equations in which the additional Reynolds stresses, and the introduced variables (i.e. turbulence kinetic energy, κ (J kg^{-1}), specific dissipation rate, ω (s^{-1})) can be solved.

Substituting expressions for the mean and fluctuating components into the instantaneous continuity and momentum Navier-Stokes equations yields the Reynolds-averaged Navier-Stokes equations (Fluent-Theory, 2010),

$$\frac{\partial \rho}{\partial t} + \frac{\partial}{\partial x_i}(\rho \overline{u_i}) = 0 \tag{2.7}$$

and

$$\frac{\partial}{\partial t}(\rho \overline{u_i}) + \frac{\partial}{\partial x_j}\left(\rho \overline{u_i}\,\overline{u_j}\right) = -\frac{\partial p}{\partial x_i} + \frac{\partial}{\partial x_i}\left[\mu\left(\frac{\partial \overline{u_i}}{\partial x_j} + \frac{\partial \overline{u_j}}{\partial x_i} - \frac{2}{3}\delta_{ij}\frac{\partial \overline{u_l}}{\partial x_l}\right)\right] + \frac{\partial}{\partial x_j}\underbrace{\left(-\rho\overline{u_i' u_j'}\right)}_{\substack{Reynolds \\ stresses}} \tag{2.8}$$

The effects of turbulence are represented by the Reynolds stresses, which must be modelled to close Eq. 2.8. A frequently used method to relate the Reynolds stresses to the mean velocity gradients is the Boussinesq hypothesis (Fluent-Theory, 2010),

$$-\rho\overline{u_i' u_j'} = \mu_t\left(\frac{\partial u_i}{\partial x_j} + \frac{\partial u_j}{\partial x_i}\right) - \frac{2}{3}\left(\rho\kappa + \mu_t\frac{\partial u_k}{\partial x_k}\right)\delta_{ij} \tag{2.9}$$

where μ_t (kg m^{-1} s^{-1}) is the turbulent viscosity.

There exist a number of established turbulence models to model the turbulence viscosity. The reasons for the choice of turbulence model will be presented. However, the underlying theories behind the turbulence models are well established and it was felt

that a detailed explanation would contribute little to the overall project. If the reader wishes to know more about the exact development of various turbulent models they are referred to "An Introduction to Computational Fluid Mechanics" by Versteeg and Malalasekera (1995).

Fluent-Theory (2010) details eight principle turbulent models. From relevant literature involving the forced-air cooling of horticultural produce the κ-ε and the κ-ω turbulence models (Defraeye et al., 2013b, 2014; Delele et al., 2007, 2008, 2009a, 2009b, 2012a, 2012b; Tutar et al., 2009) are the most frequently used.

2.5.2.2 κ-ε model

In the κ-ε model two additional transport equations (for the turbulent kinetic energy, κ (J kg^{-1}) and the turbulence dissipation rate, ε (m^2 s^{-3})) are solved. The turbulent viscosity is computed as a function of κ and ε. The standard κ-ε model has become the standard for use in practical flow engineering problems due to its robustness, relative accuracy over a wide range of turbulent flows and CPU efficiency. It is relatively simple to implement and produces stable and quickly converging solutions. Standard κ-ε models are limited in terms of their accuracy when dealing with separation and re-attachment points for curved boundary layers, and for re-circulating flows and low Reynolds number flows (Hu & Sun, 2001). The κ-ε model suffers from its insensitivity to boundary layer separation and adverse pressure gradients, often resulting in delayed and reduced separations compared to observations.

In the standard κ-ε turbulence model μ_t is defined as,

$$\mu_t = \rho C_\mu \frac{\kappa^2}{\varepsilon} \tag{2.10}$$

Where C_μ is a model constant.

The following transport equations are used to obtain κ and ε (Fluent-Theory, 2010),

$$\frac{\partial}{\partial t}(\rho\kappa) + \frac{\partial}{\partial x_i}(\rho\kappa u_i) = \frac{\partial}{\partial x_j}\left[\left(\mu + \frac{\mu_t}{\sigma_\kappa}\right)\frac{\partial \kappa}{\partial x_j}\right] - \rho\varepsilon + \underbrace{G_t + G_b}_{Soure\ terms} \tag{2.11}$$

and

$$\frac{\partial}{\partial t}(\rho\varepsilon) + \frac{\partial}{\partial x_i}(\rho\varepsilon u_i) = \frac{\partial}{\partial x_j}\left[\left(\mu + \frac{\mu_t}{\sigma_\varepsilon}\right)\frac{\partial \varepsilon}{\partial x_j}\right] - C_{2\varepsilon}\rho\frac{\varepsilon^2}{\kappa} + \underbrace{C_{1\varepsilon}\frac{\varepsilon}{\kappa}(G_t + C_{3\varepsilon}G_b)}_{Soure\ terms} \tag{2.12}$$

σ_κ (-) and σ_ε (-) are the turbulent Prandtl numbers. $C_{1\varepsilon}$, $C_{2\varepsilon}$ and $C_{3\varepsilon}$ are model constants. By default the buoyancy effects on ε are neglected, hence $C_{3\varepsilon} = 0$ (Fluent-Theory, 2010).

G_t (kg m^{-1} s^{-3}), the generation of turbulent energy due to mean velocity gradients, is defined as,

$$G_t = -\rho\overline{u_i' u_j'}\frac{\partial u_j}{\partial x_i} \tag{2.13}$$

G_b, the generation of turbulent energy due to buoyancy, is defined as,

$$G_b = \beta g_i \frac{u_t}{Pr_t}\frac{\partial T}{\partial x_i} \tag{2.14}$$

where β (K^{-1}) is the coefficient of thermal expansion and T (K) is the temperature.

2.5.2.3 κ-ω model

The κ-ω model is similar to the κ-ε model. However, it is the specific dissipation rate ω (s^{-1}) that is solved by the second additional transport equation. Advantages over the κ-ε model include its ability to describe the viscous sublayer and predict adverse pressure gradient boundary layer flows and separation. However, the model is extremely sensitive to the input values of κ- and ω- outside the shear layer, making the standard version unsuitable for implementation in Fluent. The SST κ-ω model is less sensitive to the freestream κ- and ω- values. For this reason it is commonly employed to describe aerodynamic flows.

2.5.3 Wall functions

For turbulence modelling an approach is required to model the near-wall region. The approach is dependent on the y^+ value. y^+ is a dimensionless wall distance for fluid flow past wall surfaces and is used to describe the expected flow behaviour. Close to the wall ($y^+ \leq 1$) a viscous sub-layer, where the flow is almost laminar, exists. At the outer layer ($y^+ > 30$) fully turbulent flow is present (Fluent-Theory, 2010). Between these two regions there is a buffer or blending region. Traditionally two approaches have been employed for modelling this region. The region can be meshed extremely fine and resolved all the way down to the wall surface (this is often impractical due to the high mesh requirements) or wall functions can be used.

Semi-empirical functions, termed wall functions, can be employed to bridge the viscosity affected region and the fully turbulent region. Wall functions require that the

mesh is sufficiently coarse. If the y^+ value is too small ($y^+ < 30$) then the first calculation point in the simulation will be within the viscous sub-layer and wall functions will be no longer valid.

Recent versions of ANSYS provide an Enhanced Wall Treatment (EWT) option (Fluent-Theory, 2010). The EWT is a two-layer model that divides the turbulent flow region into a viscosity-affected region and a fully-turbulent region. A near-wall modelling method is used for the viscous sub-layer ($y^+ \leq 1$) and enhanced wall functions for the fully turbulent regions ($y^+ > 30$). The EWT uses a blending function to enable the model to be used throughout the entire near-wall region that guarantees correct asymptotic behaviour $y^+ \leq 1$, $y > 30$ and reasonable approximations for the wall buffer region.

2.5.4 Energy transport

2.5.4.1 Energy conservation per unit volume

The conservation of energy in fluid regions can be expressed as (Fluent-Theory, 2010),

$$\underbrace{\frac{\partial}{\partial t}(\rho E)}_{\substack{Rate\ of \\ energy \\ change}} + \underbrace{\nabla \cdot \left(\vec{v}(\rho E + p)\right)}_{Convection\ term} = \underbrace{\nabla \cdot \left(\underbrace{k_{eff}\nabla T}_{\substack{Conduction \\ term}} - \underbrace{\sum_{a} h_a \overrightarrow{J_a}}_{\substack{Species \\ diffusion}} + \underbrace{\left(\bar{\bar{\tau}}_{eff} \cdot \vec{v}\right)}_{\substack{Viscous \\ dissipation}} \right)}_{Diffusion\ terms} \tag{2.15}$$

where E (J kg^{-1}) is the total internal energy per mass, k_{eff} (W m^{-1} K^{-1}) is the effective thermal conductivity ($k + k_t$), k is the thermal conductivity and k_t is the turbulent thermal conductivity (defined by the turbulence model chosen). J_a (kg m^{-2} s^{-1}) is the diffusion flux of species a.

In Eq. 2.15,

$$E = h - \frac{p}{\rho} + \frac{v^2}{2} \tag{2.16}$$

where h (J kg^{-1}) is the sensible enthalpy for an incompressible flow,

$$h = \Sigma_a X_a h_a + \frac{p}{\rho} \tag{2.17}$$

where X_a is the mass fraction of species a and

$$h_a = \int_{T_{ref}}^{T} C_{p,a} dT \tag{2.18}$$

where C_p (J kg^{-1} K^{-1}) is the heat capacity and T_{ref} is equal to 298.15 K.

With no species diffusion the turbulent heat transfer is modelled as,

$$\underbrace{\frac{\partial}{\partial t}(\rho E)}_{\substack{Rate\ of \\ energy \\ change}} + \underbrace{\frac{\partial}{\partial x_i}[u_i(\rho E + p)]}_{Convection\ term} = \underbrace{\frac{\partial}{\partial x_j}\left(\underbrace{k_{eff}\frac{\partial \mathrm{T}}{\partial x_j}}_{\substack{Conduction \\ term}} + u_i \underbrace{\left(\tau_{ij}\right)_{eff}}_{\substack{Viscous \\ dissipation}} \right)}_{Diffusion\ terms} \tag{2.18}$$

$(\tau_{ij})_{eff}$ is the deviatoric stress tensor,

$$\left(\tau_{ij}\right)_{eff} = \mu_{eff}\left(\frac{\partial u_j}{\partial x_i} + \frac{\partial u_i}{\partial x_j}\right) - \frac{2}{3}\mu_{eff}\frac{\partial \mu_k}{\partial \mu_k}\delta_{ij} \tag{2.19}$$

k_{eff}, the effective thermal conductivity, is,

$$k_{eff} = k + \frac{c_p \mu_t}{Pr_t} \tag{2.20}$$

2.5.3.2 Energy conservation in solid regions

The energy conservation equation used in solid regions is similar to the energy equation in fluid regions (Eq. 2.15). However, there are no terms for pressure, species diffusion or viscous dissipation. The equation can be expressed as (Fluent-Theory, 2010),

$$\underbrace{\frac{\partial}{\partial t}(\rho h)}_{\substack{Local\ change \\ with\ time}} = \underbrace{\nabla \cdot (k \nabla T)}_{\substack{Conductive \\ term}} \tag{2.21}$$

2.6 Transport mechanisms in the cooling of horticultural produce

2.6.1 Convective heat transfer

Convective heat transfer describes the heat transfer between a moving fluid and a solid object. Convective heat transfer is a result of forced and/or natural convection. In forced convection the convective heat transfer coefficient is heavily influenced by the fluid velocity (Dincer, 1995). In natural convection the fluid motion is the result of density gradients in the air due to temperature differences throughout the fluid. The influence of natural convection, or buoyancy forces, on mixed convection flows, such as those potentially found inside of a polyliner bag of horticultural produce, is measured by the ratio of the Grashof, Gr, and Reynolds, Re, numbers, expressed as (Fluent-Theory, 2010),

$$\frac{Gr}{Re^2} = \frac{g\beta\Delta TL}{u^2} \tag{2.22}$$

where β (K^{-1}) is the thermal expansion of the fluid and L (m) is the characteristic length.

If this number approaches or exceeds unity then natural convection will contribute heavily to the flow. If this number is small then buoyancy forces may be neglected.

Convective heat transfer can also be influenced by moisture loss (Woods, 1990). Differences in water vapour pressure between the surface of horticultural produce and the surrounding airflow causes evaporation of moisture from the produce. The removal of the latent heat of evaporation can accelerate the convective heat transfer.

2.6.2 Conductive heat transfer

Conduction describes heat transfer between or within solid bodies due to a temperature gradient (Singh & Heldman, 2014). For horticultural produce internal conduction is due to two processes. Heat generated through product respiration is conducted to the cooled kiwifruit surface. The surface is cooled by convection, creating a temperature gradient within the product which causes heat to conduct to the surface.

2.6.3 Radiative heat transfer

Thermal radiation is the transfer of heat from one surface to another through a vacuum or transparent medium (Singh & Heldman, 2014). Typically, in the forced-air cooling of

horticultural produce the contribution of radiation considered small compared to the convective heat transfer (Defraeye et al., 2013b).

2.6.4 Heat transfer in the forced-air cooling

In forced-air cooling heat transfer is a result of conduction, convection and radiation. It is usually a combination of all three methods, with each becoming more or less significant, for the specific system under investigation.

2.7 CFD applications in the postharvest cold chain

The refrigeration of packed produce (most times in boxes on pallets) usually leads to complicated airflow pathways. In the early 1990's numerical modelling of these systems was a recent phenomenon as it was both time-consuming and complex (Wang & Touber, 1990). Continuous advances in numerical models and computer capabilities have since facilitated the numerical analysis of increasingly complex phenomena. Today CFD has been employed as a tool to optimise and develop equipment and processing strategies in the food industry (Norton & Sun, 2006). The detailed information provided by the use of CFD models has facilitated unique opportunities to investigate alternative system designs, without the need for expensive and time consuming experiments. CFD has been applied to refrigerated rooms, horticultural packages, transport equipment and refrigerated cavities in the postharvest cold chain. Examples of knowledge obtained through the use of CFD, on the performance of current and modified package systems during the postharvest cooling and refrigeration of horticultural produce, are presented below.

2.7.1 Refrigerated rooms

CFD analysis has shown how an uneven airflow distribution in refrigerated rooms (Figure 2.2) can cause warm spots in pallets bins located in the centre and rear (furthest from the evaporator fan) sections of the room (Amos, 2005; Delele et al., 2009a). Delele et al. (2009a) developed a multiscale CFD direct simulation model of a chicory root cool store to investigate how humidification intervals can reduce chicory root weight loss during cooling. The numerical model demonstrated how low velocity cooling towards the rear of room was unable to completely remove the heat of respiration from the produce. Using the developed multiscale CFD model of the chicory root cool store Delele et al. (2009b) tested potential scenarios to improve the system. Numerical results suggested that elongating the air deflector to direct refrigerated air to the rear of the room and reducing the stack height to increase the free air space at the top of the room, would lead to an improvement in the cooling time and overall process efficiency.

2.7.2 Ventilated packaging during forced-air cooling

A series of CFD studies have demonstrated how the size and location of the openings of ventilated packages affect and can improve the rate and uniformity of forced-air cooling applications of non-polylined horticultural produce, by modifying how much air can come in contact with the product and how it is distributed inside the package (Dehghannya et al., 2008, 2011, 2012; Delele et al., 2008; Ferrua & Singh, 2009a, 2011; van der Sman, 2002; Vigneault et al., 2006). CFD has been used to simulate the effect of altering the size and location of the vents in the package and whether these changes

can improve the airflow distribution and cooling uniformity within and between the product packages.

Using a direct numerical simulation model Ferrua and Singh (2011) developed a series of design guidelines to optimise the package design as part of the forced-air cooling process of strawberry clamshells. They found that the cooling rate and uniformity could be improved by periodically reversing the direction refrigerated air was pulled through the pallet. In addition they found that increasing the vent area of the clamshells, hence forcing more air through the clamshells will not necessarily lead to improvements in the cooling rate of the process. Ferrua & Singh (2011) also found that the cooling rate and uniformity of the process could be improved by decreasing the temperature of the air being delivered at the warmest points within the system. This was achieved by bypassing half the airflow entering the pallet structure into the second part of the pallet, ensuring a supply of refrigerated air to the warmest clamshells located in the back half of the pallet. By doing this a decrease of 6 % in the time taken for the warmest part of the pallet to reach seven-eighths cooling was predicted in the CFD simulation.

Dehghannya et al. (2008, 2011, 2012) investigated the size and location of vented areas on the cooling heterogeneity using CFD. A setup, involving a forced air tunnel to draw air through a bed of solid polymer balls, was designed to simulate postharvest cooling of spherical produce inside a ventilated package. The finite element method was used to solve simultaneous 2D airflow and heat transfer models. The airflow pulled through each ventilated package was determined from experimental data. Results indicated that while cooling uniformity increased with an increase in vent area, the rate of cooling was more dependent on the distribution of the vent areas and may actually decrease if the

vents are not evenly distributed. For example, three vents, with one vent located near both edges of the package wall and one at the centre will facilitate a faster cooling rate then if the same three vents are located beside each other in the centre of the package wall (Dehghannya et al., 2012). The evenly distributed vent configuration promotes a more homogeneous distribution of the airflow throughout the package, resulting in faster cooling.

2.7.3 Transport equipment

In refrigerated transport trailers the product temperature and homogeneity are directly controlled by the airflow patterns (Moureh et al, 2009c). Refrigerated air must be delivered to all parts of the container to compensate for heat fluxes through container walls and/or the heat of respiration of the product. Combining experiments with the numerical results Moureh and Flick (2004) and Moureh et al. (2009a, 2009b) showed that air circulation within a refrigerated transport trailer containing slotted boxes filled with spheres was found to be dependent on the porosity of the boxes. For ventilated packages the refrigerated air supply jet had an increased penetration depth along the truck length compared to non-permeable boxes. Non-permeable boxes promoted short-circuiting of the airflow in the front part of the truck. This allowed produce in the front of the truck to receive a sufficient supply of refrigerated air to maintain the produce at low temperatures and remove the heat generated by respiration. However, the airflow rate was inadequate for produce located at the back of the truck promoting temperature heterogeneity within the truck.

Using the developed CFD model air-duct systems between rows of pallets in refrigerated trucks were shown to improve the overall homogeneity of the airflow, and consequently temperature, in the truck (Moureh et al., 2009c). When air-ducts were included the airflow was blown into the truck at three positions (at the front, 1/3 of the truck length from the front and 2/3 of the truck length from the front). The use of air-ducts avoided the occurrence of stagnant zones and low velocities in the rear (region furthest from the evaporator fan) of the truck, while reducing the air velocities at the front. Air-ducts were shown to prevent over-chilling of produce, due to high air velocities, in the front of the trailer and overheating of the produce, due to low air velocities, at the rear of the trailer.

2.7.4 Domestic refrigeration

In domestic refrigerators natural convection which leads to evaporation and condensation can cause product quality loss in food (Laguerre et al., 2007, 2008, 2009). Laguerre et al. (2010) developed and validated a CFD model that simulated the heat and moisture transfer in a domestic refrigerator. The model assumed steady state conditions and laminar airflow and used Fluent to solve the mass and heat transfer equations. The validated model showed the dehydration of the food product near the top the refrigerator due to a higher air temperature. Likewise, as the air flowed down towards the bottom of the refrigerator its temperature decreased resulting in condensation on the food products in that region.

Typically domestic refrigerators contain one thermostat measuring the air temperature at one specific point and assume that it is constant everywhere. To generate information on

the different temperatures within the space António and Alfonso (2011) developed a CFD model that used Fluent, and applied the standard κ-ε turbulence model, to simulate temperature gradients in a refrigerator. The numerical model showed the coldest regions to be near the cool wall (containing the evaporator fan) and the bottom. These were the optimal locations to place perishable products as they require the lowest storage temperatures.

2.7.5 Future of numerical modelling in postharvest operations

With the increased availability and affordability of computational power and numerical software packages the frequency of utilisation of numerical models in the field of postharvest refrigeration can be expected to significantly grow. Over the last 16 years alone numerical models in postharvest operations have progressed from porous medium (Alvarez et al., 2003; Haong et al., 2003; Xu & Burfoot, 1999; van der Sman, 2002; Verboven et al. 2006; Zou et al., 2006a, 2006b) and zonal models (Tanner et al., 2002a, 2002b, 2002c) to direct numerical simulation 3D models containing thousands of individual horticultural products (Defraeye et al., 2013b, 2014; Delele et al., 2009a, 2009b, 2013b, 2013c; Ferrua & Singh, 2009a, 2009d, 2011; Moureh et al. 2009a, 2009b, 2009c and Tutar et al., 2009). It can be argued that even the current numerical models are being held back by limits in the computational power available outside high performance computing centres (that is, readily available to non-computing university departments or small design offices). 3D numerical models of multiple packages still require the use of wall functions to calculate turbulence between the airflow and solids, despite their potential for inaccuracy (Defraeye et al., 2013a).

For the numerical modelling of forced-air cooling operations it can be expected that within the next five to ten years low Reynolds number modelling (using an extremely fine mesh to subdivide the volume around the fluid-solid surfaces) will not only be possible but common practice. The only thing preventing low Reynolds number modelling from being currently implemented for the 3D modelling of multiple MBPs is the practical feasibility of computational memory requirements and associated simulation time (Defraeye et al., 2013a).

2.8 Conclusions

Forced-air cooling is commonly used with horticultural produce to lower the fruit temperature and limit fruit respiration within an acceptable time frame. The MBP used for kiwifruit contains openings to allow refrigerated air to be pulled through the package to lower the temperature of the fruit while a polyliner prevents moisture loss and subsequent fruit shrivelling. The polyliner prevents moisture loss not just during forced-air cooling but also throughout the entire cold chain. As such it is a fixed constraint in the package composition. Experimental research has shown that the flowrate and distribution of air is a critical design factor in the forced-air cooling and refrigeration of horticultural food products. For forced-air cooling and refrigeration an even delivery of the airflow to each area of the system is essential to optimizing the performance of the operations.

Numerical models provide a method for optimising package design. Various numerical models exist to predict the mass, momentum and heat transfer in food operations. These numerical models range from averaged porous medium models and simplified zonal

models to direct numerical simulations that explicitly solve the associated transport equations. Direct numerical modelling, which can model kiwifruit MBPs during forced-air cooling, has already been extensively used to understand and improve package design for horticultural produce. A direct numerical model simulation of a package(s), once validated against experimental data, can be used to predict the effect of package design and operating conditions changes, without the need to create physical prototypes that are expensive, time-consuming and seasonally limited for experimental work.

The use of direct numerical simulations has been shown to facilitate improvements to the understanding of the mechanisms through which different design parameters affect the cooling rate and uniformity of the forced-air cooling process, along with the numerical assessment of different designs. CFD, using the finite volume scheme, will be used in this project. While much research has been carried out into the forced-air cooling of horticultural produce, typically, those projects did not involve systems which contained a polyliner. Usually, forced convection is the dominant heat transfer process. However, the presence of the polyliner is expected to alter the relative contribution of the heat transfer mechanisms. Before, a CFD model can be developed a series of experiments about the cooling performance of polylined horticultural produce is required to evaluate the importance of different heat transfer mechanisms, to provide information about the boundary conditions of the problem, and to provide validation data for the model. A CFD model which can simulate the primary contributing heat transfer processes, while excluding the phenomenon that have a negligible impact, can then be developed and validated.

Chapter 3

Research objectives

This project aims to combine industrial and laboratory experiments with a numerical model to determine the significant factors affecting the forced-air cooling process of polylined horticultural produce. The first step is to experimentally investigate the heat transfer mechanisms controlling the forced-air cooling performance. The experimental results can then be used to inform upon the development of a numerical model of the process. Following validation the numerical model can be used assess operating conditions (air flowrate and pressure drop) and investigate the impact of different design features in the package and their effect on the cooling performance. The primary objectives of this project were laid out as follows:

1) Experimentally investigate the heat transfer mechanisms controlling the forced-air cooling of kiwifruit MBPs
2) Use the experimental results to design and develop a numerical model that accounts for the presence of a polyliner, using computational fluid dynamics (CFD), that can simulate the transport phenomena occurring during the process
3) Validate the numerical model against experimental data for a variety of operating conditions
4) Identify the most efficient (in terms of cooling rate, uniformity and energy use) operating conditions and propose an alternative box design to improve upon the cooling efficiency
5) Develop a series of guidelines to improve the design and performance of the forced-air cooling process of polylined horticultural produce

Chapter 4

Characterising the forced-air cooling performance of polylined modular bulk packs

4.1. Introduction

Much research has been conducted into characterising the forced-air cooling of non-polylined horticultural produce in ventilated packaging (section 2.5.2). However, the relative influences of the operating conditions and design features on the cooling performance are specific to each design. For example, increasing the venting area does not always translate to reduced cooling times. Instead, there is an optimal vent area percentage, specific to each product (Pathare et al., 2012). In some cases, such as strawberry clamshells, bypassing half the airflow entering a pallet structure into the second part of the pallet can be the best way to improve the overall cooling time (Ferrua & Singh, 2011). In addition to the lack of definitive design specifications to improve the cooling process of non-polylined horticultural produce the kiwifruit modular bulk pack (MBP) contains an inner packaging liner, or polyliner. There is comparatively little information available on the impact of this polyliner (as it is not a feature of most horticultural packaging systems). Prior to the development of the numerical model an understanding of the transport phenomenon, and particularly relevant heat transfer mechanisms and pathways, occurring were required.

*Material from this chapter is included in conference papers: (a) O'Sullivan, J.L., Ferrua, M., Love, R., Verboven, P., Nicolai, B.M., & East, A. (2012). *Mechanisms and performance of the forced-air cooling process of fruit packed in polyethylene liners* [CD]. Paper presented at the CIGR Section VII International Technical Symposium on Innovating the Food Value Chain, Stellenbosch, South Africa. (b) O'Sullivan, J.L., Ferrua, M.J., Love, R.J., Verboven, P., Nicolaï, B.M., & East, A.R. (2013a). *Performance of the forced-air cooling process of fruit packed in polyethylene liners as a function of pallet orientation* [USB]. Paper presented at the 2nd IIR International Conference on Sustainability and the Cold Chain, Paris, France.

4.2 Industrial experiments

4.2.1 Objectives

The objective of the industrial experiments was to provide an initial insight into the heat transfer mechanisms occurring in polylined MBPs of kiwifruit during forced-air cooling. The industrial experiments aimed to describe the primary heat transfer pathways within MBPs and identify how the cooling performance was influenced by MBP location and pallet orientation, in a commercial setting. Results from the industrial experiments can lead towards designing more comprehensive experiments that can be run under controlled laboratory conditions.

4.2.2 Methods

The experiments were performed at a commercial packhouse and storage facility in Te Puke, New Zealand. A tunnel cooler (Section 2.2.1) was the forced-air cooling device used. Two palletised rows of produce were placed to either side of a fan. The fan created a vacuum which drew refrigerated air through the pallets. A standard ISO industrial pallet (1.2 x 1.0 m) holds 100 MBPs, evenly distributed into 10 layers. There are two possible pallet orientations that air can be pulled through (Figure 4.1). Commercially, air is pulled through the 1.0 m pallet face. This was the pallet orientation used for the first industrial experiment. The monitored pallet was one of the two centre pallets in the tunnel cooler row (Figure 2.1, section 2.2.1).

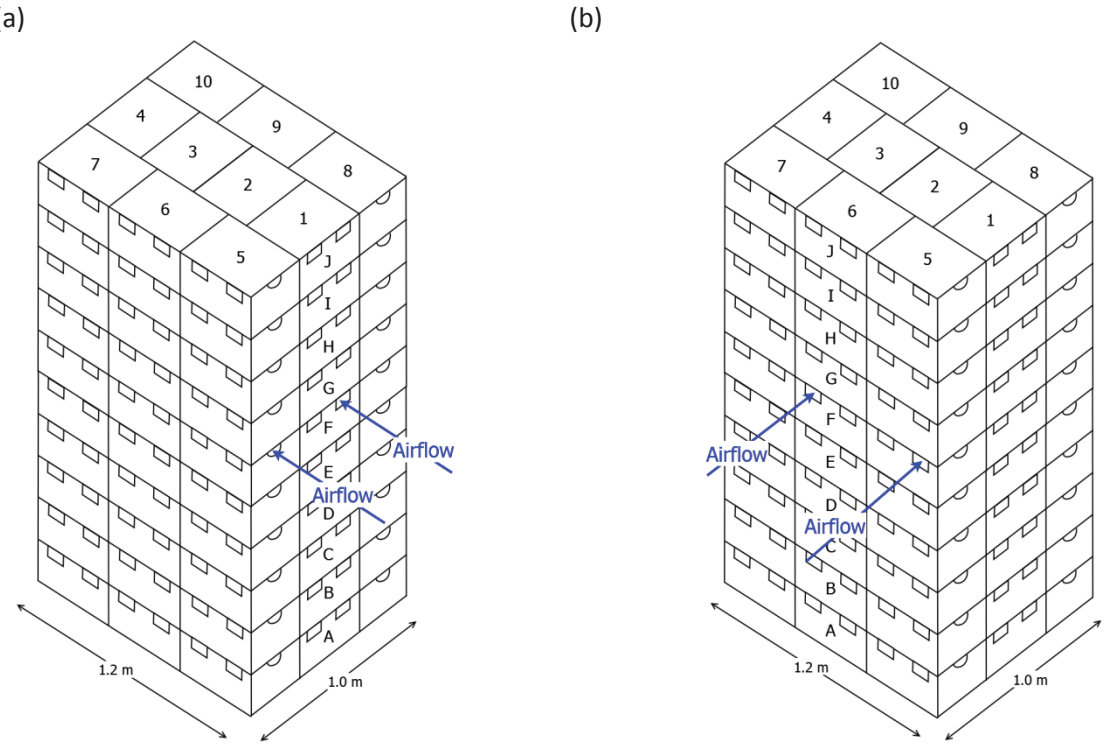

Figure 4.1. Kiwifruit pallet with MBPs numbered 1 – 10 and pallet layers "A" – "J". Air can be drawn through (a) the 1.0 m face or (b) the 1.2 m face.

Due to the geometric nature of the pallet, a line of axial symmetry was assumed down the centre of the pallet (through MBPs 1 – 4). In the 1.0 m orientation MBPs 5 and 8, 6 and 9, and 7 and 10, were replicas of each other. In the 1.2 m orientation MBPs 5 and 7, 1 and 4, 2 and 3, and 8 and 10 were replicates. Hence, measurements for MBPs with replicas, both on separate layers and due to axial symmetry, were averaged. Hence, analysis and presentation of the results was for a reduced single pallet layer (Figure 4.2).

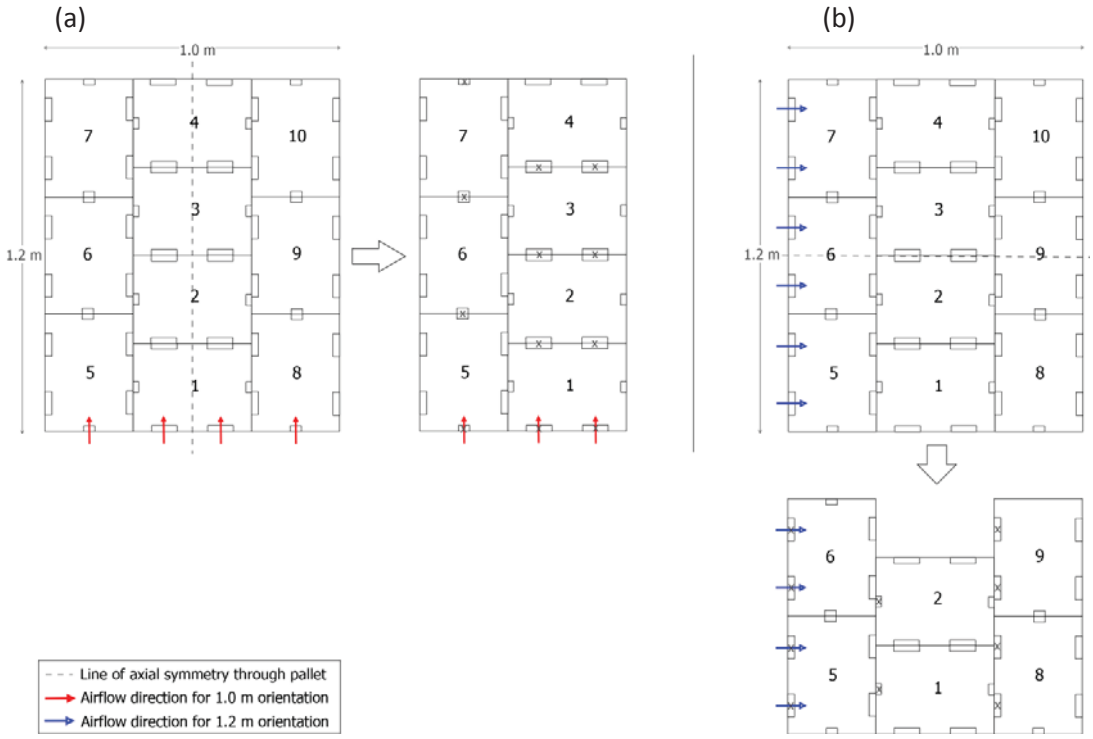

Figure 4.2. Reduced pallet row of MBPs 1 - 10, for air pulled through (a) the 1.0 m pallet orientation and (b) the 1.2 pallet orientation, on the basis of axial symmetry. "X" denotes location of thermocouples to measure air temperatures.

4.2.2.1 Air temperature

The air temperature entering each MBP was measured by thermocouples (1 per cardboard box vent orientated towards the incoming refrigerated airflow). There were 11 air measurement points per monitored pallet layer in the 1.0 m orientation and 10 air measurement points in the 1.2 m orientation. Thermocouples were placed in the front vent (i.e. vent through which air enters the MBP when being pulled linearly from the front to back of the pallet).

4.2.2.2 Impact of MBP location on the cooling rate

The kiwifruit temperatures were recorded in multiple MBPs in both pallet orientations to identify the impact of MBP location on cooling rate. Due to the time constraints

associated with running experiments at an industrial facility thermocouples were only placed in the centre of six different kiwifruit, randomly located in the top layer of fruit, per monitored MBP. The fruit were left in the same arrangement as they were commercially packed. It was assumed that, with the exception of top "J" and bottom "A" layer, the different pallet layers would experience the same cooling rates and profiles. MBPs in both layers "D" and "G" were monitored as replicates, as these were considered to be representative of the overall pallet (Figure 4.1).

4.2.2.3 Impact of kiwifruit location within a MBP on the cooling rate

When air was drawn through the 1.0 m face an experiment into the effect of cooling rate depending on the kiwifruit location within the MBP was performed. As this was a commercial operation the experimental set-up (pallet disassembly, thermocouple placement and pallet reassembly) had to be completed between 10 am and 4 pm on the same day. Due to these time constraints this experiment could only be carried out for MBP 1 in layers "E" and "F" (Figure 4.1). Layers "E" and "F" were considered to be replicates of each other. The experiment assumed that the kiwifruit were roughly divided into four layers with approximately 25 kiwifruit per layer. Kiwifruit were selected in the top and bottom fruit layers in MBP 1 (Figure 4.3) and the fruit temperatures monitored. Type-T thermocouples were placed in the centre of monitored kiwifruit. The random stacking of the kiwifruit meant the kiwifruit could only be placed in the general vicinity of the indicated locations (Figure 4.4). The kiwifruit temperature data as dependent on location within the MBP was averaged across the two pallet layers ("E" and "F").

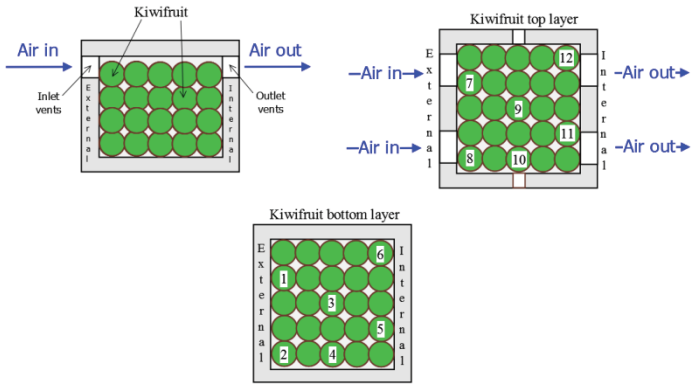

Figure 4.3. Approximate location of kiwifruit in the top and bottom kiwifruit layers for MBP 1 in layers “E” and “F” of the 1.0 m pallet orientation.

(a) (b)

Figure 4.4. Kiwifruit as packed in a commercial facility (a) excluding and (b) including Type-T thermocouples to monitor the kiwifruit temperature in MBP 1.

4.2.2.4 Pallet orientation and positioning

The experiments described above were conducted for both pallet orientations. For the second experiment, conducted approximately three weeks after the first, air was pulled through the 1.2 m face. Due to time constraints only the experiments into the impact of MBP location on the cooling rate (section 4.2.2.2) for the 1.0m orientation could be repeated for the 1.2 m orientation. For the 1.0 m orientation there were two rows of six pallets to either side of the fan, with the monitored pallet placed in the number 3 position (Figure 4.5). Due to the increased width of the pallet in the 1.2 m orientation

only five pallets could be placed in a row at either side of the fan (Figure 4.5). The monitored pallet was in the number 3 position. In both orientations the monitored pallet was in the row in the left hand side.

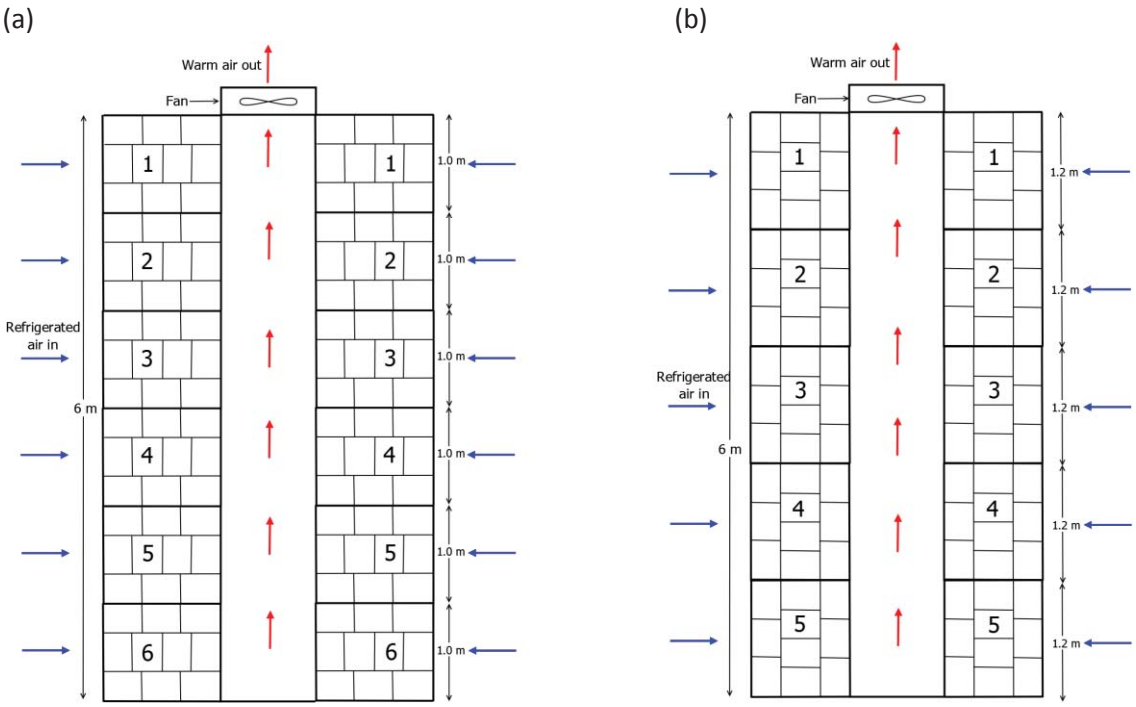

Figure 4.5. Pallet positions in an industrial tunnel cooler for the (a) 1.0 m and (b) 1.2 m orientation

4.2.3 Temperature logging

The temperature of every thermocouple was recorded every minute over a 10 h period, starting when the kiwifruit pallets were moved (from the pallet packing at ambient temperature in an assembly room open to the outside conditions) into the cool room, where the tunnel cooler was operated. It took approximately 2.5 h for all the pallets (including the monitored pallet) to be assembled into the tunnel cooler, for the tarp to be positioned and the forced-air cooling operation initiated. The forced-air cooling lasted for about 4 – 6 h, depending on pallet orientation run, after which the tunnel cooler was deactivated and the pallets left in the cool room for approximately 4 h before being moved to a refrigerated storage room. Temperatures were logged at one-minute

intervals by Grant Squirrel 64-channel dataloggers (1000 Series Squirrel Meter/Logger, Eltek Ltd, Cambridge, UK).

4.2.4 Data analysis

4.2.4.1 MBP location and pallet orientation

When comparing the cooling rates between MBP location and the pallet orientation the kiwifruit temperatures were converted to the fractional unaccomplished temperature change (FUTC), *Y*. *Y* represents the amount of possible temperature change that has yet to be accomplished (Eq. 4.1) and is a common method used to normalise cooling data to enable comparison between multiple cooling trials where initial and air cooling temperatures may differ (Brosnan & Sun, 2001).

$$Y = \frac{T - T_a}{T_i - T_a} \tag{4.1}$$

where T (°C) is the temperature of kiwifruit in MBP at the specified time of cooling, T_i (°C) is the initial temperature of individual kiwifruit in the MBP at the start of cooling, and T_a (°C) is the average temperature of the air. T_a (°C) is a single value, taken as the average temperature of the air entering the pallet over the cooling process. When calculating the averaging *Y* in a MBP *Y* was first calculated for each kiwifruit and then averaged over the number of kiwifruit recorded per MBP. The half cooling time (HCT) is defined as the time at which Y equals 0.5, when the kiwifruit has cooled halfway from their initial temperature to that of the cooling air. The seven-eighths cooling time (SECT) is when Y = 0.125.

In the 1.0 m orientation the forced-air cooling was only in operation for less than 4 h. Hence, comparisons with the 1.2 m orientation were only for the first 3.9 h of forced-air cooling. There was a relative lack of cooling (no MBP reached HCT during the first 4 h of forced-air cooling for either orientation). Hence, no statistical analysis was performed on the results. Only the general trends observed from the graphs will be briefly discussed.

4.2.4.2 Individual kiwifruit

For individual kiwifruit the temperature drop was from the initial kiwifruit temperature (approximately 20 °C) during the 3.9 h of forced-air cooling for MBP 1 in the 1.0 m orientation. When comparing the cooling rates of individual kiwifruit the amount of cooling that has occurred was expressed as $((1-Y)$ x 100$)$, which converted Y to a percentage of cooling achieved.

4.2.5 Industrial results

The data collected have deficiencies; the venue was an active commercial packing facility so the operating conditions (air temperature, initial kiwifruit temperature, duration of forced-air cooling, time between kiwifruit pallet entering cool room and start of forced-air cooling, etc.) were not able to be controlled as precisely as a laboratory experiment. However, it was possible to carry out replicates for each MBP for two pallet layers. The experiments were still valuable to provide a first insight into how palletised polylined MBPs of kiwifruit cool, and gave a sense of the conditions encountered in real commercial practice.

4.2.5.1 Air temperature

The thermocouples to record the air temperatures were placed in the middle of the inlet of the cardboard box vent orientated towards the incoming refrigerated airflow, for each MBP. Hence, the exact temperature recorded was the air temperature at the boundary between the MBPs and the air in the refrigerated room (for MBPs 1 and 5). The sudden drop in air temperature after ~ 2.5 h from the start of temperature logging in both pallet orientations, as air was pulled through the vents, indicated the start of forced-air cooling (Figure 4.6). The forced-air cooling operation was considered to be in effect (i.e. no sizeable increases to the air temperature in the room) until 6.4 h in the 1.0 m orientation (Figure 4.6(a)) and 8.2 h in the 1.2 m orientation (Figure 4.6(b)), from the start of temperature logging.

MBPs 1 and 5 were at the front of the pallet and effectively recorded the air temperature in the refrigerated rooms. As the refrigerated rooms were in an active packhouse warm air at ambient conditions was being introduced as forklifts moved in and out of the room to assemble and disassemble other tunnel coolers in the room. Hence, the air temperature in the refrigerated room oscillates throughout from the 0 °C set point as it is being increased as warm air infiltrates the room. The introduction of significant amount of warm air occurred at 6.4 h and 8.2 h in the 1.0 m and 1.2 m orientation, respectively (Figure 4.6), negating the viability of analysing this data, as the assumption of constant air temperature is significantly broken.

Air temperatures in the cool rooms showed significant variations between the pallet orientations (Figure 4.6). During the 1.0 m orientation the room temperature fluctuated

around 0 °C during forced-air cooling. However, the 1.2 m orientation, conducted in a different cool room, operated at 7 °C.

In the 1.2 m orientation the average temperature of the kiwifruit when the pallet was placed in the refrigerated room was 13.6 °C, whereas the average temperature in the 1.0 m orientation was 18.3 °C. There were numerous possible reasons for the lower kiwifruit temperatures. The 1.2 m orientation experiment was conducted three weeks after the 1.0 m orientation experiment, in mid-May. The three week gap may have witnessed a substantial drop in ambient temperature as winter approached, lowering the field heat of the kiwifruit at harvest. Additionally, following harvest and prior to packing the kiwifruit may have been stored in a cool, shaded location, for an extended time period (i.e. 3 – 7 days), lowering the fruit temperature but risking moisture loss. The relatively low fruit temperature at the start of cooling resulted in a relative low maximum air temperature. The narrow range for air temperatures in the 1.2 m orientation (~ 6.3 °C) reduced the potential change in air temperature as it was pulled through the pallet (Figure 4.6).

From observations of the tunnel coolers during the industrial trials the pallets were set-up quite poorly. Large gaps between and around individual pallets in the tunnel cooler were present, reducing the percentage of the flowrate pulled through the pallet and lowering the reduction in delivered air temperature, particularly for the MBPs at the back in for both orientations (Figure 4.6). Nevertheless, despite the deficiencies in the data, the relationship between air temperatures and cooling rate of the MBPs can still be analysed, provided the uncontrolled variables present in industrial experiments are taken into consideration.

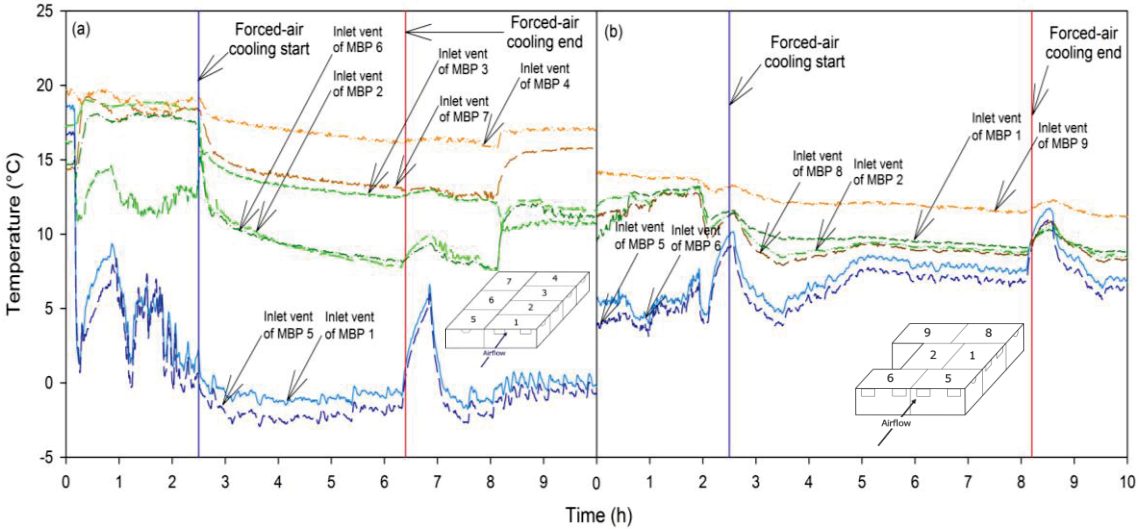

Figure 4.6. Air temperature change at the inlet vent of each MBP in a pallet row for (a) the 1.0 m orientation and (b) the 1.2 m orientation over 10 h of cooling in industry.

There was a higher increase in air temperature as it was pulled through the pallet in the 1.0 m orientation, compared to the 1.2 m orientation. The increase in air temperature in the 1.0 m orientation resulted in slower cooling rates of the corresponding MBPs, particularly MBP 4, where there was a small difference in temperature between the kiwifruit and the cooling air, reducing the driving force for heat transfer. The higher temperature difference in the 1.2 m orientation between the air and the kiwifruit, and the lower increase in air temperature between MBPs, resulted in improved cooling rates and uniformity (Figure 4.7).

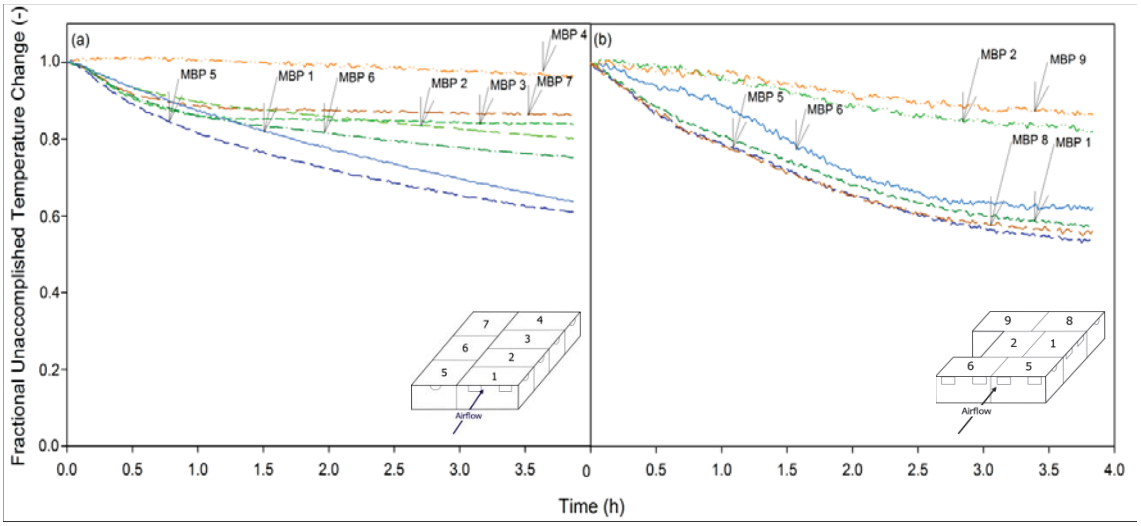

Figure 4.7. Average fractional unaccomplished temperature change, from the start of the forced-air cooling for (a) the 1.0 m orientation and (b) the 1.2 m orientation

4.2.5.2. *Y* of modular bulk packs in industry

In the 1.0 m orientation the maximum amount of cooling occurred at the front of the pallet, where MBPs 1 and 5 were directly exposed to cooling airflow. The further the back in the pallet, away from the airflow, the MBPs were located the slower the cooling rate (Figure 4.7(a)).

In the 1.2 m orientation MBPs 5, 6, 1 and 8 all cooled at similar rates. It is possible that there was a large gap between the side of the monitored pallet and the adjacent pallet. This may have allowed a high volumetric airflow rate to flow between pallets providing a substantial heat transfer pathway along the external sides of MBP 5, 1 and 8 (Figure 4.7(b)). Similarly, MBPs 6, 2 and 9, located away from potential refrigerated airflow past the side of the pallet, showed slower cooling rates then might be expected. This effect is most prominent in MBP 2, which was isolated in the centre of the pallet.

Pallets are nominally placed exactly adjacent to each other in the tunnel cooler, but frequently gaps between pallets of up to 5 cm are observed. These gaps provide additional airflow pathways and are caused either due to the pallet being slightly misaligned when the tunnel cooler is assembled, or the individual MBPs being slightly misaligned when the pallet is assembled. The procedures followed by the operators obviously influence the occurrence and extent of any gaps. As indicated by these results, gaps between pallets may in fact increase the cooling rate of the neighbouring MBPs, but at the cost of compromising the cooling rate elsewhere in the tunnel cooler (i.e. by reducing the air flowrate through the centre of the pallet).

In the 1.0 m orientation the average temperature drops for all the kiwifruit MBPs from their starting temperatures was 26 %, after 3.9 h of forced-air cooling. In the 1.2 m orientation this cooling percentage was 35 % over the same time period. The maximum difference in the amount of cooling that occurred ((*1*-*Y*) x 100) between individual MBPs was 38 % in the 1.0 m orientation, compared to 32 % in the 1.2 m orientation. The slowest cooling rates occurred in the MBPs centrally located at the back of the pallet in both orientations (MBP 4 in the 1.0 m orientation and MBP 9 in the 1.2 m orientation).

The data collected can be described as "noisy" and was difficult to derive definitive conclusions from. However, despite the uncontrolled variables the observation of a lower rise is air temperatures pulled through, and substantially faster cooling rates for the MBPs at the front of the pallet in the 1.0 m orientation were considered likely to be confirmed in laboratory experiments, which were conducted in section 4.3.

4.2.5.3. *Y* within modular bulk packs

The impact of location within the MBP on the reduction in kiwifruit temperature is presented in order of fastest cooling rates, from top to bottom, for MBP 1 in the 1.0 m orientation (Table 4.1). Kiwifruit 1 and 2 were two of the top six kiwifruit with the highest cooling rates. This implied that cooling was not solely dominated by the airflow across the top of the pallet and that cooling may have also occurred across the cardboard base. Kiwifruit 11, centrally located in the top fruit layer, cooled slower than both Kiwifruit 4 and 6. Kiwifruit 4 and 6 were located in the bottom fruit layer of the MBP.

This indicated that there were other pathways for heat transfer in addition to the airflow across the top of the polyliner.

Table 4.1. Kiwifruit location within MBP 1, temperature drop and the percentage of cooling unaccomplished during the forced-air cooling period in the 1.0 m pallet orientation. Standard deviation is shown for the data (n = 2).

Kiwifruit location	Temperature drop (°C)	1 – Y (%)
8	9.2 ± 1.0	58.0 ± 9.0
2	8.6 ± 0.2	54.5 ± 3.2
12	9.4 ± 0.7	50.0 ± 2.4
7	8.5 ± 0.1	48.6 ± 1.2
1	7.4 ± 0.3	47.1 ± 0.2
10	7.7 ± 0.7	44.1 ± 2.7
4	6.0 ± 0.3	33.2 ± 1.6
9	5.9 ± 1.1	33.2 ± 8.2
6	5.8 ± 1.0	31.2 ± 5.8
11	4.8 ± 0.2	26.2 ± 0.5
3	4.5 ± 0.1	25.2 ± 1.2
5	3.4 ± 0.0	18.1 ± 0.5

4.2.6 Conclusions (industrial experiments)

The forced-air cooling of kiwifruit MBPs was dependent on the temperature of the refrigerated air flowing through each MBP. For the 1.0 m orientation the further away from the refrigerated airflow the MBPs were located the higher the air temperature entering the MBPs and consequently, the slower the cooling rate. For the 1.2 m orientation the air entered through the 1.2 m pallet face and the distance that the cooling air travelled through the pallet was reduced. Hence, the increase in air temperature as it flowed into each MBP, compared to the 1.0 m orientation, was relatively low. The closer the air temperatures flowing into to each MBP are to the refrigerated air temperature the higher the likelihood of increased cooling rates and uniformity between the MBPs.

The MBP centrally located at the front of the pallet in the 1.0 m pallet orientation

showed substantial temperature gradients within the MBP. The industrial results indicate that there were other substantial heat transfer pathways, besides heat transfer from the refrigerated airflow pulled through the MBP through the polyliner to the top layer of kiwifruit. It is important to note that some of these pathways (heat transfer through the base of the MBP, for example) can be controlled by the box designer (i.e. by material selection). Other heat transfer pathways (heat through the side of the MBP into the gap between pallets) depend on operating procedures and will be difficult for the box designer to account for.

The industrial experiments showed the general cooling profiles that occur during forced-air cooling and provided an initial insight into the heat transfer mechanisms in polyliner modular bulk packs of horticultural produce. However, collecting this data was difficult and not conducted under controlled conditions. It was clear from the industrial experiments that the experiments would have to be repeated, under controlled laboratory conditions, with a particular emphasis on temperature gradients throughout the entire MBP, i.e. kiwifruit would have to be measured at the multiple locations within multiple MBPs, spread throughout the pallet layer. Control over the operating conditions maintained across experiments would allow stronger conclusions to be drawn about the effect of kiwifruit location within a MBP, MBP location in a pallet layer and pallet orientation on the airflow behaviour and heat transfer mechanisms occurring.

4.3 Laboratory experiments

4.3.1 Objectives

Two laboratory experiments were designed, based on the information obtained from industrial experiments. The objectives for the laboratory experiments can be broken in two parts. The first involves evaluating the cooling performance of the individual MBPs and entire pallet of kiwifruit during forced-air cooling. The second involves preliminary questions to develop a numerical model of the system.

4.3.1.1 Cooling performance

The experiments aimed to calculate what regions of the MBP cooled fastest, relative to each other and the impact of MBP location (i.e. distance from incoming refrigerated airflow) in the pallet layer on cooling rate.

4.3.1.2 Numerical model

The experiments also aimed to provide data to inform a numerical model of the forced-air cooling process of polylined horticultural produce. For example, what are the key heat transport mechanisms to include and is moisture loss likely to significantly contribute to the cooling rate?

4.4 Methods

4.4.1 Design of a forced-air cooling simulator

A laboratory apparatus was designed and constructed to simulate forced-air cooling of palletized produce stacked while allowing control over the flowrate of the refrigerated air (Figure 4.8). In terms of experimental cost, it is preferable to run experiments on half-pallets (five layers high of kiwifruit MBPs compared to the ten layers used in industry). It was assumed that the middle three layers of a five layer pallet (layers "B", "C" and "D"; Figure 4.8) would behave similarly to the middle eight layers of ten layer pallet, while the top and bottom layers (layers "E" and "A", respectively, in the five layer pallet; Figure 4.8) would behave similarly regardless whether there were three or eight layers between them. Thus, it was considered safe to construct the laboratory apparatus as a half-pallet and to extrapolate the findings to a full-pallet.

Typically, pre-coolers for horticultural produce operate with a volumetric airflow rate (given in term of per kg of product) through the pallet of 0.5 – 2.0 L kg^{-1} s^{-1} (Thompson, 2004) and a pressure drop of 60 – 750 Pa (Brosnan & Sun, 2001). With approximately 10.5 kg of kiwifruit in each MBP, the half-pallet fruit weight of the laboratory apparatus is 525 kg, thus the required airflow through the pallet is 0.26 – 1.05 m^3 s^{-1}. To meet this flowrate a variable speed drive (VSD) fan (Model AP0502AA5/16, Fantech, Wellington, NZ) capable of generating a maximum airflow rate of 2 m^3 s^{-1} was selected.

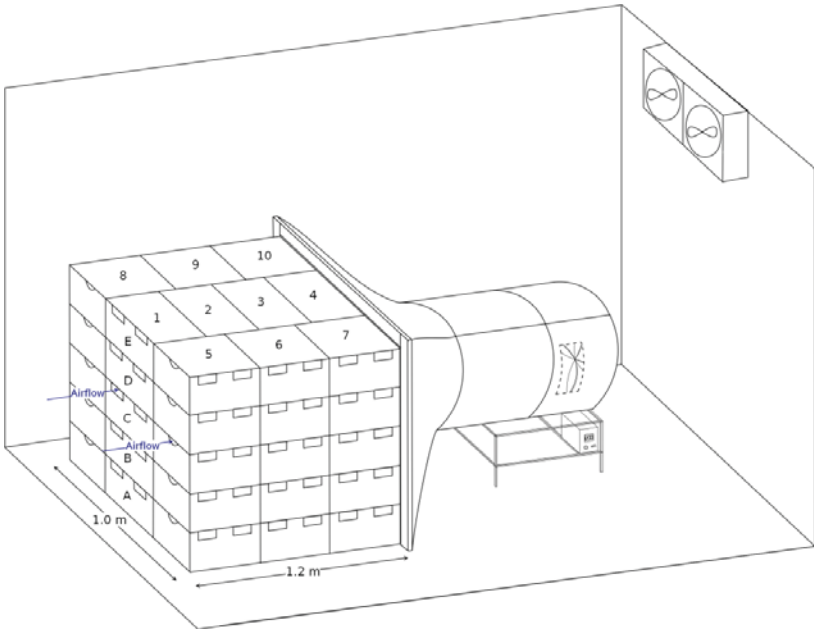

Figure 4.8 Variable speed drive fan attached to a half-pallet of kiwifruit trays inside a cool room to simulate precooling. In the illustrated configuration refrigerated air is pulled through the 1.0 m wide pallet face. However, the fan ducting/pallet interface is wide enough to allow the pallet to be rotated so that air is instead drawn through the 1.2 m wide pallet face.

4.4.1.1 Design and construction of experimental pre-cooler equipment

To simulate forced-air cooling a rig had to be designed and constructed that was portable, could pull air (via a fan) through a half-pallet of kiwifruit and measure the air flowrate, while conforming to the dimensional restrictions of the refrigerated room. The length of the available refrigerated room was 3000 mm. Practically, due to the length of the pallet (1200 mm), length of the fan (500 mm) and minimum length of 500 mm required between the fan outlet and the back wall of the room, the maximum upstream straight length of pipe between the airflow measurement device (orifice plate) and interface (to connect the half-pallet to the rest of the rig) was 500 mm or one pipe diameter. The half-pallet had a height of approximately 1 m, which including the pallet base, gave it a total height of 1.2 m. The interface had a height and width of 1200 mm.

Stainless steel 316 was the material used for the interface, pipe and orifice plate. The components and dimensions are illustrated in Figure 4.9.

When the pallet was orientated so that the air was drawn through the 1.0 m wide face (Figure 4.8) the pallet was centred in the interface and the consequent gaps at the edges of the pallet were sealed with removable steel fixtures.

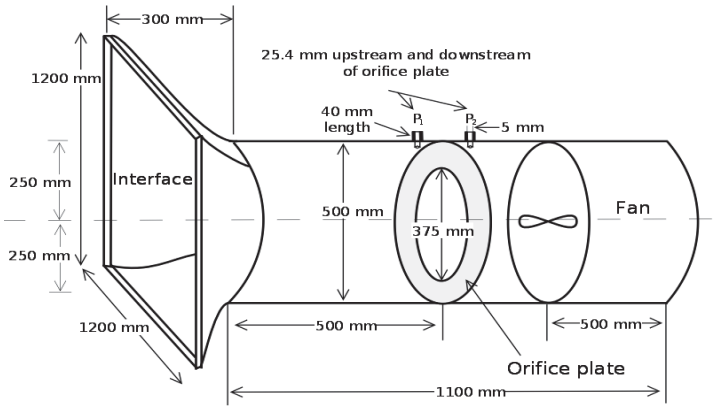

Figure 4.9. Dimensions for the variable speed drive fan, orifice plate, pressure tappings, upstream and downstream cylinder lengths and interface to attach to horticultural produce pallet to simulate forced-air cooling.

4.4.1.2 Measurement of volumetric flowrate through the pallet

To measure the flowrate pulled through the pallet an orifice plate was used. An orifice plate is a thin plate with a hole in the middle that introduces a restriction into a pipe, reducing the cross-sectional area by a known amount (Rennels & Hudson, 2012). As the airflow approaches the orifice plate it contracts and accelerates as the same mass flowrate in the pipe must pass through the smaller opening of the orifice (assuming that the air is incompressible, which is reasonable at the pressures considered here). A vena contracta (point of highest air velocity and narrowest diameter) forms slightly downstream from the orifice plate, before the air expands back to fill the pipe and the velocity reduces to its original value. This phenomenon causes a measurable drop in

pressure across the orifice, and the magnitude of the pressure drop depends upon the volumetric flowrate of the air (Rennel & Hudson, 2012). Hence, the airflow rate can be calculated from the differential pressure between pressure tappings (measurement points) located at specific distances upstream and downstream of the orifice plate (Figure 4.9).

The orifice plate was designed according to the ISO standard ISO 5167-2 (2003) and with consideration of ISO 5167-1 (2003). The standards specify the geometry and method of use (installation and operating conditions) of orifice plates when they are inserted in a conduit or pipe running full to determine the flow-rate of the fluid flowing in the conduit. The standards also outlined the dimensions, equipment and calculation methods required to measure the airflow rate, from the pressure drop across the orifice plate.

The outer diameter of the orifice plate had to be the same as the fan diameter. The fan had a diameter (D) of 500 mm and this dimension became the basis for the orifice plate and pipe calculation. The main dimensions followed from ISO 5167-2 (2003) were;

- E, thickness of the orifice plate – $0.005\ D \leq E \leq 0.02\ D$
- B, ratio of outer to internal orifice plate diameter (D/d) – $0.10 \leq B \leq 0.75$
- l'_1, distance of pressure tapping upstream (P_1) from orifice plate 25.4 ± 1 mm when $B \leq 0.6$ or $B > 0.6$
- l'_2, distance of pressure tapping downstream (P_2) from orifice plate 25.4 ± 1 mm when $B \leq 0.6$ or $B > 0.6$
- a, diameter of pressure tapping for clean fluids – 1 mm $\leq a \leq$ 10 mm
- length of pressure tapping – $< 2.5a$

To reduce the pressure drop through the orifice plate, allowing for higher pressure drops to be generated across the pallet if required, a large internal diameter, *d*, of 375 mm was chosen for the orifice plate.

4.4.1.3 Calibration of the orifice plate

Before the orifice plate can be used to measure the flow rate the discharge coefficient (C_D) of the orifice plate must be determined. This discharge coefficient is the ratio of the actual discharge to the theoretical discharge and relates the theoretical flowrate calculated from the differential pressure to the actual flowrate through the pipe. The discharge coefficient is a function of the exact location of the pressures tappings and ratio of outer to internal orifice plate diameter. As this value is specific to each system rig it is best to experimentally determine it in known flow conditions (Rennels & Hudson, 2012).

To measure the actual flowrate through the pipe a hot-wire anemometer (Dantec, model 54-N-60) measured the air velocity at five evenly spaced vertical locations (500, 375, 250, 125 and 0 mm from the bottom of the pipe) 500 mm upstream of the orifice plate at a fan speed of 300 rpm, with no obstructions to the airflow further upstream, so the vertical locations could be observed. The average air velocity, from the five measurements, was then multiplied by the cross-sectional area of the pipe to give the measured volumetric flowrate. The differential pressure between the two pressure tappings was measured by a U-tube manometer. This experiment was repeated at fan speeds of 420, 540, 660 and 780 rpm. Averaging the air speed at the five locations and multiplying by the cross-sectional area of the pipe allowed the actual flowrate to be

calculated. The theoretical flow rate was calculated from the differential pressure by (ISO 5167-2, 2003),

$$Q = C_D A_2 \left(\frac{2\Delta p}{\rho(1 - B^4)} \right)^{1/2} \tag{4.2}$$

where Q ($m^3\ s^{-1}$) is the measured volumetric flowrate, B is the ratio of outer to internal orifice plate diameter (D/d), A_2 is the internal orifice plate area (0.11 m^2), Δp (Pa) is the measured differential pressure and ρ is the fluid density (kg m^{-3}).

A plot of Q versus $A_2(2\Delta p/\rho(1-B^4))^{1/2}$ gave the experimental discharge coefficient (0.70) from the slope of the line (Figure 4.10). The length of the required pipe diameter for this specific system (i.e. downstream of a constriction immediately behind a partial obstruction) was not listed in the ISO 5167-1 (2003) or ISO 5167-2 (2003) standards. However, it can be assumed less than ideal. Additionally, the air velocity measurements were measured without a pallet in front of the pipe. However, the discharge coefficient was calculated from experiments for this specific system and not from theoretical calculations for an idealised system.

The flowrate can now be calculated from the differential pressure during forced-air cooling experiments, when the air is being pulled through a pallet. The combination of the VSD (to adjust the fan speed) and orifice plate enabled control and measurement of the total airflow through a half-pallet of kiwifruit MBPs.

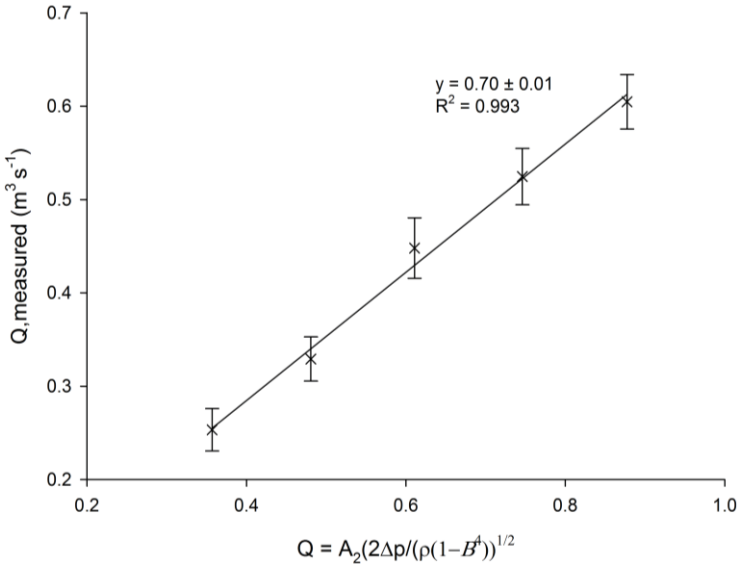

Figure 4.10. Plot of the measured volumetric flow rate (n = 5) against the theoretical flowrate (with a discharge coefficient of 1) calculated from the pressure drop across an orifice plate to find the actual discharge coefficient. Error bars represent ± S.D and are calculated from the replicates at each flowrate measurement locations.

4.4.2 Experimental structure

4.4.2.1 Cooling profiles

The effect of MBP location within the pallet was investigated by measuring the kiwifruit temperature in MBPs 1 – 7 when air was pulled through the 1.0 m pallet face (Figure 4.11(a)). To investigate the effect of pallet orientation the same experiment was carried out with refrigerated air drawn through the 1.2 m face and MBPs 5, 6, 1, 2, 8 and 9 measured (Figure 4.11(b)). The cooling profiles of kiwifruit MBPs as dependent on their location within the pallet were then related to the temperature and velocity of the air pulled through the pallet.

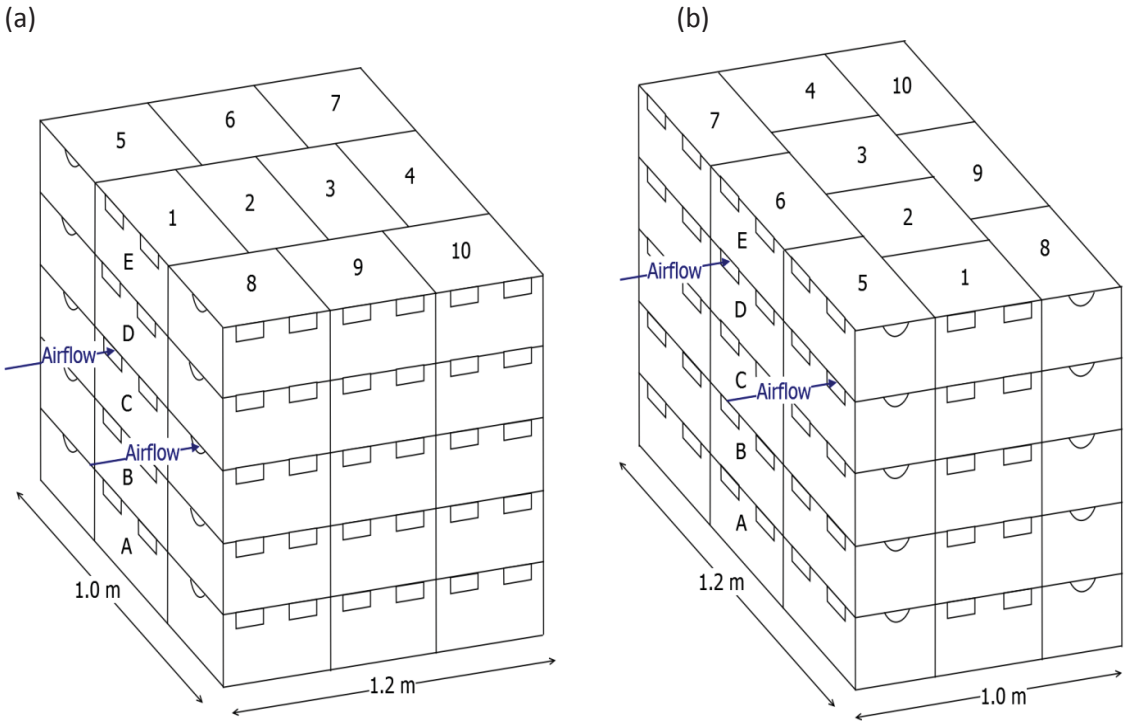

Figure 4.11 Half-pallet layout with layers assigned letters "A"-"E" when air is pulled through the (a) 1.0 m pallet face and (b) the 1.2 m pallet face.

4.4.2.2 Moisture loss

An experiment was also conducted in which the mass change for MBPs 5 – 7 in the 1.2 m pallet orientation was recorded during the first 4 h of forced-air cooling.

4.4.3. Experimental measurements

4.4.3.1 Pallet Orientations

Standard count 36 Hayward kiwifruit MBPs (Section 2.1.4) were used for all experiments. For trials conducted in the Temperature Control Room (TCR) in Massey a half pallet, 1.0 m high, was used (Figure 4.9). When the pallet was placed in the 1.0 m orientation (allowing air to flow through the 1.0 wide face) a tarp was placed over the

1.2 m lateral side walls and the free space between the interface and top MBPs of the pallet, ensuring all of the airflow entered the pallet through the 1.0 m face only. Hence, pseudo-linear airflow occurred through the pallet, parallel to the 1.2 m face. Within the five layers two layers were measured ("B" and "D"). These were considered to be representative of an overall pallet. In the 1.2 m orientation the pallet was rotated 90 degrees and the tarp placed over the 1.0 m lateral side walls. A line of axial symmetry was assumed down the centre of both pallet orientations, in the same arrangement as in Section 4.2.2.

4.4.3.2 Fruit arrangements within modular bulk packs

To ensure that airflow through each MBP was not influenced by differences in fruit stacking pattern kiwifruit were uniformly packed following a cubic centred distribution pattern (Figure 4.12(a)). For kiwifruit MBPs the air flowed over and around the polyliner and not through the stack, like in non-polylined packages. Hence, it was assumed that the polyliner would mitigate the impact that the exact stacking arrangement (i.e. cubic centred or random) had on the overall airflow patterns through a pallet, while eliminating random stacking of the produce as an experimental variable within individual MBPs (i.e. a kiwifruit could potentially block one vent of a MBP in the middle of the pallet when randomly stacked). A total of 100 count 36 kiwifruit (weight range of 93 – 103 g) were separated into four layers and arranged within each box. 30 kiwifruit were in the bottom layer, 20 in the second, 30 in the third and 20 in the top. This stacking arrangement could be replicated in the construction of the numerical model (section 5.3.3).

(a) (b)

Figure 4.12 Kiwifruit packed in a cubic centred distribution (a) excluding and (b) including the Type-T thermocouples to monitor the kiwifruit temperature.

4.4.3.3 Temperature monitoring

Type-T thermocouples were used to monitor the centre temperatures of 12 kiwifruit within each monitored MBP (Figure 4.11(b)). The thermocouple locations were chosen to fully capture the temperature gradients within a MBP. This assumption was tested in the numerical model by comparing the average temperature of the kiwifruit bulk calculated by averaging 12 measurement points against the volume-average temperature of the entire kiwifruit bulk (Appendix A2). In addition, it was assumed that averaging the kiwifruit temperature across each of these locations would give an accurate overall average fruit temperature for the MBP. Prior to insertion of the flexible thermocouple wires a hole was punctured, with a narrow screwdriver, from the kiwifruit surface to centre. The thermocouples were placed as close as possible at the centre of each monitored fruit.

To assist in visualization of the results the kiwifruit stacking were subdivided into individual areas termed, bottom, middle, top, internal and external. This enabled the cooling of kiwifruit as a function of location within the MBP to be studied (Figure

4.13). For MBPs 1 – 4 in the 1.0 m orientation the air entered the MBP through the hand vents located on the external side of the MBP. For MBPs 5 – 7 and MBPs 8 – 10 the refrigerated air was pulled through the end vents and the internal side was defined as the side in contact with MBPs 1 – 4. The external side was located on the outer edge of the pallet. For the 1.2 m wide orientation the refrigerated air entered the MBP through the hand vents of MBPs 5 – 7 and 8 – 10, located on the external side. For MBP 1 the external side was located on the outside of the pallet. For MBP 2 the external side is in contact with MBP 1.

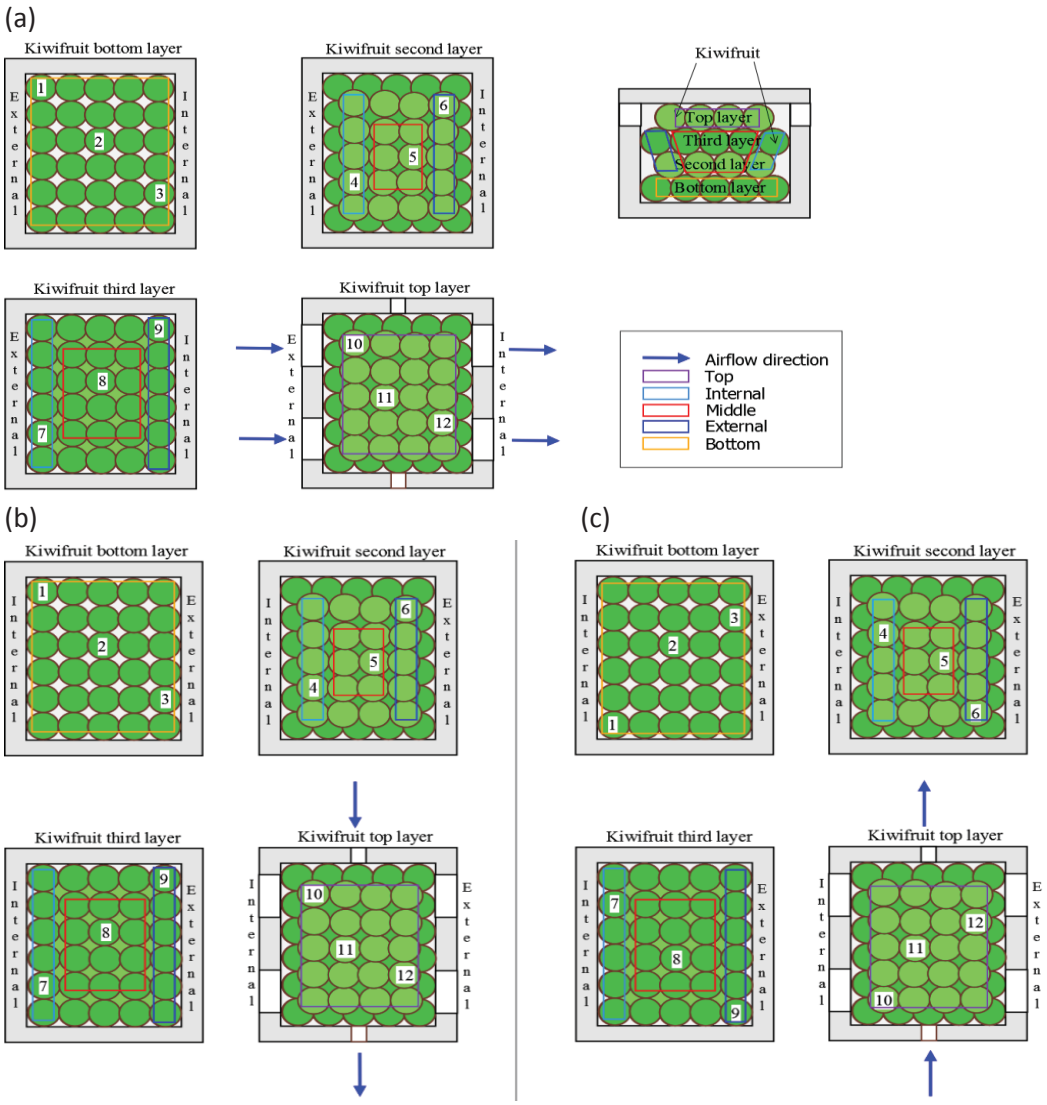

Figure 4.13. Cubic centred distribution and thermocouple location for kiwifruit in (a) MBPs 1 – 4 in the 1.0 m orientation and MBP 5, 6, 8 and 9 in the 1.2 m orientation, (b) MBP 5 – 7 in the 1.0 m orientation and (c) MBPs 1 and 2 in the 1.2 m orientation

The air temperature entering each modular bulk pack was also measured by thermocouples (1 per inlet cardboard box vent for the incoming refrigerated airflow into a MBP), giving a total of 11 air measurement points per monitored pallet layer in the 1.0 m orientation and 10 in the 1.2 m orientation. Temperatures were logged at one-minute intervals by 64-channel dataloggers (1000 Series Squirrel Meter/Logger, Eltek ltd, Cambridge, UK), over the forced-air cooling periods (approximately 8 h).

4.4.3.4 Air velocity and flowrates

Air velocities were recorded by a hot-wire anemometer (Dantec, model 54-N-60). In the 1.0 m orientation air was pulled through the end vents of MBPs 5 and 8 and the hand vents of MBP 1 (Figure 4.14), resulting in two velocity measurements per MBP/MBP replicate (i.e. MBP 5 and 8 were replicates) per pallet layer ("B" and "D"). In the 1.2 m orientation air was pulled through the hand vents of MBPs 5 – 7, giving two velocity measurements per MBP and four per MBP replicate, per pallet layer. For both orientations the velocity measurements were repeated three times.

The air flowrate ($m^3 s^{-1}$) entering through the vents of the MBPs at the front of the pallet was estimated by multiplying the point velocity recorded entering the vent by the vent area. This method assumed no variation in velocity depending on the horizontal or vertical location on the vent face. The total air flowrate entering the pallet through the vents was calculated by multiplying the total air flowrate entering a single pallet layer (i.e. adding the flowrates at each vent orientated to the incoming airflow for the MBPs at the front of the pallet) by 5 (the number of layers in a half-pallet). The flowrate

entering the pallet through the vents was compared to the total volumetric airflow rate pulled through the pallet layer (measured at the orifice plate).

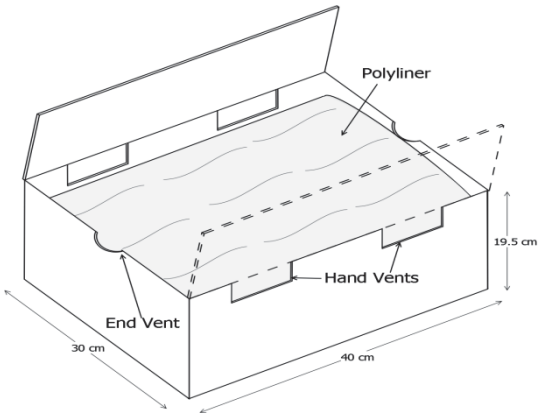

Figure 4.14. Schematic diagram for the cardboard box used in MBPs of kiwifruit.

4.4.4 Experimental set-up

Kiwifruit were stored at 0 °C for approximately 6 weeks following harvest prior to experimentation. Prior to the forced-air cooling experiments the kiwifruit were equilibrated to room temperature (approximately 20 °C), replicating the field heat observed following harvest. The temperature control room was set and maintained at 0 °C, with a relative humidity (RH) of 90 %. On experiment initiation the instrumented pallet was rolled into the room attached to the fan system and the precooling simulation initiated, within 5 minutes of kiwifruit entering the cool environment. For the 1.0 m orientation the VSD fan was set to 1500 rpm, generating an air flowrate through the pallet of 0.59 m^3 s^{-1} (1.1 L kg^{-1} s^{-1}) and pressure drop of 126 Pa across the pallet. In the 1.2 m orientation the VSD fan was set to 1500 rpm, generating an airflow rate through the pallet of 0.68 m^3 s^{-1} (1.3 L kg^{-1} s^{-1}) and a pressure drop of 83 Pa. Air flowrates and pressure drops were also recorded for fan speeds ranging from 900 rpm to 2400 rpm for both pallet orientations.

4.4.5. Moisture loss

The mass change of MBP 5 – 7 for pallet layer "B" in the 1.2 m orientation (Figure 4.10(b)) was recorded in a separate experiment. The same experimental set-up outlined in section 4.4.4 for the 1.2 m orientation was followed. The weighing scales were placed on a small table within the refrigerated room. The scales were inside a large cardboard box to prevent air velocities in the room from affecting the measurements. For mass measurements the MBP was removed from the pallet, placed on the scales and replaced in the pallet within a sixty second timeframe. The mass of MBP 5 was monitored every 21 minutes, starting at 7 minutes after the initiation of forced-air cooling, MBP 6 every 21 minutes, starting after 14 minutes, and MBP 7 every 21 minutes, starting at 21 minutes. These measurement intervals were followed for the first 4 h of cooling. The mass of all three MBPs was also recorded at the end the cooling period (after 20 h).

4.4.6. Data analysis

4.4.6.1 Data normalisation

The fractional unaccomplished temperature change, *Y*, was calculated in the same way as in section 4.2.4. When calculating *Y* for the individual areas in a MBP *Y* was calculated for each kiwifruit temperature recorded in the area and then averaged.

4.4.6.3 Average for an entire pallet layer

For a "fair" comparison of the overall cooling rate differences between an entire pallet layer in both orientations, complete temperatures for the pallet layer must be assumed. Hence, when directly comparing cooling rates between the two pallet orientations the data from MBPs 5 – 7 is assumed to represent the data for MBPs 8 – 10 in the 1.0 m orientation, giving temperatures for a complete pallet layer. In the 1.2 m orientation the data from MBP 5 is copied over to MBP 7, MBPs 1 and 2 to MBPs 3 and 4, and MBP 8 to MBP 10. Hence, the pallet average temperature is calculated from the average of 10 MBPs in both orientations. The rest of the results are presented for the reduced pallet layer.

4.4.6.4 Statistical analysis

Multiple ANOVAs were performed to identify the factors that had a significant impact on the air flowrate, HCT and SECT. The 'General Linear Model' in the statistical software package 'Minitab 16' (Minitab 16 Statistical Software, 2010) was used for the ANOVA calculations, with Tukey's honest significance test used as the mean separation test. Differences were considered to be significant at 95 % confidence ($p < 0.05$). The Lest Significant Difference, LSD, is the minimal difference for two values to be considered significantly different from each other.

4.5 Laboratory experiment results

The HCT was considered to provide more reliable indications of the cooling speed than the SECT. The rate of cooling is driven by the difference between the fruit temperature and the refrigerated air temperature. Hence, as the fruit temperature approaches the refrigerated air temperature (i.e. as $Y \rightarrow 0$) the rate of cooling becomes more influenced by small variations in air temperature. As a result SECT values are more influenced by variability in air delivery temperature around the average than the HCT values. For this reason more weight was given to the HCT over the SECT in the analysis of the results.

In both Tables 4.2 and 4.5 the number of kiwifruit temperature readings (n) are less than the number of thermocouples actually placed. The high number of thermocouples recording kiwifruit temperatures per experiment (264) meant that it was extremely difficult to get correct readings for each data point. Failure of thermocouple readings were due to variety of reasons, the most common occurring when the thermocouples were accidently pulled out of the kiwifruit, during pallet set-up, and subsequently recorded air temperatures. Unfortunately, these incorrect recordings only became apparent either during data analysis or by physical inspection of the thermocouple locations after conclusion of the experiment. For example, in Table 4.2 n was expected to be 24 in the first two data columns. However, due to failure of three thermocouples for one MBP replicate, n was 21. The loss of data due to equipment failure was considered small enough to not influence the overall results and conclusions.

4.5.1 Commercial pallet orientation (1.0 m wide orientation)

4.5.1.1 Air temperature

The refrigerated air warmed up as it was pulled through the pallet. Air temperatures measured inside MBPs 1 and 5 were 3 °C and 1 °C respectively, after 2 h of cooling (Figure 4.15(a)). As the temperature of the air was measured at the inlet vent of the MBPs, after the airflow had been drawn past the vent (see section 4.2.5.1), the discrepancy between MBP 1 and 5 could be explained by differences in the temperature of the fruit and the volumetric flowrates within the MBPs. The air temperature which flowed into MBPs 3, 4 and 7, located at the back of the pallet had warmed up, to a temperature range of 7-9 °C.

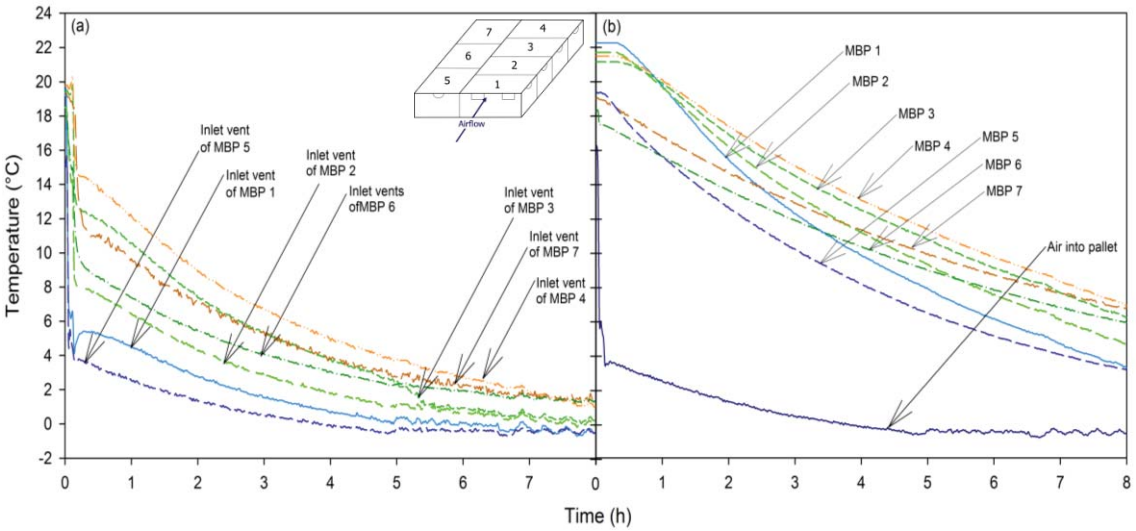

Figure 4.15. Temperatures during forced-air cooling of (a) air pulled past the inlet vent of each MBP in a pallet row and (b) average temperature change of each MBP in pallet row "B" for the 1.0 m orientation.

The rise in temperature of the cooling air as it was pulled through the pallet resulted in slower cooling rates of the MBPs at the back of the pallet (MBPs 3, 4 and 7; Figure 4.15(b)). MBP 1 had a HCT of 3.75 h, while MBPs 3 and 4 had a HCT of 5.49 h and 5.02 h, respectively (Table 4.2). No significant difference in HCT or SECT between MBPs 3 and 4 was observed (Table 4.2), although the air that flowed into MBP 4 was warmer than the air that flowed into MBP 3. The back face of MBP 4 was exposed to the surrounding air allowing for cooling, via conduction, out the back face of the pallet.

Table 4.2. Average HCT and SECT as influenced by box location, subdivision within box and pallet layer for the 1.0 m pallet orientation

MBP	HCT	SECT	Area (MBPs 1-4)	HCT	SECT	Area (MBPs 5-7)	HCT	SECT	Layer	HCT	SECT
1	3.75^{ab}	8.76^{a}	Top	3.54^{a}	8.94^{a}	Top	3.50^{a}	10.34^{a}	B	4.80^{a}	12.30^{a}
2	4.42^{abc}	9.97^{ab}	Middle	6.81^{b}	13.12^{b}	Middle	6.68^{b}	14.64^{a}	D	4.50^{a}	9.75^{b}
3	5.49^{cd}	11.46^{bc}	Bottom	4.15^{a}	9.69^{ab}	Bottom	4.30^{a}	11.85^{a}			
4	5.02^{cd}	11.22^{bc}	Internal	3.75^{a}	8.62^{a}	Internal	3.84^{a}	10.41^{a}			
5	3.45^{a}	8.56^{a}	External	5.00^{a}	11.13^{ab}	External	4.88^{ab}	12.48^{a}			
6	4.80^{bcd}	12.35^{c}									
7	5.61^{d}	14.86^{d}									
p-value	< 0.001	< 0.001		< 0.001	< 0.001		< 0.001	< 0.001		0.152	< 0.001
n	21	21		14	14		11	11		76	76
LSD	1.16	2.14		1.60	3.51		1.89	4.23		0.40	0.73

— Factors that share the same superscript letter in the same column are not significant (p=0.05)

4.5.1.2 FUTC of modular bulk packs within a pallet layer

MBPs 1 and 5 showed the greatest change in FUTC change during cooling, accomplishing 78 % of the total cooling after 8 h (Figure 4.16) with HCTs of approximately 3.6 h (Table 4.2). Both MBPs were directly exposed to the incoming refrigerated airflow and had one side, with surface areas of 8 x 10^{-2} m^2 (MBP 1) and 6 x 10^{-2} m^2 (MBP 5), orientated to this airflow.

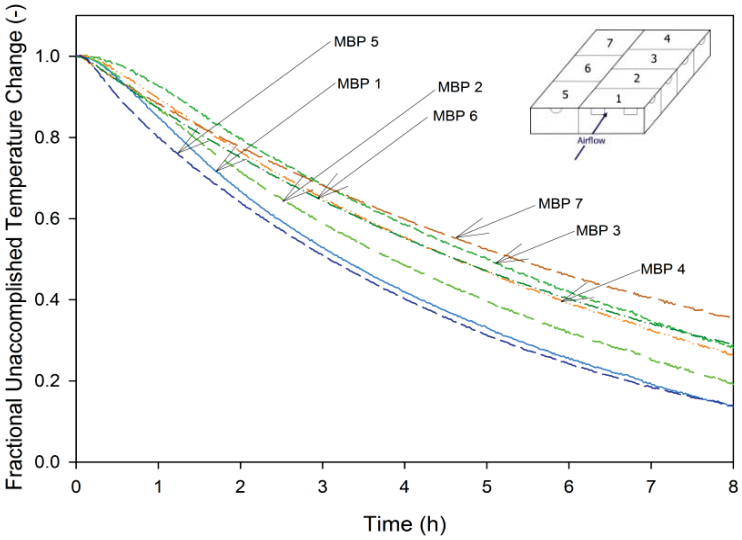

Figure 4.16. Average fractional unaccomplished temperature change, during cooling for each MBP in a pallet row for the 1.0 m orientation

No significant difference in HCT and SECT between MBPs 1 and 5 was observed (Table 4.2). Due to the orientation of MBP 5, the end vent surface area for the air to enter was only 7 x 10^{-4} m^2. The total surface area available for airflow through MBP 1, provided by the two hand vents was almost 7 times larger (48 x 10^{-4} m^2). The relatively small open area of the end vents limited the volume of air that could be pulled through MBP 5. The average velocity recorded through the end vent was 4.84 ± 0.54 m s^{-1} (volumetric flowrate of 3.39 ± 0.38 x 10^{-3} m^3 s^{-1}; Table 4.3). The average velocity recorded through the hand vents of MBP 1 was 2.68 ± 0.10 m s^{-1}. The volumetric flowrate was estimated at 12.84 x 10^{-3} ± 0.50 m^3 s^{-1}, close to a fourfold increase over MBP 5 (Table 4.3). However, higher local velocities were recorded through the end vent of MBP 5 and one side wall was only separated by a tarp from the surrounding room temperature.

Table 4.3. Point velocities (n = 12) and airflow measured at the orifice plate (n = 18) for the 1.0 m pallet orientation at a fan speed of 1500 rpm. Errors are ± 95 % confidence interval.

	1.0 m orientation		
	Velocity (m s^{-1})	**Area (m^2)**	**Airflow (m^3 s^{-1})**
MBP 1, point velocity	2.68 ± 0.10	48 x 10^{-4}	12.84 ± 0.50 x 10^{-3}
MBP 5 and 8, point velocity	4.84 ± 0.54	7 x 10^{-4}	3.39 ± 0.38 x 10^{-3}
Flowrate (sum into MBPs 1, 5 and 8 times five layers)	—	—	0.10 ± 0.01
Flowrate (calculated from Δp at orifice plate)	—	—	0.59 ± 0.02

Ferrua and Singh (2009a) showed that any attempt to increase the amount of airflow through a system, consisting of strawberries packed in clamshells, by varying the vent area, will result in no significant improvement to the rate or uniformity of the forced-air cooling process. Dehghannya et al. (2008, 2011, 2012) concluded that simply increasing the vent area, hence improving the volumetric airflow through the system, will not automatically lessen the cooling time of horticulture produce. Similarly, increasing the volumetric flowrate through each MBP beyond a specific threshold flowrate (at most 3.39 ± 0.60 x 10^{-3} m^3 s^{-1} based on the flowrates measured for this experiment) is unlikely to significantly increase the cooling rate of polylined kiwifruit MBPs.

Kumar et al. (2008) demonstrated that increasing the air velocity significantly increased the surface heat transfer coefficient of oranges and tomatoes during forced-air cooling, in a non-polylined system. There was no significant difference in HCT or SECT between MBP 5 (local air velocities of 4.84 ± 0.16 m s^{-1} pulled past the end vent), and MBP 1 (local velocities of 2.68 ± 0.85 m s^{-1}) suggesting that the air velocity acting against the polyliner did not significantly affect the heat transfer process in the MBPs.

The polyliner provides a barrier to direct contact between the refrigerated airflow and produce. Ngcobo et al. (2012) showed that grapes packed in perforated liners, which allow some contact between the refrigerated airflow and the produce possessed faster HCT than those in non-perforated liners which generate a complete barrier. The polyliner barrier may have reduced the relative influence of convective heat transfer between individual MBPs (i.e. a higher flowrate or higher local velocities through polylined produce were not as influential or had a lower effective threshold limit compared to non-polylined produce). The heat transfer phenomena (both local and overall) were quite complex and can't be simplified to a linear relationship between cooling rate and volumetric flow rate or air velocity through the vents.

The trends observed for MBPs 1 and 5 (similar cooling times regardless of potential air flowrates pulled through the individual MBPs) continued throughout the pallet layer. There was no significant difference in HCT between MBPs 3, 4, 6 and 7 (Table 4.2). MBP 7, unexpectedly, had a significantly longer SECT. The thermocouple wires may have created a partial blockage of the airflow between the aligning end vents of MBPs 5 – 7 in layer "B" of the pallet, with the effect only significantly affecting the air temperatures at the SECT, when the kiwifruit temperature approaches and becomes considerably affected by small differences in air temperature. The high standard deviation for point velocities measured for the end vents between different layers indicate that air velocities were not evenly distributed between the different pallet layers (Table 4.3). Also, as the air was pulled through pallet some proportion may have been pulled vertically down and through the gaps in the pallet base, following under the pallet to the fan. Layer "B", located closer to the pallet base, was more likely to have been affected by this. The lower the amount of cooling air pulled horizontally through

the pallet layer the lower the potential for cooling. Looking at the HCT, which gives a more reliable indication of the cooling profile there was no significant difference between the HCT for the pallet layers, with HCTs of approximately 4.65 h (Table 4.2).

4.5.1.3 FUTC of subdivisions within modular bulk packs

Kiwifruit in bottom of MBP cooled faster than the middle of the MBP, despite being located furthest from the refrigerated airflow entering the box (Figure 4.13(a)). This phenomenon was true for MBPs 1 – 4 and MBPs 5 – 7 in the pallet (Table 4.2). It was likely that the kiwifruit located at the bottom of the MBP were being cooled by the refrigerated air entering the MBP below, through the cardboard packaging. No significant difference in HCT between the top and bottom of the MBPs suggest that the cardboard base of a MBP did not constitute a significant conductive resistance to heat transfer (Table 4.2). These results suggest that as air flowed into the top of the kiwifruit MBPs it simultaneously contributed to cooling of kiwifruit below (the fruit in the MBP) and above (the fruit in the MBP stacked directly above).

There was no significant difference in HCT or SECT between the internal and external sides of the MBPs (Table 4.2). For MBPs 1 – 4 the external side was directly orientated to the incoming refrigerated airflow (Figure 4.13). For MBPs 5 – 7 the external sides are only separated from the refrigerated air in the cool room by a tarp. The fan created enough suction when it was active to pull the tarp directly onto the sides of the pallet, eliminating any observable stagnant air. Hence, a cooling pathway existed between the external sides of the MBPs and the refrigerated air. The internal sides were in contact with MBPs 1 – 4 (Figure 4.13).

Only 17% of the total volumetric airflow pulled through the pallet (measured at the orifice plate) appeared to flow through the openings (i.e. calculated from point velocities measured at the hand and end vents) of the MBP (Table 4.3). Air attempts to follow the path of least resistance. With the highest airflow resistance through the MBP via the narrow headspace created between the polyliner and bottom of the box lid the primary airflow pathways will naturally try to form along alternative routes through and/ or around the pallet.

Air was able to flow underneath the pallet, through the pallet base. With minimal resistance to airflow underneath the pallet, a large percentage of the airflow measured at the orifice plate was likely to have been pulled under the pallet base. A tarp was placed along the sides of the pallet. When the fan was activated the pressure drop pulled the tarp against the sides of the pallet. While air doesn't flow through the tarp there was still the potential for airflow between the tarp and pallet sides. The pressure across the pallet is at its highest (i.e. closest to ambient) at the front and decreases (i.e. increasing the pressure drop) towards the back of the pallet, as it gets closer to the fan. While there may not have been a direct airflow pathway between the tarp and sides of the pallet along the complete pallet length there was the potential for air to flow partway along this gap before being pulled through the pallet as the tarp was pulled tighter against the sides of the pallet, due to the increased pressure drop between the pallet and ambient room pressure. As this airflow enters through the side of the pallet it would not be recorded by the velocity measurements at the inlet vents of MBPs 1, 5 and 8.

Despite efforts to eliminate gaps in the pallet, via cords pulled tight around pallet perimeter (mimicking the set-up in industry) there were still observable horizontal gaps

between the individual MBPs. For the reasons outlined above different information about the air flowrate and pathways present in laboratory experiments, that closely resemble potential airflow pathways in industry, can be obtained from considering the flowrate entering the pallet through the inlet vents at the front of pallet and total flowrate generated by the fan.

The low percentage of air pulled through the vents in the MBPs meant that a substantial proportion of air was flowing through the gaps between the MBPs, likely following pathways of least resistance. For MBPs 5 – 7, the airflow may have provided a heat transfer pathway for the internal sides approximately equal to the heat transfer pathway through the external sides (Table 4.2).

Heat transfer from kiwifruit located in the middle of the MBP, equidistance from all six cardboard box surfaces was primarily conduction with the surrounding kiwifruit and natural convection. This lead to significantly longer HCTs compared to the top, internal and bottom sub-areas, for both MBPs 1 – 4 and MBPs 5 – 7 (Table 4.2).

4.5.2 Alternate pallet orientation (1.2 m orientation)

4.5.2.1 Pressure drop as influenced by pallet orientation

For fan speeds above 900 rpm the pressure drop when the pallet was orientated by the 1.0 m face was higher than the pressure drop when the pallet was orientated by the 1.2 m face (Figure 4.17). The higher pressure drop of the 1.0 m orientation may have been a result of the additional pallet length. In this orientation the refrigerated air passed

through a 1.2 m pallet length compared to the 1.0 m length in the alternative orientation. For the 1.0 m orientation there were six MBPs (5 – 7, and 8 – 10) orientated so that their end vents were exposed to the incoming airflow, compared to four MBPs (1 – 4) in the 1.2 m orientation (Figure 4.18(a)). The end vents created higher entrance losses than the hand vents, due to their smaller area, increasing the pressure drop through the pallet. The 1.0 m orientation also reduced the total vent area per pallet row orientated to the incoming airflow (6.2 x 10^{-3} m^2) compared to the 1.2 m orientation (14.4 x 10^{-3} m^2).

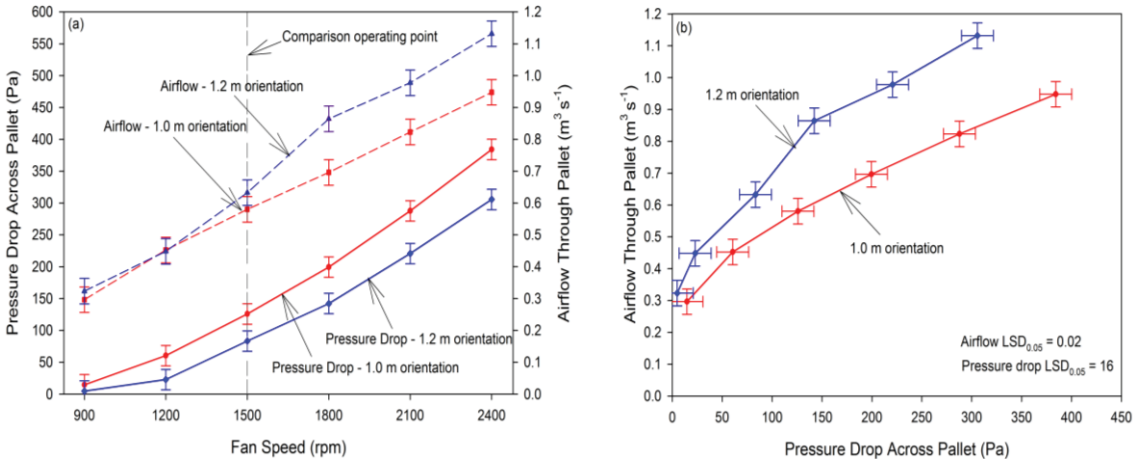

Figure 4.17. Plot of (a) airflow and pressure drop across the pallet as a function of fan speed with LSD bars and (b) airflow as a function of pressure drop for both pallet orientations. Error bars represent $LSD_{0.05}$ (n = 18).

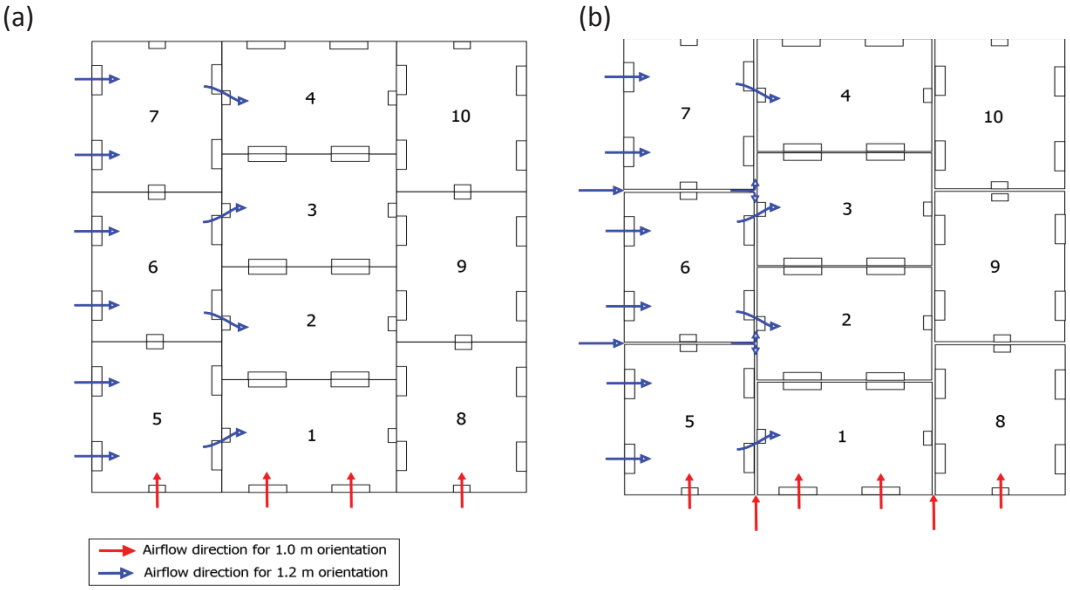

Figure 4.18. Airflow pathways pulled through the pallet (a) without and (b) with gaps between MBPs for both the 1.0 m and 1.2 m orientation

The pressure drop and airflow relationship was further complicated by the probability of gaps between the MBPs for both pallet orientations (Figure 4.18). If each MBP was in direct contact (i.e. no gaps for airflow between individual MBPs) than the airflow through the vents would be expected to be lower in the 1.2 m orientation, due to the high airflow resistance caused by the small airflow pathways between MBPs 5 and 1, and between MBPs 6 and 2 (Figure 4.18(a)). Instead gaps between individual MBPs most likely provided alternative airflow pathways through the pallet layer (Figure 4.18(b)).

The relationship between box vent hole ratio, directly exposed to the refrigerated airflow, and resistance to airflow has been shown in numerous works involving the forced-air cooling of non-polylined horticultural produce (van der Sman, 2002; Vigneault et al., 2006; Delele et al., 2008). In each case the pressure drop was shown to decrease when the area available for airflow was increased. However, for fan speeds ≤ 1500 rpm there was no significant difference in airflow rate pulled through the different pallet orientations (Figure 4.17). This may have been due to the more tortuous airflow pathways present in the 1.2 m orientation compared to the 1.0 m (Figure 4.18).

In the 1.0 m orientation relatively linear airflow pathways existed. The air can be pulled through the connecting vents of MBPs 1 – 4, 5 – 7 and 8 – 10. In the 1.2 m orientation there were limited connecting airflow pathways, via the alignment of vents between individual MBPs (Figure 4.18). Fan speeds ≥ 1800 rpm may have generated enough airflow to overcome this resistance and/or pulled the air through gaps between individual MBPs. This may explain why the airflow through the 1.2 m orientation was only significantly higher when the fan speed is ≥ 1800 rpm (Figure 4.17).

4.5.2.2 Air temperature

Initially for the front and middle rows in the 1.2 m orientation the air temperatures entering the MBPs were relatively cool (Figure 4.19). The air temperatures warmed up by the time they reached the MBPs in the back row (8 and 9), as it mixed with the warm air exiting the preceding MBPs. This was due in part to the complexity of the available airflow pathways promoting airflow mixing (Figure 4.18). Both Ferrua and Singh (2009b) and Meana et al. (2005) demonstrated that as air is pulled through ventilated packages of horticultural products it can either flow through or around the packages but the air entering packages at the back of a pallet will warm up due to air mixing.

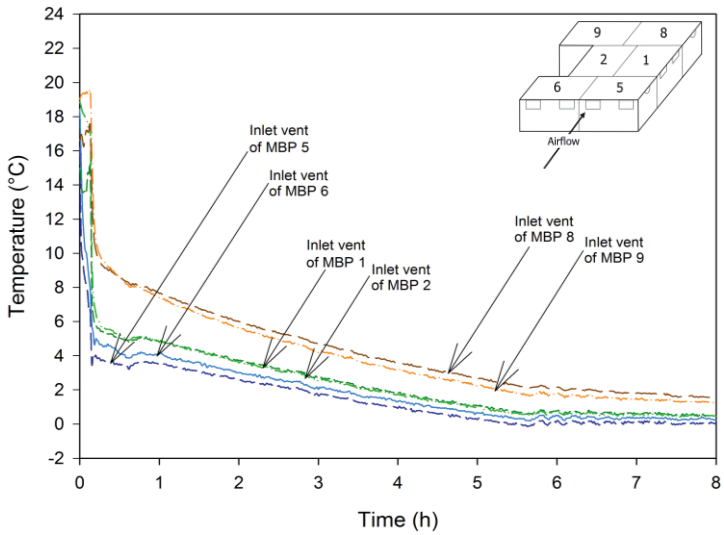

Figure 4.19. Air temperature change at the inlet vent of each MBP in a pallet row during cooling for the 1.2 m orientation

4.5.2.3. FUTC of modular bulk packs between pallet orientations

The total amount of airflow that entered through the vents of the MBPs (5 and 6) at the front of the pallet in the 1.2 m pallet orientation was approximately double that of the MBPs (1 and 2) at the front of the 1.0 m orientation (Table 4.4). The experimental set-

up (i.e. minimal airflow resistance underneath the pallet) was the same as the 1.0 m orientation set-up. Hence, the more complex airflow pathways through gaps between MBPs in the 1.2 m orientation likely provided a higher airflow resistance than the linear airflow pathways between the central and side MBPs in the 1.0 m orientation (Figure 4.18). This may have led to a higher percentage of airflow flowing through the vents of the MBPs at the front of the pallet (which offered a lower resistance to airflow than gaps between individual MBPs) in the 1.2 m orientation.

A comparison of average pallet layer HCT and SECT showed an improvement for the 1.2 m orientation (Table 4.5). However, there was a higher flowrate through the 1.2 m orientation (Table 4.4). More importantly, only ten pallets can be set-up in a tunnel cooler for industrial operations, due to the increased width of the face orientated to the airflow, compared to twelve pallets in the 1.0 m orientation (Figure 4.5). Despite the small improvement in cooling rate for the 1.2 m orientation the reduction in total number of pallets cooled per forced-air cooling operation, make the 1.0 m orientation the better option for industrial tunnel coolers.

Table 4.4. Air velocities for MBPs 1 and 5 (n = 12) in the 1.0 m orientation and for MBPs 5 and 7 (n = 24) and MBP 6 (n = 12) in the 1.2 m orientation and airflow measured at the orifice plate (n = 18) pulled through both pallet orientations for a fan speed of 1500 rpm. Errors are ± 95 % confidence interval.

	1.0 m orientation				1.2 m orientation		
	Velocity ($m\ s^{-1}$)	Area (m^2)	Airflow ($m^3\ s^{-1}$)		Velocity ($m\ s^{-1}$)	Area (m^2)	Airflow ($m^3\ s^{-1}$)
MBP 1, point velocity	2.68 ± 0.10	48×10^{-4}	$12.84 \pm 0.50 \times 10^{-3}$	**MBP 6, point velocity**	2.31 ± 0.16	48×10^{-4}	$11.07 \pm 0.07 \times 10^{-3}$
MBP 5 and 8, point velocity	4.84 ± 0.54	7×10^{-4}	$3.39 \pm 0.38 \times 10^{-3}$	**MBP 5 and 7, point velocity**	3.35 ± 0.33	48×10^{-4}	$16.08 \pm 0.16 \times 10^{-3}$
Flowrate (sum into MBPs 1, 5 and 8 times five layers)	—	—	0.10 ± 0.01	**Flowrate (sum into MBPs 1, 5 and 8 times five layers)**	—	—	0.22 ± 0.01
Flowrate (calculated from Δp at orifice plate)	—	—	0.59 ± 0.02	**Flowrate (calculated from Δp at orifice plate)**	—	—	0.68 ± 0.02

Table 4.5. Average HCT and SECT as influenced pallet orientation.

Orientation	HCT	SECT
1.0 m	4.54[b]	11.17[b]
1.2 m	4.12[a]	10.05[a]
p-value	< 0.05	< 0.05
n	208	208
LSD	0.34	0.68

— Factors that share the same superscript letter in the same column are not significant (p=0.05)

4.5.2.4. FUTC of modular bulk packs within both pallet orientations

For comparison purposes, in the 1.0 m orientation MBPs 1 and 5 are at the front of the pallet, MBPs 2, 3 and 6 at the centre and MBPs 4 and 7 at the back. In the 1.2 m orientation MBPs 5 and 6 are at the front, MBPs 1 and 2 at the centre and MBPs 8 and 9 at the back of the pallet. The FUTC profiles for both orientations are shown in Figure 4.20.

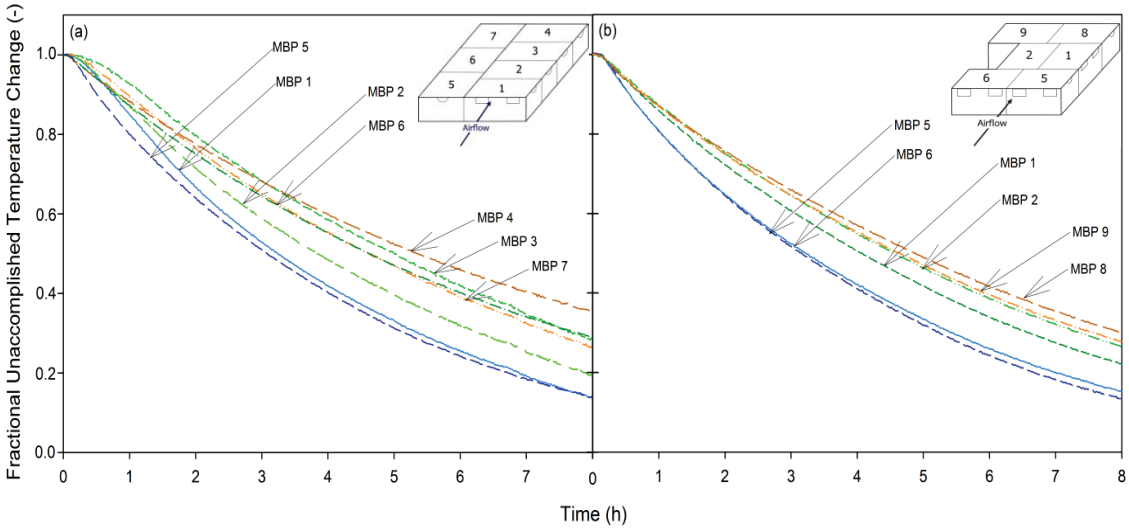

Figure 4.20. Average fractional unaccomplished temperature change, during cooling for each box in a pallet row for the (a) 1.0 m orientation (same data presented in Figure 4.13) and (b) for the 1.2 m orientation.

In the 1.2 m orientation MBPs at the centre of the pallet did not have significantly faster HCT than the MBPs at the front or back. In the 1.0 m orientation the centrally located MBPs had significantly longer HCT than those at the front of the pallet, 4.90 h

compared to 3.61 h (Table 4.6). The lack of significant difference in HCT between the front and centre MBPs in the 1.2 m orientation was likely due to relatively cool air temperatures flowing into the MBPs (Figure 4.19). However, this air warmed up by the time it flowed into the MBPs at the back of the pallet resulting in no significant difference in HCT between the MBPs at the back of the pallet due to pallet orientation (Table 4.6). The likely explanations for the significant difference in SECT between pallet layers "B" and "D" are the same as those discussed in section 4.5.1.2.

Table 4.6. Average HCT and SECT as influenced by general box location in each pallet orientation, pallet layer and pallet orientations for both pallet orientations.

Orientation & Box Location	HCT	SECT	Layer	HCT	SECT
1.0 m, Front	3.61^{a}	8.68^{a}	B	4.48^{a}	11.44^{a}
1.0 m, Centre	4.90^{bc}	11.24^{bc}	D	4.33^{a}	9.72^{b}
1.0 m, Back	5.32^{c}	13.06^{d}			
1.2 m, Front	3.50^{a}	8.50^{a}			
1.2 m, Centre	4.21^{ab}	9.92^{ab}			
1.2 m, Back	4.90^{bc}	12.05^{cd}			
p-value	< 0.001	< 0.001		0.3	< 0.001
n	39	39		139	139
LSD	0.79	1.58		0.29	0.59

— Factors that share the same letter in the same column are not significant (p=0.05)

4.5.3 Moisture loss

The overall mass of the MBPs increased by approximately 5 – 9 g (0.048 – 0.086 % of the fresh fruit weight) during forced-air cooling (Figure 4.21). This is in direct contradiction to the assumption of moisture loss. The relatively small changes in mass may have been effected by air velocities in the room interfering with the measurements, despite the presence of the enclosure for the measurement scales. However, the same trend was observed in all three MBPs. The mass of the MBPs increased until approximately 3.5 h before "levelling off" and eventually decreased slightly by the end of cooling. Prior to the experiment the MBPs were equilibrated to the ambient

conditions in the laboratory. The temperature in the laboratory was approximately 20 °C and RH would have been approximately 40 % - 60 % for that time of year. The TCR was kept at 90 % RH. Hence, the cardboard in the MBPs may have absorbed some moisture from the airflow in the room at the start of the experiment, leading to a net gain in moisture for the MBPs. The moisture content of corrugated cardboard boxes can increase from 8.1 % (dry basis (db)) at ambient testing conditions to 20 % (db) in horticultural cool stores (Nevins, 2008). After 3.5 h there was a net reduction in mass as either the rate of moisture loss exceeded the rate of moisture absorption or the corrugated cardboard reached its maximum moisture content. However, this net moisture loss was only 1 – 4 g, depending on the MBP.

The small quantities of moisture loss recorded can be considered reasonable. Wiley et al. (1999) recorded moisture loss at 0.7 % of fresh fruit weight after 18 weeks of storage, for non-perforated liners in kiwifruit MBPs. While the experiments failed to quantify the exact amount of moisture loss from the fruit, the small amount observed by the experiment and the minute quantities reported in published work during kiwifruit storage, means that the effect of moisture loss on the cooling rate can be assumed negligible.

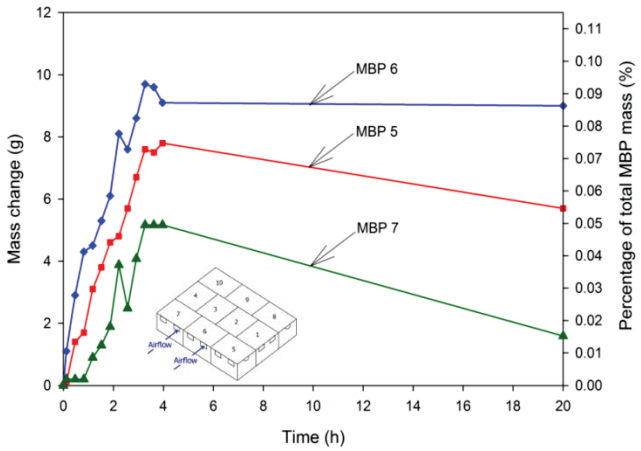

Figure 4.21. Mass change of MBPs 5 – 7 in the 1.2 m pallet orientation during forced-air cooling

4.6. Laboratory experiments conclusions

4.6.1 Heat transfer mechanisms

Significant temperature gradients existed within MBPs during forced-air cooling. Kiwifruit located in the middle of the MBPs cooled significantly slower than all other areas (top, bottom, external and internal side of the pack). The lack of significant difference between the top and the bottom of the MBP appears to indicate a substantial cooling pathway provided by air flowing through the MBP stacked directly below, with cooling via conduction across the cardboard base.

For both pallet orientations the cooling rate of polylined kiwifruit was a function of the location of the MBP within the pallet layer. Kiwifruit in the front of the pallet cooled the fastest. The air warmed up as it was pulled through the pallet. Hence, the further away from the entering airflow the MBPs were located, the lower the cooling rate.

4.6.2 Informing numerical model development

It is difficult to replicate the heat transfer occurring through the external walls without calculating experimental heat transfer coefficients, which would be specific to a certain package design. Ideally the boundary conditions in the numerical model will not require experimental inputs as this will limit the potential for numerically assessing alternative package designs.

The experiment to calculate the mass change of the MBPs during forced-air cooling failed to quantify the impact of moisture loss on the cooling process. However, the experiment did show a lack of significant mass change. Minute quantities of moisture loss have been reported in published work involving polylined kiwifruit. The high probability (informed from experiments and literature) of minute quantities of moisture transferred during forced-air cooling was considered sufficient evidence to assume moisture loss and/ or transfer as negligible in this project.

These experiments (both industry and laboratory), performed near the start (chronologically) of this project, gave an early insight into the complex transport phenomena occurring during the forced-air cooling of polylined horticultural produce. The experiments provided extremely valuable information into the cooling profiles within the pallet. However, the uncontrolled variables (gaps between MBPs, airflow under pallet, heat flow through tarp, etc. …) make it difficult to clearly identify the relative influence of the heat transfer mechanisms occurring. For example, no relationship could be established between cooling rate and flowrate, or velocity, into the MBPs. A numerical model, validated against well controlled experiments, can quantify the exact airflow and heat transfer rates throughout the pallet and how they impact the cooling performance. A combination of experimental and numerical information can then be used to improve cooling performance, whether by optimising the operating conditions (i.e. flowrate and pressure drop) and/ or designing a new MBP.

Chapter 5

Numerical model development

5.1. Introduction

Numerical models can be used to simulate the forced-air cooling process of horticultural produce. These models can be used to investigate the effect of changes to operating conditions and package design on the performance of the process, such as the effect of altering the size and location of vents in horticultural produce packing on the cooling rate and uniformity, without having to conduct experimental trails (Dehghannya et al., 2008, 2011, 2012; Delele et al., 2008; Ferrua & Singh, 2009a; van der Sman, 2002).

Compared to numerical models of forced-air cooling of non-polylined horticultural produce the relative contribution of the various heat transfer mechanisms (forced and natural convection, conduction, radiation and heat of respiration) is likely to be different for polylined produce. Hence, it can be dangerous to base the inclusion/ exclusion of the various heat transfer mechanisms solely on published numerical models in literature. However, including all the mechanisms could make the numerical model too complex to solve with modest computing resources. Therefore, the significance of each of the mechanisms must be investigated analytically to determine possible simplification of the model without compromising on accuracy.

*Material from this chapter is included in the conference paper: O'Sullivan, J.L., Ferrua, M.J., Love, R.J., Verboven, P., Nicolaï, B.M., & East, A.R. (2013b). *Mathematical modelling of kiwifruit packaging undergoing forced-air cooling*. Paper presented at the 26th Symposium on Packaging, Espoo, Finland.

5.2. Objectives

This chapter aims to develop a suitable mathematical model that simulates the forced-air cooling of a pallet of polylined kiwifruit modular bulk packs (MBPs). To achieve this goal the following objectives were;

1) To create the geometrical model of the shape and packaging structure of kiwifruit in a MBP.
2) To build a numerical model of a pallet layer (10 MBPs).
3) Determine the required heat transfer mechanisms to be considered by the model.

5.2.1 Software package

The numerical model was developed using the ANSYS v.15 software package, which uses the finite volume scheme to directly solve transport phenomenon via iterative processes. For this project “Design Modeler” was used to create the geometrical model, “Meshing” to mesh or divide the system into minute elements and “Fluent” to solve the relevant transport phenomenon.

5.3 Geometrical model

The packaging structure to be reproduced in the MBP consists of kiwifruit, wrapped in a polyliner and placed in a cardboard box. The numerical MBP construction is discussed in the following sub-sections.

5.3.1. Kiwifruit physical model

Zespri International provided three 2D images of the kiwifruit dimensions, within the average weight range (93 – 103 g; count 36). These images gave the external dimensions through the centre of the kiwifruit, for the raised view (cut horizontally through the centre lengthwise), flat view (cut vertically through the centre lengthwise) and end view (cut vertically through the center widthwise) of Hayward green kiwifruit. The 2D images were converted to Cartesian coordinates, with the raised view representing the xy-plane, the flat view the xz-plane and the end view the yz-plane.

For the raised view the values along the y-axis corresponding to specific points on the x-axis were noted. In ANSYS, geometries can be drawn in the geometry editor (DesignModeler, 2010). Using this tool the line coordinates for the raised view of a kiwifruit on the xy-plane were read into DesignModeler (Figure 5.1). This creates a 2D image of the kiwifruit. The image was comprised of 20 individual segments.

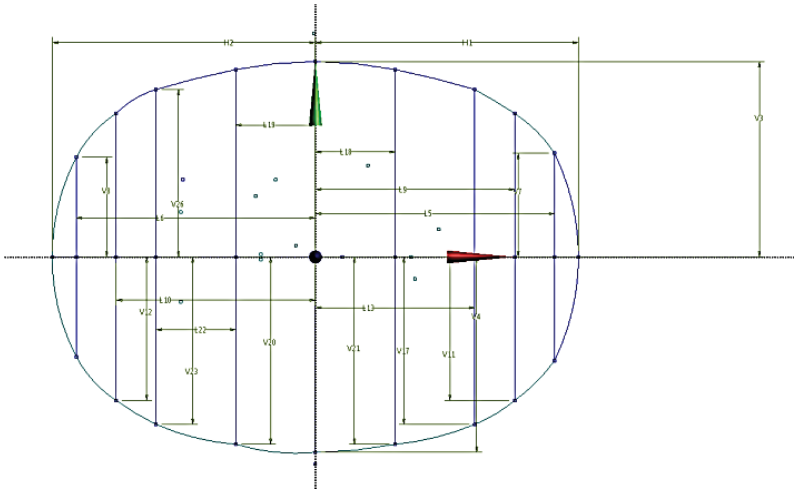

Figure 5.1. The raised view of Hayward green kiwifruit drawn along the xy-axis in Design Modeler.

Applying the same method recreates the flat view, implemented on the xz-plane (Figure 5.2(a)). Connecting the xy- and xz-planes forms an outline of the three-dimensional kiwifruit, consisting of 40 individual segments (Figure 5.2(b)).

(a) (b)

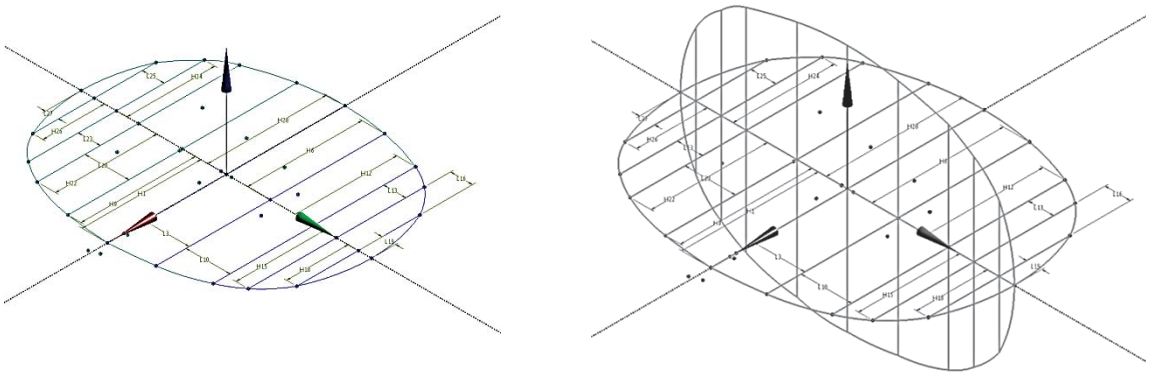

Figure 5.2. The (a) flat view of Hayward green kiwifruit along the xz-plane in DesignModeler and (b) 3D outline of the kiwifruit.

The 3D image was completed with coordinates from the end view (yz-plane). The area for each external segment was converted to a surface (Figure 5.3). The separate surfaces were joined together, completing the construction of a geometrical model of the kiwifruit (Figure 5.3). Each kiwifruit model has a total surface area and volume of 103.1 x 10^{-4} m^2 and 95.8 x 10^{-6} m^3, respectively. Multiplying the numerical volume by the kiwifruit density (1037 $kg.m^{-3}$; determined in section 6.3.2) yields a mass of 99.3 g, which is in the centre of the count 36 weight range.

(a) (b)

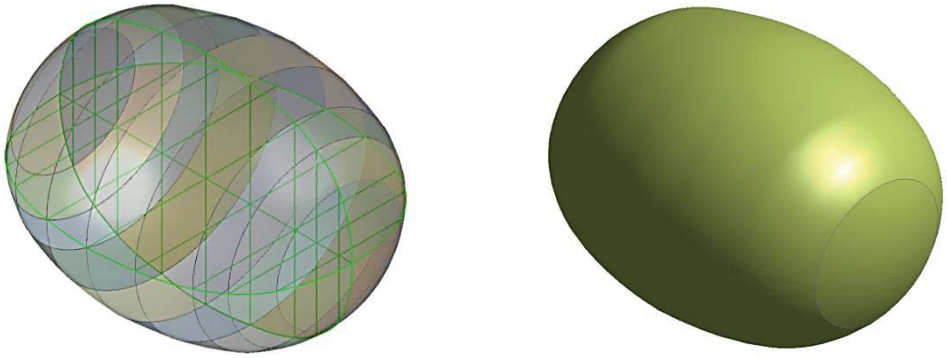

Figure 5.3. Completed construction of an anatomically correct 3D Hayward green kiwifruit, formed by joining the individual surfaces together.

5.3.2 Cardboard box

The cardboard box was constructed with the same external (40 x 30 x 19.5 cm) and internal (38.4 x 29.2. x 18.7 cm) dimensions as the physical construct (Figure 5.4). The cardboard thickness was 0.4 cm, for the top, bottom, front and back of the box. The front and back of the box refer to the walls where the hand vents are located. The cardboard overlapped at the ends of the box, for a thickness of 0.8 cm on each of the end box walls.

Some simplification was made to the box, reducing the complex geometry. The hemispherical end vents were replaced with rectangular vents that had the same effective area (Figure 5.4). The top and base of the cardboard box both had a thickness of 4 mm. The area directly above the end vents created by the gap between the cardboard lids was included in the effective area of the rectangular end vents.

When kiwifruit MBPs are stacked in a pallet the refrigerated air that enters through the vents cools not only the kiwifruit in the MBP but also the kiwifruit in MBP directly above, through conduction across the base of the cardboard box (section 4.5.1). To

simulate this phenomenon a periodic boundary condition to link heat transfer from the top of the box to the bottom of the box was required. However, the CFD solver software used (Fluent) cannot simulate a periodic boundary condition between a fluid (air in the gap between the cardboard lid) and a solid (cardboard base). Hence, the gap in the cardboard lid was not included. Instead the top of the cardboard was assumed to be one homogeneous solid. This simplification is unlikely to cause unrealistic airflow and heat transfer patterns as when MBP are stacked on top of each other there are no air gaps through the box lid (excluding the MBP at the top of the pallet which has a tarp placed over it). The top and bottom of the MBP, both modelled as a continuous solid (cardboard), were linked by the periodic boundary condition in the numerical set-up (section 5.6.2).

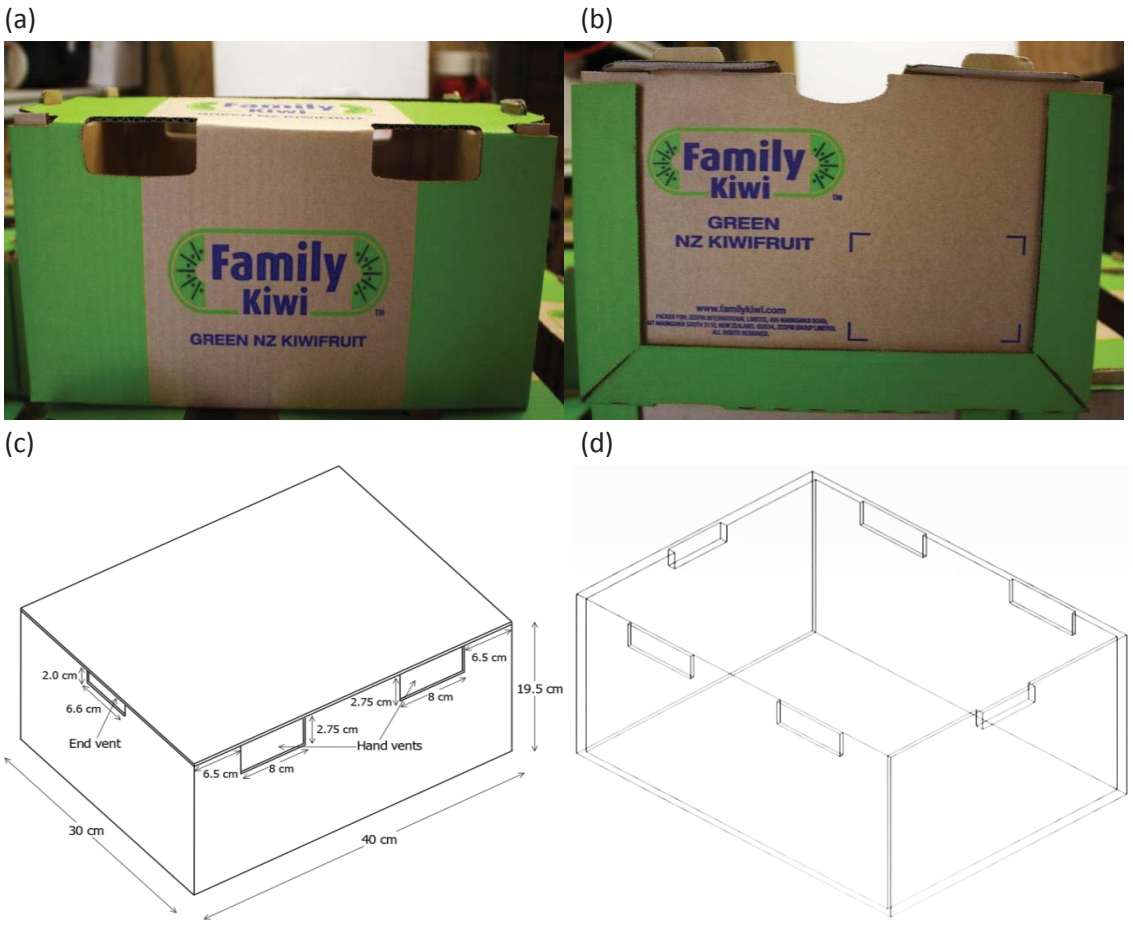

Figure 5.4. Image of (a) photo of front view (b) photo of end view (c) simplified geometry schematic diagram and (d) the numerical model construction of the cardboard box.

5.3.3 Modular bulk pack

There are approximately 100 kiwifruit (count 36 size) in each MBP. In the numerical model the kiwifruit were arranged in four layers within each box, following the stacking arrangement used in the laboratory experiments (30 in the bottom, 20 in the second, 30 in the third and 20 in the top layer; section 4.4.3). This stacking arrangement could be replicated in the experimental validation of the numerical model (section 7.2.2) and eliminated random stacking as a variable between experimental and numerical set-ups of the kiwifruit MBPs. Single contact points between individual produce can create an unstable and distorted mesh, which can negatively impact upon the solution accuracy and stability (Ferrua & Singh, 2009a). To promote the mesh integrity each individual kiwifruit was placed slightly apart (~ 2 mm) from each other, and the box walls where applicable, in the bottom layer (Figure 5.5). 2 mm was found to be the minimum distance (determined through trial and error) that could be used before instabilities began to appear in the numerical simulation. The same distance (~ 2 mm) was maintained between the kiwifruit in the bottom and second layer. While the horizontal distance between kiwifruit varied in the second layer (as the arrangement was determined by the spacing in the bottom layer) a minimum distance of 2 mm was enforced (Figure 5.6). The arrangement for the bottom and second layer was repeated for the third and top layer. The minimum height between the highest point of the kiwifruit curvature in the top layer and bottom of the cardboard lid was 4 mm. The 100 kiwifruit had a combined surface area and volume of 103.1×10^{-2} m^2 and 95.8×10^{-4} m^3, respectively.

(a) (b)

Figure 5.5. Image of (a) photo and (b) the numerical model construction of the bottom layer of count 36 kiwifruit in the modular bulk pack.

(a) (b)

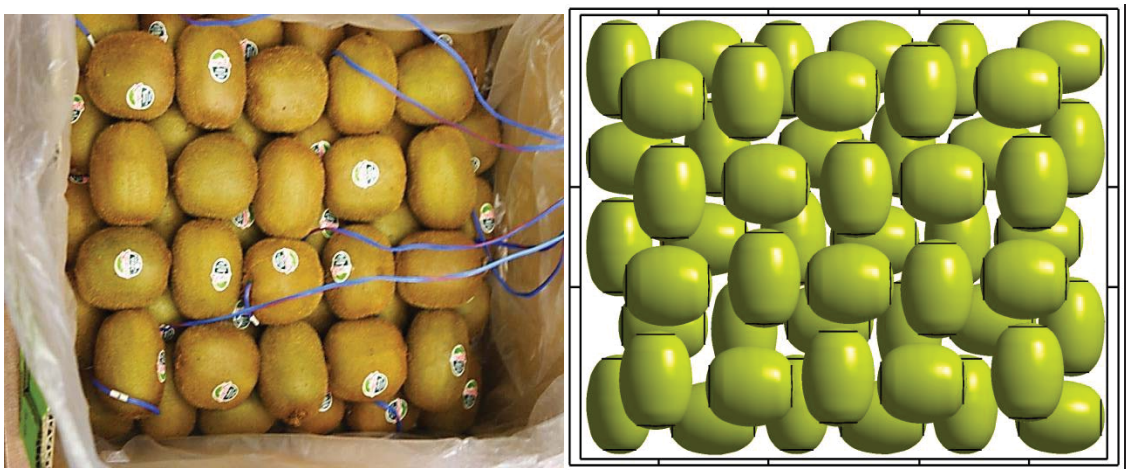

Figure 5.6. Image of (a) photo and (b) the numerical model construction of the bottom and second layer of count 36 kiwifruit in the modular bulk pack.

The kiwifruit was encased in a polyliner. The material in the polyliner was high density polyethylene with a thickness of 10 μm. In essence the polyliner is a plastic barrier which wraps around and moulds onto the shape of the external kiwifruit.

Although it is preferable to avoid excessive contact points, placing the kiwifruit slightly apart from the polyliner would create an insulation layer of air, with the associated thermal properties (i.e. extremely low thermal conductivity). This would reduce the heat transfer between the kiwifruit, through the polyliner to the refrigerated air flowing

through the MBP and simulate an unrealistic heat transfer process. Hence, the polyliner was placed in direct contact with the each external kiwifruit (to a depth of 5 mm) that were in contact with the kiwifruit in reality (every kiwifruit in the top layer, and the edge kiwifruit in the bottom, second and third layers; Figure 5.7). A depth < 5 mm introduced instabilities (non-converging residuals) to the numerical simulation. Any depth > 5 mm qualitatively appeared to be unrepresentative of reality. If the amount of contact was increased, for example by 40 % the cooling profiles would change slightly, by initially experiencing faster cooling, but ultimately retain the similar cooling times (Appendix A1). In the numerical model set-up the kiwifruit surfaces outside of the polyliner were prescribed the properties of the polyliner. This simulated the heat transfer from kiwifruit, through the polyliner to the refrigerated airflow. Hence, an effective polyliner surface, combining the polyliner surface and external kiwifruit surfaces, was created. To reduce the complexity of the mesh the polyliner was modelled as a series of rectangles.

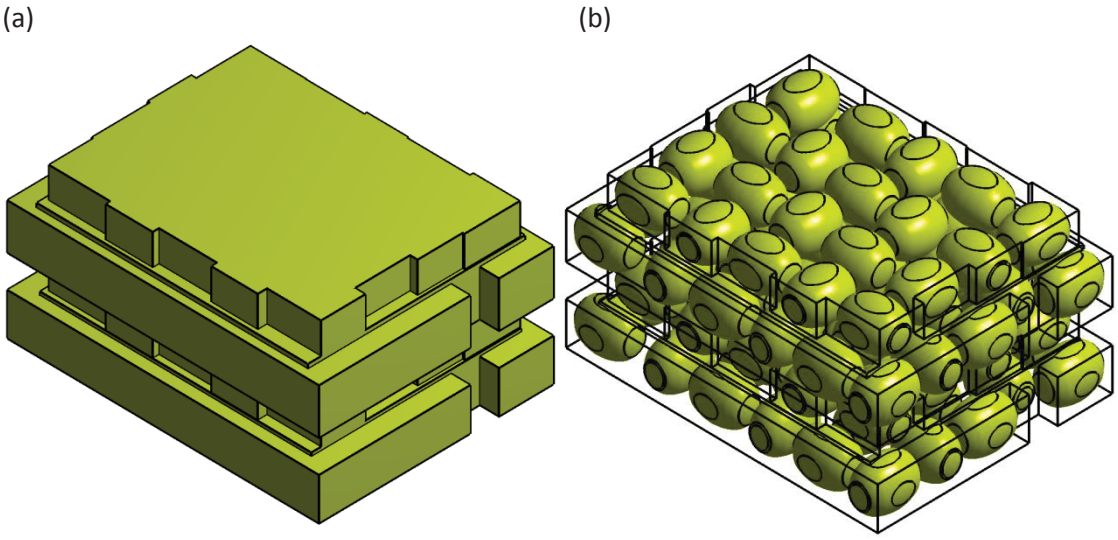

Figure 5.7. Image of (a) independent polyliner shape and (b) effective polyliner surface and kiwifruit bulk.

The extremely narrow thickness of the polyliner (10 μm) was expected to only provide a physical barrier to airflow but not thermal barrier to heat transfer. Hence, the polyliner thickness was not included in the numerical model. This assumption was tested in Appendix A1.

To prevent the simulation of an unrealistic airflow pathway between the bottom of the polyliner bag and the cardboard box, the polyliner was in direct contact with cardboard base (Figure 5.8). The effective polyliner surface intersects the base of the cardboard base to a depth ~ 1 mm, where the kiwifruit extrude through the polyliner. 1 mm was the minimum depth possible (determined through trial and error) that could be used before instabilities started to appear in the numerical simulation.

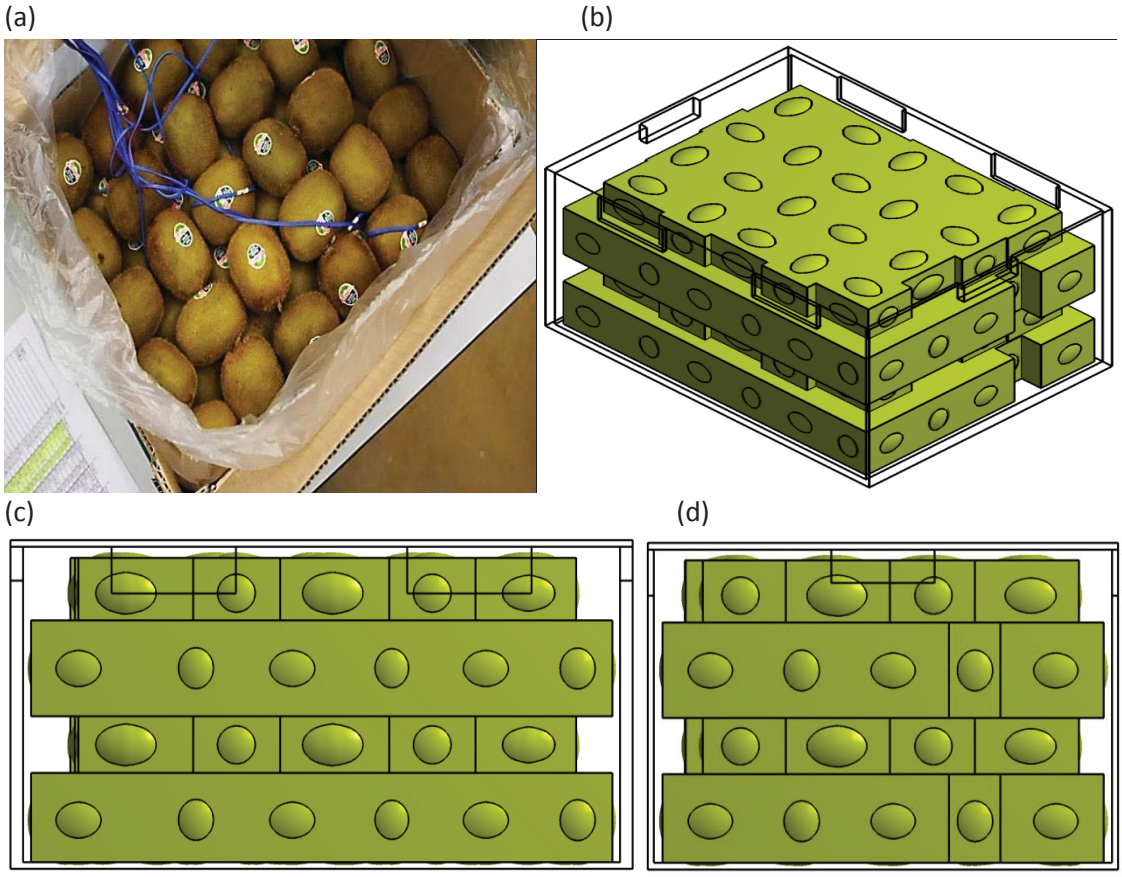

Figure 5.8. Image of (a) photo of a Hayward green kiwifruit modular bulk pack alongside (b) isometric (c) long-side and (d) short-side view of the numerical model construction containing 100 fruit, the effective polyliner surface and the cardboard box.

5.4 Pallet footprint

The single MBP was expanded to a pallet layer, with MBPs 5 – 7 and 8 – 10 rotated 90° to reproduce the pallet footprint (Figure 5.9) observed in industrial applications (section 4.2.2). The MBPs were assumed to fit perfectly together with no space between MBPs. Refrigerated air was pulled through the 1.0 m pallet face. To prevent the inlet and outlet boundary conditions from influencing the airflow near the MBPs the inlet boundary was located 100 cm upstream of the MBP and the outlet boundary 150 cm downstream of the MBP (Figure 5.10). 150 cm was chosen as this provided an adequate distance for the fluid to return to a stable profile after exiting the pallet (Appendix A1).

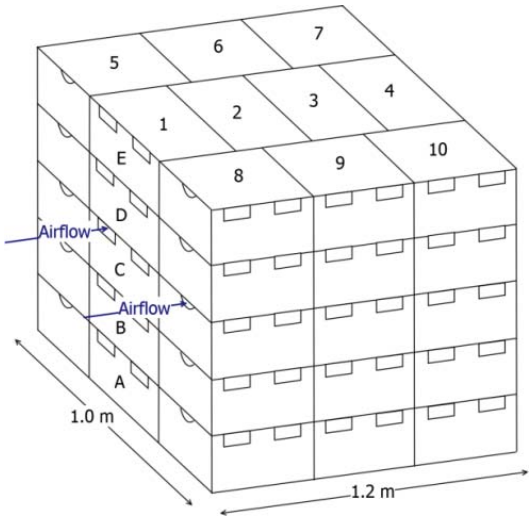

Figure 5.9. Half-pallet layout with layers "A"-"E" and MBPs 1 – 10. Refrigerated air is pulled through the 1.0 m pallet face during forced-air cooling.

(a)

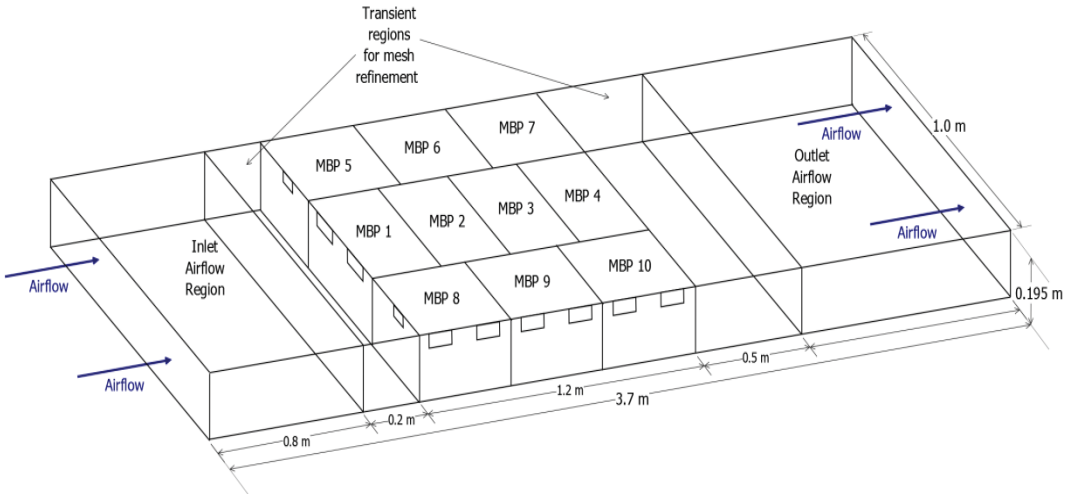

(b)

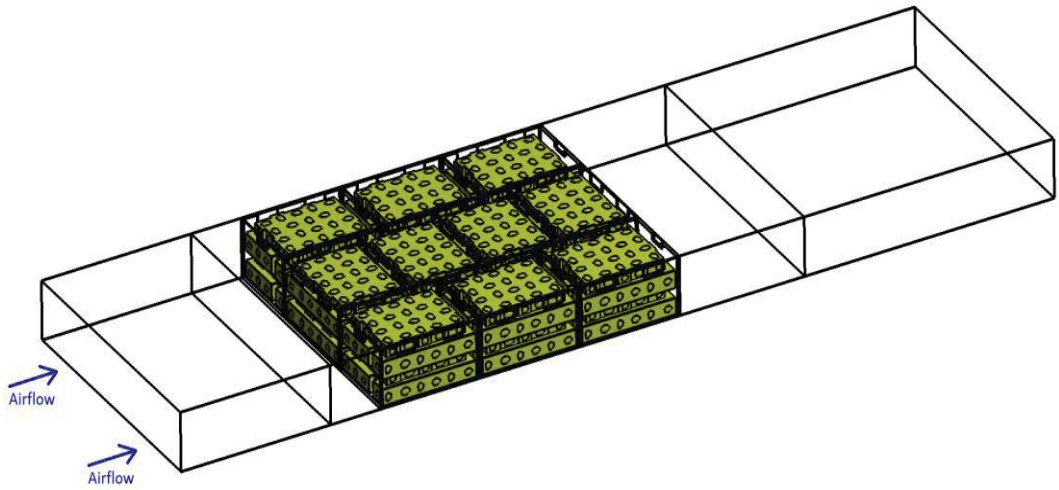

Figure 5.10. (a) 3D schematic diagram and (b) numerical construct of the computational pallet layer for the forced-air cooling of a single pallet layer, when air is pulled through 1.0 m pallet face.

5.4.1 Mesh generation

Unless otherwise stated the default settings were used. The mesh was generated using the CFD physics and Fluent solver preference. The coarse span angle centre, with the default angle of 70 degrees, was used. The maximum size on any individual face was limited to 7.5 mm and the local minimum size was kept at the default value (1.81 mm). The growth rate or expansion ratio between cells was kept at 1.2, below the maximum of 1.3 recommended in Franke et al. (2007). This expansion ratio was found to produce

a stable numerical solution without drastically increasing the grid size. The maximum face size and expansion ratio ensured that the mesh in the likely turbulent flow regime (airflow between the box lid and the polyliner) was properly refined (Figure 5.11). The total number of elements was 7.4 $x10^6$, with 1.9 $x10^6$ nodes. The grid had an average element quality of 0.83 and average orthogonal quality 0.85, with a minimum orthogonal quality of 0.026. The element quality ranges between 0 (which indicates an element with zero or negative volume) and 1 (which indicates a perfect cube; (Meshing, 2010)). The higher the value of the element quality the faster the mesh is likely to produce a converged solution. The range for orthogonal quality is 0 (worst) – 1 (best). If the minimal orthogonal quality is below 0.01 then the mesh is highly skewed and distorted and it is unlikely to produce stable and converging solutions.

The spatial discretization error was calculated from the Richardson extrapolation at 1.1 % (Appendix A1). The Richardson extrapolation for spatial discretisation quantifies the error of a specified variable by extrapolating the exact solution from a series of solutions that get more accurate (i.e. exhibit asymptotic converge) as the number of elements used in the mesh increase. A detailed explanation and derivation of the Richardson extrapolation for both mesh size and time step can be found in Appendix A1.

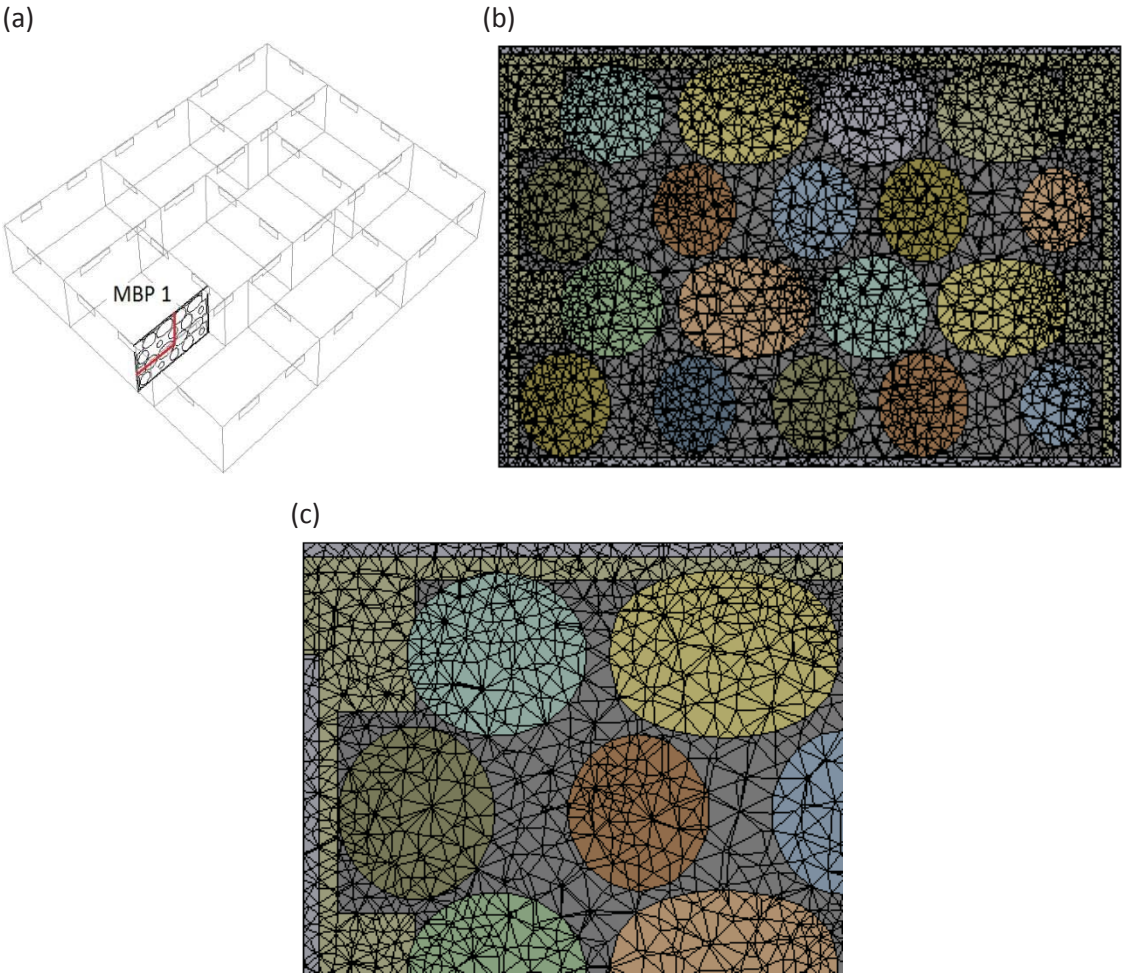

Figure 5.11. (a) Location of cross-sectional area for MBP 1 and ¼ view of MBP 1; computational grid of (b) MBP 1 and (c) ¼ view of MBP 1.

5.5. Transport phenomenon during forced-air cooling

The precooling process of polylined horticultural produce involves a number of transport phenomena. Fluid flow can be either laminar or turbulent. Heat transfer mechanisms include: forced convection (between the refrigerated airflow and the box/polyliner), natural convection (inside the polyliner between the air and the polyliner/kiwifruit), conduction (between the cardboard/polyliner/kiwifruit and cardboard/polyliner/kiwifruit) and radiation (between the cardboard/polyliner/kiwifruit and cardboard/polyliner/kiwifruit), respiration heat generation and latent heat of evaporation and condensation due to moisture transfer and/or loss.

Using information from laboratory experiments into the transport phenomenon occurring during forced-air cooling (section 4.5) a numerical model that includes the heat transfer mechanisms outside (Figure 5.12) and inside (Figure 5.13) the polyliner was developed.

Outside the polyliner, forced convection occurs between the cardboard/polyliner surface and the refrigerated airflow (Figure 5.12). Conduction occurs across and within the cardboard walls, including conduction between MBPs vertically stacked. Conduction also occurs between the cardboard base and effective polyliner surface.

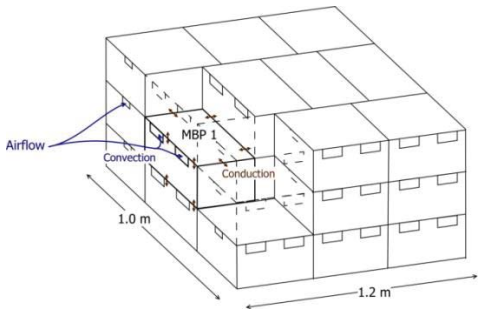

Figure 5.12. The primary external heat transfer mechanisms for MBP 1 during forced-air cooling.

Natural convection occurs inside the polyliner (Figure 5.13). The heat transfer process within the polyliner may also be affected by radiation, the respiratory heat generation by the fruit and the latent heat of evaporation from the fruit surface (absorbing heat – increasing cooling rate) and condensation on cool surfaces (releasing heat - reducing cooling rate) due to moisture transfer.

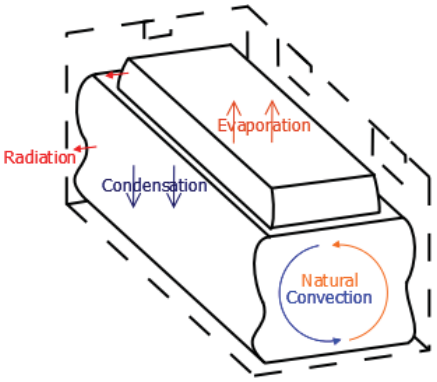

Figure 5.13. Some of the internal heat transfer mechanisms for a MBP of polylined kiwifruit during forced-air cooling, where the primary airflow direction is perpendicular to the hand vents.

5.5.1 Flow regimes in the numerical model

The Reynolds number for the refrigerated air pulled through the pallet was estimated to determine whether the flow should be considered laminar or turbulent. The minimal flowrate per mass of fruit used in experimental validation of the numerical model was 0.34 L kg^{-1} s^{-1} (section 7.2.2). Converting to flowrate pulled through the single layer of the numerical model yields 0.034 m^3 s^{-1}. The total open area, A, (7.0 x10^{-3} m^{-2}) orientated towards the incoming airflow pulled through the pallet was calculated from two hand vents (MBP 1) and two end vents (one each for MBP 5 and 8). The associated total open area perimeter was 0.774 m. The hydraulic diameter, D_H = 4A/Perimeter, was 0.143 m. Hence the Reynolds number (Holman, 2010) was calculated for air at 0 °C, using the air properties for viscosity, μ (kg m^{-1} s^{-1}), and density, ρ (kg m^{-3}), defined in section 6.4, as

$$Re = \frac{\rho Q D_H}{\mu A} = \frac{(1.293)(0.034)(0.143)}{(1.73 \times 10^{-5})(7.0 \times 10^{-3})} = 51323 \quad (5.1)$$

Alternatively the Reynolds number can be calculated for the airflow through the headspace in the MBPs. The height between the polyliner and the bottom of the cardboard lid (not including the protrusions in the polyliner caused by the kiwifruit) was 9 mm. If a height of 9 mm is assumed constant everywhere in the MBP (i.e. not accounting for the change in height of the polyliner near the box walls as it follows the shape of the kiwifruit bulk) and using the internal length (0.384 m) and width (0.292 m) of the box the cross-sectional area of the headspace perpendicular to the airflow is 3.5 $x10^{-3}$ m^2 for MBP 1 and 2.6 $x10^{-3}$ m^2 for MBPs 5 and 8. The overall hydraulic diameter is calculated as 0.018 m. The Reynolds number can be calculated by substituting the new values into Eq. 5.1,

$$Re = \frac{\rho Q D_H}{\mu A} = \frac{(1.293)(0.034)(0.018)}{(1.73 \times 10^{-5})(8.7 \times 10^{-3})} = 5190 \tag{5.2}$$

Although the Reynolds number for turbulent flow is specific to each system, values above 5190 were considered sufficiently high for the flow to be well within the turbulent regime, both when the air was pulled past the inlet vents of the pallet and when it passed through the headspace within the MBPs.

It should be noted that in CFD the different turbulence models perform well when the airflow is essentially laminar (Re < 300, Defraeye et al., (2013)) Discrepancies with empirical data are found at higher Reynolds numbers. Provided the flow regions where the turbulence model is applied is not completely enclosed, possibly necessitating the inclusion of natural convection, the importance of choosing and applying the correct turbulence model is amplified at higher Reynolds numbers and becomes less important as the Reynolds number decreases.

5.5.2 Heat transfer mechanisms in the numerical model

Heat transfer due to conduction and convection were included in the numerical model. The relative influence of moisture transfer, natural convection, radiation and the heat of respiration were analytically evaluated to determine whether to include or exclude the heat transfer mechanisms in the numerical simulation.

5.5.2.1 Moisture transfer

Moisture transfer loss was determined to have a negligible impact on the heat transfer process (section 4.5.3). There is the potential for heat released from the system due to moisture condensing from the air inside the polyliner. At a worst case scenario the air in the polyliner was at 20 °C and 100 % RH at the start of forced-air cooling. Over cooling the air in the polyliner could potentially drop to 0 °C and 90 % RH (RH the TCR was kept at. From psychometric charts (Singh & Heldman, 2014) the maximum moisture condensing into the system was 0.0122 $g_w/g_{dry\text{-}air}$. The numerical model reported the air volume inside the polyliner of each MBP as 0.0073 m^3, or 0.0088 kg at 20 °C. The latent heat of condensation of water, $\lambda_{condensation}$, is approximately 2260 kJ kg^{-1} (Datt, 2011). Hence, the maximum potential contribution by latent heat of condensation is,

$$Heat_{condensation} = (m_w)(\lambda_{condensation}) = (0.0122)(0.0088)(2260) = 0.24\ kJ \quad (5.3)$$

The sensible heat load to be removed from a single MBP during cooling can be calculated from the mass of fruit, m_f, heat capacity, C_p, estimated as 3.713 J kg^{-1} K^{-1} for kiwifruit (section 6.4)and temperature difference, ΔT (K^{-1}),

$$Heat_{overall} = m_f C_p \Delta T = 10.5 \times 3.713 \times 20 = 780\ kJ \tag{5.4}$$

Hence, the potential addition due to the latent heat of condensation from the air within the polyliner during cooling was deemed negligible at < 0.04 %.

Moisture evaporated, if any, from the kiwifruit was assumed to transfer to water vapour within the polyliner bag, before condensing back as water droplets on cool surfaces within the polyliner during the forced-air cooling process. Hence, the latent heats of evaporation and condensation due to moisture evaporated from the kiwifruit and later condensing on cool polyliner and kiwifruit surfaces were assumed to be equal and opposite to each other, providing no net increase/decrease to the overall heat balance.

Another potential contribution is water condensing on fruit surfaces enhancing heat transfer due to the higher thermal conductivity of water. However, kiwifruit is 80 – 90 % water (Burdon et al., 2004) its thermal conductivity is 0.542 W m^{-1} K^{-1} (section 6.4.2), marginally lower than the thermal conductivity of water (0.577 W m^{-1} K^{-1} at 20 °C; Singh & Heldman, 2014). Hence, the increased heat transfer through the fruit surface, even if moisture condensate was present on a substantial percentage was considered negligible, particularly as the moisture condensate won't change the thermal conductivity elsewhere in the fruit volume.

5.5.2.2 Natural convection

The region inside the polyliner can be considered an enclosed space. Within enclosed systems the Grashof number calculates the ratio of natural convection, also termed buoyancy forces, to viscous forces acting on a fluid (Holman, 2010);

$$Gr = \frac{g\beta(\Delta T)L^3}{\nu^2} \tag{5.5}$$

Where ν (m^2 s^{-1}) is the kinematic viscosity, g (m s^{-2}) is gravity, β (K^{-1}) is the thermal expansion coefficient, ΔT (K^{-1}) is the temperature difference between two surfaces and L (m^{-1}) is the characteristic length between the surfaces.

Density differences generated within a fluid by a temperature difference within the domain induce fluid motion that facilitates the movement of energy; a process termed natural convection. At extremely low Grashof numbers (< 1700) the fluid motions generated by natural convection can be considered negligible, and heat transfer mainly occurs via conduction across the stagnant fluid layer. As the Grashof number increases different flow regimes (transitional and then turbulent) with increasing levels of fluid motion that progressively facilitate energy transport are encountered.

To estimate the Grashof number L is the height of the polyliner (~ 18.3 cm). At the start of precooling the refrigerated air temperature is 0 °C and the kiwifruit is 20 °C. Assuming the air temperature inside the polyliner has an average temperature of 10 °C (halfway between the fruit and refrigerated air temperature), allows ν (1.42 x 10^{-05}

m^2 s^{-1}) and β (3.53 x 10^{-3} K^{-1}) to be estimated (Singh & Heldman, 2014). Applying Eq. 5.5 yields,

$$Gr = \frac{g\beta(\Delta T)L^3}{\nu^2} = \frac{9.81 \times 0.00353(20)0.183^3}{(1.42x10^{-05})^2} = 2.1x10^7 \quad (5.6)$$

Based on the Grashof number (2.1 x 10^7) it was assumed that natural convection was a significant heat transfer mechanism within the polyliner. Hence, natural convection was included in the numerical simulation. The assumption to include natural convection was justified later in the project when cooling simulations were run with and without natural convection enabled (Appendix A1).

5.5.2.3 Radiation

Typically, in the forced-air cooling of horticultural produce the influence of radiation is expected to be small compared to the convective heat transfer (Defraeye et al., 2013b). However, the presence of the polyliner, and the subsequent stagnation of some internal air space, reducing convective/buoyancy effects, may result in heat transfer due to radiation having a substantial influence on the overall cooling performance.

One method of analysing the potential influence of radiation is to compare the heat flux, *q/A* (W m^{-2}), due to radiation to the heat flux via conduction through a stagnant air layer of 2 mm (distance enforced between the kiwifruit/polyliner/cardboard surfaces; section 5.3.2), within the polyliner. The heat transfer coefficient due to conduction through the stagnant air layer ($h.t.c._{cond,air}$), using an average distance between kiwifruit and

kiwifruit/polyliner of 2 mm, and assuming a temperature difference of 20 °C, was estimated from (Holman, 2010);

$$h.t.c._{cond,air} = \frac{k_{air}}{L} = \frac{0.0243}{0.002} = 11.75\ W\ m^{-2}\ K^{-1} \tag{5.7}$$

The heat flux due to conduction through this stagnant air layer in the polyliner was estimated as,

$$(q/A)_{cond} = h.t.c._{cond,air}\,\Delta T = 11.75 \cdot 20 = 235\ W\ m^{-2} \tag{5.8}$$

For polyethylene the emissivity, ϵ, is equal to 0.96 (Burg, 2004). No literature exists to the author's knowledgeϵ of the emissivity of kiwifruit. The emissivity of Golden delicious apples will be used as a substitute. Hellebrand et al. (2002) measured the emissivity of apples (Golden delicious) between 0.94 and 0.97. Hence, ϵ was assumed to equal 0.96. The heat flux due to radiation through air, between the polyliner and kiwifruit can be estimated as (Holdman, 2010),

$$(q/A)_{rad} = \frac{\sigma(T_1^4 - T_2^4)}{\frac{1}{\epsilon_1} + \frac{1}{\epsilon_2} - 1} = \frac{5.67 \times 10^{-08}(293.15^4 - 273.15^4)}{\frac{1}{0.96} + \frac{1}{0.96} - 1} = 96\ W\ m^{-2} \tag{5.9}$$

From the above calculation $(q/A)_{rad}$ potentially contributes to 29 % of the heat flux through stagnant air within the polyliner. This calculation is an extremely rough analytical estimate. The values for analysing the radiative heat transfer are for worst case scenarios as the real life temperature differences are expected to be much lower, especially once the fruit begins to cool. The calculation assumes two parallel surfaces facing each other, which is not the case between ellipsoidal/ spherical fruit and a polyliner, where view factors (i.e. the actual surface of the fruit in a direct line of sight

with the polyliner) will further diminish the effect of radiation. As the heat flux due to radiation was so much lower than that of conduction through a stagnant air layer, which in turn was expected to have a small contribution to the primary heat transfer mechanisms (forced-convection and conduction) it was considered negligible in the model construction. However, there were a lot of assumptions involved in neglecting radiation. To provide further evidence for the exclusion of radiation a simulation was run with radiation included for the numerical model and the impact was shown to be relatively small (Appendix A1).

5.5.2.4 Heat of Respiration

During forced-air cooling the heat of respiration is unlikely to have a significant impact on the cooling rate of horticultural produce (Gowda et al., 1997), largely because the forced-air process occurs over a short time period. However, as this numerical model involves polylined horticultural produce a brief analytical calculation to the contribution of the heat of respiration was performed.

In section 4.5.2 the slowest HCT during forced-air cooling for a MBP (MBP 7) was 5.6 h. Dividing the heat load to be removed by time, t (s), gives the total heat flow rate, q (W) to cool from 20 °C to 10 °C,

$$q = \frac{mC_p\Delta T}{t} = \frac{10.5 \times 3.713 \times (20 - 10)}{3600 \times 5.6} = 19.3\ W \tag{5.10}$$

Since the heat of respiration of kiwifruit at 15 °C is 0.64 W (Crisosto et al., 2013) the contribution of respiration to the amount of heat to be removed would be 3.3 %. The

heat of respiration is at its maximum during initial cooling and rapidly decreases as the temperature of the kiwifruit drop. The percentage contribution drops to 1.6 % between HCT and SECT. As the heat of respiration represents such a small percentage of total heat load during the worst case scenario (at the start of cooling) it was considered negligible for a complete pallet layer over the full forced-air cooling process.

5.5.3 Transport equations in the numerical model

Section 2.5 outlined the conservation equations used in Fluent to solve the transport phenomenon. Definitions of the vector quantity, $\vec{v}$, and partial derivate operator, ∇, and how the terms are expressed in Cartesian coordinates were also in section 2.5. The following sub-headings detail the actual equations solved by Fluent due to the inclusion and exclusion of the various source terms deemed relevant or negligible, respectively.

5.5.2.1 Mass transport

There was no mass dispersion or mass source terms included in the numerical model. The transport of mass within the fluid phase resulted in eq. 5.11,

$$\frac{\partial}{\partial t}(\rho) + \nabla \cdot (\rho \vec{v}) = 0 \tag{5.11}$$

where $\vec{v}$ (m s^{-1}) is the overall velocity vector.

5.5.2.2 Momentum transport

Reynolds averaging was used to account for the presence of turbulence, where the standard κ-ε turbulence model was employed. The effect of gravity was included in the numerical model. There were no other external body forces, hence the fluid flow equation in conservation form, reduced to,

$$\frac{\partial}{\partial t}(\rho\vec{v}) + \nabla \cdot (\rho\vec{v}\vec{v}) = -\nabla p + \nabla \cdot (\bar{\bar{\tau}}) + \rho\vec{g} \tag{5.12}$$

where p (Pa) is the pressure and $\bar{\bar{\tau}}$ (N m^{-2}) is the stress tensor.

Eq. 5.12 for a Newtonian fluid (air can be assumed to be Newtonian) and including Reynolds averaging for turbulent flow can be further expanded, using Cartesian co-ordinates, to,

$$\frac{\partial}{\partial t}(\rho u_i) + \frac{\partial}{\partial x_j}(\rho u_i u_j) = -\frac{\partial p}{\partial x_i} + \frac{\partial}{\partial x_i}\left[\mu\left(\frac{\partial u_i}{\partial x_j} + \frac{\partial u_j}{\partial x_i} - \frac{2}{3}\delta_{ij}\frac{\partial u_l}{\partial x_l}\right)\right] + \frac{\partial}{\partial x_j}\underbrace{\left(-\rho\overline{u_i' u_j'}\right)}_{Reynolds\ stresses} \tag{5.13}$$

The Reynolds stresses were modelled by the Boussinesq hypothesis (which relates the Reynolds stresses to the mean velocity gradients),

$$-\rho\overline{u_i' u_j'} = \mu_t\left(\frac{\partial u_i}{\partial x_j} + \frac{\partial u_j}{\partial x_i}\right) - \frac{2}{3}\left(\rho\kappa + \mu_t\frac{\partial u_k}{\partial x_k}\right)\delta_{ij} \tag{5.14}$$

where κ (J kg^{-1}) is the turbulent kinetic energy and μ_t (kg m^{-1} s^{-1}) is the turbulent viscosity.

The standard κ-ε turbulence model was selected, which defines μ_t as (Fluent-Theory, 2010),

$$\mu_t = \rho C_\mu \frac{\kappa^2}{\varepsilon} \tag{5.15}$$

where ε (m^2 s^{-3}) is turbulence dissipation rate and C_μ is a model constant.

The standard κ-ε turbulence model uses the following transport equations to obtain κ and ε,

$$\frac{\partial}{\partial t}(\rho\kappa) + \frac{\partial}{\partial x_i}(\rho\kappa u_i) = \frac{\partial}{\partial x_j}\left[\left(\mu + \frac{\mu_t}{\sigma_\kappa}\right)\frac{\partial \kappa}{\partial x_j}\right] - \rho\varepsilon + G_t \tag{5.16}$$

and

$$\frac{\partial}{\partial t}(\rho\varepsilon) + \frac{\partial}{\partial x_i}(\rho\varepsilon u_i) = \frac{\partial}{\partial x_j}\left[\left(\mu + \frac{\mu_t}{\sigma_\varepsilon}\right)\frac{\partial \kappa}{\partial x_j}\right] - C_{2\varepsilon}\rho\frac{\varepsilon^2}{\kappa} + C_{1\varepsilon}\frac{\varepsilon}{\kappa}(G_t) \tag{5.17}$$

where σ_κ (-) and σ_ε (-) are the turbulent Prandtl numbers, and $C_{1\varepsilon}$ and $C_{2\varepsilon}$ are model constants.

G_t (kg m^{-1} s^{-3}), the generation of turbulent energy due to mean velocity gradients, is defined as,

$$G_t = -\rho\overline{u_i' u_j'}\frac{\partial u_j}{\partial x_i} \tag{5.18}$$

The model constants for the standard κ-ε turbulence model were set to their default values for the semi-empirical correlation,

$C_{1\varepsilon}$ = 1.44, $C_{2\varepsilon}$ = 1.92, C_μ = 0.09, σ_κ =1.0 and σ_ε = 1.3.

5.5.2.3 Energy transport

Energy conservation equation for fluids

The energy conservation equation does not need to include species diffusion, viscous dissipation or source terms,

$$\frac{\partial}{\partial t}(\rho E) + \underbrace{\nabla \cdot \left(\vec{v}(\rho E + p)\right)}_{convective\ transport} = \nabla \cdot \left(\underbrace{k_{eff} \nabla T}_{\substack{effective \\ conductivity}} \right) \tag{5.19}$$

where E (J kg^{-1}) is the total energy per unit mass, k_{eff} (W m^{-1} K^{-1}) is the effective thermal conductivity ($k + k_t$) and k_t, the turbulent thermal conductivity, is,

$$k_t = \frac{c_p \mu_t}{Pr_t} \tag{5.20}$$

The energy is related to the enthalpy by,

$$E = h - \frac{p}{\rho} + \frac{v^2}{2} \tag{5.21}$$

h (J kg^{-1}) is the sensible enthalpy,

$$h = \int_{T_{ref}}^{T} C_p dT \tag{5.22}$$

where T_{ref} is equal to 298.15 K.

Energy conservation equation for solids

There were no heat source terms for the solids. The energy conservation equation in the solid regions (kiwifruit, polyliner and cardboard) of the numerical model reduced to,

$$\frac{\partial}{\partial t}(\rho h) = \nabla \cdot (k \nabla T) \tag{5.23}$$

5.6 Numerical setup

5.6.1 Material thermophysical properties

The thermophysical properties of the fluids and solids are shown in Table 5.1. The air properties at 0 °C were used for the air, both inside and outside the polyliner. However, natural convection was only enabled for air inside the polyliner. Materials properties are defined and a comprehensive sensitivity analysis performed in section 6.4.

Table 5.1. Material properties of the air and solid materials, in the numerical model. See section 6.4 for sources of property data.

	Material				
Properties	**Air (0 °C) outside polyliner**	**Air (0 °C) inside polyliner**	**Kiwifruit**	**Cardboard**	**Polyliner**
Density (kg m^{-3})	1.293	1.293	1037	195	960
Specific heat capacity (J kg^{-1} K^{-1})	1006	1006	3713	1700	2300
Thermal conductivity (W m^{-1} K^{-1})	0.0243	0.0243	0.542	0.065	0.48
Viscosity (kg m^{-1} s^{-1})	1.73 x10^{-05}	1.73 x10^{-05}	–	–	–
Expansion coefficient (K^{-1})	–	0.00367	–	–	–

5.6.2 Problem setup

5.6.2.1 Boundary conditions

The top, bottom and lateral boundaries upstream and downstream of the MBPs were modelled as symmetry boundary conditions (no-slip walls). This assumes that the normal velocity components and gradients are zero at the boundary. The kiwifruit, polyliner and cardboard surfaces were modelled as no-slip walls with zero roughness. The refrigerated air pulled through the MBP was never in direct contact with the kiwifruit, due to the presence of the polyliner, while a laminar zone and natural convection was simulated inside the polyliner. Hence, the assumption of no-slip walls for the kiwifruit surfaces was considered reasonable.

During experimental validation insulation blocks were placed to either side of the pallet layer. Hence, a heat flux of zero was assumed through the side walls of the pallet layer. A periodic boundary condition was enabled between the top and bottom of the MBPs. The temperatures within the computational domain were initially set to specified value. For each validation experiment (Chapter 7) the exact temperature was specific to the ambient temperature in the laboratory that the kiwifruit were equilibrated at (18.9 – 20.1 °C). For sensitivity analysis (Chapter 6) and comparison of different operating conditions and MBP designs (Chapter 8) the temperatures were set to 20 °C, to replicate the field heat of kiwifruit following harvest.

5.6.2.2 Operating conditions

The inlet of the computational domain was defined as a pressure inlet and set to the ambient atmospheric pressure (i.e. the condition in the temperature control room). The outlet of the computational domain was defined as a pressure outlet with an underpressure imposed, to represent the underpressure created by a fan in a forced-air tunnel cooler device. The pressure drop can be varied until the desired flowrate through the pallet is achieved. The inlet and outlet of the computational domain were set to the temperature of the refrigerated room (~ 0 °C, depending on the specific experimental conditions).

In the experimental validation setup (section 7.2) a screen duct with wire-meshes at the entrance and inlet was placed in front of the half pallet. Hence, a low turbulence intensity (1 %) was the initial condition defined at the pressure inlet. The hydraulic diameter, 0.34 m, was the other initial turbulence parameter prescribed at the pressure inlet. The same intensity and hydraulic diameter were set at the pressure outlet.

5.6.2.3 Turbulence model

The κ-ε turbulence model employs wall functions to model the near-wall regions (i.e. the boundary layers between the airflow and cardboard/ effective polyliner surfaces). When using wall functions the y^+ (wall distance for fluid flow past surfaces used to describe the expected flow behaviour) calculated during simulation should > 30, for the approach to be valid (section 2.5.3). The current mesh settings were expected to produce average $y^+ > 30$ for each pressure drop tested. However, low Reynolds numbers in the

airflow were expected within areas that receive a small percentage of the total airflow distribution (e.g. outside of the straight airflow pathways between vents, such as the top and bottom corners of the box). Hence, the y^+ values vary throughout the MBP along the airflow and cardboard/ effective polyliner surface boundary, causing local $y^+ < 30$. This creates a situation where the mesh will constantly have to be refined/ coarsened locally. While possible to achieve for a specific vent configuration and air flowrate this will become extremely cumbersome if any design features or operating conditions change, necessitating a complete re-mesh of the computational domain. To account for this the Enhanced Wall Treatment (EWT) option, a y^+ insensitive wall function approach was used

The standard κ-ε was the turbulence model used, due to its robustness, relative accuracy over a wide range of turbulent flows and CPU efficiency (Fluent-Theory, 2010). The EWT was enabled for the near-wall modelling. While the standard κ-ε turbulence model, with EWT, was expected to give the best performance a variety of turbulence models were numerically tested (Appendix A1).

5.6.3 Numerical simulation

The numerical simulations were performed with the ANSYS Fluent 15 software package (Fluent, 2010). The SIMPLE algorithm was used for pressure-velocity coupling. Second order spatial discretization schemes were used throughout for each of the solution methods (pressure, turbulent kinetic energy, specific dissipation rate and energy). The Green-Gauss Cell Based option was used for gradient discretization, to ensure second order interpolation, as recommended by Fluent (2010). The under-

relaxation factors for each of the relevant terms (pressure, density, body forces, momentum, turbulent kinetic energy, turbulent viscosity and energy) were kept at the default settings recommended in Fluent (2010).

Prior to simulation of the transient forced-air cooling process, steady state simulations were performed to obtain the initial airflow field and temperature conditions. The flow was initialized by assuming no flow and a uniform, atmospheric pressure field.

5.6.4 Iterative convergence

Starting from an initial guess of the flow variables throughout the computational domain the equations were solved until a specific error was reached. For fluid flow and turbulence equations normalised residuals in the range of 10^{-3} indicated that the solution was practically converged (Fluent, 2010). The default energy residual convergence was even tighter ($< 10^{-6}$).

To reduce the total computational time the flow field was initialized and solved at steady-state, independent of temperature. The initial steady state simulations were run until each of the relevant residuals (continuity, x-, y- and z-velocity, turbulent kinetic energy, turbulent viscosity) were below the required threshold for convergence. This was approximately 400 iterations for all conditions tested. Following steady-state convergence the transient simulation was run at a time step of 60 s, with a maximum of 20 iterations per time step. A temporal analysis on the time step size was performed using the Richardson extrapolation in Appendix A1, with a temporal discretization error of 3.1 % found. The influence of natural convection on the heat transfer meant that the

flow field could not be assumed independent of temperature. Hence, the flow and turbulence equations were calculated along with the energy equation during transient simulation. The simulations (for 14 h) took approximately 24 h, on an i5-4570 Intel Core processor (3.2 GHz) with 8 GB RAM memory.

5.7 Conclusions

A numerical model to simulate the forced-air cooling for a single pallet layer, containing 10 MBPs, has been constructed. A periodic boundary condition linking heat transfer between the top and bottom the MBPs is included to simulate the cooling effect of the airflow entering MBPs in the pallet layers directly below.

Direct contact between individual produce or produce and a polyliner can create an inconsistent mesh around the contact points causing unstable calculations (i.e. non-converging residuals) in the simulation stage. However, a combination of a relatively low number of contact points (only between the polyliner and kiwifruit surfaces in contact with the polyliner) and a high mesh size meant that the mesh around the contact areas could be locally refined to the point that the mesh was stable.

Analytical steady-state calculations showed that radiation and heat generation due to product respiration could be excluded. Natural convection was shown to provide a substantial contribution to the overall heat transfer process. Hence, the momentum and energy calculations were coupled during transient simulation. The standard κ-ε turbulence model with enhanced wall treatment was used to allow the numerical model to be applied across a range of air flowrates.

Before the numerical model can be experimentally validated the sensitivity of the model to the material properties prescribed must be determined.

Chapter 6

Impact of the thermal characterisation of the numerical model inputs

6.1 Introduction

A numerical model of a single pallet layer, containing ten modular bulk packs (MBPs), of polylined horticultural produce has been developed. Prior to validating the numerical model against experimental data it is important to test the robustness of the model to the thermal characterisation of the system under study. Unfortunately, exact values could not be obtained for all of the material thermal properties. The properties of the air can change with respect to temperature, while the properties of the solids, such as the exact thermal conductivity and specific heat capacity for Hayward kiwifruit do not exist in current published literature, to the knowledge of the author. This led to various assumptions about the exact material properties during the set-up of the numerical model (section 5.6.1). These assumed values were tested before experimental validation of the numerical model.

6.2 Objectives

This chapter aims to investigate the sensitivity of the numerical model to the various input values. This includes the thermophysical properties of the fluids and solids (density, thermal conductivity, heat capacity, viscosity, expansion coefficient). If the model is adapted to function for other horticultural produce or even different varieties of kiwifruit then the input parameters that the model is most sensitive to will already be

known and the researcher can ensure that effort is efficiently concentrated to establish true values for the highly sensitive variables.

6.3 Methods

The impact of the material properties was analysed by comparing the change in average temperature across the pallet layer after a specific time period (the approximate HCT) against a "standard" version of the numerical model. The HCT gave a reliable indication of cooling performance in laboratory experiments (section 4.5). The "standard" model, which generated the base line values for comparison against, had the geometrical construct and set-up (including material properties) outlined in sections 5.3 and 5.6, respectively, for a pressure drop of 850 Pa (the highest pressure drop the numerical model was experimentally validated against; section 7.2) and flowrate of 0.71 L kg^{-1} s^{-1} across the pallet layer. The inlet temperature of the refrigerated air was 0 °C and the temperatures within the computational domain were set to 20 °C.

6.4 Sensitivity of the numerical model results to the thermal property input values

6.4.1 Thermophysical properties of air

The thermophysical properties of air change depending on the air temperature and relative humidity (RH). ANSYS Fluent does provide the option to calculate the various properties with respect to temperature and RH during simulations (Fluent, 2010). However, this will add to the computation time and expense. Tsilingiris (2008) details the thermal properties of air for temperatures between 0 – 100 °C and a RH range of 0 –

100 %. During forced-air cooling refrigerated air is pulled through the pallet at approximately 0 °C and can't exceed the maximum temperature of the fruit (20 °C). At low air temperatures (i.e. < 20 °C) increasing the RH from 0 % to 100 % has a negligible effect on the thermal properties of density, heat capacity, thermal conductivity and viscosity (Tsilingiris, 2008). Differences in air properties, due to RH, do not become apparent until temperatures around 40 °C. Hence, air properties were calculated from values readily available in literature for dry air, which are included in Holman (2010).

Within kiwifruit MBPs air was either within the box but outside the polyliner (turbulent region) or trapped within the enclosed space of the polyliner (laminar region). Two separate sets of thermal properties were used, depending on region the air was located in. A sensitivity analysis was performed on the air properties to ensure that assuming constant values (i.e. values that did change with respect to temperature) did not adversely affect the results. The high values were calculated for an air temperature of 20 °C (the air temperature inside the polyliner at the start of simulation; Table 6.4). The properties of dry air are well established in literature, hence, the sensitivity analyses was only performed when all air properties, either inside or outside the polyliner, were at 20 °C, and compared to the standard model, where all the air properties were for a dry air temperature of 0 °C (Table 6.4).

6.4.2 Thermophysical properties of kiwifruit

6.4.2.1 Kiwifruit density

The density range for the kiwifruit was established from current literature for Hayward kiwifruit (Actinidia deliciosa) harvested in New Zealand. Jordan et al. (2000) found a density range of 1025.5 – 1038.2 kg m^{-3} and Jordan and Seelye (2009) reported a range of 1031.3 – 1049.9 kg m^{-3}. From these values an average of 1037 kg m^{-3} was used in the numerical model with high and low values of 1049.9 kg m^{-3} and 1025.5 kg m^{-3}, respectively, tested in the sensitivity analysis (Table 6.4).

6.4.2.2 Kiwifruit specific heat capacity and thermal conductivity

Exact data for the thermal properties of Hayward kiwifruit could not be found in current literature. However, many models exist for estimating the specific heat capacity and thermal conductivity of food materials based on the water content (X_w) of the produce (Sweat, 1994).

Following harvest the typical water content of Hayward kiwifruit is 80 – 90 % (Burdon et al., 2004). For Hayward kiwifruit harvested in New Zealand the dry matter range is 15.1 – 19.0 % (X_w of 81.0 – 84.9 %; Table 6.1). A dry matter content of 17 % (X_w of 83 %) was used in the numerical model, based on the average values reported in Table 6.1.

Table 6.1. Dry matter content of Hayward (Actinidia Deliciosa) kiwifruit harvested in New Zealand.

Author	Dry matter content (%)	Water content, X_w (-)
Macrae et al. (1989)	15.6 – 18.5	0.815 – 0.844
McGlone and Kawano (1998)	15.9 – 18.4	0.816 – 0.841
Mowat and Maguire (2007)	15.7 – 17.2	0.828 – 0.843
Wang et al (2011)	15.1 – 19.0	0.810 – 0.849

Sweat (1994) reviewed the correlations for estimating the specific heat capacity and thermal conductivity, based on the water content (in decimal form; Table 6.2). Both the equation and outputs values for the average ($X_{w,avg}$ = 0.83), high ($X_{w,high}$ = 0.849) and low ($X_{w,low}$ = 0.81) water contents of kiwifruit are presented. As the correlations are based on the water content the highest and lowest values in Table 6.2 were used to calculate the high and low specific heat capacity and thermal conductivity for the sensitivity analysis. For an average water content of 0.83 the specific heat capacity and thermal conductivity were 3.713 kJ kg^{-1} K^{-1} and 0.542 W m^{-1} K^{-1}, respectively.

Table 6.2. Heat capacity and thermal conductivity models for foods based on the water content

		$X_{w,avg}$ = 0.83	$X_{w,high}$ = 0.844	$X_{w,low}$ = 0.815
Author	**Model**	**Specific heat capacity (kJ kg^{-1} K^{-1})**		
Siebel (1982)	$0.837 + 3.349X_w$	3.617	3.664	**3.566**
Backstrom and Emblik (1965)	$1.200 + 2.990X_w$	3.682	3.724	3.637
Comini et al. (1974)	$1.256 + 2.931X_w$	3.689	3.730	3.645
Fikiin (1974)	$1.381 + 2.930X_w$	3.813	**3.854**	3.769
Dominguez et al. (1974)	$1.382 + 2.805X_w$	3.710	3.749	3.668
Lamb (1976)	$1.470 + 2.720X_w$	3.728	3.766	3.687
Riedel (1956)	$1.672 + 2.508X_w$	3.754	3.789	3.716
Values used in sensitivity		**3.713**	**3.854**	**3.566**
		Thermal conductivity (W m^{-1} K^{-1})		
Backstrom and Emblik (1965)	$0.26 + 0.34X_w$	0.542	0.547	0.537
Bowman (1970)	$0.056 + 0.567X_w$	0.527	0.535	**0.518**
Bowman (1970)	$0.081 + 0.568X_w$	0.552	0.560	0.544
Comini et al. (1974)	$0.26 + 0.33X_w$	0.534	0.539	0.529
Sweat (1974)	$0.148 + 0.493X_w$	0.557	**0.564**	0.550
Values used in sensitivity		**0.542**	**0.564**	**0.518**

6.4.3 Thermophysical properties of cardboard and polyliner

The thermophysical properties for corrugated cardboard and high density polyethylene (polyliner bag) can be found in current literature and are summarized in Table 6.3. To determine whether the corrugated cardboard properties were a critical parameter in the numerical model the density, specific heat capacity and thermal conductivity were varied by ± 20 % in the sensitivity analysis (Table 6.4). The thermal properties of the polyliner were shown to provide a negligible resistance to heat transfer (Appendix A1). Hence, a sensitivity analysis was not performed on their possible range. However, they were still defined in the numerical model.

Table 6.3. Thermophysical properties of the corrugated cardboard and polyethylene liner

Material	Density ($kg\ m^{-3}$)	Specific heat capacity ($kJ\ kg^{-1}\ K^{-1}$)	Thermal conductivity ($W\ m^{-1}\ K^{-1}$)
Corrugated cardboard	195[a]	1700[b]	0.065[c]
High density polyethylene	960[c]	2300[c]	0.48[c]

a. Tanner (1998)
b. Amos (1995)
c. ASHRAE (1993)

Table 6.4. Sensitivity input range for fluid and solid thermophysical properties

Parameter	Nomenclature	T = 0 °C	T = 20 °C	
Air (refrigerated)				
Density ($kg\ m^{-3}$)	ρ_a	1.293	1.204	
Specific heat capacity ($J\ kg^{-1}\ K^{-1}$)	C_a	1006	1006	
Thermal conductivity ($W\ m^{-1}\ K^{-1}$)	k_a	0.0243	0.0258	
Dynamic viscosity ($kg\ m^{-1}\ s^{-1}$)	μ_a	1.73×10^{-5}	1.83×10^{-5}	
Air (in polyliner bag)				
Density ($kg\ m^{-3}$)	$\rho_{a,p}$	1.293	1.204	
Specific heat capacity ($J\ kg^{-1}\ K^{-1}$)	$C_{a,p}$	1006	1006	
Thermal conductivity ($W\ m^{-1}\ K^{-1}$)	$k_{a,p}$	0.0243	0.0258	
Dynamic viscosity ($kg\ m^{-1}\ s^{-1}$)	$\mu_{a,p}$	1.73×10^{-5}	1.83×10^{-5}	
Expansion coefficient (K^{-1})	$\beta_{a,p}$	0.00367	0.00353	
		Average	**High**	Low
Kiwifruit				
Density ($kg\ m^{-3}$)	ρ_k	1037	1049.9	1025.5
Specific heat capacity ($J\ kg^{-1}\ K^{-1}$)	C_k	3713	3854	3566
Thermal conductivity ($W\ m^{-1}\ K^{-1}$)	k_k	0.542	0.560	0.518
Cardboard				
Density ($kg\ m^{-3}$)	ρ_c	195	234	156
Specific heat capacity ($J\ kg^{-1}\ K^{-1}$)	C_c	1700	2040	1360
Thermal conductivity ($W\ m^{-1}\ K^{-1}$)	k_c	0.065	0.078	0.052

6.5 Numerical results

The numerical model simulation with "standard" or base line input values produced a HCT of approximately 3 h (Table 6.5). Hence, 3 h of forced-air cooling simulation was specified as the comparison point for the average pallet temperature. The numerical model was found to be particularly robust. With the exception of the specific heat capacity of kiwifruit, no material property input value caused a change of > 1.0 % in the average pallet temperature. The greatest variation in temperature, for the highest potential kiwifruit heat capacity, was only 0.22 °C or 2.1 %. The relative sensitivity of the numerical model to the specific heat capacity of kiwifruit was expected as the cooling rate of a solid is proportional to the heat capacity of the solid. However, the relative changes in the numerical results due to the change in the material property values were too small to try to draw any conclusions about the heat transfer process occurring or what mechanisms it may be dependent on.

Table 6.5. Sensitivity analysis for the impact of thermal properties on the numerical model.

	Temperature at t = 3 h (°C)	**Change in temperature at t = 3 h**	
Base line values	10.65	–	
Model inputs		**(°C)**	**(%)**
Inputs* at T_a = 20 °C	10.69	+ 0.05	+ 0.4
Inputs* at $T_{a,p}$ = 20 °C	10.62	- 0.02	- 0.2
ρ_k = 1049.9 kg m^{-3} (↑)	10.71	+ 0.06	+ 0.6
ρ_k = 1025.5 kg m^{-3} (↓)	10.58	- 0.07	- 0.6
C_k = 3854 J kg^{-1} K^{-1} (↑)	10.86	+ 0.22	+ 2.1
C_k = 3566 J kg^{-1} K^{-1} (↓)	10.46	- 0.17	- 1.6
k_k = 0.560 W m^{-1} K^{-1} (↑)	10.62	- 0.02	- 0.2
k_k = 0.518 W m^{-1} K^{-1} (↓)	10.70	+ 0.06	+ 0.6
ρ_c = 243 kg m^{-3} (↑)	10.65	+ 0.00	+ 0.0
ρ_c = 156 kg m^{-3} (↓)	10.63	- 0.01	- 0.1
C_c = 2040 J kg^{-1} K^{-1} (↑)	10.73	+ 0.08	+ 0.8
C_c = 1360 J kg^{-1} K^{-1} (↓)	10.70	- 0.06	- 0.6
k_c = 0.078 W m^{-1} K^{-1} (↑)	10.56	- 0.08	- 0.8
k_c = 0.052 W m^{-1} K^{-1} (↓)	10.72	+ 0.07	+ 0.7

*All model inputs (ρ, C, k, μ, β) set to their respective values for the specified temperature (T (°C))
(↑)/(↓) indicate if the input value is higher/lower than the base line input value

6.6 Conclusions

The numerical model was not sensitive to the thermophysical properties of the materials (within the likely range of input values). This verified the property values specified in the set-up of the model and eliminated potential sources for discrepancy between numerical results and experimental data. With the robustness of the numerical model confirmed the model can be experimentally validated.

Chapter 7

Numerical model validation

7.1 Introduction

A numerical model of polylined horticultural produce during forced-air cooling, including the local phenomena underlying the cooling performance of individual modular bulk packs (MBPs) has been developed (Chapter 5). The objective of this chapter is to validate this model by proving its ability to predict the temperature profiles of individual MBPs within a pallet layer against experimental temperature data.

7.2 Experimental system for validation

The experimental set up used to validate the model was similar to the set-up used in section 4.4. However, some modifications, detailed below, were required. The modifications ensured that all the air pulled through the system flowed through the pallet layers, the air coming into the pallet was uniformly distributed and there were no additional sources of energy transport between the packed fruits and the refrigerated room other than transfer via the airflow pulled through the pallet (i.e. there was no energy transfer through the sides of the pallet). These modifications were carried out so that the operating and boundary conditions in the experiments could be set up in a way that could reproduce the numerical conditions, while minimising uncertainties. By controlling the parameters and boundary conditions the accuracy of the CFD model can be determined by comparison with experiments (Defraeye et al., 2013b).

7.2.1 Experimental system set-up

A test duct with a solid wooden base, to prevent air from being pulled under the pallet, was built (Figure 7.1). The test duct was built with 15 cm of space to either side of the pallet and 30 cm of space at the top of the pallet, to match the dimensions of the fan system, detailed in section 4.4.1. Blocks of insulation where used to fill all the space around the sides of the pallet. This imposed a zero flux condition though the side walls of the pallet. An insulation block was also used to fill the remaining space between the top of the pallet and the fan system. The top and side walls of the test duct were constructed from transparent plastic polycarbonate sheets. A metal duct, containing a wire-mesh at the entrance and exit, was placed in front of the test duct. This promoted a uniform airflow distribution of air pulled through the pallet during experiments. The length between insulation blocks was 1000 mm, the exact width of the pallet when air is pulled through the 1.0 m face. This ensured that there was a minimal amount of space between individual MBPs for the air to flow through (i.e. nearly all of the airflow was forced through the vents of the MBPs). The modifications ensured that the vast majority of airflow generated flowed through the pallet before flowing past the orifice plate. By eliminating any other airflow pathways, which potentially occurred during laboratory experiments (i.e. air under the pallet and through the pallet base, air through gaps between individual MBPs and air along the sides of the pallet; section 4.5.1) the entire volumetric flowrate recorded from the pressure drop at the orifice plate can be assumed to have been pulled through the front of the pallet.

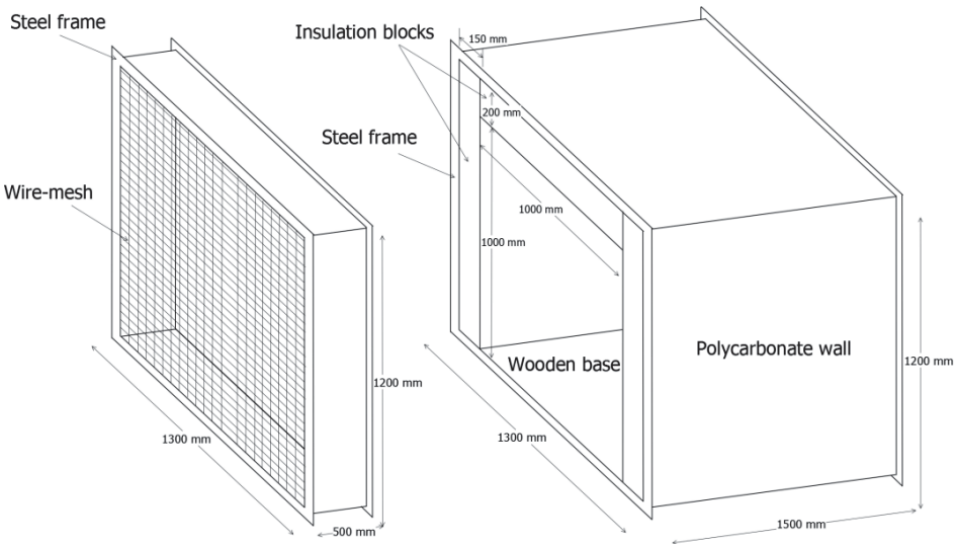

Figure 7.1. Wire mesh and insulated test duct attachments for the forced-air cooling system

For experiments the metal duct containing the wire-mesh, the insulated test duct and fan system were all attached together (Figure 7.2).

(a) (b)

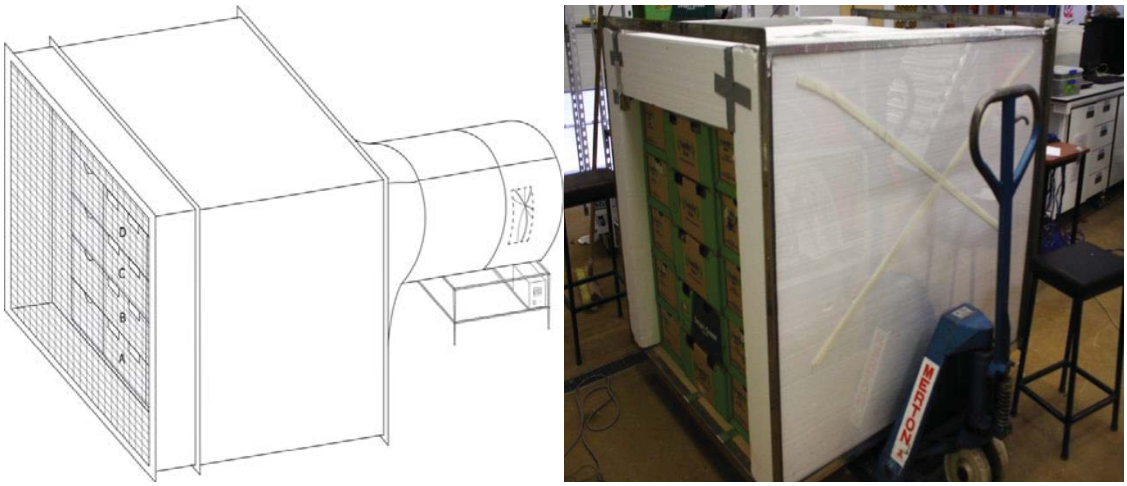

Figure 7.2. (a) Schematic diagram, including the wire mesh and fan system, and (b) photo of the insulated test duct, containing 5 layers of kiwifruit MBPs, to validate the numerical model.

7.2.2 Experimental methods

The fan system operated the same as in the set-up detailed in section 4.4.1 (the airflow pulled through the pallet was measured by the pressure drop across an orifice plate). The presence of the wire mesh prevented the use of a hot-wire anemometer to record the

air velocities past the inlet vents of the pallet. The MBPs were stacked 5 layers high (half-pallet height). In a temperature control room (TCR) the fan pulled refrigerated air through the pallet. A different TCR to the TCR used for experiments in section 4.4.4, was used. The new TCR had dimensions measuring 1.0 m by 5.0 m to accommodate the length of the experimental validation system.

Three different flowrates (0.34, 0.51, 0.71 L kg^{-1} s^{-1}) were tested, ranging from low rates (below those for typical precooling operations) to rates within the range (0.5 – 2.0 L kg^{-1} s^{-1}; Thompson, 2004). Laboratory experiments (section 4.5.1) indicated that a flowrate of 1.1 L kg^{-1} s^{-1} was likely beyond the threshold flowrate for significant improvement to cooling rate. Additionally, the range for typical precooling operations does not consider the presence of a polyliner, which can be expected to lower the threshold flowrate, due to decreased contact area between the produce and cooling air (the polyliner may provide a negligible thermal resistance but it still prevents airflow through the kiwifruit bulk). Hence, all three tested flowrates were chosen to be relatively low.

Kiwifruit where stacked in a cubic centred distribution and thermocouples were inserted into the centre of 12 kiwifruit per MBP (Figure 7.3), for MBPs 1 – 7 in both layers "B" and "D" (Figure 7.4). Due to symmetry MBPs 5 – 7 and 8 – 10 were expected to be replicates of each other. The same technique was used in section 4.2.2. Hence, only the kiwifruit temperatures in MBPs 5 – 7 were monitored. The kiwifruit arrangement and thermocouple placement was the same used in the laboratory experiment for 1.0 m orientation (section 4.4.3).

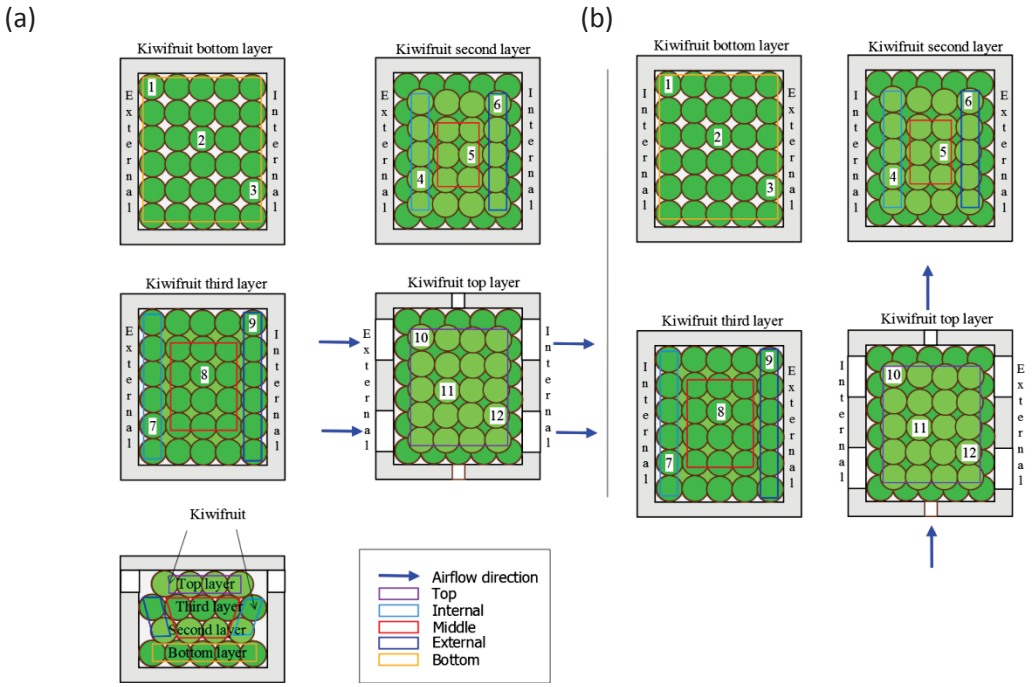

Figure 7.3. Cubic centred distribution and thermocouple location for kiwifruit in (a) MBPs 1 – 4 and (b) MBP 5 – 7. Images first appears in Figure 4.13.

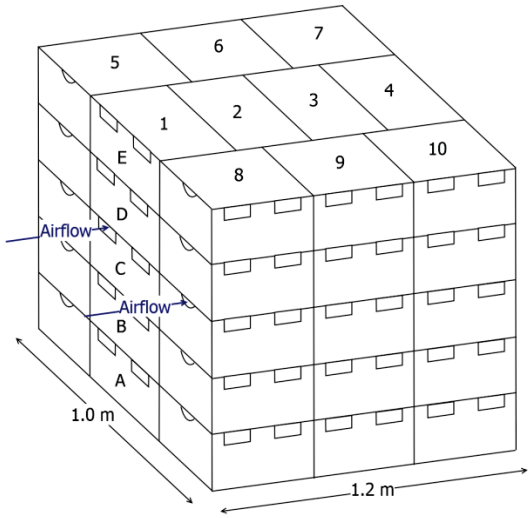

Figure 7.4 Half-pallet layout with layers assigned letters "A"-"E". Air is pulled through the 1.0 m pallet. Image first appears in Figure 4.10

Table 7.1. Fan speeds, flowrate and corresponding pressure drop across the half-pallet tested

Fan speed (rpm)	$Q_{half\text{-}pallet}$ ($m^3\ s^{-1}$)	Q ($L\ kg^{-1}\ s^{-1}$)
1320	0.17	0.34
1800	0.25	0.51
2340	0.35	0.71

7.3 Model validation simulations

Certain experimental variables, such as the exact size and shape of the individual kiwifruit were difficult to accurately reproduce during the numerical trials. The product size can affect the airflow resistance through random stacking of horticultural produce in vented boxes (Delele et al., 2008). During industrial postharvest operations, before delivery to the laboratory, the kiwifruit were sorted into MBPs, based on the produce weight range. Count 36 kiwifruit (weighing between 93 – 103 g) have been used throughout this project, for both experiments and the numerical model construct. The exact size and shape of each kiwifruit can vary, within the weight range, in each MBP. These variables could influence the temperature profiles of the individual fruit. A specific cubic centred distribution of the kiwifruit was employed in each MBP to eliminate random product stacking as a variable. Additionally, by using the average fruit temperature (average of all monitored kiwifruit) per MBP it was assumed that the effect of kiwifruit shape and exact thermocouple location within the fruit on the temperature profile of the kiwifruit within the MBPs was minimised. Hence, a comparison between the experimental and numerical average temperature of the kiwifruit per MBP was used as the validation tool.

The numerical model followed the set-up procedure described in section 5.6. The air temperature at the numerical model inlet was set to the average air temperature in the TCR during experiments. The underpressure, at the numerical system outlet, was varied to achieve the flowrate (L kg^{-1} s^{-1}) generated in the experiments. For each simulation the initial fruit and cardboard box temperature were set to the initial fruit temperature in

each MBP for the corresponding experiment. The total starting temperature range across the three experiments was 18.9 – 20.1 °C.

7.4 Validation methods

Validation of the numerical model was performed by comparing the predicted and experimental cooling profiles of MBPs 1 – 7. The same MBP replicates (5 and 8, 6 and 9, 7 and 10) used in experiments (section 7.2.2) were used to present the results for the numerical model. The HCT and SECT were calculated following the calculation method outlined in section 4.2.4. The experimental uncertainty (standard error) was calculated per MBP. The experimental average temperature was calculated by averaging each temperature data point (12) in each MBP. The standard error was calculated from 24 data points (12 per box in each of the two monitored layers). The predicted temperatures were an average of all 100 kiwifruit in a MBP.

7.5 Comparison of the numerical and experimental temperatures

The underpressure imposed on the system outlet, in the numerical model, produced airflow rates of 0.34, 0.51 and 0.71 $L.kg^{-1}s^{-1}$ for underpressure values of 200, 420 and 850 Pa, respectively.

7.5.1 Comparison of the numerical and experimental temperature profiles

Separating the pallet layer into MBPs 1 – 4 (through the centre of the pallet layer) and MBPs 5 – 7 (along the side of the pallet layer), with error bars only presented for MBPs

1, 4, 5 and 7, allowed for a more detailed comparison of the individual MBP temperature profiles at flowrates of 0.34 L kg^{-1} s^{-1} (Figure 7.5), 0.51 L kg^{-1} s^{-1} (Figure 7.6) and 0.71 L kg^{-1} s^{-1} (Figure 7.7).

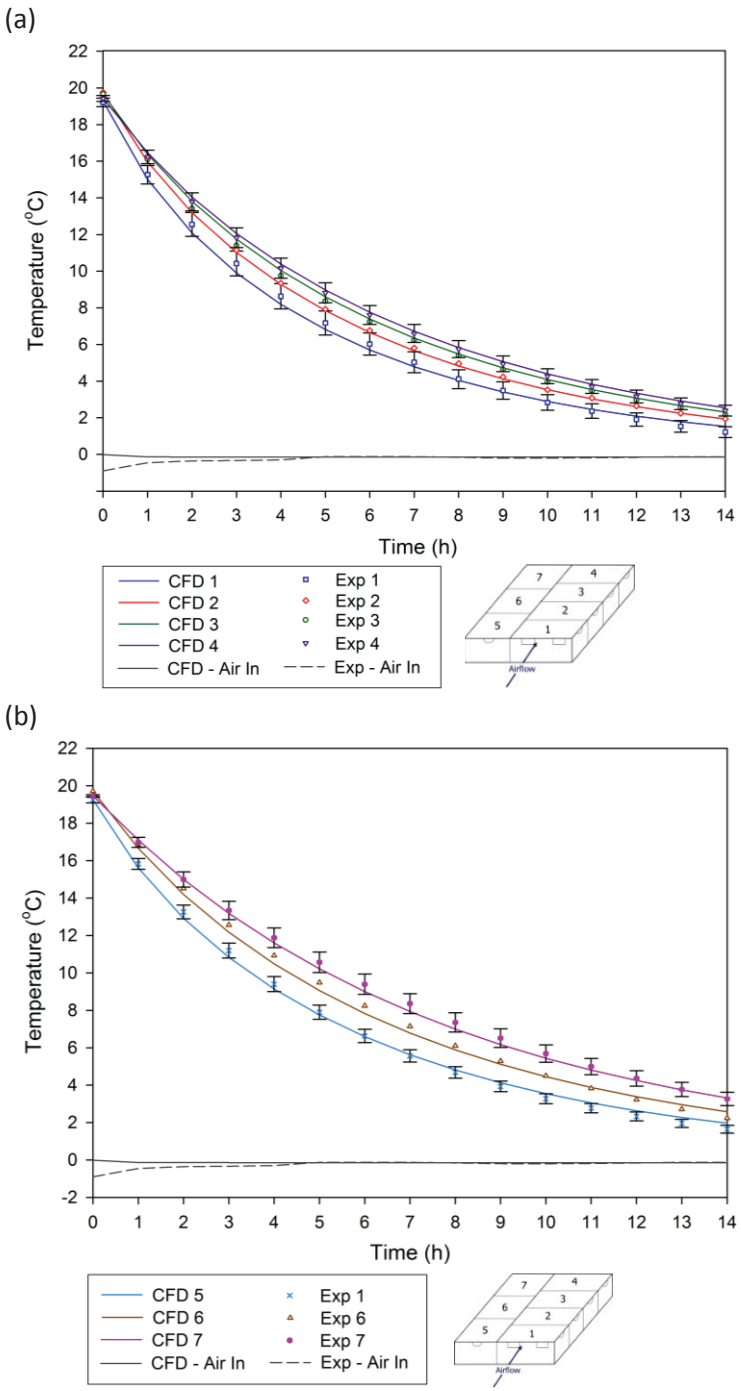

Figure 7.5. Comparison between predicted and experimental numerical average temperatures, during 14 h of forced-air cooling from an approximate initial product temperature of 20 °C at 0.34 L kg^{-1} s^{-1}, for (a) MBPs 1 - 4 and (b) MBPs 5 - 7. Standard error bars are shown for MBPs 1, 4, 5 and 7. Experimental and simulated air temperatures, averaged between the inlet vents of MBPs 1 and 5, are also shown.

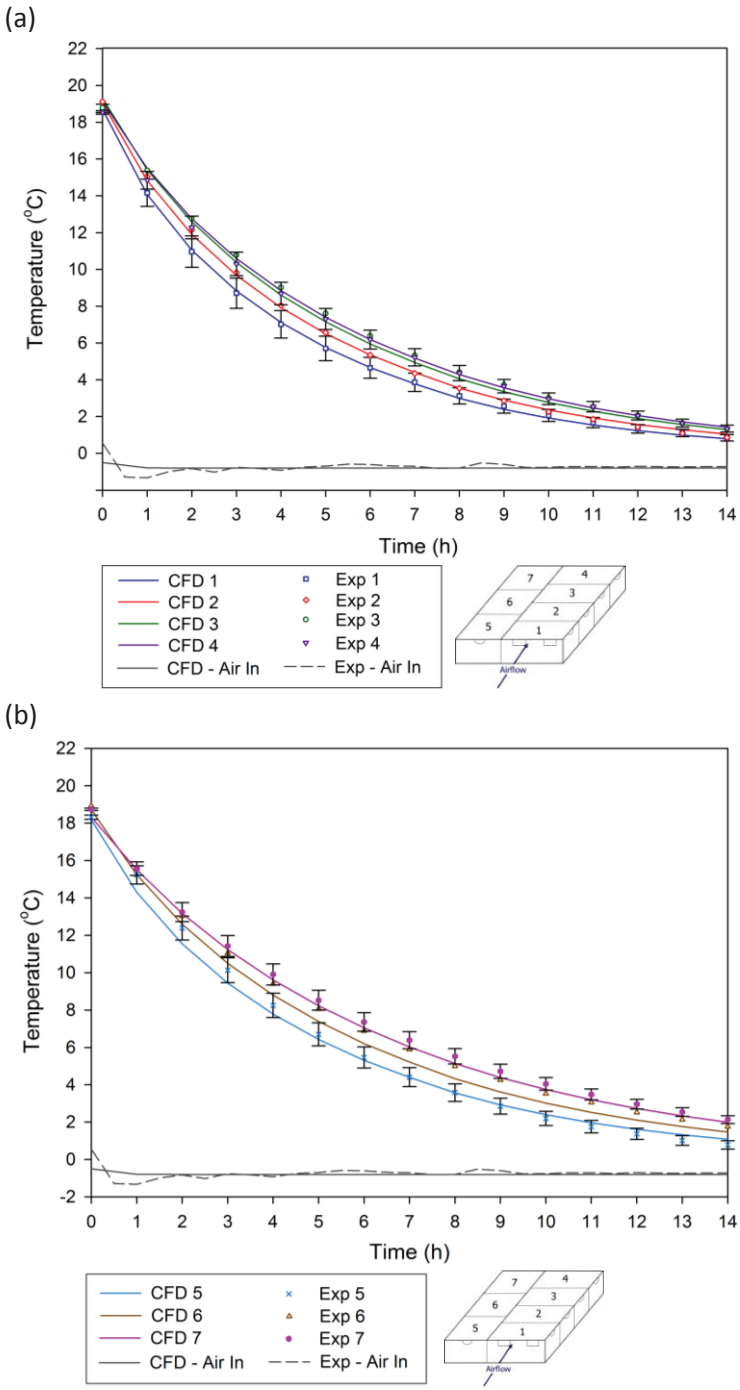

Figure 7.6. Comparison between predicted and experimental numerical average temperatures, during 14 h of forced-air cooling from an approximate initial product temperature of 20 °C at 0.51 L kg^{-1} s^{-1}, for (a) MBPs 1 - 4 and (b) MBPs 5 - 7. Standard error bars are shown for MBPs 1, 4, 5 and 7. Experimental and simulated air temperatures, averaged between the inlet vents of MBPs 1 and 5, are also shown.

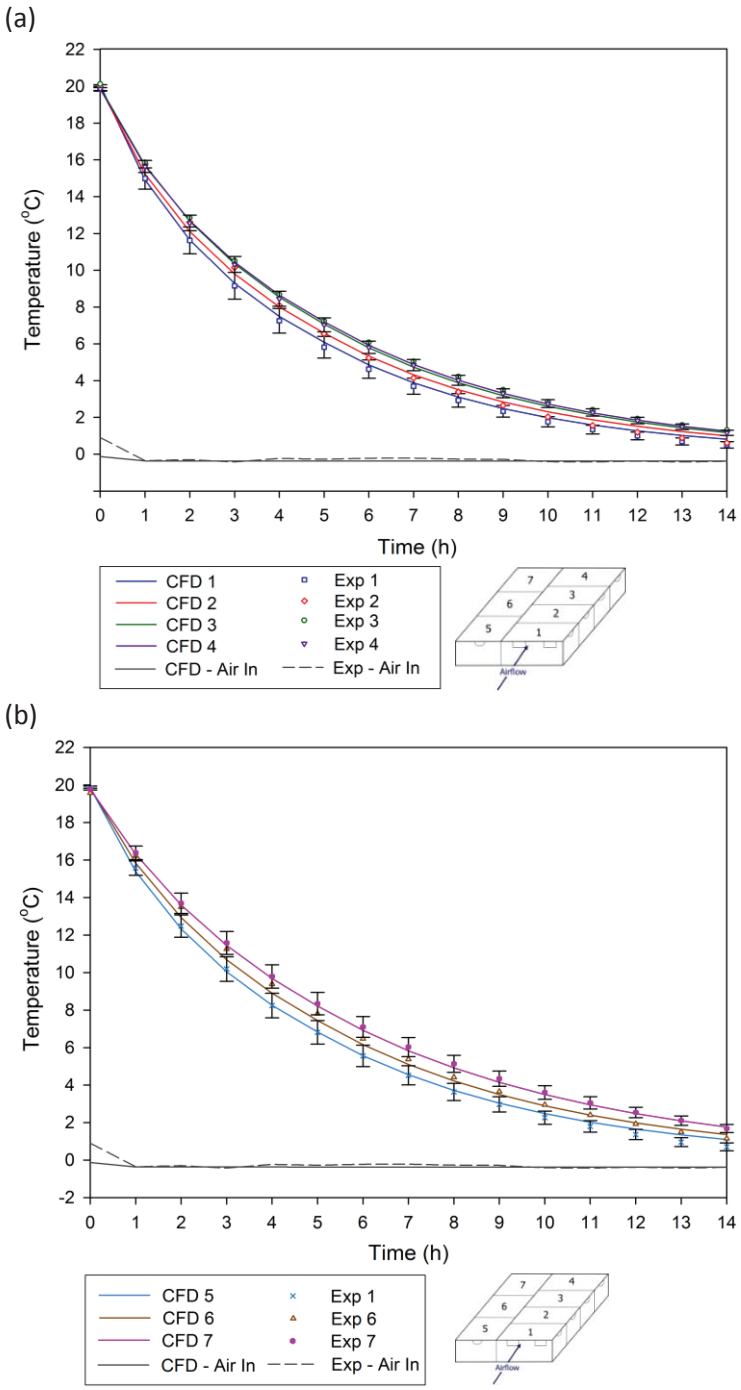

Figure 7.7. Comparison between predicted and experimental numerical average temperatures, during 14 h of forced-air cooling from an approximate initial product temperature of 20 °C at 0.71 L kg^{-1} s^{-1}, for (a) MBPs 1 - 4 and (b) MBPs 5 - 7. Standard error bars are shown for MBPs 1, 4, 5 and 7. Experimental and simulated air temperatures, averaged between the inlet vents of MBPs 1 and 5, are also shown.

The predicted temperature profiles fell within the standard error bars of the experimental data for MBPs 1, 4, 5 and 7 (Figures 7.5, 7.6 & 7.7). While the predicted temperatures remained within the error bars for the duration of the simulation they tended to over predict the temperate drop at the start of cooling (0 – 4 h) and under predict the kiwifruit temperatures at end of the cooling operation (12 – 14 h). Overall, the location of the predicted temperature profiles, within the error bars of the experimental data, showed that the CFD model was quite accurate, especially considering the large mass of fruit per MBP (~10 kg) and long duration (14 h) of the forced-air cooling operation.

7.5.2 Comparison of the numerical and experimental HCT and SECT

Validation of the numerical model was also achieved by examining the numerical and experimental HCT and SECT for each MBP at flowrates of 0.34 L kg^{-1} s^{-1} (Figure 7.8), 0.51 L kg^{-1} s^{-1} (Figure 7.9) and 0.71 L kg^{-1} s^{-1} (Figure 7.10).

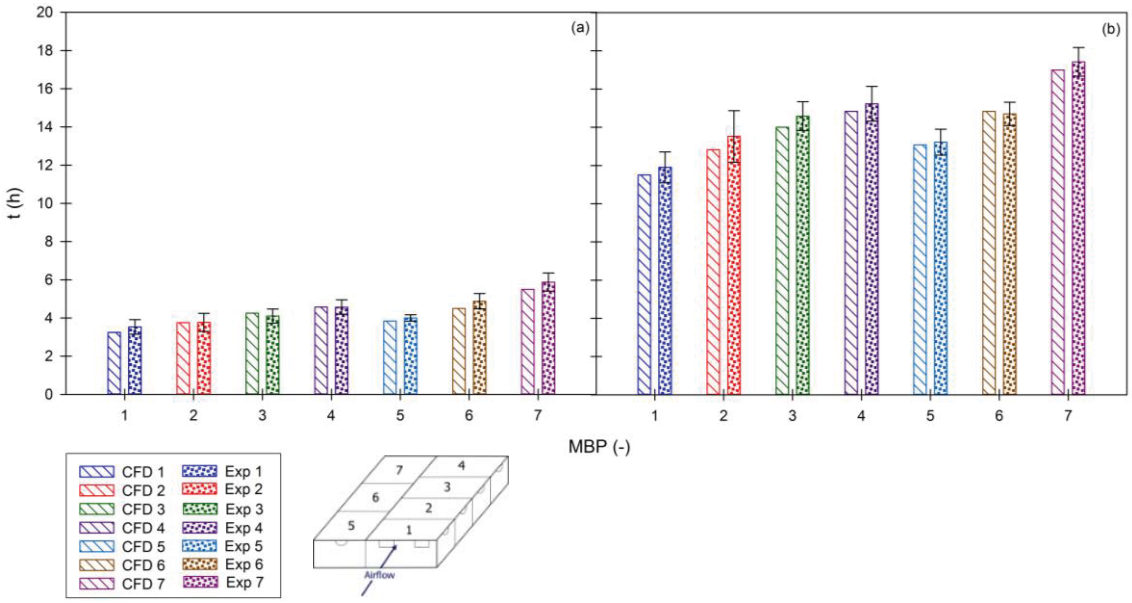

Figure 7.8. Predicted and experimental cooling times for MBPs 1 – 7 at 0.34 L kg^{-1} s^{-1}, for (a) HCT and (b) SECT. Standard error bars are shown for each MBP.

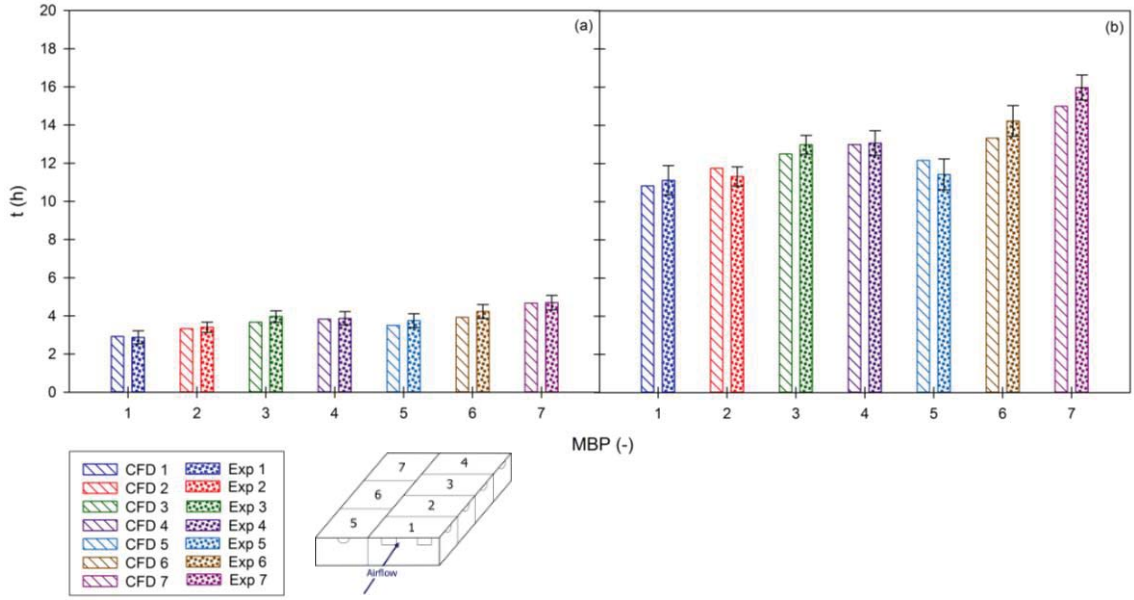

Figure 7.9. Predicted and experimental cooling times for MBPs 1 – 7 at 0.51 L kg^{-1} s^{-1}, for (a) HCT and (b) SECT. Standard error bars are shown for each MBP.

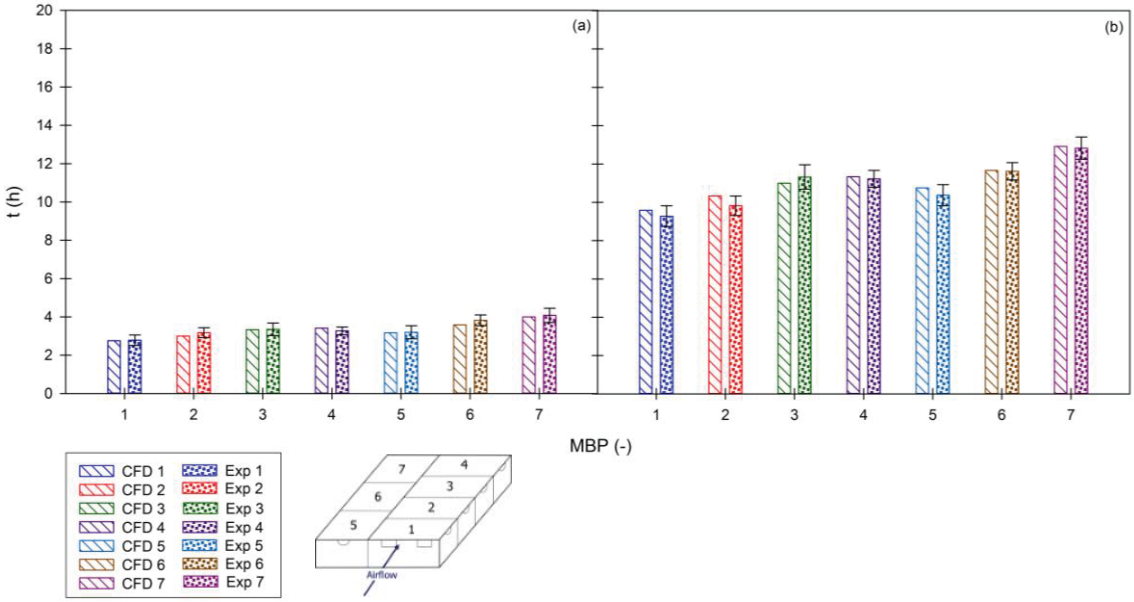

Figure 7.10. Predicted and experimental cooling times for MBPs 1 – 7 at 0.71 L kg^{-1} s^{-1}, for (a) HCT and (b) SECT. Standard error bars are shown for each MBP.

With the exception of the SECT for MBP 6 and 7 at a flowrate of 0.51 L kg^{-1} s^{-1} the HCT and SECT predicted by the numerical model fall within the error bars of the experiments for each of the tested flowrates (Figures 7.8, 7.9 & 7.10).

7.5.3 Experimental uncertainties

The most likely explanation for the minor over prediction of cooling (i.e. kiwifruit temperatures were predicted lower than experimental values) at the start of the simulation (Figures 7.5 and 7.6) was the exact thermocouple location. During experiments the thermocouples were placed as close to the centre of the kiwifruit as possible (i.e. the slowest cooling point within the fruit). However, the numerical model monitors the average temperature of the entire kiwifruit volume (including those lower temperatures that immediately start developing close to the fruit surface). Additionally, for the 0.51 L kg^{-1} s^{-1} and 0.71 L kg^{-1} s^{-1} experiments for the first hour the refrigerated air temperature was elevated, due to the sudden heat load (the kiwifruit heat-pallet) placed in the TCR, reducing the potential for cooling.

In experiments the wires may have caused some blockage of the vents in the MBPs. A blockage would have a greater impact on MBPs 5 – 7 due to the smaller effective vent area orientated perpendicular to the incoming refrigerated airflow (13 cm^2 compared to 44 cm^2 for MBPs 1 – 4). This could explain why the numerical model predicted a faster SECT (outside the error bars) for MBP 6 and 7 at a flowrate of 0.51 L kg^{-1} s^{-1} (Figure 7.6).

The possible reasons (thermocouple location, thermocouple wire blockage) for minor discrepancies, both in temperature profiles and HCT and SECT, are only a spread of the explanations for the difference in prediction accuracy between the numerical model and experiments. In the numerical model the exact cause of the difference is difficult to identify due to the complexity of the transport phenomena within the system. However, considering the number of assumptions required to develop the numerical model and the uncertainties in the various assumed constants (such as the thermophysical properties of the kiwifruit and cardboard) certain degrees of discrepancy are to be expected.

7.6 Conclusions

The capability of the numerical model to predict the average fruit temperature per MBP was quantitatively validated. A good agreement was found between the experimental and predicted values of the HCT and SECT for each MBP. Numerous assumptions were required to model the transport phenomena within the complex polylined packaging system. There were challenges associated with reproducing the numerical boundary conditions in experiments and the thermocouple wires may have had an impact on the experimentally determined cooling profiles. Considering the assumptions and challenges associated a good agreement between the experimental and predicted profiles of the average fruit temperature per MBP was obtained. This numerical model can be used to predict the transport phenomenon within the individual MBPs during forced-air cooling applications. This analysis can be used inform the researcher on optimal operating conditions, in terms of cooling rate and flowrate required, and potential alternative design features to improve cooling performance.

Chapter 8

Numerical model applications

8.1 Introduction

A numerical model to simulate the forced-air cooling of a pallet layer of polylined horticultural produce has been developed and experimentally validated. The model can be used develop a detailed understanding of the key mechanisms and design features controlling the forced-air cooling performance. The model can also find the optimal operating point of any given design.

Increasing the airflow pulled through the pallet will reduce the time taken for the produce to reach HCT. However after a certain airflow rate the improvement in HCT will be relatively minor compared to the increase in power costs. The higher the air flowrate (or pressure drop) applied, the higher the power required by the fan and the higher the cost of electricity. Finding an airflow rate that produces sufficient cooling, in a reasonable time period, without consuming excess amounts of power is essential for the kiwifruit industry.

The numerical model can be used to analyse the local air velocities and distribution, between and within the MBPs, and their subsequent impact on the cooling rate of the kiwifruit. The actual transport phenomena occurring inside and outside the polyliner bag and the relative contribution of the various heat transfer methods can now be

quantified. Finally, the numerical model allows for an in-depth assessment of potential alternative design features for the MBP.

8.2 Objectives

The chapter aims to analyse the different operating conditions (flowrate/ pressure drop) for the current MBP design to find the practical limit between increased energy input and cooling time for the current MBP system. By analysing the influence of the temperature profile and distribution of the airflow within the pallet the key design features controlling the cooling performance of the process can be identified. This information can then be used to propose a potential alternative box design to improve cooling performance.

8.3 Operating conditions investigated and power calculations

8.3.1 Operating conditions

Lower pressure drops, starting at 25 Pa and successively doubled until 200 Pa, were tested in order to find the point of maximum efficiency between successive increases to pressure drop and reduction in HCT. Higher pressure drops (up to 850 Pa) have already been tested in section 7.5. Although it is not ideal to extrapolate the model for simulations outside of the range of validation conditions the tested conditions were not radically different. The only change was a reduction in pressure drop. All temperatures (including set air temperatures entering the numerical model and initial kiwifruit

temperatures were kept within the validation range). Hence, conclusions based on these numerical results can be considered valid.

The airflow distribution between MBPs will be discussed in terms of the relative amount (as a percentage of the total flowrate though the pallet) pulled through each MBP.

Due to the pallet geometry there is a line of axial symmetry down the centre of the pallet (through MBPs 1 – 4). MBPs 5 and 8, 6 and 9, and 7 and 10, represent replicas of each other (Figure 8.1). Hence, results (HCT, airflow distribution, air temperature) are only given for MBPs 1 – 7 (Figures 8.3, 8.4, & 8.12 and Tables 8.1 & 8.2.) Air flowrate and temperature distribution plots are shown for the full pallet layer.

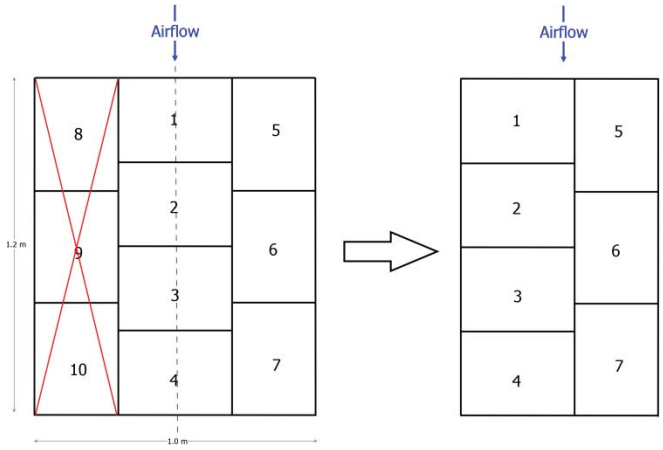

Figure 8.1. Reduced pallet layer of MBPs 1 – 10, on the basis of axial symmetry.

Prior to transient simulation of the cooling process the numerical model was first initialised and run at steady-state conditions until residual convergence (section 5.6.4). The air entering the system (i.e. at the inlet of numerical model) was assigned a set temperature of 0 °C. The kiwifruit and cardboard box temperatures were initially set to 20 °C. Kiwifruit temperature refers to average temperature of the entire kiwifruit bulk within each individual MBP (section 7.3).

8.3.2 Power requirements

The power cost (kWh) for the pallet was calculated from the HCT of the slowest cooling MBP. Hence, the active running time of the fan to sufficiently cool the pallet was dependent on the cooling rate of the slowest cooling MBP.

The power (P (W)) requirement for the forced-air cooling of a single pallet layer can be estimated from a product of the pressure drop (p (Pa)) and flowrate (Q (m^3 s^{-1})) across the pallet layer:

$$\Delta W = \Delta pQ \tag{8.1}$$

The numerical system is for a single pallet layer. A full pallet contains 10 layers. Assuming that the airflow is evenly distributed between each pallet layer (i.e. that each layer offers the same resistance to airflow) then the total amount of air required in a full pallet can be estimated by multiplying the flowrate by 10 ($Q_{pallet} = Q_{single\text{-}layer}$ x 10) The pressure drop for a single pallet layer will be the same for the full pallet. Hence,

$$P_{pallet} = \Delta pQ_{single-layer} \times n_{\text{layers}} = \Delta pQ_{pallet} \tag{8.2}$$

The power cost (kWh) to cool a single pallet to HCT (h) can be calculated from the product of power requirement and HCT of the slowest cooling MBP,

$$Power\ cost = P_{pallet} t_{HCT} \tag{8.3}$$

For this analysis 12 pallets were assumed to be cooled at a time, as is common practice in forced-air tunnel coolers (O'Sullivan et al., 2014). Assuming that during the kiwifruit harvest season the forced-air cooling operation is active for 24 h a day then the amount of kiwifruit pallets cooled per week can be estimated as,

$$\frac{Pallets}{week} = \frac{no.cooling\ runs}{day} \times \frac{no.pallets}{run} \times \frac{days}{week} \Rightarrow \frac{24}{t_{HCT}} \times 12 \times 7 \tag{8.4}$$

Associated power cost per week is,

$$\frac{Power\ cost}{week} = \frac{Power\ cost}{pallet} \times \frac{Pallets}{week} \tag{8.5}$$

It is important to note that when estimating the power required for forced-air cooling operations the flowrate generated is also dependent on the fan and motor efficiency. The actual power requirements for the fan will thus be greater than the estimates considered here. However, model predictions of the relative changes in power cost at different conditions should be accurate, as long as the fan is equally efficient at the conditions of insert. For answering questions about operating facilities, where the fans are already in place, then the model results should be combined with fan curves (specific to the system) that indicate the fan (and motor) efficiencies at various conditions.

8.4 Optimal operating point

This section aims to find an optimised point between efficient HCT in terms of power cost and practical HCT in terms of the quantity of kiwifruit (on a number of pallets per week scale) that can be cooled. Testing various operating conditions allows the model

to find the point at which it is no longer practically beneficial (in terms of power cost) to continue increasing the air flowrate and pressure drop, for the sake of diminished returns in the reduction of cooling times. In the previous chapter (section 7.5) numerical results for pressure drops between 220 and 850 Pa showed that approximately doubling the pressure drop between tests resulted in relatively small improvements (< 12 %) in terms of the relative reduction of the average pallet HCT between successive tests. Hence, the effective maximum was defined as when the relative improvement in HCT was < 12 % when the pressure drop was doubled between simulations. A survey into the pressure drops across palletized kiwifruit MBPs currently being achieved by precoolers in industrial packhouses in New Zealand found a range of approximately 0 – 140 Pa (Shim et al., 2016). The survey was carried out for 22 precoolers, spread across 7 industrial sites. Hence, the survey results are at least representative of a significant fraction of the industry. Based on numerical results and what is apparently achievable in industry pressure drops of 25, 50, 100 and 200 Pa were tested with the numerical model. The HCT presented is the HCT of the slowest cooling MBP, as this is the limiting MBP to cooling rate.

8.4.1 Numerical results

There was a substantial improvement in cooling rate and therefore number of pallets that could be cooled up to a pressure drop of 100 Pa (0.243 m^3 s^{-1}; Figure 8.2). Increasing the pressure drop from 25 Pa to 50 Pa increased the number of pallets that could be cooled from 196 to 249 and the power requirements from 5.8 kWh to 16.8 kWh. The relative power cost per pallet was 0.029 kWh at 25 Pa and 0.067 kWh at 50 Pa. Further increases in the pressure drop, to 100 Pa, allowed 310 pallets to be cooled

by a single tunnel cooler per week. However, 100 Pa required a power requirement of 49.0 kWh and raised the relative power cost to 0.16 kWh per pallet. At 200 Pa 367 pallets could be cooled per week but at a relative cost of 0.38 kWh per pallet.

Over the course of two forced-air cooling experiments conducted in industry the precooler was observed to be active for a maximum of duration of 6.0 h (section 4.2.5). At 200 Pa the HCT of the slowest cooling MBP was 5.5 h (Figure 8.2), thus 6 h will be sufficient to achieve the HCT of all MBPs. However, a pressure drop of 200 Pa requires a power requirement of 0.384 kWh per pallet, and is above the maximum pressure drop (140 Pa) observed in operating industrial precoolers (Shim et al., 2016). If the precooling duration can be extended to 6.5 h then HCT of the slowest cooling MBP can achieved for a pressure drop of only 100 Pa (reducing the power cost to 0.16 kWh per pallet). If pressure drops of only 50 Pa and 25 Pa are available the HCT of the slowest cooling MBP is achieved in 8.1 h and 10.3 h, respectively. Such long HCTs may be outside the practical time period available for forced-air cooling during the short (~ 1 month) kiwifruit harvest season.

Industrial operators should thus strive to achieve a constant pressure drop of at least 100 Pa across all pallets in a tunnel cooler, in order to achieve reasonable cooling within the typical time available in the pre-cooler at a justifiable cost. In 2014 the cost of electricity for industry was 11.98 c/kWh (Ministry of Business, Innovation and Employment, 2015). Operating at a pressure drop of 100 Pa allows 310 pallets to be cooled per tunnel cooler per week at an estimated operating cost of NZ $ 594. At 200 Pa the cost is NZ $ 1,688 for 367 pallets. Hence, it costs NZ $ 1,094 to cool an extra 57

pallets. The money saved by operating at 100 Pa instead of 200 Pa could potential be used to invest in another tunnel cooler.

The cost estimates can be scaled up to evaluate the impact if the optimal operating point was applied across the entire kiwifruit industry in New Zealand. From 2012 – 2014 the amount of kiwifruit processed, in terms of equivalent number of trays (weighing 3.6 kg each), averaged 105 million trays (Fresh Facts, 2014). One MBP holds the equivalent kiwifruit mass of approximately 3 trays. Hence, the equivalent of 0.35 million pallets, containing a total of 35 million MBPs could be forced-air cooled annually. If it costs NZ $ 594 to cool 310 pallets to HCT at 100 Pa then the cost to cool 0.35 million is NZ $ 0.7 million. The cost when operating at 200 Pa is NZ $ 1.6 million. Hence, choosing the appropriate operating point could potentially save the kiwifruit industry NZ $ 0.9 million annually. It should be noted that the estimation of the fan operating cost does not account for the fan and motor efficiency which will increase the power required to actually generate the desired flowrate. Hence, the potential monetary savings can be considered a conservative estimate.

The extra power cost, coupled with the diminishing reduction in improvement to HCT, make substantial increases to pressure drop beyond 100 Pa an inefficient method of improving the forced air cooling process of polylined horticultural produce.

It should be noted that the recommendation of 100 Pa is a compromise, applicable to most potential scenarios, between cooling rate and power cost, that can be changed based on the specific circumstances. For example if a large quantity of kiwifruit has to be cooled or if there is only a small number of kiwifruit pallets awaiting cooling

(possible due to bad weather inhibiting harvest) then the flowrate/ pressure drop can be adjusted accordingly.

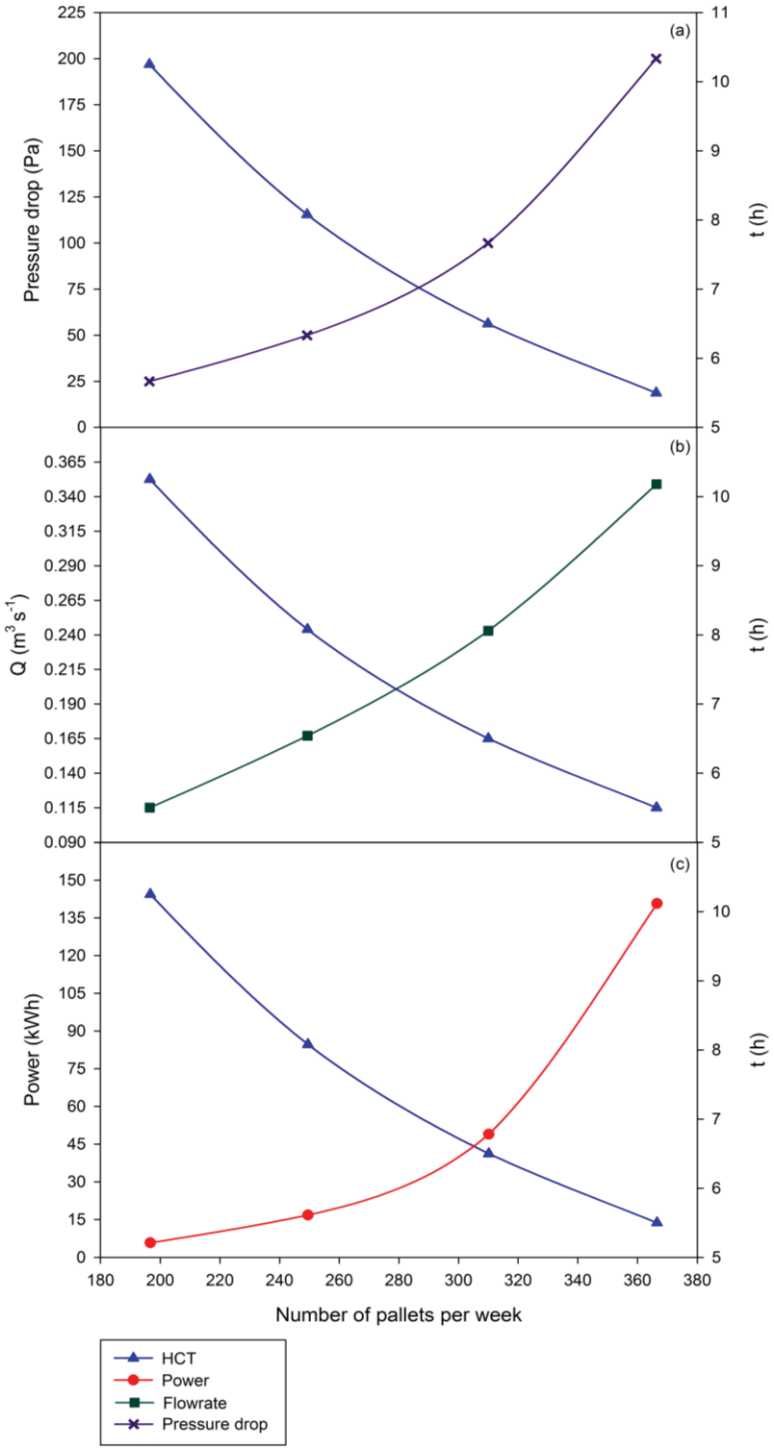

Figure 8.2. HCT of slowest cooling MBP and no. of pallets that can be cooled to this HCT per week against (a) pressure drop per pallet (b) flowrate per pallet and (c) total power requirement.

8.5 Significant factors affecting the cooling performance

Along with finding the optimal operating conditions to use in an industrial setting the numerical model allows the response of the system to successively doubling the pressure drop (25, 50, 100 and 200 Pa) to be analysed in terms of a reduction in HCT for each MBP.

8.5.1 Impact of air flowrate and pressure drop on the cooling performance

The largest reduction in average HCT for the pallet layer, 1.26 h (18 %), occurred for a pressure drop increase from 25 Pa to 50 Pa (Table 8.1). The reduction in average pallet layer HCT was 1.02 h (17 %) when the pressure drop was doubled from 50 Pa to 100 Pa, and only 0.58 h (< 12 %, the effective maximum) for an increase in pressure drop from 100 Pa to 200 Pa. The relative increase in flowrate remained constant, at approximately 31 %, between each of the tested conditions. Hence, a pressure drop of 100 Pa (0.243 L kg^{-1} s^{-1}) was considered the effective maximum.

Table 8.1. HCT, and the relative reduction in HCT, between the tested pressure drops/air flowrates for MBPs 1 – 7 in a pallet layer

		HCT (h)							
Δp (Pa)	**Q (L kg^{-1} s^{-1})**	**MBP 1**	**MBP 2**	**MBP 3**	**MBP 4**	**MBP 5**	**MBP 6**	**MBP 7**	**Pallet $layer_{avg}$**
25	0.115	4.17	5.83	7.50	8.58	5.17	7.50	10.25	7.19
50	0.167	3.75	4.92	6.00	6.75	4.58	6.25	8.08	5.93
100	0.243	3.42	4.17	4.83	5.35	4.08	5.17	6.50	4.93
200	0.349	3.25	3.75	4.25	4.58	3.75	4.58	5.50	4.35
		Relative reduction in HCT (%) between successive pressure drop increases							
25	0.115	–	–	–	–	–	–	–	–
50	0.167	10.1	15.6	20.0	21.3	11.4	16.7	21.2	17.5
100	0.243	8.8	15.2	19.5	20.7	10.9	17.3	19.6	16.9
200	0.349	5.0	10.1	12.0	14.4	8.1	11.4	15.4	11.8

As discussed in sections 4.5 and 4.6, while other heat transfer mechanisms occur, forced convection has a substantial impact on the cooling rate of polylined horticultural produce. Forced-convection cooling mainly occurs between the polyliner and refrigerated airflow pulled through the pallet. Differences in HCT due to forced-convection cooling result from changes to the heat transfer coefficient (h.t.c) and/or the temperature difference between the cooling air and the polyliner. Reductions in HCT of MBPs 1 and 5 are largely associated with an increase in h.t.c as the air temperature entering the MBPs was effectively constant, due to the MBP location at the front of the pallet. The HCT for MBPs 1 and 5 were at an effective maximum (< 12 % improvement for each successive pressure drop increase; Table 8.1). This suggests that the comparatively larger reductions in HCT for MBPs 3, 4, 6 and 7 were largely due to the temperature gradient between the fruits and the air forced through these MBPs.

The h.t.c, between the effective polyliner surface and the refrigerated airflow, increased relatively linearly between the tested air flowrates, for each individual MBP (Figure 8.3). The h.t.c. was higher in the central MBPs as the higher vent area orientated to the incoming refrigerated airflow, compared to the MBPs at the side of the pallet, allowed a higher percentage of the airflow to flow through these MBPs. From the proportional and linear increase in h.t.c. for the MBPs it could be hypothesised that the differences observed in their relative rates of cooling as the airflow was increased should be associated with the increased temperature gradient between the refrigerated airflow and the kiwifruit, particularly for the MBPs located at the back of the pallet.

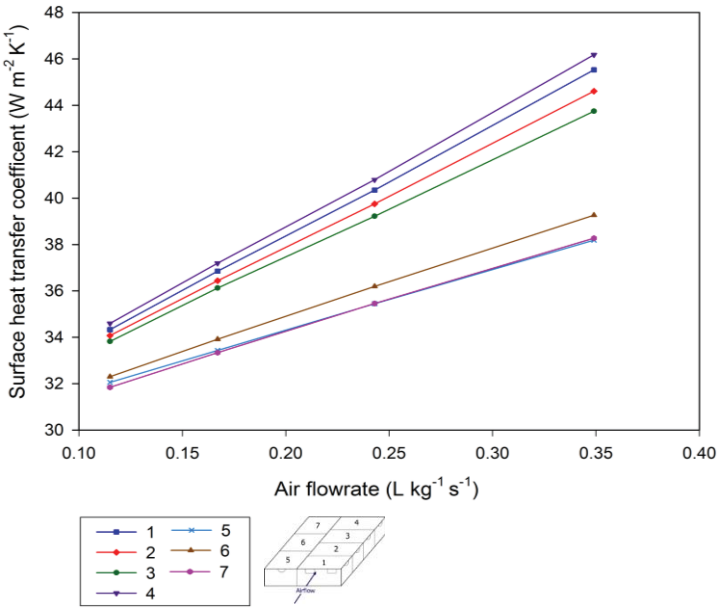

Figure 8.3 Average wall function surface heat transfer coefficients between the refrigerated airflow and effective polyliner surface

If the air and kiwifruit mixture inside the polyliner is considered as a lumped parameter Fluent can calculate the Biot number from the average temperature of the refrigerated air in the MBP ($T_{air\text{-}MBP}$), the average temperature at the polyliner surface ($T_{polyliner\text{-}MBP}$) and the temperature at the centre of the enclosed space in the polyliner ($T_{centre\text{-}MBP}$). Using MBP 1, at the pallet average HCT (4.93 h) and flowrate of 100 Pa, as an example the Biot number is calculated as (Davies, 2011),

$$Bi = \frac{\left(T_{centre} - T_{polyliner}\right)}{\left(T_{polyliner} - T_{air}\right)} = \frac{(13.5 - 1.9)}{(1.9 - 0.8)} = 10.5$$

The high Biot number demonstrates that the resistance to heat transfer within the enclosed space of the polyliner is high relative to the resistance presented by the forced convection process at the surface of the polyliner, which is in direct contact with the refrigerated airflow. The high resistance within the polyliner limits the impact of increasing the air flowrate, and subsequently forced convective heat transfer rate, as the

low heat transfer rate within the polyliner will persist at high flowrates and limit the improvement to cooling rate.

8.5.2 Impact of air temperature on the cooling performance

Increasing the pressure drop reduced the increase in air temperature as the air was pulled through the pallet layer (Figure 8.4). At 25 Pa the air temperature entering MBP 7 was 7.2 °C after 4 h of cooling, with a corresponding HCT for MBP 7 of 10.25 h (Table 8.1). At 50 Pa, 100 Pa and 200 Pa the air temperature entering MBP 7, after 4 h, were 5.5 °C, 3.8 °C and 2.8 °C, respectively. The corresponding HCT for the MBPs were 8.08 h, 6.50 h and 5.50 h.

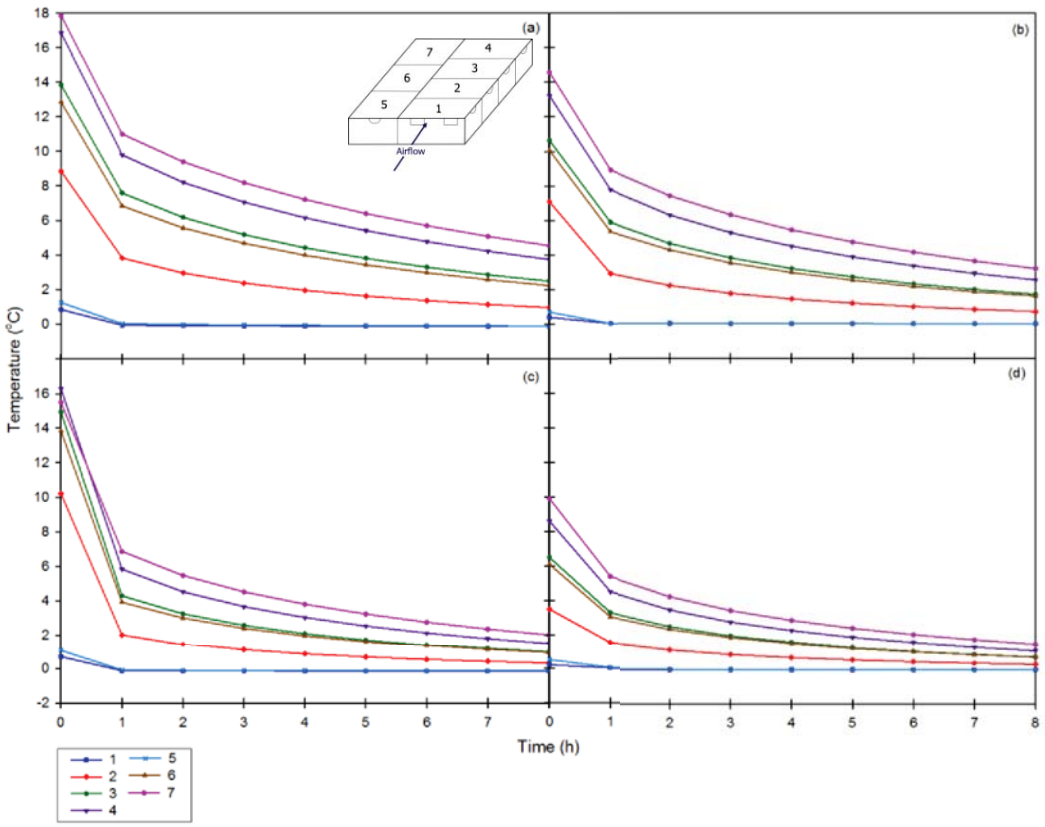

Figure 8.4. Average air temperature at the inlet vents (perpendicular to the incoming refrigerated air pulled through the pallet layer) for MBPs 1 – 7 at pressure drops of (a) 25 Pa (0.115 L kg^{-1} s^{-1}), (b) 50 Pa (0.167 L kg^{-1} s^{-1}), (c) 100 Pa (0.243 L kg^{-1} s^{-1}) and (d) 200 Pa (0.349 L kg^{-1} s^{-1}).

The relatively large increase in the cooling rate of MBPs 3, 4, 6 and 7 (compared to MBPs 1 and 5) for successive pressure drop increases suggest that the improvements to HCT were primarily driven by the air temperature entering the MBPs. These results indicate that the cooling process may be improved (i.e. become more uniform) by delivering cooler air to the warmest MBPs.

8.6 Air flowrate and temperature distribution within the pallet

This numerical model allows for an in-depth analysis of the airflow and temperature distribution within the MBPs during forced-air cooling. This detail can be used to inform the researcher of the primary heat transfer pathways and how potential design features might alter the cooling performance. Results are discussed for a flowrate of 0.243 L kg^{-1} s^{-1} as this was the optimal condition found (section 8.4.1).

8.6.1 Air flowrate and temperature distribution within MBPs

The airflow distribution within each MBP caused relatively high air velocities immediately behind the inlet vents of each MBP that quickly dissipated along and across the package (Figure 8.5). The airflow distribution causes a corresponding distribution in air temperature within the MBPs.

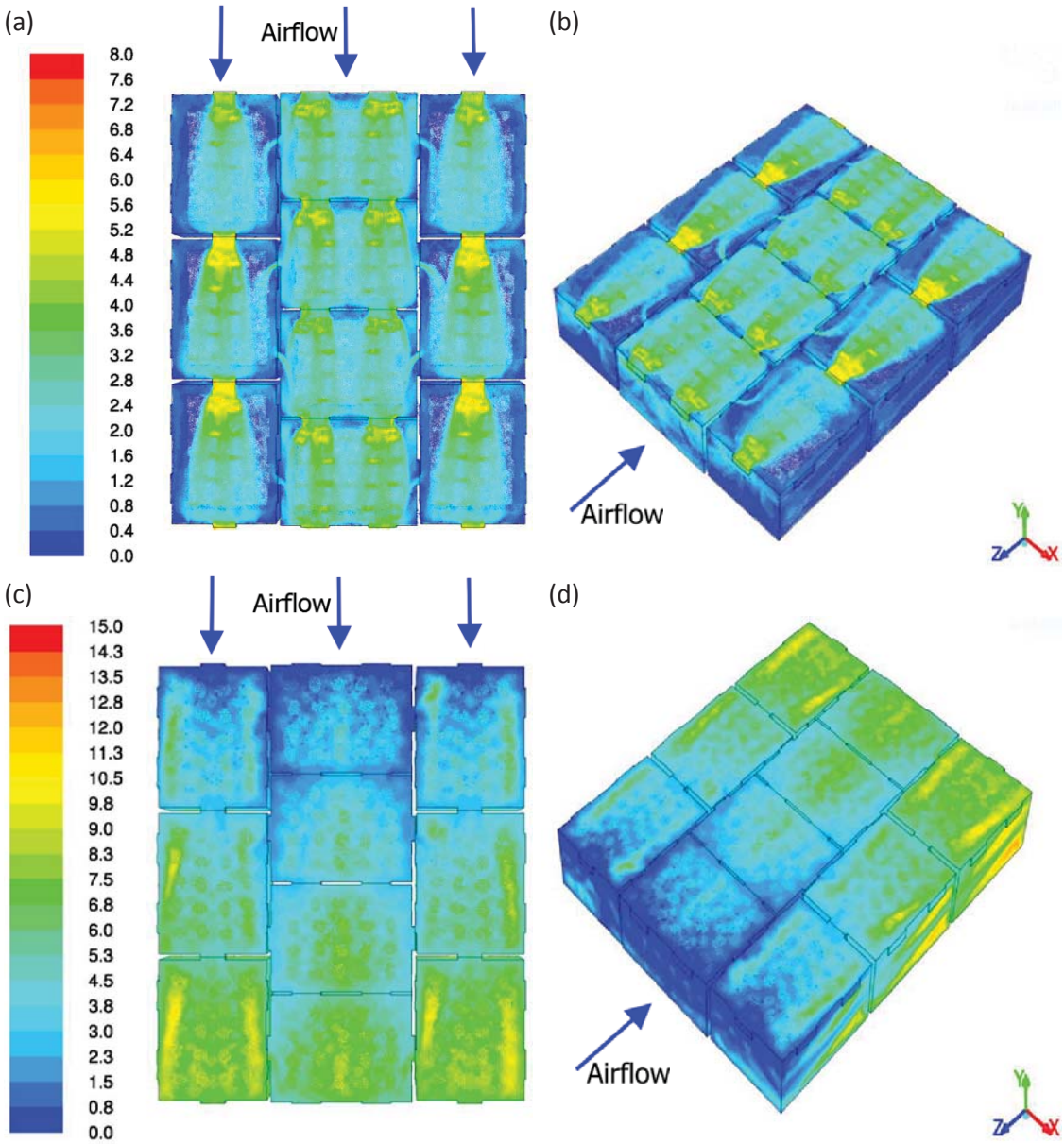

Figure 8.5. Distribution of air velocities (m.s^{-1}) for an (a) top-down view and (b) isometric view, and air temperatures (°C) for an (c) top-down view and (d) isometric view. Images were taken after 2 h of forced air cooling for a pressure drop of 100 Pa (0.243 L kg^{-1} s^{-1}).

Both the airflow distribution and air temperature within each MBP impacted upon the kiwifruit temperatures. After 4.93 h (average pallet HCT) of forced-air cooling the kiwifruit in contact with the polyliner at the location of high air velocities had lower surface temperatures than the adjoining kiwifruit (Figure 8.6). As the temperature of the air increased the temperature of the kiwifruit increased from the front to the back of the pallet. For kiwifruit towards the centre of the fruit bulk, cooling occurred primarily via

conduction or natural convection. As expected, kiwifruit in the centre of the MBP cooled relatively slowly. This created large temperature gradients between the kiwifruit, within each MBP (Figure 8.6).

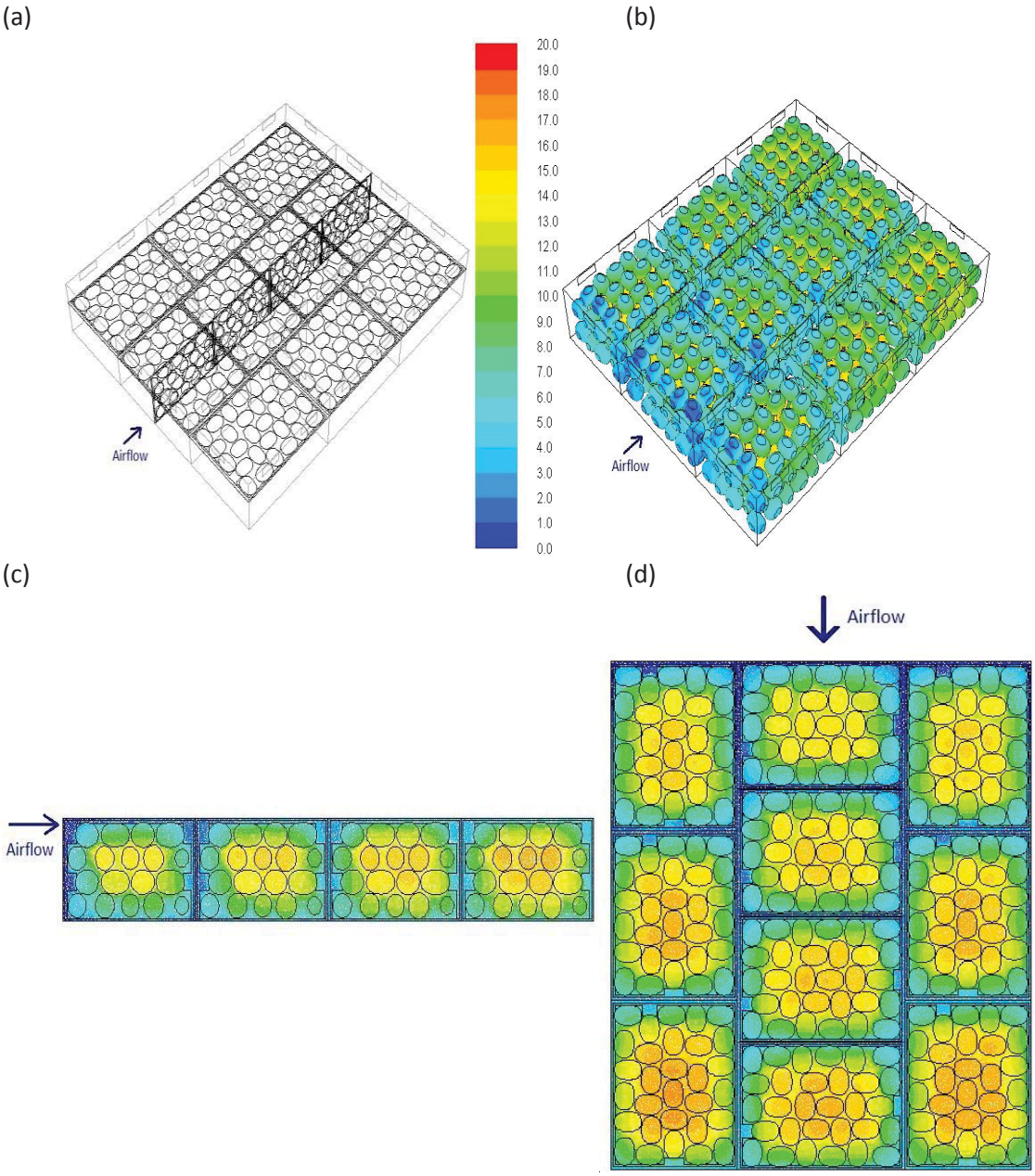

Figure 8.6. (a) Location of vertical and horizontal cross-sectional area through the pallet layer. Temperature distribution (°C) for (b) an isometric view of the kiwifruit temperature in each MBP, along the (c) vertical and (d) horizontal cross-sectional area, after 4.93 h (average pallet layer HCT) of forced air cooling for a pressure drop of 100 Pa (0.243 L kg^{-1} s^{-1}).

8.6.2 Air flowrate and temperature distribution between MBPs

At a pressure drop of 100 Pa (0.243 L kg^{-1} s^{-1}) 55.2 % of the airflow entering the front of the pallet flowed into MBP 1, located in the centre (Figure 8.7). The remaining 44.8 % was split evenly between MBPs 5 and 8, located at the side of the pallet. The airflow was pulled from the front to the back of the pallet with only a small exchange of airflow (< 3.9 %) between MBPs located along the centre and side of the pallet when the vents aligned. There was a net transfer of air from MBP 1 to 5, MBP 2 to 6, from MBPs 6 to 3 and from MBPs 7 to 4 (Figure 8.7). For the airflow through the centre of the pallet (MBPs 1 – 4) there was net increase of 0.9 % between the percentage of total airflow pulled through the entrance vents of MBP 1 (at the front of the pallet) and the exit vents of MBP 4 (at the back of the pallet). From a design modification standpoint manipulation and possible creation of additional alignment between the various vents between MBPs offers the potential for control of the location and quantity of airflow exchanged between MBPs.

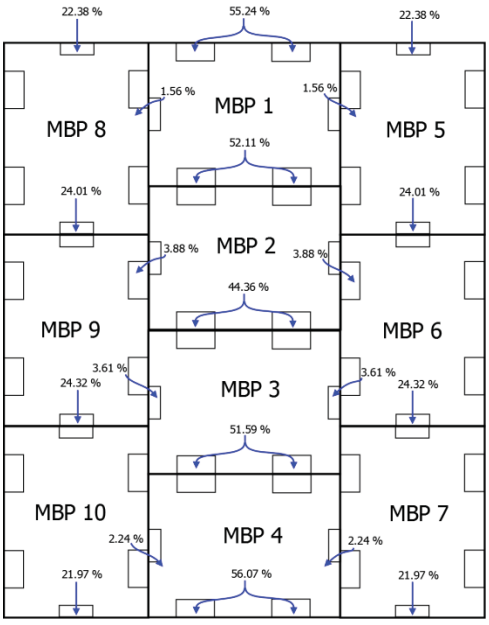

Figure 8.7. Volumetric flowrate (L kg^{-1} s^{-1}) distribution between MBPs (total entering and exiting the pallet layer of 100 %)

8.7 Alternative MBP design

For CFD based design studies the complementary information from experiments and numerical studies should be utilised (Defraeye et al., 2013b). Over the course of this dissertation a combination of experimental and numerical results have lent information towards understanding how any potential design modifications may impact the cooling performance. Primarily:

- The cooling rate of the MBPs decrease from the front to the back of the pallet, corresponding to the increase in air temperature as it is pulled through the pallet.
- Due to MBP orientation there is an uneven airflow distribution entering the MBPs at the front of the pallet, which affects cooling rates between MBPs located at the centre and side of the pallet

The numerical studies have expanded the knowledge base to include the following:

- Increasing the air flowrate, beyond a relatively low threshold flowrate, has a reduced impact on the cooling rate.
- Faster cooling rates can be achieved by lowering the temperature of the airflow reaching the MBPs at the back of the pallet
- Within the pallet airflow can be exchanged between MBPs, on the side and centre of the pallet, when the vents align.

Based on the relative impact of air flowrate and temperature on the HCT of the MBPs an efficient method of improving the cooling performance of the pallet layer would be to redistribute the airflow within the pallet to deliver cool air to MBPs 3, 4, 6 and 7,

hence, improving cooling uniformity without having to increase the air flowrate and consequently fan power requirements.

This section aims to propose a new MBP design that can be used to reduce the cooling heterogeneity in the pallet, by increasing the HCT of coolest MBP and reducing the HCT of the warmest MBP.

8.7.1 Geometry

There are various limitations associated with any alternative MBP design. The design cannot cause significant mechanically weaknesses to the box. The polyliner must remain, so as to prevent moisture loss. Any new MBP must be simple to implement in an industrial environment (i.e. it would not be very practical to suggest 10 different box types for each MBP location within the pallet as this would lengthen the time taken to package the fruit, following harvest). Also the more complicated the system the increased likelihood that something will go wrong. Ideally, an alternative box design will prioritise cooling uniformity (i.e. reduce the difference in average kiwifruit temperature between different MBPs) over improved cooling rate, as cooling uniformity is better for fruit quality.

The proposed alternative box design and pallet layout is a two pronged approach, focused on controlling the airflow distribution within the pallet layer. In the pallet layer the current box design can be retained for MBPs 1, 2, 3, 4, and 7, while a new box design is used for MBPs 5 and 6. The new box design has additional vents on the end faces of MBPs 5 and 6. Increasing the overall vent area perpendicular to the incoming

refrigerated airflow, in the new design allows a higher volumetric airflow to be forced through MBPs 5 and 6. The additional vents are located near the edges of the box so as to create airflow channels between the polyliner and inner walls of the box, delivering cool air along the side of the pallet towards MBP 7. However, simply utilising the new design for each MBP will further lower the airflow resistance through the side of the pallet. With less air flowing through the centre of the pallet the air temperatures pulled through the centre will increase. This will lengthen the HCT of MBPs 1 – 4. While MBP 1 and 2 would most likely still cool at similar rates to MBP 5, due to their proximity to the incoming refrigerated airflow, MBP 4 would become the slowest cooling MBP. Hence, the new design would fail to improve cooling uniformity. Instead the current design is retained for MBP 7. This diverts the cool air channelled through the left-hand side (LHS) of MBP 6 into MBP 3 and subsequently MBP 4, while MBP 7 benefits from the cool air channelled through the right-hand side (RHS) of MBP 6 (Figure 8.8).

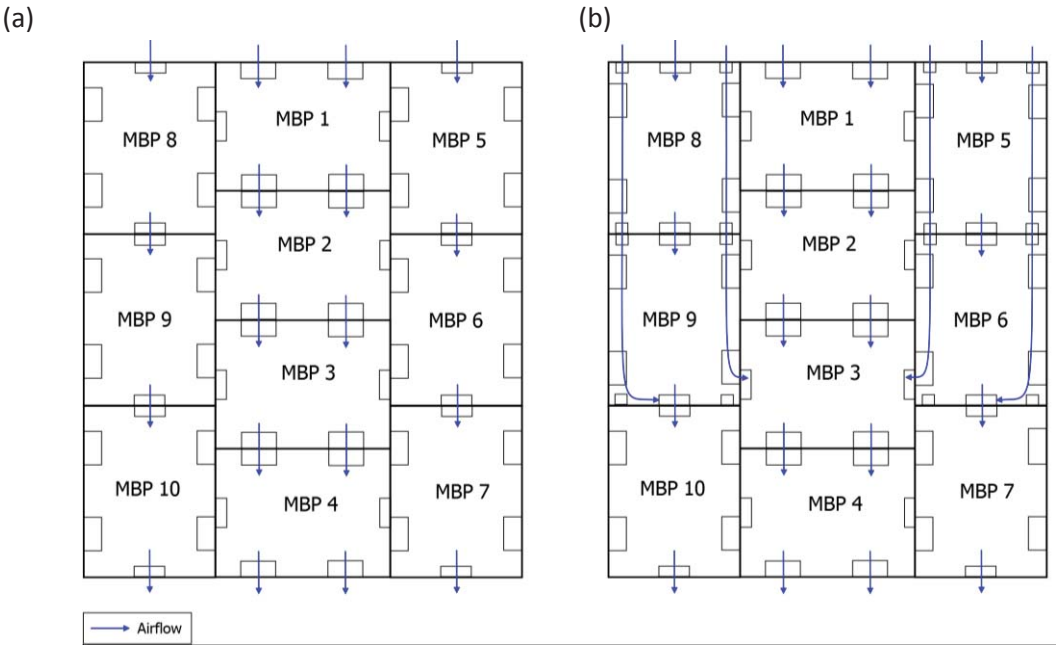

Figure 8.8. Conceptual sketch of the primary airflow pathways through (a) current and (b) new box design.

For the new box design the additional vents on the end faces have a total open area of 12.5 cm^2; approximately doubling the existing open area on the end faces of MBPs 5 and 6 (Figure 8.9(b)). They are placed 1.4 cm in from the box edges, so as not to unduly mechanically weaken the box. The hand vents for MBPs 5 and 6 are not orientated towards the incoming airflow. As such they do not play a significant role in airflow distribution within the corresponding MBPs. Hence, the hand vents in the new box design can be moved towards the box edges and extended slightly (0.8 cm) in length. The hands vents are 4.1 cm in from the edge of the box for MBPs 5 and 6 (Figure 8.9(b)) compared to 6.5 cm for the current design (Figure 8.9(a)). This increases the open area cross over between the hand vents of MBPs 6 and the end vents of MBP 3, forcing more air through MBP 3, and subsequently MBP 4. By combining two different box designs the alignment of vents between central and side MBPs is modified. This alignment, hence airflow exchange between MBPs, is limited at the front (between MBP 5 and 1, and MBP 6 and 2) and increased towards the back of the pallet (between MBP 6 and 3).

It is important to note that the numerical model used geometrical simplification to replace the hemispherical end vents in the current box design with an effective (rectangular) vent area. When manufacturing the box for use in industry the rectangular design for the end vents should be implemented, to achieve the same exchange of airflow between MBPs due to vent alignment.

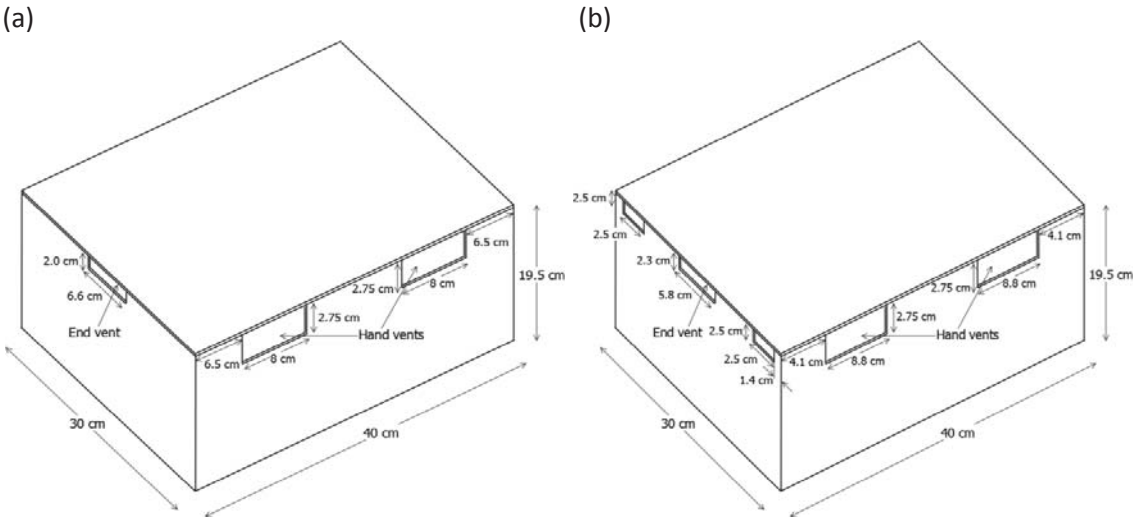

Figure 8.9. Schematic diagram for (a) the current box and (b) alternative box for MBPs 5 and 6

8.7.2 Comparison methods

When considering any change to the package design it is important to note that modifying the vent area of some or all of the MBPs will also change the airflow-pressure drop relationship across the pallet. Maintaining the pressure drop for the comparison will result in a higher volumetric flowrate through the new pallet design, as the more ventilated MBPs will have less resistance to airflow. While at constant flowrate the refrigerated airflow will have the same cooling capacity. Hence, a more direct analysis of the package design features and the impact of redistributing the same quantity of refrigerated air on the cooling rate and uniformity of the pallet will be generated.

8.7.3 Results

For the numerical simulations the cooling profiles for the new pallet composition were first compared at a constant flowrate and then at a constant pressure drop, across the pallet. Airflow distribution between pallet compositions was compared at a constant

flowrate. A flowrate of 0.243 L kg^{-1} s^{-1} and pressure drop of 100 Pa (the optimal operation conditions found in section 8.4.1) were the constant values used.

8.7.3.1 Airflow distribution

The air distributed as expected in the new box design and pallet composition. Due to the additional vent areas on the end faces of MBPs 5 and 6 only 38.7 % of the airflow entered the pallet layer through MBP 1, compared to 55.24 % in the current set-up (Figure 8.10). The airflow exchange between MBPs 1 and 2 and the side MBPs (5 and 6) was < 1.4 % in the new design (down from 3.9 % in the current design). Retaining the current design for MBP 7 reduced the area available for airflow between MBPs 6 and 7. This caused a large percentage (7.9 %) of the airflow to seek a path of lower resistance, by flowing from MBP 6 to MBP 3. Only 3.6 % of the airflow transferred from MBP 6 to 3 in the current design.

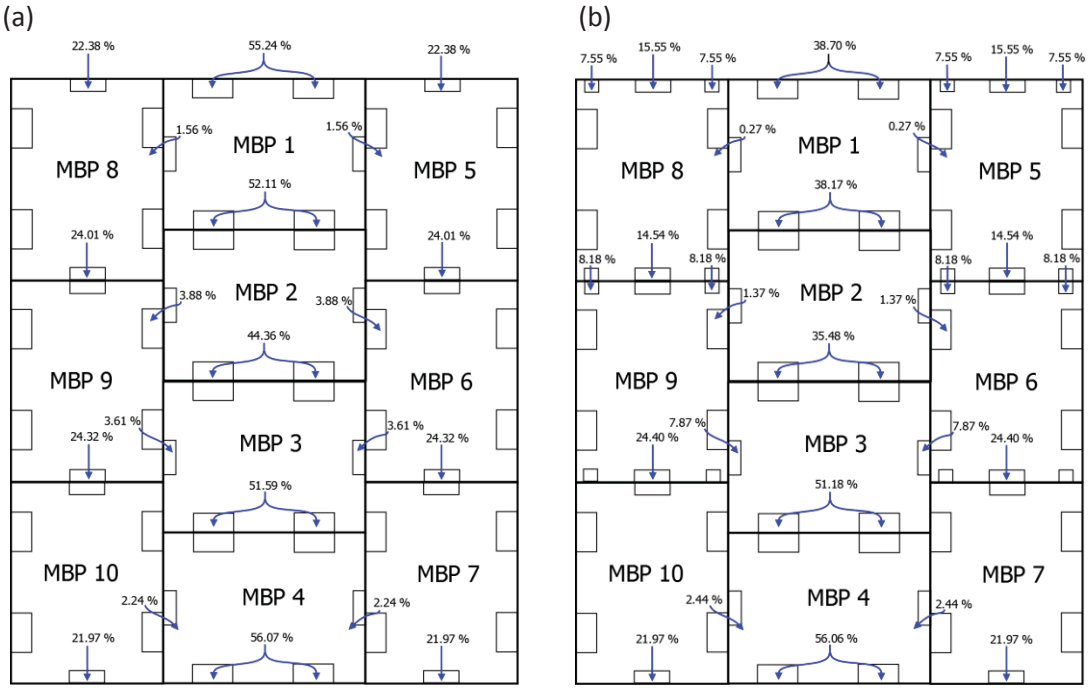

Figure 8.10. Airflow distribution (total though pallet layer of 100 %) through each MBP for (a) the current and (b) the new box design

8.7.3.2 Constant volumetric flowrate

Keeping the flowrate (0.243 L kg^{-1} s^{-1}) constant between the current and new box design resulted in similar HCTs (Table 8.2). However, more uniform cooling (i.e. the difference in HCT between the coolest and warmest MBPs) was observed. The HCTs of MBPs 1, 2, 3, 4 and 6 increased, while the HCTs of MBP 5 and 7 were reduced. It might be expected that the HCT of MBP 6 would also decrease. Although, in total, more air was forced through MBP 6 (including additional end vents) in the new design (30.9 % compared to 24.0 %; Figure 8.10) a significant percentage (7.9 %) flowed into MBP 3, reducing the amount of air available to cool the fruit in MBP 6. The warmest MBP (MBP 7) improved its HCT by 0.25 h, while the HCT of the coolest MBP (MBP 1) increased by 0.33 h, improving cooling uniformity (Table 8.2).

Table 8.2. HCT for each MBP and the pallet layer average for the current box design and the new box design. Comparisons are provided at both constant flowrate and constant pressure drop.

			HCT (h)							
Box types	**Δp (Pa)**	**Q (L kg^{-1} s^{-1})**	**MBP 1**	**MBP 2**	**MBP 3**	**MBP 4**	**MBP 5**	**MBP 6**	**MBP 7**	**Pallet $layer_{avg}$**
Current	100	0.243	3.42	4.17	4.92	5.33	4.08	5.17	6.50	4.93
With new design	76	0.243	3.75	4.67	5.33	5.50	4.00	5.25	6.25	5.03
With new design	100	0.280	3.58	4.33	4.92	5.08	3.83	4.92	5.83	4.71

The most important result from the new box design and pallet composition is the improvement in the overall cooling uniformity of the pallet. The temperature difference between the coolest and warmest MBPs shows the improvement at any time in the cooling operation (Figure 8.11). After 5 h (the approximate average pallet layer HCT) of cooling the temperature difference between MBP 1 and MBP 7 was 3.4 °C for the new box design, an improvement of 19 % over the current design.

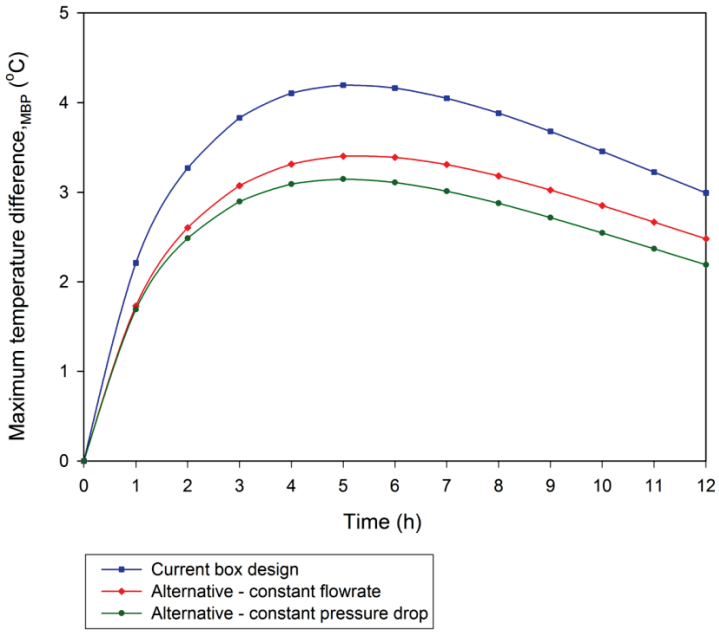

Figure 8.11. Maximum difference between average MBP temperatures in the pallet layer for the current design and alterative design tested at a constant flowrate (L kg^{-1} s^{-1}) and pressure drop (Pa).

8.7.3.3 Air temperature profile across pallet

The temperature profile of the air measured at the original (excluding the additional vent areas) vents in both box designs remained similar (Figure 8.12). The new box design did not negatively affect the air temperature entering each MBP. Hence, the channelled airflow was able to improve the cooling of the warmest MBPs without having to compensate for higher air temperatures entering the original vent areas due to the new box design.

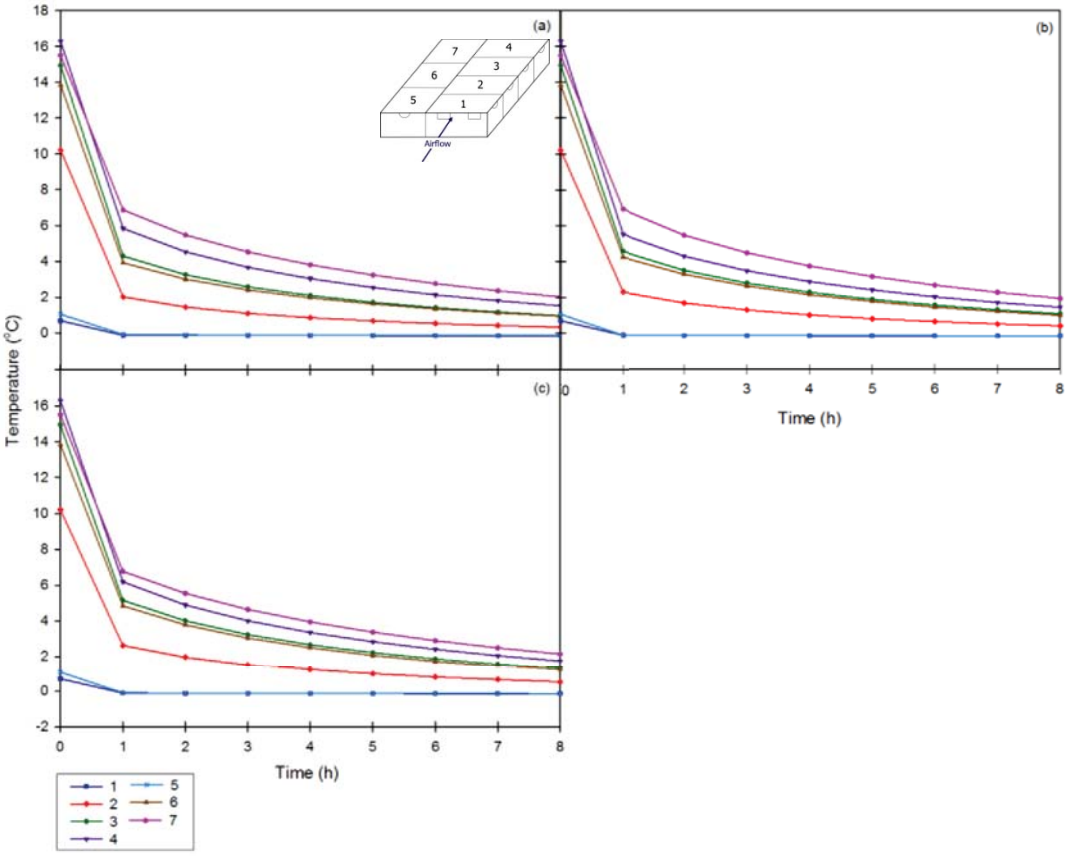

Figure 8.12. Average air temperature at the primary vents (not the newly created vents) orientated towards to the incoming refrigerated air pulled through (a) the current box design (b) the new box design at the same pressure drop and (c) the new box design at the same flowrate.

8.7.3.4 Air flowrate and temperature distribution within MBPs

The new box design created high air velocities along the newly created channels at the end faces of MBPs 5 and 6 (Figure 8.13). These high air velocity pathways delivered cool air to the MBPs located centrally and at the back of the pallet. MBP 3 and subsequently MBP 4 received cool air channelled along the LHS of MBP 6 and into MBP 3. The cool air channelled along the RHS and to the back of MBP 6 helped cool the kiwifruit in MBP 7.

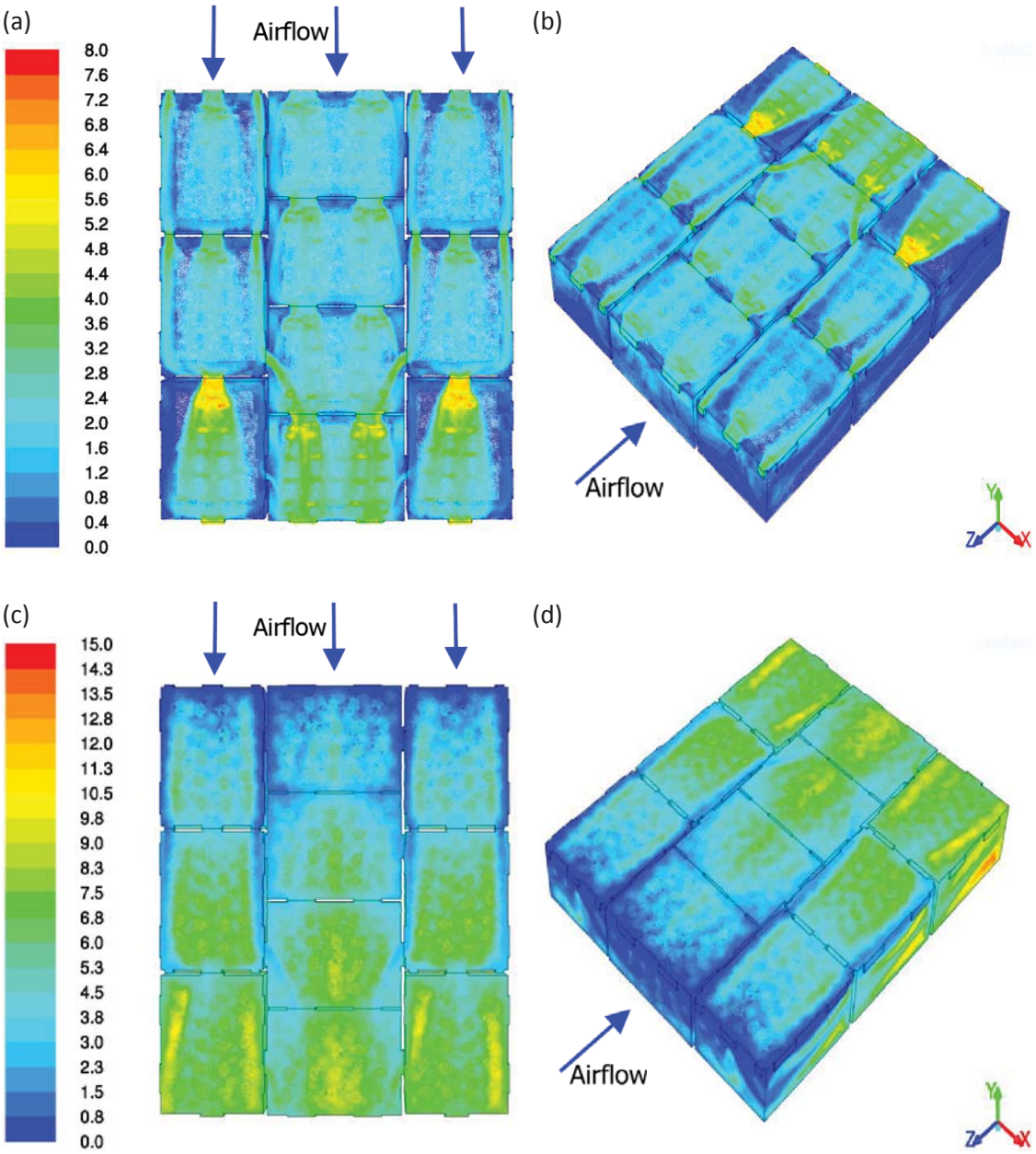

Figure 8.13. Distribution of air velocities ($m.s^{-1}$) for the new box design for an (a) top-down and (b) isometric view, and air temperatures (°C) for an (c) top-down and (d) isometric view. Images were taken after 2 h of forced air cooling for a pressure drop of 76 Pa (0.243 L kg^{-1} s^{-1}).

After 5.03 h (average pallet HCT) of forced-air cooling the high air velocities along the sides of MBP 5 and 6 and into MBP 3 and 4 caused cooler kiwifruit temperatures along the sides of the corresponding MBPs (Figure 8.14) compared to the primarily front to back cooling of the current box design (Figure 8.6). The channelling of cool air along the RHS to the back of MBP 6 (Figure 8.13) cooled the kiwifruit at the back of MBP 6

(Figure 8.14). The kiwifruit at the front of MBP 7 were cooled (via conduction) due to their proximity to the kiwifruit at the back of MBP 6.

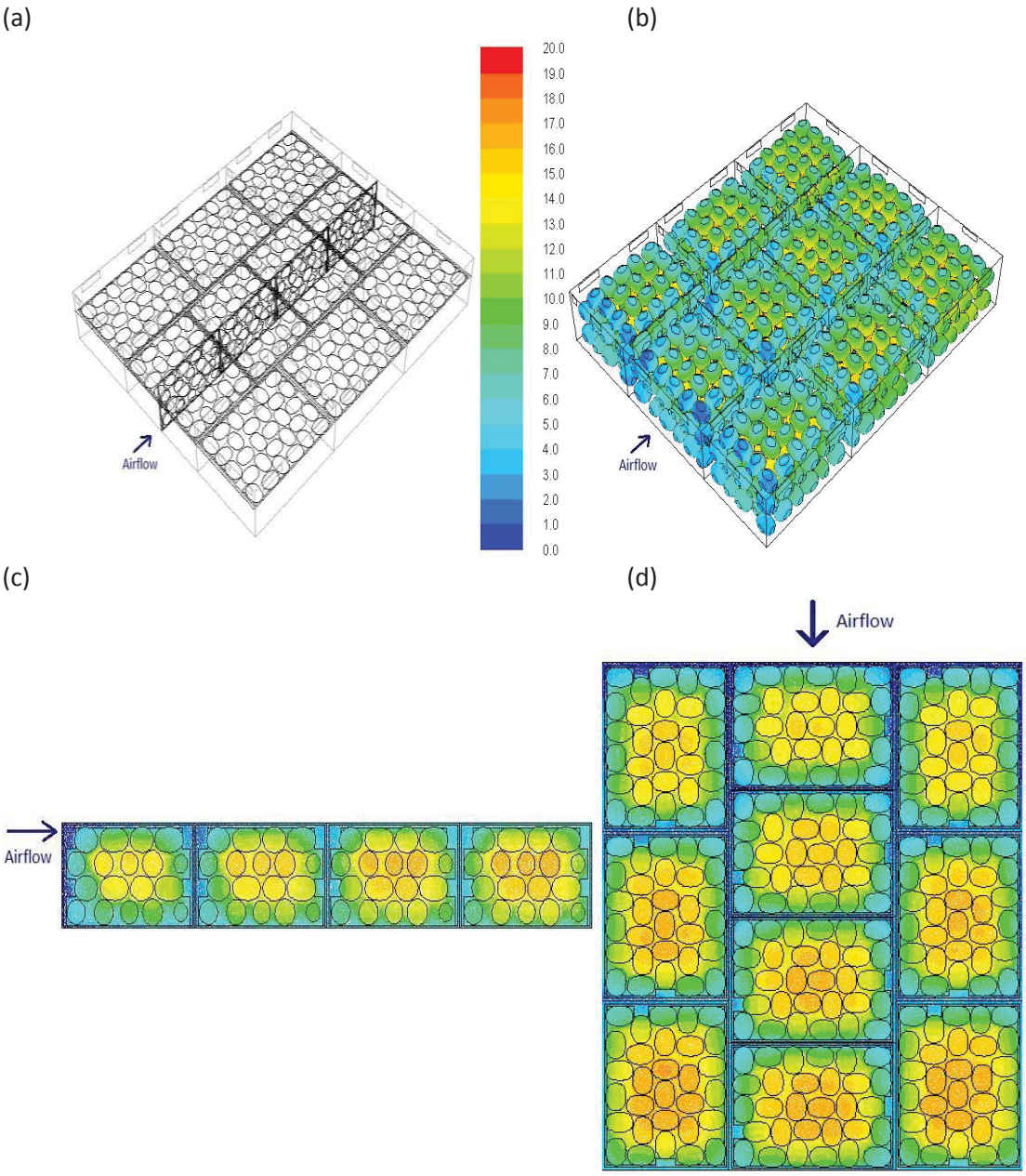

Figure 8.14. (a) Location of vertical and horizontal cross-sectional area through the pallet layer with the new design. Temperature distribution (°C) for (b) an isometric view of the kiwifruit temperature in each MBP, along the (c) vertical and (d) horizontal cross-sectional area, after 5.00 h (average pallet layer HCT) of forced air cooling for a pressure drop of 76 Pa (0.243 L kg^{-1} s^{-1}).

8.7.3.5 Constant pressure drop

When a constant pressure drop of 100 Pa was maintained the flowrate pulled through the new pallet composition increased to 0.280 L kg^{-1} s^{-1}, or by 13 % (Table 8.2). The average pallet HCT improved from 4.93 h to 4.71 h. The HCT of MBP 7 (warmest MBP) improved by 0.87 h and the HCT of MBP 1 (coolest MBP) increased by 0.16 h, for an overall improvement to cooling uniformity. After 5 h of cooling the temperature difference between MBP 1 and 7 was 3.1 °C, an improvement of 26 % over the current design (Figure 8.11).

8.7.3.6 Energy inputs

The relationship between airflow, pressure drop, energy requirement, HCT and pallet throughput per week was improved in the new box design (Figure 8.15). Along with improving cooling uniformity the new box design required a much lower pressure drop (76 Pa) to generate the same flowrate (0.243 L kg^{-1} s^{-1}) as the current design. The lower HCT time of slowest cooling MBP increased the number of pallets that could be cooled per week from 310 to 322, while reducing the total energy input from 49.0 kWh to 37.2 kWh. Estimating the cost of electricity for industry at 11.98 c/kWh (Ministry of Business, Innovation and Employment, 2015) than the operating cost per tunnel cooler per week is NZ $ 453 for 322 pallets. This leads to a saving of NZ $ 141 over the current MBP design, with an additional 12 pallets also cooled per week. Scaling up to an industry wide application in New Zealand and the forced-air cooling of 0.35 million pallets (section 8.4.1) gives an estimated costing of NZ $ 0.5 million for the new box design, when operating at constant pressure drop. Hence, switching to the new design

offers a potential saving, using an extremely conservative estimation of electricity requirements to power the fan, of NZ $ 0.2 million annually, across the entire industry. At constant pressure the number of pallets that can be cooled per week increased from 310 to 345, with an increase in total energy use of 49.0 kWh to 56.4 kWh.

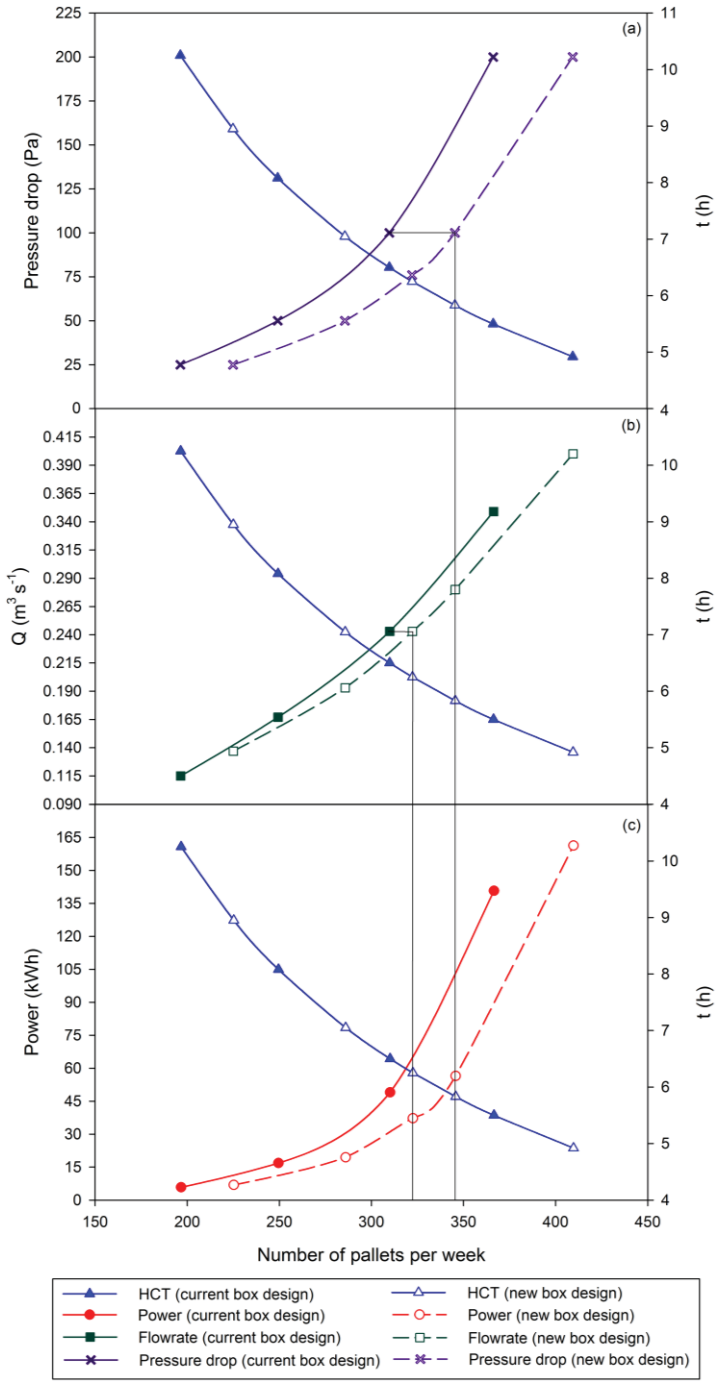

Figure 8.15. HCT of slowest cooling MBP and no. of pallets that can be cooled to this HCT per week, for the current and new box design against (a) pressure drop per pallet (b) flowrate per pallet and (c) power requirement. Data for current box design is reproduced from Figure 8.2.

8.8 Conclusions

The numerical model is a valuable research tool in understanding and improving the cooling process for polylined horticultural produce. The model has identified a pressure drop of 100 Pa and corresponding flowrate of 0.243 L kg^{-1} s^{-1} as the optimal point to ensure rapid cooling of the kiwifruit without incurring excessive operating costs to run the fan.

Beyond a relative low threshold flowrate (0.243 L kg^{-1} s^{-1}) increases in flowrate are an ineffective method to improve the cooling rate and uniformity of the pallet. Instead the airflow distribution can be manipulated to deliver cool air to the warmest MBPs (located centrally and at the back of the pallet). An alternative box design, with additional vent areas, creating airflow channels along the side and into the middle of the pallet has been presented. This alternative box design has benefits at either constant volumetric flowrate (as an energy saving method) or at constant pressure drop (to increase the pallet cooling rate). Both methods improve the cooling uniformity. This allows the individual pre-cooling operator to decide on what to prioritise.

Chapter 9

Discussion

9.1 Introduction

This project has developed a numerical model that can describe and predict the temperature profiles of polylined modular bulk packs (MBPs) of horticultural produce undergoing forced-air cooling. This project takes advantage of the advances and availability in computational power and numerical software packages developed through the later part of the 20th century and the start of the 21st. Following validation the numerical model has determined the operating point (in terms of pressure drop and flowrate across the pallet) to ensure rapid cooling of the produce without incurring excessive operational costs due to the running of the fan equipment. A working numerical model allows for the testing of some alternative processing conditions, such as air temperature and flowrate, and some alternative design features in the construction of the MBP. The capability to numerically simulate the cooling performance of the MBP and system variations, unconstrained by the availability of product (horticultural harvest season) and without the expense and time requirement of physical prototype testing is an extremely beneficial research tool.

9.2 Output of project in terms of the wider field of postharvest research

This project has been completed at a time where similar numerical studies into rapid and uniform cooling of horticultural produce are being published globally. While the

product varies from table grapes (Delele et al., 2013a) and citrus fruit (Defraeye et al., 2013b, 2014; Delele et al., 2013b, 2013c) in South Africa to strawberries in the USA (Ferrua & Singh, 2011) and to solid polymer balls that can represent any spherical produce in Canada (Dehghannya et al. 2008, 2011, 2012) there is a clear movement towards utilising the recent advances and availability in computational power and numerical model packages as a primary research tool. A common theme to emerge from these geographically diverse labs is that the cooling performance (frequently defined as cooling uniformity, rather than average, fastest, or slowest cooling time) is best achieved via controlling the airflow distribution within the pallet layers. Whether it is lowering the airflow resistance by removing entire faces from the container (Defraeye et al., 2013b, 2014), changing the location and size of the various open areas (Dehghannya et al. 2008, 2011, 2012) or creating specific bypass routes to deliver cool air directly to the back half of pallet (Ferrua & Singh, 2011) the principle of controlling or improving the airflow distribution remains the same. The efficiency of the forced-air cooling process is determined by the rate and uniformity of product cooling in comparison to the energy input required (de Castro et al., 2004a, 2004b). It is no coincidence that lowering the airflow resistance through pallets of produce has the additional benefit of reducing the fan requirements to generate the same volumetric flowrate through the pallet and hence lower power requirements, which can be an important cost saving measure. Like the research described above this project has combining improved cooling uniformity, via controlled airflow distribution, with a reduction in power requirement.

This project does share some similarities with recent numerical models involving the forced-air cooling of ventilated horticultural produce (Defraeye et al., 2013b, 2014;

Dehghannya et al., 2008, 2011, 2012; Delele et al., 2009a, 2009b, 2013a, 2013b, 2013c; Ferrua & Singh, 2009a, 2009b, 2009c, 2011 and Tutar et al., 2009). However, this work is one of the first to address the issue of how to incorporate the presence of a polyliner. Partially, this is because polyliners are not used in the cool chains of all horticultural products. Some numerical models do exist for polylined produce, specifically table grapes (Delele et al., 2013a). However, in the work by Delele et al. (2013a) while the carton box may have been explicitly modelled the interior components (produce and polyliner bag) used the porous medium approach (section 2.3.1) and thus fail to provide much insight into the heat transfer mechanisms occurring within the polyliner. As such, there was little previous literature to refer to on how to address the problem of a polyliner and none existing (to the knowledge of the author) involving the creation within a computational fluid dynamics (CFD) modelling environment of an effective polyliner surface (combining the faces of the kiwifruit in contact with polyliner and the polyliner itself into one effective surface).

9.3 Specific challenges and data sets required in the project

When this project first started there was limited knowledge into the actual heat transfer process occurring within polylined horticultural produce during cooling. Although it is possible to estimate the relative importance of various heat transfer mechanisms using approaches based on dimensionless numbers (section 5.5.1), this sort of analysis is sensitive to the identification of characteristic dimensions and times that best represent the cooling process. However, it is not always clear which dimensions should be chosen. Often, the only choice is to use best guess values. For example, the high relative importance of vertical heat transfer between MBP stacked on top of each other was not

apparent. Unlike the cooling of produce without a polyliner there is no direct contact between refrigerated airflow and produce. As a result the conductive cooling through the base of the cardboard box, supplied by the airflow pulled through the MBP directly beneath has a greater influence on the overall heat transfer rate and must be included in the numerical model. This is not apparent to an analysis that (for example) only considers conduction within the radial dimension of individual fruit, or between the areas of contact between individual fruit.

As this project involves horticultural produce, experiments were limited to the kiwifruit harvest season, which only occurs once a year. Consequently, over the duration of this four year project there were only three harvest seasons to conduct experiments. The first two seasons were spent obtaining a detailed understanding of the heat transfer processes occurring during forced-air cooling. This knowledge was required as a numerical model can’t be built if the transport phenomena and relative importance of each method are unknown. For all practical purposes this left one kiwifruit season to conduct experiments, that reproduced the numerical boundary conditions, to validate the numerical model. The key data sets required, aside from the correct geometrical dimensions of the individual components, were both fruit and air temperatures, with respect to flowrate and pressure drop across the pallet.

9.4 Major findings of the study

9.4.1 Experimental

During forced-air cooling the half-cooling time (HCT) of the kiwifruit MBPs is dependent on their location within the pallet layer. Cooling primarily occurs from the front to the back of the pallet, relating to the air temperature entering each MBP. Changing the pallet orientation (i.e. rotating the pallet by 90 °) will not substantially change this temperature profile during cooling. As long as the air either absorbs heat as it passes through the package or mixes with warm air exiting the preceding packages it will warm up, reducing the cooling potential of the air reaching the back of the pallet. This is consistent with the findings of Ferrua and Singh (2009b) and Meana et al. (2005) for the forced-air cooling of strawberry clamshell packages.

MBPs are either located at the centre or side of the pallet. For MBPs located at the front of the pallet in the 1.0 m commercial orientation cooling rates showed no significant differences between the centre and side MBPs, despite flowrates over three times higher entering the centre MBP. This suggested that for polylined kiwifruit MBPs there is a threshold flowrate, above which the improvement to cooling will be minimal. Practically, there were a limited number of experiments that could be run for any given kiwifruit harvest season. However, the numerical model allowed a variety of flowrates to be tested to find the point where it is no longer efficient to increase the flowrate.

9.4.2 Numerical model

Along with corroborating the major findings of the experimental studies the numerical model found the threshold flowrate pulled through the pallet to be 0.243 L kg^{-1} s^{-1}. Above this flowrate diminished returns (< 12 %) in terms of relative improvement to average pallet layer HCT were observed. The threshold flowrate for polylined produce is likely to fall below the typical range recommended in industry (0.5 – 2.0 L kg^{-1} s^{-1}; Thompson, 2004) for the forced-air cooling of non-polylined horticultural produce. For example, De Castro et al. (2004a) showed that, for the forced-air cooling of non-polylined horticultural produce, increasing the air flowrate from 2 to 4 L kg^{-1} s^{-1} only reduced the HCT by a further 11 %, compared to a 26 % reduction in HCT when increasing the air flowrate from 1 to 2 L kg^{-1} s^{-1}.

When operating with polylined produce the polyliner prevents direct contact between the refrigerated air and the produce. The polyliner, which moulds to the roughly rectangular shape of the external fruit bulk, creates a much smaller surface area for the air to contact than the potential surface area if the refrigerated air flowed between and around each individual product. The polyliner also creates an enclosed space, consisting of air and the produce where the primary methods of heat transfer are natural convection and conduction, which both offer a high resistance to heat transfer, particularly when compared to the resistance to forced convective heat transfer at the polyliner surface. Increasing the air flowrate and improving the forced convective heat transfer rate will have a minimal effect on the natural convective and conductive heat transfer rates within the polyliner. Hence, a lower surface area for contact between refrigerated air and produce (or polyliner in this case) and relatively high resistance to heat transfer

within the polyliner, result in a lower optimal volumetric flowrate, than typically observed for non-polylined produce, likely being required to reach the effective cooling limit, beyond which relatively small improvements to cooling time for drastically increasing power requirements occur.

9.4.3 Improving cooling performance

For the forced-air cooling of ventilated packages of horticultural produce the optimal vent area is specific to each product (Pathare et al., 2012). For non-polylined produce the vent area can be as low as 6 % (Ladaniya & Singh, 2002) and 7 % (Delele et al., 2013c) for citrus fruit, up to 13 % for strawberry clamshells (Thompson & Knutson, 1997), and finally 25 % for apples and onions (Vigneault & Goyette, 2002a). Using polymer balls to represent horticultural produce de Castro et al. (2005) found the ideal open area range at 8 % to 16 %. However, for polylined horticultural produce the reported optimal vent area is lower, ranging from 2.5 % for peaches (Singh et al., 2003) to 5 % for table grapes (Aswaney, 2007). The total open area in kiwifruit MBPs is approximately 4 % (6 % on the hand vent faces). Hence, increases to this area are unlikely to improve cooling.

Uniform cooling promotes uniform produce quality (Dehghannya et al., 2010; Nahor et al., 2005). Hence one method of maintaining product quality through refrigerated storage is to improve cooling uniformity. Like the observations in laboratory experiments the numerical model showed the reliance of the MBPs at the back of the pallet on the delivered air temperature. In the numerical model, over half the total airflow pulled through the pallet flowed through MBP 1 (centrally located and at the

front of the pallet), with little airflow exchange between the centre and side MBPs throughout the pallet layer. Hence, an efficient option to improve the cooling uniformity of the pallet, and importantly the cooling rate of slowest cooling MBPs is to control the airflow distribution, and relative temperature increase of the air as it is pulled through the pallet layer.

The airflow can be improved by using two different box designs within the same pallet layer. One box design, situated along the sides and at the front of the pallet has additional open areas on the end faces to promote or channel an increased amount of airflow through the side of the box. After passing through a number of MBPs the relatively cool, channelled air is directed towards warmest MBPs (Figure 9.1). In the numerical model such a design was predicted to cool the product more evenly (i.e. the predicted HCT of the fastest and slowest cooling MBPs were relatively close to each other).

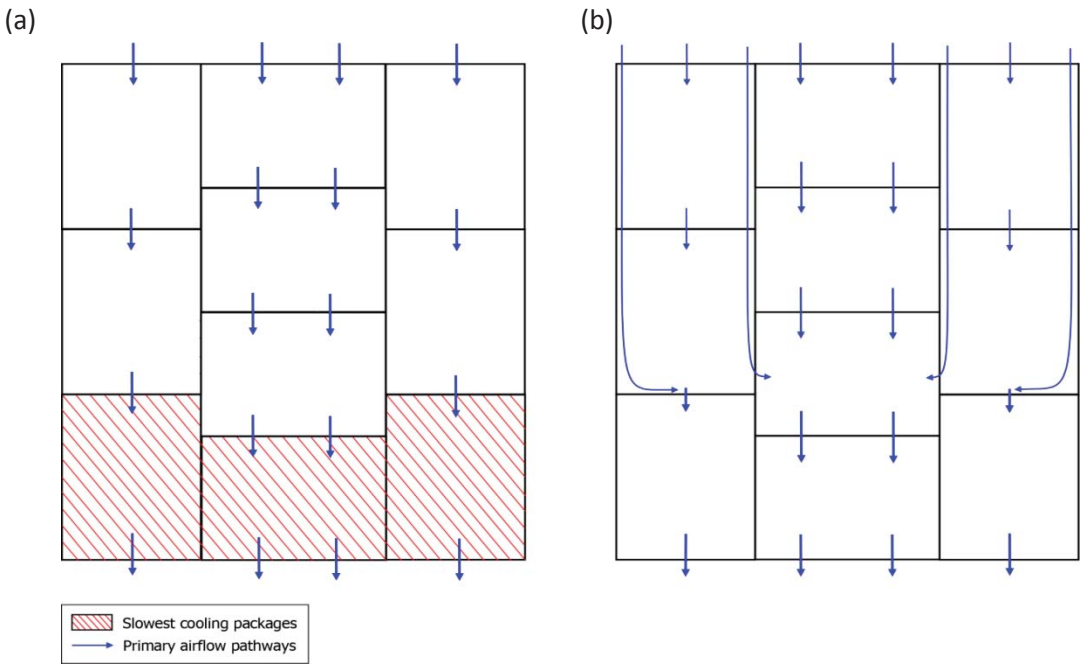

Figure 9.1. Conceptual model of the primary airflow distribution through a pallet layer of polylined horticultural produce (a) without and (b) with additional open areas to promote air bypass channelling through some packages at the side of the pallet

Dehghannya et al. (2008, 2011, 2012) found that changing the venting area alters the airflow distribution so that the amount of air in contact with the produce is changed. This can reduce the airflow distribution and subsequent cooling rates in a single package. However, poor or controlled airflow distribution within certain MBPs can aid in improving the overall cooling uniformity of the pallet. Work by Dehghannya et al. (2008, 2011, 2012) only focused on the cooling of a single package. However, if the research output of this project is to have a practical benefit to improving cooling operations in industry then it must consider an entire pallet layer.

The formation of air channels in polylined packages during forced-air cooling is not limited to kiwifruit. Delele et al., (2013a) reported that the polyliner in boxes of table grapes may have allowed cool air to bypass the fruit by forming airflow channels between the polyliner and the inner walls of the boxes.

This pressure drop is affected by the vent area of the packages (Delele et al., 2008; van der Sman, 2002; Vigneault et al., 2006). For a specific volumetric flowrate, the pressure drop across the pallet will decrease as the area available for airflow within it is increased. The new box design lowers the pressure drop required (and associated fan speed) to generate the same volumetric flowrate of air. This provides the option to either reduce the operating cost or generate a greater volumetric flowrate of air through the pallet with the existing fan system.

Using a numerical model for the forced-air cooling of citrus fruit, Defraeye et al. (2014) maintained a pressure drop across three different, non-polylined package designs. The air flowrate increased for the higher vent area packages and their HCTs improved,

agreeing with the observations from this project. When the flowrate was kept constant similar HCTs were reported for each of the three package designs. However, the designs with the larger vent areas required a lower pressure drop leading to reductions in the energy input required, in conformance with the option provided by the new box design presented in this project.

9.5 Application of numerical model findings

The cornerstone and industrial relevance of CFD based design studies is that improving the operating conditions and design features in CFD, with the aid of experimental results, will then lead to improvements that translate to and propagate throughout industrial operations. Therefore, the next logical step for this project is to construct a new box, containing the alternative design features that showed success in numerical simulations, and test its performance under industrial conditions. In terms of application in industry only one box needs to be manufactured. Removable pre-cuts can be built into the box, at the locations indicated (Figure 9.2a). When assembling the pallet the pre-cuts can be removed only on the desired MBPs (Figure 9.2b). This should minimise the complication in pallet assembly and not introduce unnecessary and time consuming complications that would be encountered if two completely different box designs were required.

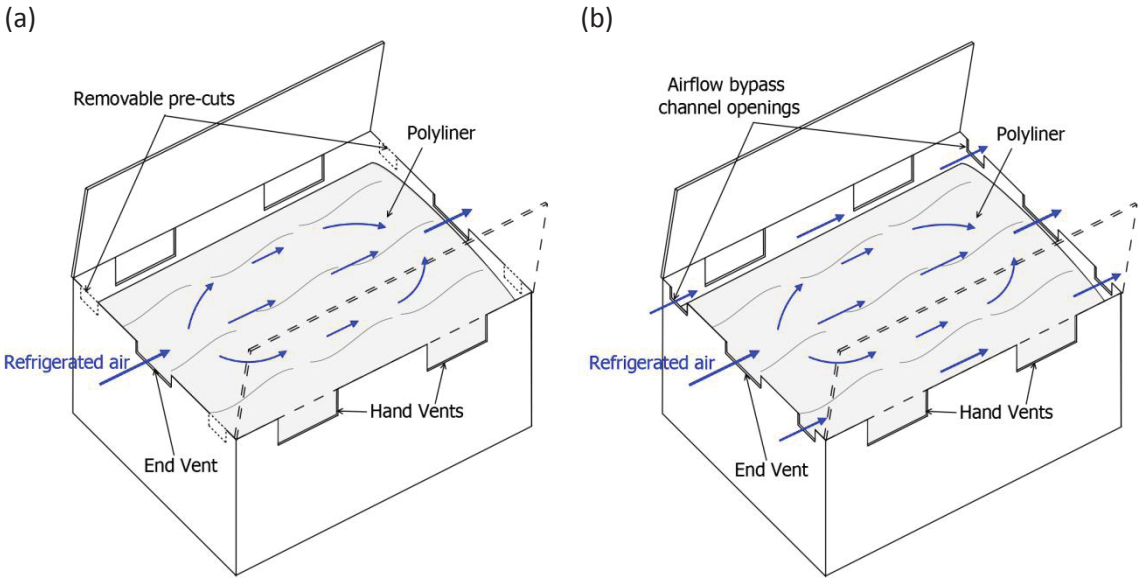

Figure 9.2. Expected airflow distribution within a ventilated package of polylined horticultural produce (a) without and (b) with additional open areas to promote airflow bypass channelling.

Practically, depending on the specific product, it may not be possible to remove the pre-cuts during pallet assembly. Instead the researcher or pre-cooler operator may wish to focus on the key aspect of the alternative pallet layout; to channel cool air partway along the side of the pallet, before redirecting part of the cool air into the centre of the pallet. This could be achieved by using the new design (Figure 9.2b) for each MBP in the pallet. However, vertical cardboard sheets could be used to redirect the channelled airflow. After pallet assembly vertical cardboard sheets, that block only the airflow bypass channel openings between the desired MBPs at the side of the pallet, can be inserted. This should retain the benefits of using two alternative box designs to control the flowrate and temperature change of the airflow throughout the pallet while reducing the complication in pallet assembly.

9.6 Potential data sets to enhance and expand the numerical model

It would be worthwhile to measure the air flowrate between different packages and within the pallet layer. The common techniques, reviewed in O'Sullivan et al. (2014), to measure airflow for forced-air cooling operations are either direct airflow measurements (thermal anemometry, vane anemometry and differential pressure flowmeters), which can disrupt the flow field, or non-invasive methods (LDA and PIV), which are expensive and often restricted to the use of a single package. The review of the available measurement techniques and associated advantages and disadvantages can be found in Appendix A3.

Specifically, for this numerical model validation of the air velocity field within the pallet layer would have involved the use of LDA or PIV. However, this presents a number of difficulties. For LDA or PIV a representative system which uses a liquid, such as mineral oil (Ferrua & Singh 2008, 2009b), to seed the particles to be traced by the camera must be used. The package and produce materials would have to be replaced by a transparent media, possibly fused silica. However, these changes to the system may create unrepresentative velocity profiles. The pallet footprint, consisting of different box orientations, presents additional challenges. If the particle tracking camera is placed horizontally it can only capture the air velocities of the MBPs orientated in one direction (i.e. it can't capture the velocity profiles of the MBPs in the centre of the pallet and the MBPs with a different orientation at the side the pallet) as the air is pulled from the front to the back of the pallet. Removing the side MBPs, to capture the velocity field of the MBPs through the centre of the pallet, risks changing the airflow behaviour by removing the airflow pathways between the central and side MBPs. Positioning the

camera so that it points straight down at the pallet layer would fail to capture the vertical air velocities as they flowed around the polyliner.

Knowledge of the velocity field does not translate to an exact prediction of the produce temperatures. The goal of this dissertation was to develop a numerical model that could predict kiwifruit temperatures during cooling. Hence, temperature validation was the priority with validation of the air velocity field a data set for potential future investigation.

In this dissertation the exact amount of contact between the polyliner and kiwifruit, and subsequent volume inside the polyliner, was not experimentally quantified. The polyethylene sheet folds around the kiwifruit bulk and is assumed to be contact (to a depth of approximately 5 mm) with each external face, if the kiwifruit bulk is viewed as one homogeneous solid. Moving forward, an experiment, while difficult to carry out to a high degree of accuracy, could be conducted to quantify the exact volume inside the polyliner. This volume can then be compared to the numerical calculation.

One possible method to measure this internal polyliner volume is through the use of a computerized axial tomography (CAT) scan of the kiwifruit MBP. A CAT scan can generate a series of cross-sectional images of the kiwifruit MBP, and construct a 3D body from the images. However, the extremely narrow thickness of the polyliner (10 μm) will make the sheet difficult to see in any CAT scan. To make to sheet more visible the polyliner could be coated in radiographic contrast medium liquid (i.e. iohexol). Additionally, the kiwifruit and cardboard box should be replaced with synthetic analogues (possible made out of polycarbonate, polymer or fused silica) that would not

show up (or least to small degree) on the CAT scan. If the polyliner can be identified in the 3D body then the volume it occupies can be calculated. It should be noted that this method would probably prove difficult to implement and there is a danger that replacing the kiwifruit and cardboard box may make the calculation of the polyliner volume unrepresentative of reality.

The numerical model can be modified to simulate the cooling of different kiwifruit size counts. Currently count 36 Hayward kiwifruit, with a mass of 93 – 103 g and approximately 100 per MBP, are used. Depending on the count size the quantity of fruit per MBP would change. This will require a different stacking arrangement. The different stacking arrangement will modify the airflow pattern through each individual MBP. However, once the stacking arrangement is completed for one MBP it can be used for each subsequent MBP in the numerical model, provided the same arrangement is used in any numerical validation experiments. While the new stacking arrangement would not be expected to significantly alter the cooling profiles it may require the numerical model to be validated again, using the same techniques employed for the current system, to confirm this assumption.

For complete accuracy of the numerical model inputs experiments could be conducted to find the exact density, heat capacity and thermal conductivity of the specific corrugated cardboard and kiwifruit used in the numerical validation of the model. However, the lack of the sensitivity of the numerical model, within the expected range of the values, mean that the return in defining these properties may not be worth the investment (time and cost) associated with the experiments.

9.6.1 Including moisture loss and transfer in the numerical model

It is possible that going forward the postharvest kiwifruit industry may consider perforated liners, which allow some contact between the refrigerated airflow and produce, instead of the current non-perforated liners which generate a complete barrier. Currently non-perforated liners are used. If moisture loss exceeds 4 % of fresh kiwifruit weight than shrivelling becomes visible (Burdon & Lallu, 2011). However, perforated liners have been shown to reduce the forced-air cooling time of kiwifruit (Wiley et al., 1999). Table grapes have also been identified as possessing faster cooling times when packed in perforated liners compared to non-perforated liners (Ngcobo et al., 2012).

Perforated liners increase the moisture loss during kiwifruit storage (Wiley et al., 1999) and will probably require moisture loss to be included in the numerical model. If a perforated liner is used than the amount of moisture loss during storage could become measurable. Wiley et al. (1999) recorded moisture loss at 5.2 % after 18 weeks of storage, for perforated liners in kiwifruit MBPs. This value was only 0.7 % for non-perforated liners. A higher amount of moisture loss during forced-air cooling would also be expected to contribute to the rate of heat transfer via the additional removal of heat due to the latent heat of evaporation. The difficultly here lies in actually measuring the moisture loss, especially as a function of time during the forced-air cooling operation. A moisture barrier would be required, possibly in the form of an impermeable wax, for the cardboard box, to prevent direct moisture transfer from the fruit to cardboard, to avoid a net weight change of zero. While possible for a single box this becomes extremely challenging when considering an entire pallet layer, or indeed pallet.

In developing the numerical model the heat absorbed due to moisture evaporation from the kiwifruit, if any, was assumed to be released back into the enclosed space in the polyliner upon condensation, providing no net increase/ decrease to the overall heat balance. However, as moisture condenses on the cool polyliner surface in contact with the refrigerated air heat released by condensation is removed by the refrigerated air, giving rise to a thermosyphon effect and increasing the heat transfer within the polyliner.

Any calculation into the potential effect of a thermosyphon on heat transfer is subject to extremely rough estimations for both the percentage of heat due to condensation removed by the refrigerated airflow and the quantity of moisture condensate. If an assumption of a film of moisture of 0.1 mm is created by condensation on the polyliner surface in contact with the refrigerated air (determined in the geometry editor as 0.34 m^2) then a total of 3.4 $x10^{-5}$ m^3 of moisture has been evaporated from the kiwifruit. Converting to a mass of water and multiplying by the latent heat of evaporation (2260 kJ kg^{-1}; Datt, 2011) yields a latent heat of 77 kJ. The sensible heat load to be removed during cooling of a single MBP is 780 kJ (section 5.5.2), leading to a potential contribution of 9.9 %. For comparison excluding natural convection from the simulation decreased the HCT of the MBPs between 11.5 % and 21.9 %, depending on location within the pallet (Appendix A1). However, the thermosyphon calculation is subject to a large number of uncertainties. The moisture is unlikely to occupy 100 % of the polyliner surface and the moisture film depth could be considerably larger or smaller. With so much ambiguity, an experiment to quantify the amount is required.

Unfortunately quantifying the amount of moisture condensate is extremely difficult. Measuring the mass of the kiwifruit (minus the polyliner and cardboard box) before and after experiments to calculate the mass of moisture evaporated is unlikely to produce reliable data. Measuring in a high/ low humidity environment and/ or opening the polyliner to remove the kiwifruit can cause further moisture evaporation/ condensation. With such small moisture quantities expected any additional change in the amount of condensate after cooling could significantly alter the results. Moisture condensate on the polyliner could potentially be identified by a CAT scan, provided they form as droplets larger than the minimum scan resolution. A CAT scanner with a resolution high enough to identify moisture condensate would most likely have to be a piece of specialised equipment.

In addition to difficulties in quantifying the amount of moisture condensate, information on the potential thermosyphon effect as a function of time would also be required if the effect is to be included in a numerical model.

It is important to note that while mass transfer can be simulated by a numerical model Fluent does not provide a direct means of achieving this. To include the mass transfer of moisture, user defined codes, which must be numerically validated, are required. Following modification of the numerical model experiments would then be required to quantify amount of moisture loss and/or transfer and validate the mass transfer predictions.

9.7 Recommendations

Unfortunately, there is no universal package configuration or operating conditions that will provide the best cooling performance for every product. However, general guidelines can be applied to improve the cooling performance of polylined horticultural produce. Alternate package configurations can be designed through numerical models, experiments, reference to similar published literature or most likely a combination of the research methods.

9.7.1 Industrial tunnel coolers

To ensure consistent cooling between the individual MBPs and pallets and to gain the full benefits from the recommended operating conditions and/ or an alternative package design, in an industrial tunnel cooler, certain practices should be adhered to. Gaps between pallets stacked in a tunnel cooler should be eliminated. However, this can difficult to achieve as pallets are positioned via forklifts. Alternatively, strips of tarp can be placed between pallets to block the airflow pathways between them. Tarp strips should also be used to block gaps under the pallet, through the pallet base. MBPs in a pallet should be placed as close together as possible to ensure the air flowed into, rather than around the individual MBPs.

9.7.2 Developing a numerical model of polylined horticultural produce

When experimentally validating a numerical model of polylined horticultural produce the fewest possible number of thermocouples per individual MBP, that can still

accurately measure the average fruit bulk temperature during cooling, should be used. Fewer wires can reduce the sources of experimental uncertainty, particularly those around the wires allowing some small volumetric flowrate of air into the polyliner and the wires blocking the airflow paths between MBPs.

When dealing with polylined produce the researcher should be aware of the potential lower threshold flowrates for cooling efficiency, compared to traditional non-polylined produce. Numerical validation experiments should be run at these flowrates. This can be tricky to achieve as, practically speaking, there are only a limited number of experiments that can be run prior to numerical validation. Hence, the flowrate range can only be estimated from the most similar published research before the numerical model is used to find the actual range.

If developing a numerical model of polylined horticultural produce the effect of natural convection should be included. The contribution of radiation, heat of respiration and moisture loss can most likely be neglected. However a thermosyphon effect may occur and the appropriate transport phenomenon to account for the moisture transfer should be included if necessary. Care must be taken if any of the product qualities are radically different from those of kiwifruit. It is up to the researcher to determine which heat transfer mechanisms are likely to play a significant role for the specific product.

9.7.3 Differences between cooling of polylined and non-polylined horticultural produce

When considering alternative operating conditions and design features to improve cooling performance there are of number of differences between polylined and non-

polylined horticultural produce. However, there is a large amount of published literature about the forced-air cooling of non-polylined produce. If the researcher is aware of the probable differences (lower threshold flowrate and optimal vent area) then a combination of work involving polylined produce and general observations from non-polylined produce can be combined to develop a new box design to improve cooling uniformity or identify what operating conditions to choose.

9.7.4 Improving the cooling performance of polylined horticultural produce

For kiwifruit MBPs the numerical model is set-up so that it can assess current operating conditions and alternative design features and output results, without having to depend on trial and error experiments. External ideas (which could appear anywhere in the scientific community, from packhouse operators to published papers involving postharvest cooling from any research group worldwide) can also be incorporated into the numerical model and their impact tested and assessed. The results can be evaluated in terms of cooling rate and uniformity, air flowrate, pressure drop or energy requirement.

While the new design presented was developed for kiwifruit MBP the general features are expected to be applicable to most polylined horticultural produce. The key design features (additional open areas and airflow channelling to deliver cool air to the warmest MBPs) of the presented package can be utilised. The new package design and pallet composition can enable the forced-air cooling process to benefit from a reduced energy requirement, without sacrificing cooling rate and improving cooling uniformity.

References

Alvarez, G., Bournet, P.E., & Flick, D. (2003). Two-dimensional simulation of turbulent flow and transfer through stacked spheres. *International Journal of Heat and Mass Transfer*, 46(13), 2459-2469. doi:10.1016/S0017-9310(02)00546-X

Amos, N.D. (1995). *Mathematical modelling of heat and mass transfer and water vapour transport in apple coolstores* (Doctoral dissertation, Massey University, Palmerston North, New Zealand). Retrieved from http://hdl.handle.net/10179/2925

Amos, N.D. (2005). Characterisation of air flow in a commerical cool store using a carbon monoxide gas tracer tracer technique. *Acta Horticulturae,* 687, 305-312. doi:10.17660/ActaHortic.2005.687.37

António, C.C., & Alfonso, C.F. (2011). Air temperature fields inside refrigeration cabins: a comparison of results from CFD and ANN modelling. *Applied Thermal Engineering,* 31(6-7), 1244-1251. doi:10.1016/j.applthermaleng.2010.12.027

Ashby, B.H. (1995). *Protecting perishable foods during transport by truck (handbook no. 669).* Retrieved from https://www.ams.usda.gov/sites/default/files/media/Protecting%20Perishable%20Foods%20During%20Transport%20by%20Truck.pdf

ASHRAE. (1993). *1993 ASHRAE handbook: fundamentals*. Atlanta, GA: American Society of Heating, Refrigeration and Air-Conditioning Engineers.

Aswaney, M. (2007). Forced-air precooling of fruits and vegetables. *Air Conditioning and Refrigeration Journal*, 57–62. Retrieved from http://www.pre-coolers.net/documents/forced-air-precooling-of-fruits-and-vegetables.pdf

Bano, S., & Scrimgeour, F. (2012). The export growth and revealed comparative advantage of the New Zealand kiwifruit industry. *International Business Research,* 5(2), 73-82. doi:10.5539/ibr.v5n2p73

Brosnan, T., & Sun, D-W. (2001). Precooling techniques and applications for horticultural products – a review. *International Journal of Refrigeration,* 24(2), 154-170. doi:10.1016/S0140-7007(00)00017-7

Burdon, J., McLeod, D., Lallu, N., Gamble, J., Petley, M., & Gunson, A. (2004). Consumer evaluation of "Hayward" kiwifruit of different at-harvest dry matter contents. *Postharvest Biology and Technology*, 34(3), 245-255. doi: 10.1016/j.postharvbio.2004.04.009

Burdon, J., & Lallu, N. (2011). Kiwifruit. In: E.M. Yahia (Ed.), *Postharvest biology and technology of tropical and subtropical fruits. Volume 3: coconut to mango* (pp. 326-360). Cambridge, UK: Woodhead Publishing Limited

Burg, S.P. (2004). *Postharvest physiology and hypobaric storage of fresh produce*. Cambridge, MA: CAB Publishing

Chourasia, M.K., & Goswami, T.K. (2006a). Simulation of transport phenomena during natural convection cooling of bagged potatoes in cold storage, part I: fluid flow and heat transfer. *Biosystems Engineering*, 94(1), 33-45. doi:10.1016/j.biosystemseng.2006.02.003

Chourasia, M.K., & Goswami, T.K. (2006b). Simulation of transport phenomena during natural convection cooling of bagged potatoes in cold storage, part II: mass transfer. *Biosystems Engineering*, 94(2), 207-219. doi:10.1016/j.biosystemseng.2006.02.015

Chourasia, M.K., & Goswami, T.K. (2007a). CFD simulation of effects of operating parameters and product on heat transfer and moisture loss in the stack of bagged potatoes. *Journal of Food Engineering*, 80(3), 947-960. doi:10.1016/j.jfoodeng.2006.07.015

Chourasia, M.K., & Goswami, T.K. (2007b). Steady state CFD modeling of airflow, heat transfer and moisture loss in a commercial potato cold store. *International Journal of Refrigeration*, 30(4), 672-689. doi:10.1016/j.ijrefrig.2006.10.002

Crisosto, C.H., Mitcham, E.J., & Kader, A.A. (2013). *Kiwifruit: recommendations for maintaining postharvest quality.* Retrieved from http://postharvest.ucdavis.edu/PFfruits/Kiwifruit/

Datt, P. (2011). Latent heat of vaporization/ condensation. In: V.P. Singh, P. Singh & U.K. Haritashya (Eds.), *Encyclopedia of snow, ice and glaciers* (pp. 703). Dordrecht, Netherlands: Springer Netherlands.

Davies, T.W. (2011). *Biot number*. Retrieved from http://www.thermopedia.com/content/585/. doi:10.1615/AtoZ.b.biot_number

de Castro, L.R., Vigneault, C., & Cortez, L.A.B. (2004a). Effect of container opening area on air distribution during precooling of horticultural produce. *Transactions of American Society of Association Executives*, 47(6), 2033–2038. doi:10.13031/2013.17792

de Castro, L.R., Vigneault, C., & Cortez, L.A.B. (2004b). Container opening design for horticultural produce cooling efficiency. *Food, Agriculture and Environment*, 2(1), 135–140. Retrieved from http://world-food.net/wfl/download/journals/2004-issue_1/f24.pdf

de Castro, L. R., Vigneault, C., & Cortez, L.A.B. (2005). Cooling performance of horticultural produce in containers with peripheral openings. *Postharvest Biology and Technology*, 38(3), 254–261. doi:10.1016/j.postharvbio.2005.07.004

Defraeye, T., Verboven, P., & Nicolaï, B.M. (2013a). CFD modelling of flow and scalar exchange of spherical food products: turbulence and boundary-layer modelling. *Journal of Food Engineering*, 114(4), 495-504. doi:10.1016/j.jfoodeng.2012.09.003

Defraeye, T., Lambrecht, R., Tsige, A.A, Delele, M.A., Opara, U.L., Cronjé, P., Verboven, P., & Nicolaï, B.M. (2013b). Forced-convective cooling of citrus fruit: package design. *Journal of Food Engineering*, 118(1), 8-18. doi:10.1016/j.jfoodeng.2013.03.026

Defraeye, T., Lambrecht, R., Delele, M.A., Tsige, A.A, Opara, U.L., Cronjé, P., Verboven, P., & Nicolaï, B.M. (2014). Forced-convective cooling of citrus fruit: cooling conditions and energy consumption in relation to package design. *Journal of Food Engineering*, 121, 118-127. doi:10.1016/j.jfoodeng.2013.08.021

Dehghannya, J.M., Ngadi, M., & Vigneault, C. (2008). Simultaneous aerodynamic and thermal analysis during cooling of stacked spheres inside ventilated packages. *Chemical Engineering & Technology,* 31(11), 1651-1659. doi:10.1002/ceat.200800290

Dehghannya, J.M., Ngadi, M., & Vigneault, C. (2010). Mathematical modeling of airflow and heat transfer during forced convection cooling of produce: a review. *Food Engineering Reviews,* 2(4), 227-243. doi:10.10.1007/s12393-010-9027-z

Dehghannya, J.M., Ngadi, M., & Vigneault, C. (2011). Mathematical modeling of airflow and heat transfer during forced convection cooling of produce considering various package vent areas. *Food Control,* 22(8), 1393-1399. doi:10.1016/j.foodcont.2011.02.019

Dehghannya, J.M., Ngadi, M., & Vigneault, C. (2012). Transport phenomena modelling during produce cooling for optimal package design: thermal sensitivity analysis. *Biosystems Engineering,* 111(3), 315-324. doi:10.1016/j.biosystemseng.2012.01.001

Delele, M.A., Jaeken, P., Debaer, C., Baetens, K., Endalew, A.M., Ramon, H., Nicolaï, B.M., & Verboven, P. (2007). CFD prototyping of an air-assisted orchard sprayer aimed at drift reduction. *Computers and Electronics in Agriculture,* 55(1), 16-27. doi:10.1016/j.compag.2006.11.002

Delele, M.A., Tijskens, E., Atalay, Y., Ho, Q., Ramon, H., Nicolaï, B.M., & Verboven, P. (2008). Combined discrete element and CFD modelling of airflow through random stacking of horticultural products in vented boxes. *Journal of Food Engineering,* 89(1), 33-41. doi:10.1016/j.jfoodeng.2008.03.026

Delele, M.A., Schenk, A., Tijskens, E., Ramon, H., Nicolaï, B.M., & Verboven, P. (2009a). Optimization of the humidification of cold stores by pressurized water atomizers based on a multiscale CFD model. *Journal of Food Engineering,* 91(2), 228-239. doi:10.1016/j.jfoodeng.2008.08.027

Delele, M.A., Schenk, A., Ramon, H., Nicolaï, B.M., & Verboven, P. (2009b). Evaluation of a chicory root cold store humidification system using computational fluid dynamics. *Journal of Food Engineering,* 94(1), 110-121. doi:10.1016/j.jfoodeng.2009.03.004

Delele, M.A., Vorstermans, B., Creemers, Tsige, A.A., Tijskens, E., Schenk, A., Nicolaï, B.M., & Verboven, P. (2012a). CFD model development and validation of a thermonebulisation fungicide fogging system for postharvest storage of fruit. *Journal of Food Engineering,* 108(1), 59-68. doi:10.1016/j.jfoodeng.2011.07.030

Delele, M.A., Vorstermans, B., Creemers, Tsige, A.A., Tijskens, E., Schenk, A., Nicolaï, B.M., & Verboven, P. (2012b). Investigating the performance of thermonebulisation fungicide fogging system for loaded fruit storage room using CFD model. *Journal of Food Engineering,* 109(1), 87-97. doi:10.1016/j.jfoodeng.2011.09.030

Delele, M.A, Ngcobo, M.E.K., Opara, U.L., & Meyer, C.J. (2013a). Investigating the effects of table grape package components and stacking on airflow, heat and mass transfer using 3-D CFD modelling. *Food and Bioprocess Technology,* 6(9), 2571-2585. doi:10.1007/s11947-012-0895-5

Delele, M.A, Ngcobo, M.E.K., Getahun, S.T., Chen, L., Mellmann, J., & Opara, U.L. (2013b). Studying airflow and heat transfer characteristics of horticultural produce packaging system using 3-D CFD model. Part I: model development and validation. *Postharvest Biology and Technology,* 86, 536-545. doi:10.1016/j.postharvbio.2013.08.014

Delele, M.A, Ngcobo, M.E.K., Getahun, S.T., Chen, L., Mellmann, J., & Opara, U.L. (2013c). Studying airflow and heat transfer characteristics of a horticultural produce packaging system using 3-D CFD model. Part II: effect of package design. *Postharvest Biology and Technology,* 86, 546-555. doi:10.1016/j.postharvbio.2013.08.015

DesignModeler. (2010). Canonsburg, PA: Ansys Inc.

Dick, E. (2009). Introduction to finite element methods in computational fluid dynamics. In J.F. Wendt (Ed.), *Computational fluid dynamics* (3rd ed., pp 235-274). Berlin Heidelberg, Germany: Springer-Verlag

Dincer, I. (1995). Air flow precooling of individual grapes. *Journal of Food Engineering,* 26(2), 243-249. doi:10.1016/0260-8774(94)00049-F

East, A.R., Sabarez, H.T., Tanner, D.J., & Cleland, D.J. (2003). *Validation of a packaging design tool: case study for apple packaging.* Paper presented at the 21st IIR International Congress of Refrigeration, Washington, D.C.

East, A.R., & Smale, N.J. (2008). Combining a hybrid genetic algorithm and a heat transfer model to optimise an insulated box for use in the transport of perishables. *Vaccine,* 26(10), 1322-1334. doi:10.1016/j.vaccine.2007.12.055

East, A.R., Jeffery, P.B., & Love, R.J. (2013) *Investigating asymmetrical packaging as a technique to reduce heterogeneity during pre-cooling of fresh produce* [USB]. Paper presented at the 2nd IIR International Conference on Sustainability and the Cold Chain, Paris, France.

Endalew, A.M., Hertog, M., Delele, M.A., Baetens, K., Persoons, T., Baelmans, M., Ramon, H., Nicolaï, B.M., & Verboven, P. (2009a). CFD modelling and wind tunnel validation of airflow through plant canopies using 3D canopy architecture. *International Journal of Heat and Fluid Flow,* 30(2), 356-368. doi:10.1016/j.ijheatfluidflow.2008.12.007

Endalew, A.M., Hertog, M., Gebrehiwot, M.G., Baelmans, M., Ramon, H., Nicolaï, B.M., & Verboven, P. (2009b). Modelling airflow within model plant canopies using an integrated approach. *Computers and Electronics in Agriculture,* 66(1), 9-24. doi:10.1016/j.compag.2008.11.002

Endalew, A.M., Debaer, C., Rutten, N., Vercammen, J., Delele, M.A., Ramon, H., Nicolaï, B.M., & Verboven, P. (2010a). Modelling pesticide flow and deposition from air-assisted orchard spraying in orchards: a new integrated CFD approach. *Agricultural and Forest Meteorology,* 150(10), 1383-1392. doi:10.1016/j.agrformet.2010.07.001

Endalew, A.M., Debaer, C., Rutten, N., Vercammen, J., Delele, M.A., Ramon, H., Nicolaï, B.M., & Verboven, P. (2010b). A new integrated CFD modelling approach towards air-assisted orchard spraying. Part I. Model development and effect of wind speed and direction on sprayer airflow. *Computers and Electronics in Agriculture,* 71(2), 128-136. doi:10.1016/j.compag.2009.11.005

Endalew, A.M., Debaer, C., Rutten, N., Vercammen, J., Delele, M.A., Ramon, H., Nicolaï, B.M., & Verboven, P. (2010c). A new integrated CFD modelling approach towards air-assisted orchard spraying - part II: validation for different sprayer types. *Computers and Electronics in Agriculture,* 71(2), 137-147. doi:10.1016/j.compag.2009.11.007

Ezeike, G., & Hung, Y.-C. (2009). Refrigeration of fresh produce from field to home: refrigeration systems and logistics. In: W.F. Florkowski, R.L. Shewfelt, B. Brueckner & S.E. Prussia (Eds.), *Postharvest handling: a systems approach* (2nd ed, pp. 513-537). San Diego, CA: Academic Press.

Ferrua, M.J., & Singh, R.P. (2008). A nonintrusive flow measurement technique to validate the simulated laminar fluid flow in a packed container with vented walls. *International Journal of Refrigeration,* 31(2), 242-255. doi:10.1016/j.ijrefrig.2007.05.013

Ferrua, M.J., & Singh, R.P. (2009a). Modeling the forced-air cooling process of fresh strawberry packages, part I: numerical model. *International Journal of Refrigeration,* 32(2), 335-348. doi:10.1016/j.ijrefrig.2008.04.010

Ferrua, M.J., & Singh, R.P. (2009b). Modeling the forced-air cooling process of fresh strawberry packages, part II: experimental validation of the flow model. *International Journal of Refrigeration,* 32(2), 349-358. doi:10.1016/j.ijrefrig.2008.04.009

Ferrua, M.J., & Singh, R.P. (2009c). Modeling the forced-air cooling process of fresh strawberry packages, part III: experimental validation of the energy model. *International Journal of Refrigeration,* 32(2), 359-368. doi:10.1016/j.ijrefrig.2008.04.011

Ferrua, M.J., & Singh, R.P. (2009d). Design guidelines for the forced-air cooling process of strawberries. *International Journal of Refrigeration,* 32(8), 1932-1943. doi:10.1016/j.ijrefrig.2009.07.011

Ferrua, M.J., & Singh, R.P. (2011). Improved airflow method and packaging system for forced-air cooling of strawberry packaging. *International Journal of Refrigeration,* 34(4), 1162-1173. doi:10.1016/j.ijrefrig.2011.01.018

Fluent. (2010). Canonsburg, PA: Ansys Inc.

Fluent-Theory. (2010). Canonsburg, PA: Ansys Inc.

Franke, J., Hellsten, A., Schlünzen, H., & Carissimo, B. (2007) *Best practice guideline for CFD simulation of flows in the urban environment. COST action 732: quality assurance and improvement of microscale meteorological models.* Hamburg, Germany: University of Hamburg.

Fresh Facts. (2014). Retrieved from http://www.freshfacts.co.nz

Gerasopoulos, D., Chlioumis, G., & Sfakiotakis, E. (2006). Non-freezing points below zero induce low-temperature breakdown of kiwifruit at harvest. *Journal of the Science of Food and Agriculture,* 86(6), 886-890. doi:10.1002/jsfa.2429

Gowda, B.S., Narasimham, G.S.V.L., & Murthy, M.V.K. (1997). Forced-air precooling of spherical foods in bulk: a parametric study. *International Journal of Heat and Fluid Flow*, 18(6), 613-624. doi:10.1016/S0142-727X(97)00028-3

Guo, Z., & Zhao, T.S. (2005). A lattice Boltzmann model for convection heat transfer in porous media. *Numerical heat transfer, part B: fundamentals*, 47(2), 157-177. doi:10.1080/10407790590883405

Hellebrand, H.J., Beuche, H., & Linke, M. (2002). *Determination of thermal emissivity and surface temperature distribution of horticultural products*. Retrieved from https://www.researchgate.net/publication/267809674

Holman, J.P. (2010). *Heat transfer* (10th ed.). New York, NY: McGraw-Hill.

Hu, Z., & Sun, D.-W. (2001). Predicting local surface heat transfer coefficients by different turbulent k-ϵ models to simulate heat and moisture transfer during air-blast chilling. *International Journal of Refrigeration*, 24(7), 702-717. doi:10.1016/S0140-7007(00)00081-5

ISO 5167-1. (2003). *Measurement of fluid flow by means of pressure differential devices inserted in circular cross-section conduits running full - part 1: general principles and requirements.*

ISO 5167-2. (2003). *Measurement of fluid flow by means of pressure differential devices inserted in circular cross-section conduits running full - part 2: orifice plates.*

Jordan, R.B., Walton, E.F., Klages, K.U., & Seelye, R.J. (2000). Postharvest fruit density as an indicator of dry matter and ripened soluble solids of kiwifruit. *Postharvest Biology and Technology*, 20(2), 163-173. doi:10.1016/S0925-5214(00)00125-3

Jordan, R.B., & Seelye, R.J. (2009) Relationship between taste perception, density and soluble solids concentration in kiwifruit (Actinidia Deliciosa). *New Zealand Journal of Crop and Horticultural Science*, 37(4), 303-317. doi:10.1080/01140671.2009.9687585

Kumar, R., Kumar, A., & Murthy, U.N. (2008). Heat transfer during forced air precooling of perishable food products. *Biosystems Engineering*, 99(2), 228-233. doi:10.1016/j.biosystemseng.2007.10.012

Ladaniya, M., & Singh, S. (2002). Packaging of horticultural produce with special reference to citrus fruits. *Packaging India*, 34(5), 9-22.

Laguerre, O., Amara, S.B., Moureh, J., & Flick, D. (2007). Numerical simulation of air flow and heat transfer in domestic refrigerators. *Journal of Food Engineering*, 81(1), 144-156. doi:10.1016/j.jfoodeng.2006.10.029

Laguerre, O., Amara, S.B., Charrier-Mojtabi, M.-C., Lartigue, B., & Flick, D. (2008). Experimental study of air flow by natural convection in a closed cavity: application in a domestic refrigerator. *Journal of Food Engineering*, 85(4), 547-560. doi:10.1016/j.jfoodeng.2007.08.023

Laguerre, O., Remy, D., & Flick, D. (2009). Airflow, heat and moisture transfers by natural convection in a refrigerating cavity. *Journal of Food Engineering*, 91(2), 197-210. doi:10.1016/j.jfoodeng.2008.08.029

Laguerre, O., Benamara, S., & Flick, D. (2010). Numerical simulation of simultaneous heat and moisture transfer in a domestic refrigerator. *International Journal of Refrigeration*, 33(7), 1425-1433. doi:10.1016/j.ijrefrig.2010.04.010

Macrae, E. A., Bowen, J.H., & Margaret, G.H.S. (1989). Maturation of kiwifruit (Actinidia Deliciosa cv. Hayward) from two orchards: differences in composition of the tissue zones. *Journal of the Science of Food and Agriculture,* 47(4), 401-416. doi:10.1002/jsfa.2740470403

McGlone, V.A., & Kawano, S. (1998). Firmness, dry-matter and soluble-solids assessment of postharvest kiwifruit by NIR spectroscopy. *Postharvest Biology and Technology,* 13(2), 131-141. doi:10.1016/S0925-5214(98)00007-6

Meana, M.B., Chau, K.V., Emond, J.P., & Talbot, M.T. (2005). Forced-air cooling of strawberries in reusable plastic containers. *Proceedings of Florida State Horticultural Society*, 118, 379-382. Retrieved from http://fshs.org/proceedings-o/2005-vol-118/118/379-382.pdf

Meshing. (2010). Canonsburg, PA: Ansys Inc.

Minitab 16 Statistical Software. (2010). [Computer software]. Massey University, New Zealand: Minitab, Inc. (www.minitab.com).

Ministry of Business, Innovation & Employment. (2015). *Nominal annual average fuel prices*. Retrieved from http://www.mbie.govt.nz/info-services/sectors-industries/energy/energy-data-modelling/statistics/prices

Mirade, P.-S., & Daudin, J.-D. (2011). Computational fluid dynamics prediction and validation of gas circulation in a cheese-ripening room. *International Dairy Journal*, 16(8), 920-930. doi:10.1016/j.idairyj.2005.08.007

Moureh, J., & Flick, D. (2004). Airflow pattern and temperature distribution in a typical refrigerated truck configuration loaded with pallets. *International Journal of Refrigeration*, 27(5), 464-474. doi:10.1016/j.ijrefrig.2004.03.003

Moureh, J., Tapsoba, M., & Flick, D. (2009a). Airflow in a slot-ventilated enclosure partially filled with porous boxes: part I - measurements and simulations in the clear region. *Computers & Fluids*, 38(2), 194-205. doi:10.1016/j.compfluid.2008.02.006

Moureh, J., Tapsoba, M., & Flick, D. (2009b). Airflow in a slot-ventilated enclosure partially filled with porous boxes: part II - measurements and simulations within porous boxes. *Computers and Fluids*, 38(2), 206-220. doi:10.1016/j.compfluid.2008.02.007

Moureh, J., Tapsoba, M., Derens, E., & Flick, D. (2009c). Air velocity characteristics within vented pallets loaded in a refrigerated vehicle with and without air ducts. *International Journal of Refrigeration*, 32(2), 220-234. doi:10.1016/j.ijrefrig.2008.06.006

Mowat, A., & Maguire, K. (2007). Canopy management and dry matter of 'Hayward' kiwifruit. *Acta Horticulturae,* 753, 333-340. doi:10.17660/ActaHortic.2007.753.41

Nahor, H.B., Hoang, M.L., Verboven, P., Baelmans, M., & Nicolai, B.M. (2005). CFD model of the airflow, heat and mass transfer in cool stores. *International Journal of Refrigeration,* 28(3), 368-380. doi:10.1016/j.ijrefrig.2004.08.014

Nevins, A. L. (2008). *Significant factors affecting horticultural corrugated fibreboard strength* (Doctoral dissertation, Massey University, Palmerston North, New Zealand). Retrieved from http://hdl.handle.net/10179/1248

Ngcobo, M.E.K., Opara, U.L., & Thiart, G.D. (2012). Effects of packaging liners on cooling rate and quality attributes of table grape (cv. Regal Seedless). *Packaging Technology and Science*, 25(2), 73-84. doi:10.1002/pts.961

Norton, T., & Sun, D.-W. (2006). Computational fluid dynamics (CFD) – an effective and efficient design and analysis tool for the food industry: a review. *Trends in Food Science and Technology,* 17(11), 600-620. doi:10.1016/j.tifs.2006.05.004

O'Sullivan, J.L., Ferrua, M.J., Love, R.J., Verboven, P., Nicolaï, B.M., & East, A.R. (2012). *Mechanisms and performance of the forced-air cooling process of fruit packed in polyethylene liners* [CD]. Paper presented at the CIGR Section VII International Technical Symposium on Innovating the Food Value Chain, Stellenbosch, South Africa.

O'Sullivan, J.L., Ferrua, M.J., Love, R.J., Verboven, P., Nicolaï, B.M., & East, A.R. (2013a). *Performance of the forced-air cooling process of fruit packed in polyethylene liners as a function of pallet orientation* [USB]. Paper presented at the 2nd IIR International Conference on Sustainability and the Cold Chain, Paris, France.

O'Sullivan, J.L., Ferrua, M.J., Love, R.J., Verboven, P., Nicolaï, B.M., & East, A.R. (2013b). *Mathematical modelling of kiwifruit packaging undergoing forced-air cooling*. Paper presented at the 26th Symposium on Packaging, Espoo, Finland.

O'Sullivan, J.L., Ferrua, M.J., Love, R.J., Verboven, P., Nicolaï, B.M., & East, A.R. (2014). Airflow measurement techniques for the improvement of forced-air cooling, refrigeration and drying operations. *Journal of Food Engineering*, 143, 90-101. doi:10.1016/j.jfoodeng.2014.06.041

Pathare, P.B., Opara, U.L., Vigneault, C., Delele, M.A., & Al-Said, F.A. (2012). Design of packaging vents for cooling fresh horticultural produce. *Food and Bioprocess Technology,* 5(6), 2031-2045. doi:10.1007/s11947-012-0883-9

Rennels, D.C., & Hudson, H.M. (2012). *Pipe flow - a practical comprehensive guide*. Hoboken, NJ: Wiley.

Roache, P.J. (1997). Quantification of uncertaintity in compuational fluid dynamics. *Annual Reviw of Fluid Mechanics*, 29, 123-160. doi:10.146/annurev.fluid.29.1.123

Shim, Y.M., Olatunji, J.R., Zhao, J., Love, R.J., Ferrua, M.J., & East, A.R. (2016). *Industry survey on the pressure drop across palletised horticultural produce during precooling*. Paper presented at the 4th IIR International Conference on Sustainability and the Cold Chain, Auckland, New Zealand.

Simson, S. P., & Straus, M.C. (2010*). Post-harvest technology of horticultural crops*. New Delhi, India: Oxford Book Company.

Singh, D., Mandal, G., & Jain, R.K. (2003). Effect of ventilation on shelf life and quality of peaches. *Acta Horticulturae*, 696, 519-522. doi:10.17660/ActaHortic.2005.696.91

Singh, R.P., & Heldman, D.R. (2014). *Introduction to food engineering* (5th ed.). San Diego, CA: Academic Press

Smale, N. J. (2004). *Mathematical modelling of airflow in shipping systems: model development and testing* (Doctoral dissertation, Massey University, Palmerston North, New Zealand). Retrieved from http://hdl.handle.net/10179/1718

Smale, N.J., Moureh, J., & Cortella, G. (2006). A review of numerical models of airflow in refrigerated food applications. *International Journal of Refrigeration*, 29(6), 911-930. doi:10.1016/j.ijrefrig.2006.03.019

Sweat, V.E. (1994). Thermal properties of food. In M.A. Rao & S.S.H. Rizvi (Eds.), *Engineering properties of foods* (2nd ed., pp. 99-138). New York, NY: Marcel Dekker, Inc.

Tanner, D.J. (1998*). Mathematical modelling for design of horticultural packaging* (Doctoral dissertation, Massey University, Palmerston North, New Zealand). Retrieved from http://hdl.handle.net/10179/2824

Tanner, D.J., Cleland, A.C., Opara, U.L, & Robertson, T.R. (2002a). A generalised mathematical modelling methodology for design of horticultural food packages exposed to refrigerated conditions: part 1, formulation. *International Journal of Refrigeration,* 25(1), 33-42. doi:10.1016/S0140-7007(01)00019-6

Tanner, D.J., Cleland, A.C., & Opara, L.U. (2002b). A generalised mathematical modelling methodology for the design of horticultural food packages exposed to refrigerated conditions. Part 2. Heat transfer modelling and testing. *International Journal of Refrigeration,* 25(1), 43-53. doi:10.1016/S0140-7007(01)00018-4

Tanner, D.J., Cleland, A.C., & Robertson, T.R. (2002c). A generalised mathematical modelling methodology for design of horticultural food packages exposed to refrigerated conditions: part 3, mass transfer modelling and testing. *International Journal of Refrigeration,* 25(1), 54-65. doi:10.1016/S0140-7007(01)00017-2

The Treasury. (2015). *New Zealand Economic and Financial Overview 2015.* Retrieved from http://www.treasury.govt.nz/economy/overview/2015

Thompson, J., & Chen, Y. (1988). Comparative energy use of vacuum, hydro, and forced air coolers for fruits and vegetables. *American Society of Heating, Refrigeration and Air-Conditioning Engineers Transactions*, 92, 1427-1433. Retreived from http://ucanr.edu/datastoreFiles/234-1044.PDF

Thompson, J., & Knutson, J. (1997). Forced air cooling of strawberries in clamshell baskets. *Perishable Handling Newsletter Issue No. 90*, pp. 29-30. Retreived from http://ucanr.edu/datastoreFiles/234-157.pdf

Thompson, J. (2004). Pre-Cooling and Storage Facilities. In USDA (Ed.), *USDA agriculture handbook 66: the commercial storage of fruits, vegetables, and florist and nursery Stocks* (pp. 1-10). Washington, DC: USDA.

Tsilingiris, P.T. (2008). Thermophysical and transport properties of humid air at temperature range between 0 and 100 °C. *Energy Conversion and Management*, 49(5), 1098-1110. doi:10.1016/j.enconman.2007.09.015

Tutar, M., Erdogdu, F., & Toka, B. (2009). Computational modeling of airflow patterns and heat transfer prediction through stacked layers' products in a vented box during cooling. *International Journal of Refrigeration,* 32(2), 295-306. doi:10.1016/j.ijrefrig.2008.05.003

van der Sman, R.G.M. (1999). Solving the vent hole design problem for seed potato packagings, with the lattice boltzmann scheme. *International Journal of Computational Fluid Dynamics,* 11(3-4), 237-248. doi:10.1080/10618569908940877

van der Sman, R.G.M. (2002). Prediction of airflow through a vented tray by the Darcy–Forchheimer equation. *Journal of Food Engineering,* 55(1), 49-57. doi:10.1016/S0260-8774(01)00241-2

Verboven, P., Hoang, M.L., & Nicolaï, B.M. (2003). Modelling turbulent air flow in cool rooms for horticultural products. *Acta Horticulturae,* 599, 435-441. doi:10.17660/ActaHortic.2003.599.55

Verboven, P., Flick, D., Nicolaï, B.M., & Alvarez, G. (2006). Modelling transport phenomena in refrigerated food bulks, packages and stacks: basics and advances. *International Journal of Refrigeration*, 29(6), 985-997. doi:10.1016/j.ijrefrig.2005.12.010

Versteeg, H.K., & Malalasekera, W. (1995). *An introduction to computational fluid dynamics: the finite volume method*. Essex, England: Longman Scientific & Technical.

Vigneault, C., & Goyette, B. (2002). Design of plastic container opening to optimize forced-air precooling of fruits and vegetables. *Applied Engineering in Agriculture,* 18(1), 73-76. doi:10.13031/2013.7697

Vigneault, C., Goyette, B., & de Castro, L.R. (2006). Maximum slat width for cooling efficiency of horticultural produce in wooden crates. *Postharvest Biology and Technology,* 40(3), 308-313. doi:10.1016/j.postharvbio.2006.01.005

Vigneault, C., Thompson, J., Wu, S., Hui, K.P.C., & LeBlanc, D.I. (2009). Transportation of fresh horticultural produce. *Postharvest Biology and Technology*, 2, 1-24. Retreived from http://ucanr.edu/datastoreFiles/234-1291.pdf

Wang, H., & Touber, S. (1990). Distributed dynamic modelling of a refrigerated room. *International Journal of Refrigeration*, 13(4), 214-222. doi:10.1016/0140-7007(90)90033-S

Wang, L., & Sun, D.-W. (2002a). Modelling vacuum cooling process of cooked meat - part 1: analysis of vacuum cooling system. *International Journal of Refrigeration*, 25(7), 854-861. doi:10.1016/S0140-7007(01)00094-9

Wang, L., & Sun, D.-W. (2002b). Modelling vacuum cooling process of cooked meat - part 2: mass and heat transfer of cooked meat under vacuum pressure. *International Journal of Refrigeration*, 25(7), 862-871. doi:10.1016/S0140-7007(01)00095-0

Wang, L., & Sun, D.-W. (2003). Recent developments in numerical modelling of heating and cooling processes in the food industry - a review. *Trends in Food Science and Technology,* 14(10), 408-423. doi:10.1016/S0924-2244(03)00151-1

Wang, M.Y., MacRae, E. Wohlers, M., & Marsh, K. (2011). Changes in volatile production and sensory quality of kiwifruit during fruit maturation in Actinidia Deliciosa 'Hayward' and Actinidia Chinensis 'Hort16A'. *Postharvest Biology and Technology,* 59(1) 16-24. doi:10.1016/j.postharvbio.2010.08.010

Whitaker, S. (1969). Advances in theory of fluid motion in porous medium. *Industrial & Engineering Chemistry,* 61(12), 14-28. doi:10.1021/ie50720a004

Wiley, P., Crisosto, C.H., & Mitchell, F.G. (1999). Adapting perforated box liners to the California kiwifruit industry. *Acta Horticulturae,* 498, 299-306. doi:10.17660/ActaHortic.1999.498.35

Woods, J.L. (1990). Moisture loss from fruits and vegetables. *Postharvest News and Information,* 1 (3), 195-199. Retrieved from http://www.cabi.org/cabdirect/FullTextPDF/Pre2000/19910300834.pdf

Xu, Y., & Burfoot, D. (1999). Simulating the bulk storage of foodstuffs. *Journal of Food Engineering,* 39(1), 23-29. doi:10.1016/S0260-8774(98)00139-3

Zou, Q. (2002). A CFD modelling system for airflow and heat transfer in ventilated packaging systems during forced-air cooling of fresh produce (Doctoral dissertation, Massey University, Palmerston North, New Zealand). Retrieved from http://hdl.handle.net/10179/2073

Zou, Q., Opara, L.U., & McKibbin, R. (2006a). A CFD modeling system for airflow and heat transfer in ventilated packaging for fresh foods: I. Initial analysis and development of mathematical models. *Journal of Food Engineering*, 77(4), 1037-1047. doi:10.1016/j.jfoodeng.2005.08.042

Zou, Q., Opara, L.U., & McKibbin, R. (2006b). A CFD modeling system for airflow and heat transfer in ventilated packaging for fresh foods: II. Computational solution, software development, and model testing. *Journal of Food Engineering*, 77(4), 1048-1058. doi:10.1016/j.jfoodeng.2005.08.043

Appendix A1

Further numerical model testing

A1.1 Introduction

In Chapter 6 the impact of changing the material thermal properties defined in the numerical set-up was tested. In the sensitivity analysis of the thermal characteristics of the numerical model the values used in the calculations were changed. However, how the calculations were performed (i.e. turbulence model used), model geometry (i.e. amount of contact between the kiwifruit and the polyliner, including thickness of the polyliner), temporal discretisation (i.e. time step), number of elements solved (i.e. mesh sizing) and transport phenomenon involved (i.e. natural convection but no radiation) were unchanged. The reasoning behind each step in the development of the numerical model was outlined in Chapter 5. To ensure the numerical model was as robust as possible additional tests into the turbulence model, transport phenomenon, mesh size, time step size and model geometries were performed.

Unless otherwise stated testing of the numerical model followed the procedure outlined in section 6.3 (inlet air temperature of 0 °C, initial temperatures within pallet of 20 °C, pressure drop of 850 Pa, flowrate of 0.71 L kg^{-1} s^{-1}).

A1.2 Turbulence models

The impact of various turbulent models on the temperature prediction during the forced-air cooling process of kiwifruit modular bulk packs (MBPs) was evaluated. When choosing a turbulence model for complex geometries, such as food packaging systems, a compromise must be made between expected prediction accuracy and practical mesh size. Defraeye et al. (2013a) evaluated the performance of several turbulence models for spherical food products. Low-Reynolds number modelling (LRNM) exhibited the best performance. However, for this project the excessively high number of mesh elements (> 10 mil) required to explicitly resolve the mesh down to the boundary layer and subsequent computational cost was not practically feasible. Instead wall functions (WF), which use semi-empirical functions to describe the boundary layer and require much lower grid resolutions, were employed. However, standard WFs have been reported to produce inaccurate predictions (Defraeye et al., 2013a). Recent versions of Fluent provide an enhanced wall treatment option (EWT) that can be combined with the κ-ε and κ-ω turbulence models (Fluent, 2010). This EWT option can be used across a wide range of mesh sizes and Reynolds numbers.

Prior to specifying a turbulence model the standard κ-ε model, with standard WFs and EWT, and the standard κ-ω turbulence model (which employs the EWT as default) were tested. The κ-ε and κ-ω are commonly employed in the numerical modelling of food operations (section 2.4.2). Defraeye et al. (2013a) note that, in CFD, most turbulence models perform well for Reynolds numbers below 300. Hence, the turbulence model evaluation for this project was performed for the highest flowrate simulated (0.71 L kg^{-1}

s^{-1}; section 7.5). A flowrate of 0.71 L kg^{-1} s^{-1} generated local $y^+ > 300$. For comparison fully turbulent flow is present when $y^+ > 30$ (Fluent-Theory, 2010).

For the individual MBPs there were minimal differences between the standard κ-ε model (with the EWT prescribed) and the standard κ-ω model, over 12 h of forced-air cooling (Figure A1.1). When standard wall functions were applied to the κ-ε model temperature discrepancies were observed (Figure A1.2).

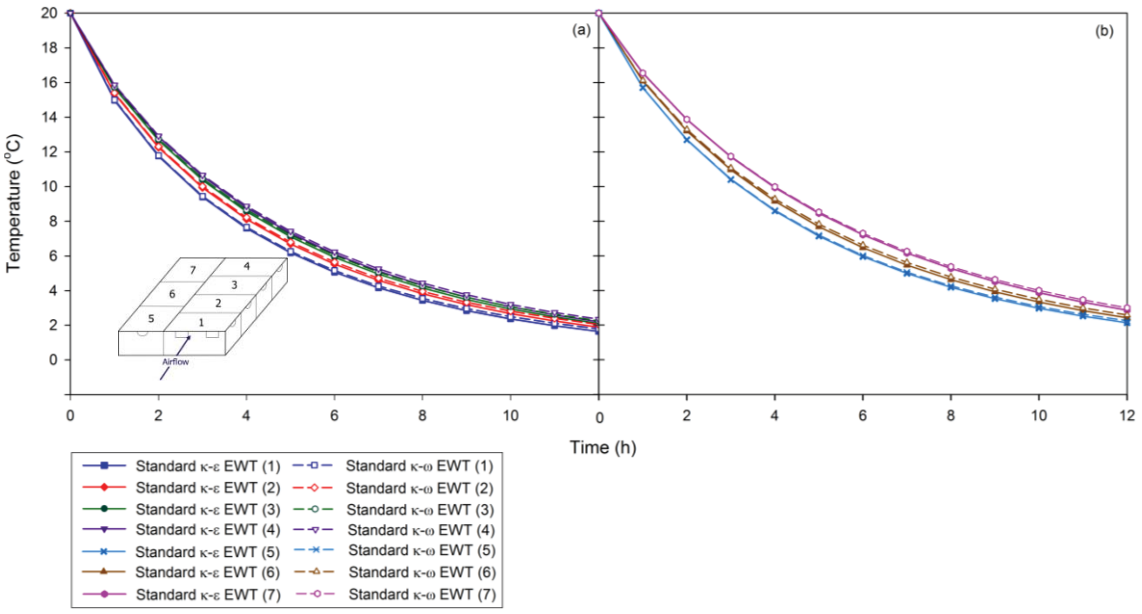

Figure A1.1. Temperature predictions for (a) MBPs 1 – 4 and (b) MBPs 5 – 7, during forced-air cooling, for a pressure drop of 850 Pa (0.71 L kg^{-1} s^{-1}), between the κ-ε (EWT) and κ-ω turbulence models.

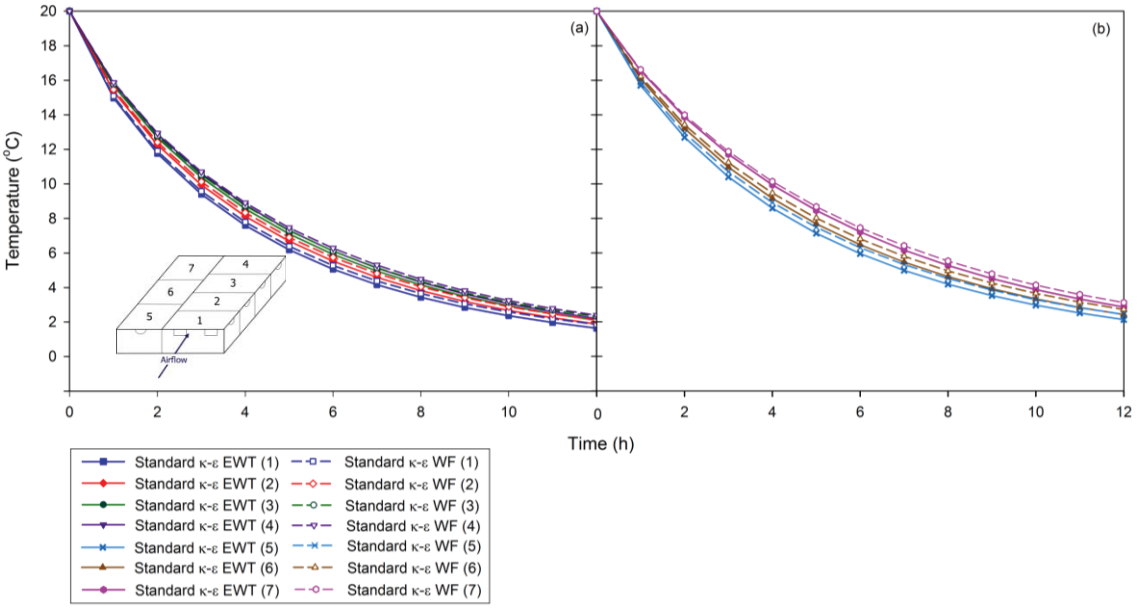

Figure A1.2. Temperature predictions for (a) MBPs 1 – 4 and (b) MBPs 5 – 7, during forced-air cooling, for a pressure drop of 850 Pa (0.71 L kg^{-1} s^{-1}), between the κ-ε (EWT) and κ-ε (standard WF) turbulence models.

The average half-cooling time (HCT) for the pallet layer was approximately 3 h. Hence, the differences in temperature prediction, compared to the baseline values generated for the standard κ-ω turbulence model, were calculated at 3 h after initiation of the forced-air cooling simulation (Table A1.1). From the results either the standard κ-ε (with EWT) or the standard κ-ω turbulence model can be employed. During turbulence model testing the standard κ-ε EWT model showed faster convergence for the first time step (~ 10 iterations) compared to the standard κ-ω turbulence model (~ 30 iterations). This was essential from a practical stand point when solving a simulation where the flow field and turbulence equations must be calculated, with the energy equations, at each time step. Hence, the standard κ-ε EWT model was employed for the numerical model.

Table A1.1. Difference in temperature prediction after 3 h of forced-air cooling for the numerical model tests, at a flowrate of 0.71 L kg^{-1} s^{-1} (850 Pa).

	Temperature (°C)							
Model alterations	**MBP 1**	**MBP 2**	**MBP 3**	**MBP 4**	**MBP 5**	**MBP 6**	**MBP 7**	**Average**
Standard	**9.40**	**9.94**	**10.37**	**10.60**	**10.40**	**10.96**	**11.72**	**10.65**
κ-ε turbulence model (Standard WF)	+ 0.18	+ 0.19	+ 0.15	+ 0.09	+ 0.30	+ 0.27	+ 0.16	+ 0.21
κ-ω turbulence model (EWT)	+ 0.05	+ 0.08	+ 0.09	+ 0.06	+ 0.03	+ 0.11	+ 0.03	+ 0.06
Polyliner thickness included	- 0.01	+ 0.00	- 0.02	- 0.06	- 0.01	+ 0.01	- 0.08	- 0.03

A1.3 Model geometry

A1.3.1 Contact between polyliner and kiwifruit

Finding an exact value for the amount contact between the kiwifruit and polyliner proved elusive in this project. Additionally, due to the highly malleable nature of the polyliner (which behaves as a plastic bag) the exact percentage of contact was expected to change between each MBP in a pallet. Hence, any experimentally determined number would have a large range of values. In the numerical model development the polyliner was placed in direct contact with each external face of the kiwifruit bulk, to a depth of 5 mm (section 5.3.3). This was the minimal depth achievable to ensure solution stability. However, it was possible to increase the amount of contact. In the interest of comprehensively evaluating the possible variables the amount of contact was increased by 40 %. This increase stretched the amount of contact to the upper limit of what could potentially occur in reality, a judgement formed from 4 years of working with kiwifruit MBPs.

For the current numerical set-up the surface area of the polyliner in contact with the air was 39.6 $x10^{-2}$ m^2, with 5.4 $x10^{-2}$ m^2 (14 %) in contact with kiwifruit bulk. The amount of contact was increased by 40 % to 7.6 $x10^{-2}$ m^2. The increased contact initially caused

slightly faster temperature drops for the MBPs due to increased forced convective cooling from the refrigerated-air, through the polyliner, to the kiwifruit (Figure A1.3). However, after initial cooling of the external kiwifruit bulk the differences in cooling profiles became minimal. This simulation was carried out at the highest flowrate tested over the course of this project (0.71 L kg^{-1} s^{-1}), where the impact of increased contact area, due to increased potential for forced convection would have been highest. Hence, provided a sensible amount of contact was prescribed then the numerical model was relatively unaffected by the exact value.

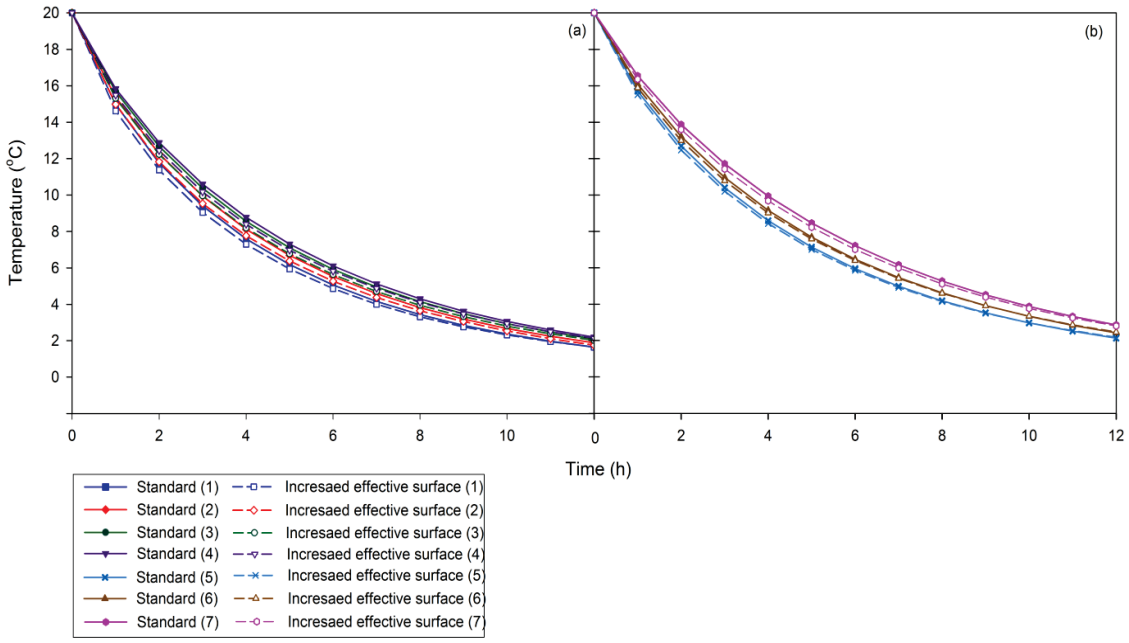

Figure A1.3. Effect of increasing the effective surface area between the kiwifruit and polyliner by 40 %, compared to standard numerical set-up, in the forced-air cooling simulation. Temperature profiles are shown for (a) MBPs 1 – 4 and (b) MBPs 5 – 7. Simulations were run for a pressure drop of 850 Pa (0.71 L kg^{-1} s^{-1}).

A1.3.2 Polyliner thickness

In the development of the numerical model the polyliner was expected to provide a physical but not thermal barrier to heat transfer, due to the narrow thickness (10 μm) of the polyliner. This assumption was tested by comparing the temperature of the MBPs,

after 3 h of forced-air cooling, with and without the polyliner thickness (Table A1.1). The maximum difference in temperature, after 3 h of cooling was 0.07 °C, for MBP 7. Hence, the thickness of the polyliner was neglected.

A1.4 Richardson extrapolation

The scripts used for the Richardson extrapolation are used to represent various terms (i.e. specified variable, mesh size, order of accuracy, etc.), hence they are independent of the nomenclature listed on page xiv. The Richardson extrapolation, also known as h^2 extrapolation, is a posteriori error estimator, which quantifies the error of a specified variable, *f*. The extrapolation can be used for both spatial and temporal discretisation, where *h* represents time step or mesh size, depending the discretisation error under investigation. The extrapolation will be discussed for spatial discretisation but the temporal discretisation can be calculated by substituting the inverse of the time step (to ensure increasing time step values with refinement) for mesh size in the equations. The discrete solution is assumed to have a series representation of (Franke et al., 2007; Roache, 1997),

$$f_k = f_{exact} + g_p h_k^p + g_{p+1} h_k^{p+1} + g_{p+2} h_k^{p+2} + \ldots \tag{A.1}$$

where *k* denotes the mesh size (i.e. 1 = fine, 2 = medium and 3 = coarse mesh), *p* is the order of accuracy and *g* are coefficients. Provided the solution for h_k is in the asymptotic range all terms of higher order then *p* are neglected and *p* and *g* do not depend on h_k.

With three unknowns on the right hand side of Eq. A.1, three equations with three different mesh sizes are required. From the three mesh sizes (h_1, h_2 and h_3) where $h_1 > h_2 > h_3$, two mesh refinement ratios can be introduced,

$$r_{21} = h_2/h_1\,, \qquad r_{32} = h_3/h_2 \tag{A.2}$$

The series expansions can now be written as,

$$\begin{aligned} f_1 &= f_{exact} + g_p h_1^p = f_{exact} + g_p h_1^p \\ f_2 &= f_{exact} + g_p h_2^p = f_{exact} + g_p (r_{21} h_1)^p \\ f_3 &= f_{exact} + g_p h_3^p = f_{exact} + g_p (r_{21} r_{32} h_1)^p \end{aligned} \tag{A.3}$$

If monotonic converge of the variable is present, defined as when the range of the ratio of solution changes, $R = (f_2 - f_1)/(f_3 - f_2)$, is $0 < R < 1$, p can be calculated from the following transcendental equation with an iterative method,

$$p = \frac{ln[(f_3 - f_2)/(f_2 - f_1)]}{ln(r_{21})} - \frac{1}{ln(r_{21})}\left[ln\left(r_{32}^p - 1\right) - ln\left(r_{21}^p - 1\right)\right] \tag{A.4}$$

Eliminating g_p in Eq. A.3 allows the exact solution to be estimated,

$$f_{exact} = f_1 + \frac{f_1 - f_2}{r_{21}^p - 1} \tag{A.5}$$

The spatial discretisation errors for each of the mesh sizes are then calculated from,

$$\begin{aligned} DE_1 &= f_1 - f_{exact} = \frac{f_2 - f_1}{r_{21}^p - 1} \\ DE_2 &= f_2 - f_{exact} = \frac{r_{21}^p (f_2 - f_1)}{r_{21}^p - 1} = r_{21}^p DE_1 \\ DE_3 &= f_3 - f_{exact} = \frac{r_{32}^p r_{21}^p (f_2 - f_1)}{r_{21}^p - 1} = (r_{32} r_{21})^p DE_1 \end{aligned} \tag{A.6}$$

A.1.4.1 Time Step

The time step was determined via the Richardson extrapolation. The unsteady-state temperature was used instead of a steady-state variable (i.e. heat transfer coefficient from the kiwifruit). A heat transfer coefficient at steady-steady state between the refrigerated air and effective polyliner surface would not account for the kiwifruit at the centre of the bulk and not be representative of the entire system. The average temperature of the kiwifruit in the pallet after 3 h of forced-air cooling the variable tested. The inverse of the time step (this increases with smaller time steps) was used in place of the number of control volumes. Relative errors were 0.3 %, 1.0 % and 3.1 % for times steps of 15 s, 30 s and 60 s, respectively (Figure A1.4). A time step of 30 s extended the simulation time more than two fold, from 24 h to 52 h. At a time step of 60 s the temporal discretisation error was estimated at 3.1 % making 60 s an acceptable compromise between solution accuracy and computation time.

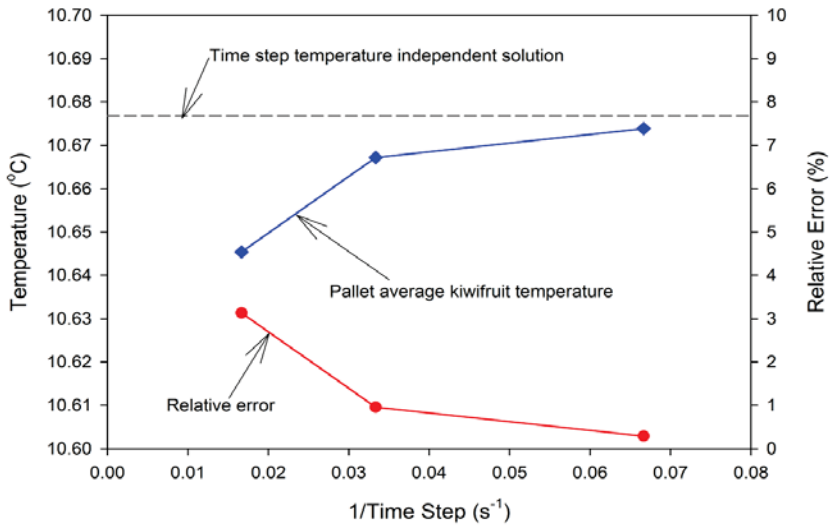

Figure A1.4. Time step convergence for the pallet average kiwifruit temperature compared to the Richardson solution and the relative error, at a pressure drop of 850 Pa (0.71 L kg^{-1} s^{-1}).

The time step was evaluated at a constant mesh size of 7.6 x10^6, the mesh size used in the numerical model (A1.4.2). Hence, the time step error and temperature discrepancies are the 3.1 % error within the mesh error. A graphical representation of the target variable (fruit temperature) was simulated for time steps of 15 s and 60 s (Figure A1.5), following the recommended procedure outlined by Franke et al. (2007).

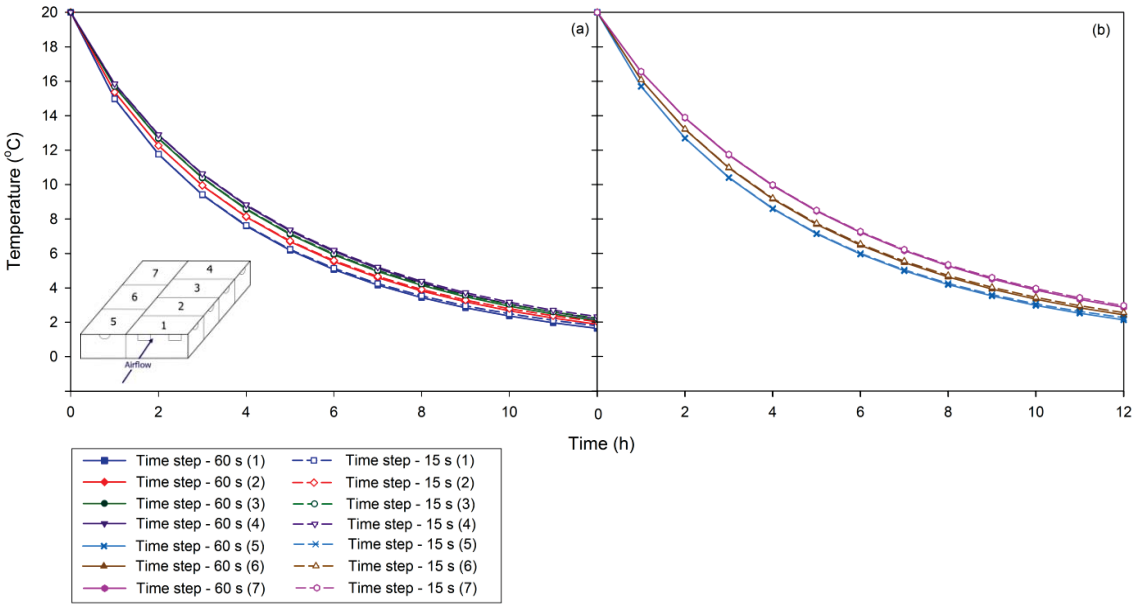

Figure A1.5. Numerical temperature predictions for (a) MBPs 1 – 4 and (b) MBPs 5 – 7, during forced-air cooling, for a pressure drop of 850 Pa (0.71 L kg^{-1} s^{-1}), for time steps of 15 s and 60 s.

A1.4.2 Mesh sizing

Mesh sensitivity was originally evaluated at a pressure drop of 850 Pa. However, to ensure that the results generated for new box design, calculated at pressure drops between 76 and 100 Pa, remained valid the Richardson extrapolation for the mesh sizing was re-calculated at a pressure drop of 100 Pa. To avoid supplying superfluous information only the results at a pressure drop of 100 Pa are presented.

While doubling the mesh size is the most commonly employed technique, this is actually not the most useful or desirable technique (Roache, 1997). With the high mesh sizes involved overestimating the mesh size required could significantly extend the computational time. Hence, mesh sizing was based on the difference, caused by a 30 % increase in the number of mesh elements, in predicted temperatures after a specific forced-air cooling time period (5 h, the approximate HCT).

Total mesh size was 7.35 x10^6 elements with a maximum face size of 7.5 mm. A lower mesh (5.70 x10^6 elements) was generated with a maximum face size of 9.0 mm and a higher mesh (9.50 x10^6 elements) with a size of 6.7 mm. The relative error in temperature was 5.6 %, 1.1 % and 0.2 % for mesh sizes of 5.70 x10^6, 7.35 x10^6 and 9.50 x10^6 elements, respectively (Figure A1.6). The mesh size of 7.35 x10^6 elements was a compromise between relative error and computational expense.

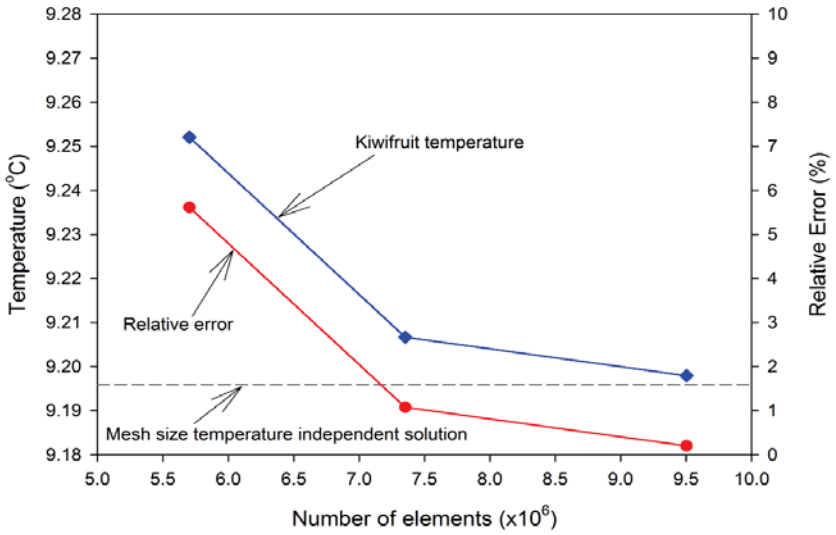

Figure A1.6. Convergence, with increasing mesh size, for the kiwifruit temperature compared to the Richardson solution and the relative error, at a pressure drop of 100 Pa (0.243 L kg^{-1} s^{-1}).

Comparing temperatures over time showed minute differences between mesh sizes of 7.35 x10^6 and 9.50 x10^6 elements (Figures A1.7 and A1.8).

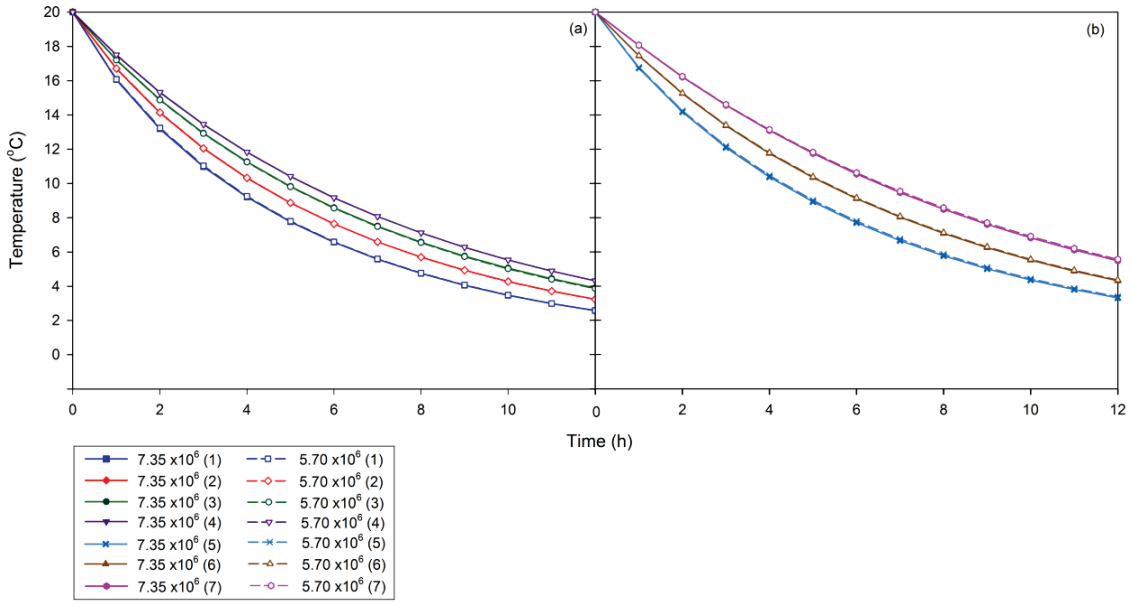

Figure A1.7. Numerical temperature predictions for (a) MBPs 1 – 4 and (b) MBPs 5 – 7, during forced-air cooling, for a pressure drop of 100 Pa (0.243 L kg^{-1} s^{-1}), for mesh sizes of 5.70 x10^6 and 7.35 x10^6 elements observed.

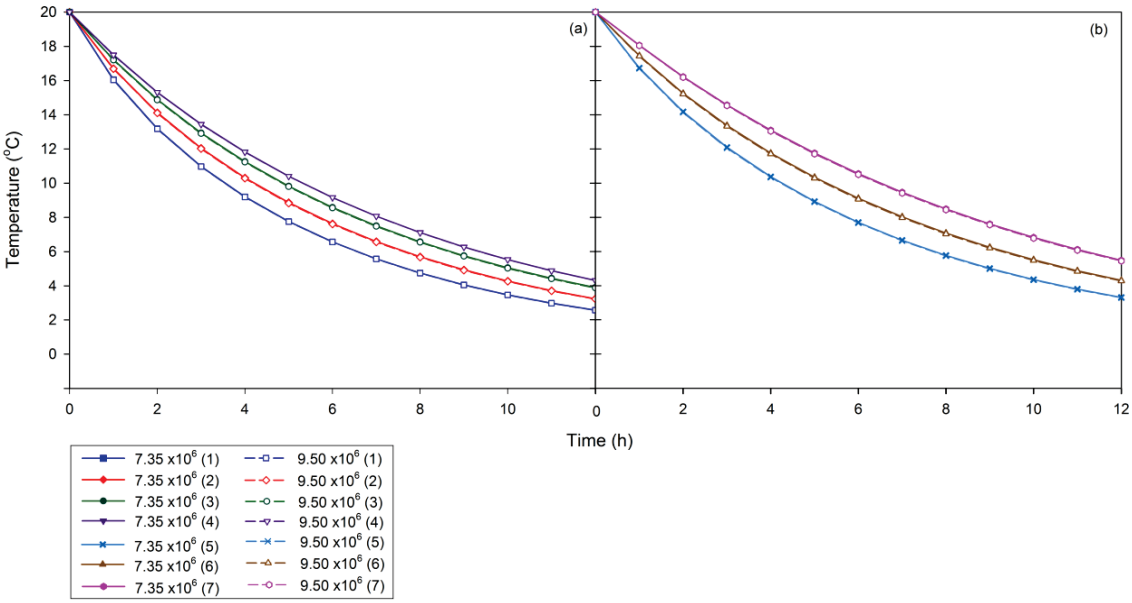

Figure A1.8. Numerical temperature predictions for (a) MBPs 1 – 4 and (b) MBPs 5 – 7, during forced-air cooling, for a pressure drop of 100 Pa (0.243 L kg^{-1} s^{-1}), for mesh sizes of 7.35 x10^6 and 9.50 x10^6 elements.

A1.5 Transport phenomenon solved

Unlike the rest of the numerical tests natural convection had a significant influence on the cooling performance. Hence, the impact of natural convection was evaluated at the optimal operating conditions (100 Pa; 0.243 L kg^{-1} s^{-1}), used to compare the alternative box design. Radiation was not expected to have a significant impact. However, as the transport phenomenon of natural convection was evaluated at 100 Pa, the contribution radiation was assessed at the same conditions.

A1.5.1 Natural convection

To exclude natural convection from the numerical simulation gravity was deactivated and the air inside the polyliner was assigned the same thermal properties as the refrigerated air pulled through the pallet (section 6.4.1). The impact of natural convection was relatively minor at the start of the simulation, when the majority of the heat transfer took place through the kiwifruit in contact with polyliner, exposed to the refrigerated airflow pulled through the MBPs (Figure A1.9). However, following the initial rapid cooling along the outside of the kiwifruit bulk heat transfer due to natural convection had a greater relative influence on the process. Discrepancies, due to the exclusion of natural convection, between the kiwifruit temperatures appeared earlier on (< 2 h after initialisation) for the MBPs at the front of pallet (MBPs 1 and 5). The faster the kiwifruit on the outside of the bulk cooled the faster that natural convection started to have a substantial influence on the rate of heat transfer.

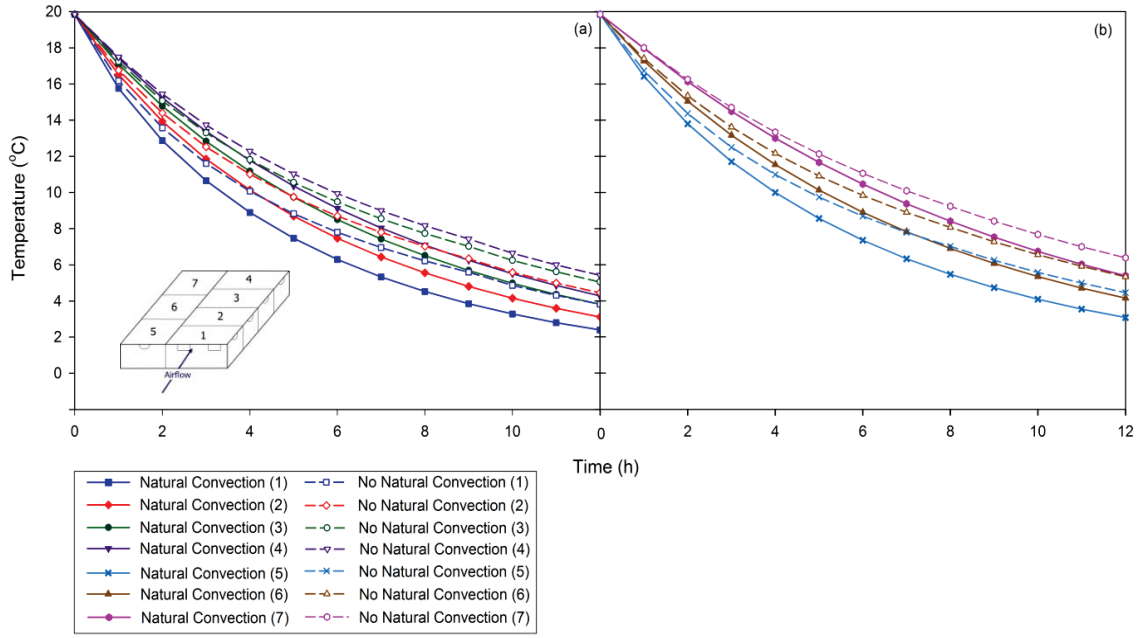

Figure A1.9. Influence of including and excluding natural convection, in the forced-air cooling simulation. The temperature profiles are shown for (a) MBPs 1 – 4 and (b) MBPs 5 – 7. Simulations were run for a pressure drop of 100 Pa (0.243 L kg^{-1} s^{-1}).

Natural convection generated a flow field, with velocities up to 0.1 m s^{-1}, inside polyliner (Figure A.10). The exclusion of natural convection, and the subsequent velocity field, caused the numerical model to predict HCTs between 21.9 % (MBP 1) and 11.5 % (MBP 7) slower than when natural convection was simulated (Table A1.2).

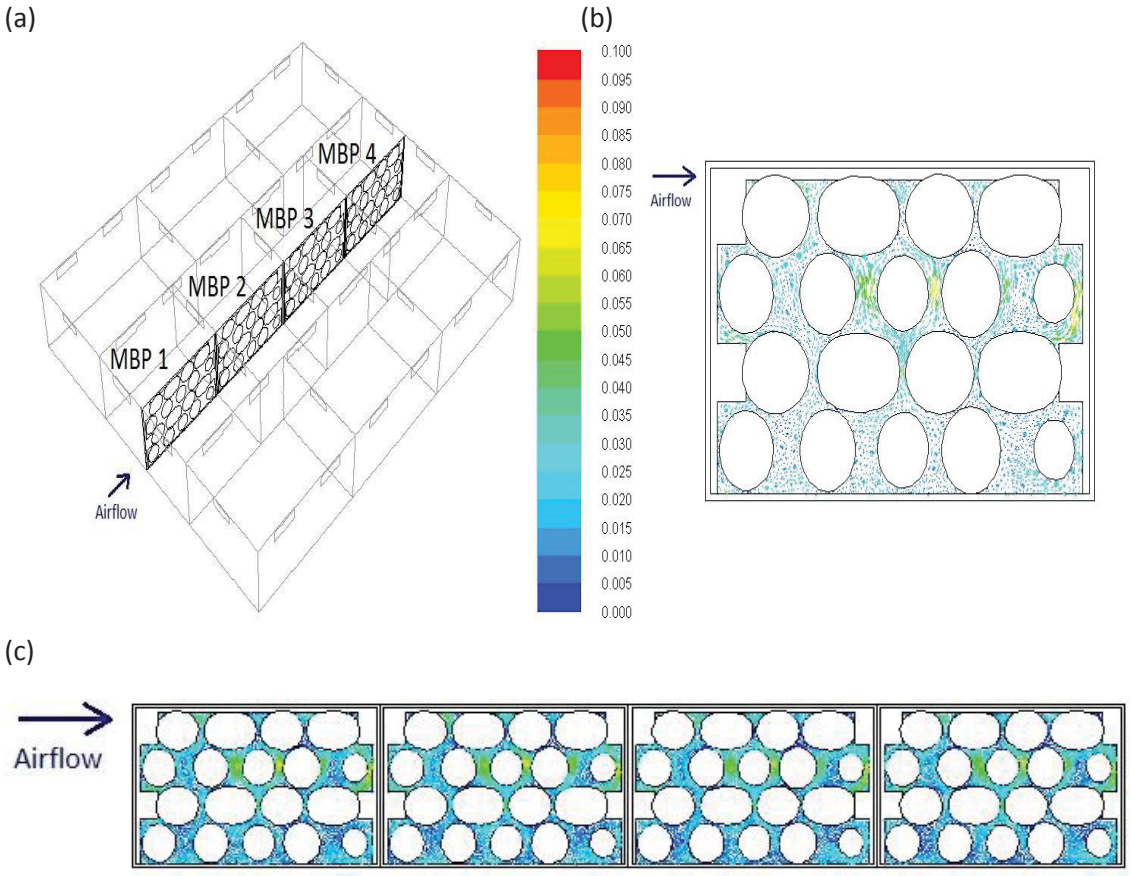

Figure A.10. (a) Location of horizontal cross-sectional area through the pallet layer. Velocity field (m s^{-1}) due to natural convection along the horizontal cross-sectional area through (b) MBP 1 and (c) MBPs 1 - 4, after 5.00 h for a pressure drop of 100 Pa (0.243 L kg^{-1} s^{-1}).

Table A.2. Effect of simulating natural convection in the numerical model on the HCT for MBPs 1 – 7

			HCT (h)							
Natural Convection	**ΔP (Pa)**	**Q (L.kg^{-1}.s^{-1})**	**MBP 1**	**MBP 2**	**MBP 3**	**MBP 4**	**MBP 5**	**MBP 6**	**MBP 7**	**Pallet layer$_{avg}$**
Included	100	0.243	3.42	4.17	4.92	5.33	4.08	5.17	6.50	4.93
Excluded	100	0.243	4.17	4.83	5.58	6.00	4.83	5.92	7.17	5.64

A1.5.2 Radiation

The discrete ordinates (DO) model was used to simulate radiative heat transfer. It was the only available model for optically thin media (air) that can be used for a pressure-based solver containing periodic boundary conditions, despite the associated computational expense (Fluent-Theory, 2010). Air was considered to be a transparent medium (e.g. it did not absorb or reflect the radiation) between the radiating surfaces. Hence, it did not participate in the radiation calculations.

For the DO model participating surfaces were defined as opaque walls, where radiation could be absorbed, reflected and/or emitted, but not transmitted directly through. There were no black bodies in the computational system hence all surfaces participating in radiation were considered grey. Wall surfaces were assumed to follow Kirchhoff's law of thermal radiation (i.e. the wall absorptivity, α, was assumed equal to the emissivity, ε). For cardboard and polyethylene ε was equal to 0.9 and 0.96, respectively (Burg, 2004). For kiwifruit ε was equal to 0.96 (section 5.5.2).

Including radiation in the numerical model resulted in a difference of 2.6 % in the average pallet temperature after 5 h (the approximate HCT) of forced-air cooling (Figure A1.10). The maximum difference, after 5 h, was 3.1 % for MBP 4. Such small differences in temperature confirmed the assumption that radiation could be excluded (section 5.5.1).

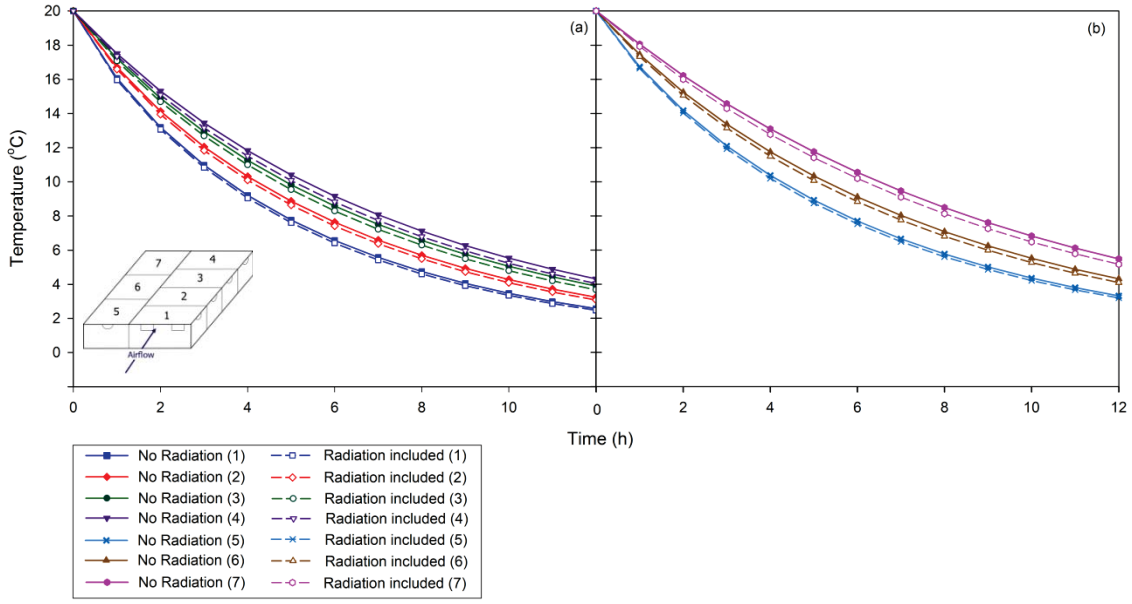

Figure A1.11. Influence of including and excluding radiative heat transfer, in the forced-air cooling simulation. The temperature profiles are shown for (a) MBPs 1 – 4 and (b) MBPs 5 – 7. Simulations were run for a pressure drop of 100 Pa (0.243 L kg^{-1} s^{-1}).

A1.6 Conclusions

The choice of turbulence model, amount of contact between the polyliner and kiwifruit, exclusion of the polyliner thickness, time step size and mesh size have been tested and justified. The numerical model identified the relative importance of natural convection to the heat transfer mechanisms and the necessity of its inclusion in the modelling of the forced-air cooling polylined horticultural produce.

General guidelines found in the user manual for the Fluent software package (Fluent, 2010) and in Franke et al. (2007) were used to initially set the mesh sizing and settings, along with the solver methods. However, these guidelines are only general and are a best guess of what can be expected to work over a wide range of systems. With respect to the overall page count and attempts to excluded unnecessary and excessive information, it is difficult to show each individual step that lead to the choice of each

setting/scheme for this specific system for the range of conditions. Ultimately, many of the final settings (i.e. expansion ratio in the meshing program or spatial discretization gradient in Fluent) were based on testing the alternatives and general knowledge, in terms of impact to solution speed and convergence, gained over the course of this project.

Appendix A2

Monitored kiwifruit location

In experiments the temperatures of 12 kiwifruit were recorded by thermocouples in each monitored modular bulk pack (MBP). The kiwifruit locations (described in section 4.4.3) were selected to both fully capture the temperature gradients within a MBP and give an accurate average temperature of the kiwifruit bulk upon averaging the data from each location. The choice of kiwifruit location was qualitative. After development of the numerical model a test comparing the temperature of the kiwifruit bulk generated by averaging the 12 measurement points against the volume-average temperature was performed.

To save computational time the test was performed for a single MBP. The numerical model was a reduced version of the full pallet layer (Figure A2.1) and used the same MBP geometry, mesh setting and simulation set-up as outlined for the full pallet layer in Chapter 5. The simulation was run for a pressure drop of 100 Pa.

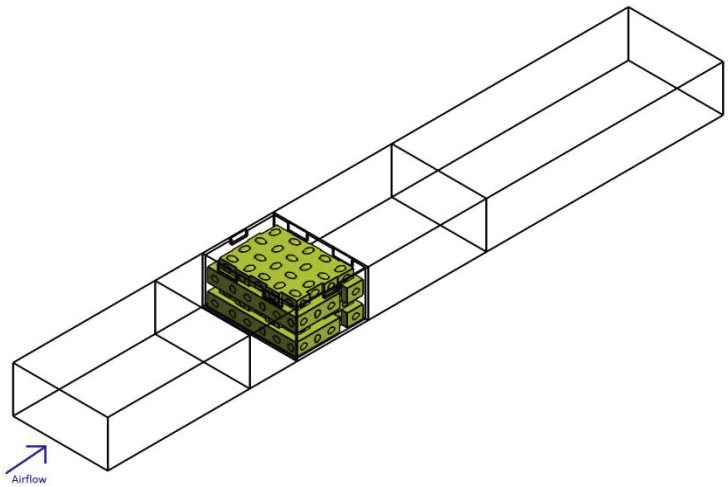

Figure A2.1. 3D schematic diagram of the computational pallet layer for the forced-air cooling of a single modular bulk pack, when air is pulled through 1.0 m pallet face.

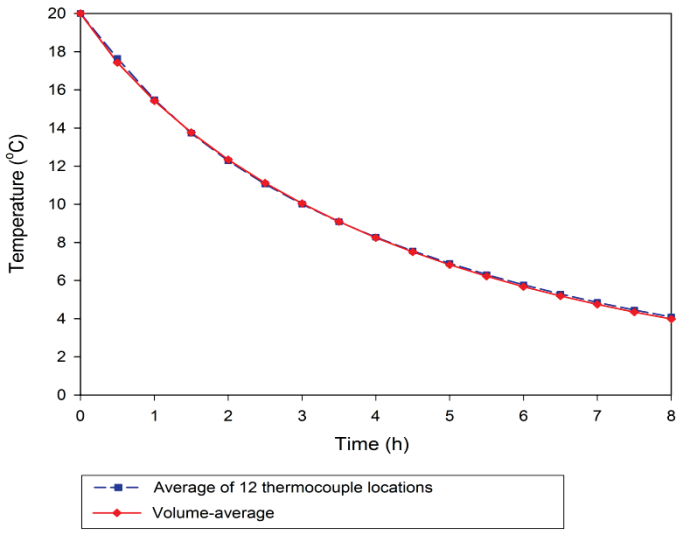

Figure A2.2 Comparison of average temperature of kiwifruit bulk, calculated by averaging 12 data points and by the volume-average temperature

There was a slight temperature difference for the first 0.5 h of cooling (Figure A2.2). The point measurements had to wait until the temperatures at their specific locations (the centre of the kiwifruit) began to cool before the temperature drop was registered. The volume-average temperature calculates the temperature across the entire kiwifruit bulk (including the kiwifruit surfaces which began to cool immediately). Hence, the volume-average measurement technique predicted slightly faster cooling at the start of the simulation. Apart from the first 0.5 h the results show an almost identical temperature prediction when the kiwifruit bulk temperature was either calculated from the average temperature of 12 points representing the 12 thermocouple locations and the volume-average of the entire kiwifruit bulk.

MASSEY UNIVERSITY
GRADUATE RESEARCH SCHOOL

STATEMENT OF CONTRIBUTION TO DOCTORAL THESIS CONTAINING PUBLICATIONS

(To appear at the end of each thesis chapter/section/appendix submitted as an article/paper or collected as an appendix at the end of the thesis)

We, the candidate and the candidate's Principal Supervisor, certify that all co-authors have consented to their work being included in the thesis and they have accepted the candidate's contribution as indicated below in the *Statement of Originality*.

Name of Candidate: Justin O'Sullivan

Name/Title of Principal Supervisor: Dr. Andrew East

Name of Published Research Output and full reference:

Journal Paper: O'Sullivan, J.L., Ferrua, M.J., Love, R.J., Verboven, P., Nicolaï, B.M. and East, A.R. (2014). Airflow measurement techniques for the improvement of forced-air cooling, refrigeration and drying operations, Journal of Food Engineering, 143(0), 90-101.
Conference Paper (1): O'Sullivan, J.L., Ferrua, M., Love, R., Verboven, P., Nicolai, B.M. & East, A. (2012). Mechanisms and performance of the forced-air cooling process of fruit packed in polyethylene liners, CIGR Section VII International Technical Symposium on Innovating the Food Value Chain, Stellenbosch, South Africa.
Conference Paper (2): O'Sullivan, J.L., Ferrua, M.J., Love, R.J., Verboven, P., Nicolaï, B.M. & East, A.R. (2013a) Performance of the forced-air cooling process of fruit packed in polyethylene liners as a function of pallet orientation, Proc. 2nd IIR International Conference on Sustainability and the Cold Chain, Paris, France.
Conference Paper (3): O'Sullivan, J.L., Ferrua, M.J., Love, R.J., Verboven, P., Nicolaï, B.M. & East, A.R. (2013b) Mathematical modelling of kiwifruit packaging undergoing forced-air cooling, Proc. 26th Symposium on Packaging, Espoo, Finland.

In which Chapter is the Published Work: Chapter 2, 4 and 5

Please indicate either:

- The percentage of the Published Work that was contributed by the candidate:

  and / or

- Describe the contribution that the candidate has made to the Published Work:

  The candidate carried out experimental work, data analysis and report writing. Co-authors edited the work and helped with experimental and numerical model design.

Justin O'Sullivan
Digitally signed by Justin O'Sullivan
DN: cn=Justin O'Sullivan, o=Massey University, ou=IFNHH, email=j.osullivan@massey.ac.nz, c=NZ
Date: 2015.09.18 20:26:38 +12'00'

Candidate's Signature

18-09-2015

Date

a.r.east@massey.ac.nz
Digitally signed by a.r.east@massey.ac.nz
DN: cn=a.r.east@massey.ac.nz
Date: 2015.09.19 06:22:47 +12'00'

Principal Supervisor's signature

19-09-2015

Date

Journal of Food Engineering 143 (2014) 90–101

Contents lists available at ScienceDirect

Journal of Food Engineering

journal homepage: www.elsevier.com/locate/jfoodeng

Review

Airflow measurement techniques for the improvement of forced-air cooling, refrigeration and drying operations

Justin O'Sullivan [a,*], Maria Ferrua [b], Richard Love [a], Pieter Verboven [c], Bart Nicolaï [c], Andrew East [a]

[a] Centre for Postharvest and Refrigeration Research, Massey University, Private Bag 11-222, Palmerston North 4442, New Zealand
[b] Riddet Institute, Massey University, Private Bag 11-222, Palmerston North 4442, New Zealand
[c] BIOSYST-MeBioS, University of Leuven, Willem de Croylaan 42, Heverlee, Belgium

ARTICLE INFO

Article history:
Received 25 February 2014
Received in revised form 6 June 2014
Accepted 29 June 2014
Available online 8 July 2014

Keywords:
Numerical model validation
Experimental
Laser doppler anemometry
Particle image velocimetry
Thermal anemometry
Flow visualisation

ABSTRACT

Flowrate and distribution of air is a critical design factor in the cooling, refrigeration and drying of horticultural food products. These operations rely on a constant supply of air distributed throughout bulk arrangements of the produce. Local distribution of the air is critical to optimising the design and efficiency of these processes. Identification of the key parameters affecting the airflow distribution has been done either experimentally (using intrusive point-wise or bulk measurement techniques) or numerically. The detailed information provided by the use of computational fluid dynamic models has facilitated unique opportunities to investigate alternative system designs, without the need for expensive and time consuming experiments. This study provides a review of the techniques available to measure airflow (thermal and rotatory vane anemometry, pressure differential devices, tracer gases, LDA and PIV). Their advantages and disadvantages (accuracy, resolution, application range, cost, and ease of use) as well as their application in the validation of numerical models are reviewed. The novel and scientifically based design guidelines developed by a better understanding of the airflow behaviour within the system for each of the operations under study are also presented.

Contents

* Corresponding author. Tel.: +64 6 350 4336; fax +64 6 350 5657.
E-mail address: j.osullivan@massey.ac.nz (J. O'Sullivan).

http://dx.doi.org/10.1016/j.jfoodeng.2014.06.041
0260-8774/

1. Introduction

Common cooling and drying operations of food are typically based on the heat exchange between a food product and a constant supply of airflow through the system (Ghisalberti and Kondjoyan, 1999). For the cooling, refrigeration and drying of food the flowrate, distribution and temperature of the airflow throughout the entire packaging structure ultimately determines the rate, uniformity and efficiency of these processes. As uniform temperatures are desired in all three operations any operating and/or design feature capable of affecting the local distribution of the airflow behaviour within the system will have a profound effect on the performance of these processes.

In forced-air cooling, the size and location of the openings of the ventilated packages have been found to have a particular effect on the rate and uniformity of the process (Defraeye et al., 2013, 2014; Delele et al., 2008; Ferrua and Singh, 2009a; van der Sman, 2002; Vigneault et al., 2006). Ventilated packaging should be designed to provide uniform airflow distribution. However, uniform cooling does not always go hand in hand with higher cooling rates, and package design is a determining factor (Defraeye et al., 2014). The vents or openings determine how much air can come in contact with the product, how it is distributed inside the package, and what the air velocity magnitude is. Hence, cooling heterogeneity within packages is often a result of uneven airflow distribution (Dehghannya et al., 2008, 2011, 2012). A comprehensive review by Pathare et al. (2012) gives the recommended vent areas for a wide range of ventilated packages for horticultural produce.

In refrigerated rooms pallet stacking patterns can result in an uneven airflow distribution. When pallets are stacked high and closely packed together those centrally located and at the rear of the room (away from the evaporator fans) will receive smaller volumetric flows of refrigerated air compared to the pallets at the front of the room (adjacent to the evaporator fans). These local differences in flowrate throughout the room cause differences in the air temperature, with warm spots developing depending on pallet location (Verboven et al., 2003). Similarly, for refrigerated transport vehicles, pallet compactness can lead to high airflow resistances and uneven airflow distribution, with the formation of stagnant zones with higher air temperatures in the rear of the vehicle (Smale et al., 2006).

Typically, in forced-convection drying, warm, dry air exits an inlet and is distributed under a bed of horticultural produce. This air tends to follow a streamline flow and if not redirected will be distributed along the centre and towards the back of system, with regions not in the main pathway receiving smaller volumetric airflows, resulting in a non-uniform final moisture content (Nagle et al., 2010). When using impinging hot air jets for drying, the location and direction of the jet can affect the rates of heat and mass transfer spatially along the product width, as a higher percentage of the airflow is directed to one section of the product (Marcroft et al., 1999).

To improve the performance of these food operations a detailed understanding of how different design parameters and operating conditions affect the airflow behaviour within the systems is essential. This information has been traditionally obtained by measuring the local distribution of the airflow within the system using a wide range of experimental techniques. In addition, experimental information collected on the behaviour of the airflow has been also recently used for the validation of numerical models of the process (Smale et al., 2006). Beginning in the 1990s engineering simulation tools, such as Computational Fluid Dynamics (CFD), have become increasingly used in the analysis of cooling and drying processes within the food industry. Relevant examples are given in Wang and Sun (2003). Advanced CFD tools can predict complex airflow patterns in food operation systems in a level of detail difficult to achieve experimentally, facilitating a better and more fundamental understanding of the effect of the design and operating conditions on the efficiency of the process.

This study reviews not only the airflow measurement techniques currently employed to characterise airflow behaviour in forced-air cooling, refrigerated and drying applications but also their application in developing a better understanding and design of these processes.

2. Airflow measurement techniques

2.1. Direct airflow measurement

Direct flow measurement techniques are generally devices placed in the flow field which measure point-values in a system. They are widely used due to their robustness, ease of use and competitive price compared to non-invasive image analysis. These techniques include thermal anemometry, vane anemometry and differential pressure flowmeters.

2.1.1. Thermal anemometers

Thermal anemometers consist of a small, electronically heated sensor, initially kept at a constant temperature above that of the fluid flow temperature. Once the sensor is placed in the flow field it experiences a certain amount of cooling. As the electrical resistance of the sensor is dependent upon its temperature, a relationship can be obtained between the flow speed and the voltage output from the sensor.

Thermal anemometers can be operated to maintain a constant temperature or constant current through the sensor. In the case of constant temperature anemometers, the sensor's resistance is constant and the required voltage (or current) to maintain the temperature is measured. Conversely, for constant current anemometers the applied current is held constant and the sensor's voltage drop (or electrical resistance) is measured (Fingerson and Freymuth, 1996). The air velocity can then be inferred from the power required to maintain the temperature or current of the sensor. The sensor placed in the fluid flow is a wire for hot-wire anemometers and a film in the case of hot-film anemometers.

Thermal anemometers can be made at a relatively low cost and when thin wires are used a high sampling frequency can be used (up to 10^5 Hz). Limitations of thermal anemometers include the requirement for regular calibration, which often involves the

device been sent back to the manufacturer once a year. The recorded velocities may be affected by impurities in the fluid that adhere to the wire, interfering with the heat transfer. Thin hot wire systems while very sensitive and accurate are very fragile and need to be combined with a portable support, positioning system, a probe calibrator, A/D converter, thermal anemometry software and a computer. Such systems can become quite expensive. For use in more industrial relevant environments, more robust (thicker hot wires) and compact solutions can be used. However, these hot wire/film anemometers are unsuitable when attempting to measure very high or low air velocities. At low air velocities (i.e. below 0.1 m s^{-1}) natural convection can become prevalent and as a result heat transfer is no longer solely dominated by forced convection (Page et al., 2009).

Alternatively, at high air velocities (i.e. above 100 m s^{-1}) the heat from the sensor tends to dissipate extremely quickly, reducing its sensitivity to changes in the velocity field (Jing et al., 2011).

The ability of hot-wire anemometers to capture turbulent high-frequency velocity fluctuations is limited by the sensor size. Depending on the level of turbulence the fluctuating components of the air velocity can have a broad frequency spectrum, from as low as 10^{-2} Hz to in excess of 10^{5} Hz (Webster, 2000). Robust hot wire systems (diameter between 0.5 and 1.0 mm) are unable to capture these high frequency velocity variations, however, the fluctuations do increase the heat transfer between the sensor and the air, causing the average velocity to be overestimated. To compensate for this a sensor with an extremely small diameter (~5 μm) and electronics that can account for the fluctuating frequencies and allow for a flat frequency response between 0 and 10^{4} Hz must be employed (Webster, 2000).

When the turbulent velocity fluctuation is more than 30% of the average velocity the probe must be moved through the flow field at a speed high enough to compensate for sudden drops in the air velocities as a result of turbulence, a technique known as "flying hot-wire system" (Jorgensen, 2002). This requires sufficient open space for the hot-wire anemometer, which is usually not found in food processing operations.

For accurate measurements the airflow direction must be known before the experiment is started and the sensor wire mounted perpendicular to the flow, unless otherwise stated by the manufacture (Jorgensen, 2002). In the case of 2D and 3D flows, multisensory hot-wire probes are used to measure the different components of the velocity field. Spherical hot wire probes that can measure the air speeds, while being insensitive to the airflow direction also exist (Lomas, 1986).

Despite the small diameter of the sensor the probe itself often has a length in excess of 0.5 m. This can create problems when investigating the airflow conditions within confined spaces such as in between horticultural packages stacked in a pallet, as the introduction of a thermal anemometer may change the airflow conditions within them (Alvarez and Flick, 1999a).

Examples of hot-wire anemometry for measuring airflow measurements in food operations include: Alvarez and Flick (1999a), Amanlou and Zomorodian (2011), Delele et al. (2008, 2009a, 2009b), Janjai et al. (2006), Kashaninejad et al. (2010), Ngcobo et al. (2013), Santonico et al. (2010) and Verboven et al., 2005.

2.1.2. Vane anemometry

Vane anemometers measure the average velocity of the airflow of a particular region within a system. A vane anemometer operates on the principle that when fluid flow hits the vanes it causes them to rotate. The higher the flow speed the faster the rotation. This rotational speed is sensed by an optical or magnetic sensor and the signal is converted to a velocity measurement.

The simplicity of vane anemometers has resulted in the manufacturing of hand held devices, which are advantageous if a portable measurement device is required. The accuracy of the anemometer is heavily dependent on the vane angle with respect to the airflow direction, which must be precisely known before any velocity measurements can be taken (Mirade and Daudin, 1998). Additionally, there is a minimal threshold velocity required to cause initial rotation of the vanes.

The relatively bulky size of vane anemometers renders them as an unsuitable selection for use within small void spaces (e.g. horticultural produce packaging), but is a viable method for measuring the airflow in larger spaces such as before or after it encounters horticultural produce.

Examples of vane anemometry for measuring airflow measurements in food measurements include: Hossain and Bala (2007), Lawrence and Maier (2011), Kadam et al. (2008), Motevali et al. (2013) and Nagle et al. (2010).

2.1.3. Differential pressure flowmeters

Differential pressure flow meters determine the flow velocity by either measuring the pressure losses over obstructions of known dimensions, such as orifice plates and Venturi meters, or by calculating the different pressure components (Coulson et al., 1999).

The devices used to record pressure differences can be classified into U-tube manometers and pressure transducers. U-tube manometers are simple to construct. However, they are not suitable when it comes to measuring very low flow rates and cannot be used in unsteady-state systems. In the case of very low rates the accuracy of the small pressure differences to be evaluated could be compromised. If the system is in transient operation the pressure difference, measured by the height difference of the fluid within each port of the U-tube, will be constantly fluctuating, making it difficult to record a single value.

Unlike U-tube manometers, pressure transducers operate by converting a pressure difference to an electrical signal that can be recorded on a data acquisition system. This represents an advantage over the U-tube manometer as it facilitates the automatic recording of pressure, including instantaneous fluctuations. They are also smaller than U-tube manometers and can operate with low airflow volumes.

Pressure devices cannot provide unobtrusive measurements of the flow in packed domains and they can only measure unidirectional flows along a streamline. Their sensitivity is limited, as they require a reasonable flowrate, to cause a detectable pressure difference. Taking the Pitot tube as an example if the flowrate is 0.6 m s^{-1} and an accuracy of 1% is required in its determination, then the manometer must be sensitive to changes of approximately 0.02 mm of a water column (Rathakrishnan, 2007). Practically, if a water column height change of 1 mm is the limiting sensitivity then the corresponding minimum air velocity that can be measured is 4 m s^{-1}. Hence, pressure devices cannot be used in room cooling or storage facilities, where low velocity and stagnant zones may exist. Due to their intrusive characteristics pressure measuring devices are generally used to measure the total flow rate into or out of a system and not within it.

Examples of differential pressure flowmeters for measuring airflow measurements in food operations include: Dehghannya et al. (2008, 2011, 2012), Gill et al. (2012), Khatchatourian et al. (2009), Mohanraj and Chandrasekar (2008), Ngcobo et al. (2012) and O'Sullivan et al. (2013).

2.2. Non-invasive qualitative methods

Non-invasive flow visualisation techniques have been pivotal in developing a better understanding of postharvest cooling and refrigeration processes, as they facilitate a more detailed and accurate assessment of airflow behaviour throughout the system. By

introducing visible particles (e.g. smoke) in the flow these methods can not only provide a better understanding of the flow patterns generated within the system but also facilitate a quantitative assessment (as discussed in the next section).

Smoke and helium bubbles make up the most common seeding particles to visualise airflow (Maghirand and Manbeck, 1993; Ruegg et al., 1994). The motion of the particles, within an illuminated thin laser light sheet is measured by tracking their location in time by a camera situated normal to the plane. The tracer particles must be sufficiently small and light so they can closely follow the flow field behaviour but large enough, so they scatter a sufficient amount of light, to be photographed or recorded with a camera.

Tracer particles are commonly generated by using a smoke-wire technique (Lohan, 2002; Wang et al., 2000). "Smoke" is generated by vaporising oil from a small diameter wire (~0.1 mm) through a resistive heating (Cornaro et al., 1999). Commonly used wire materials include steel and tungsten. This technique is limited to situations where the Reynolds number, based on the wire diameter, is small, approximately 20 since the smoke will become too dispersed in the fluid if the Reynolds number is higher. In practice, this low Reynolds number limitation restricts airflow experiments to maximum velocities of approximately 3 m s^{-1} (Rathakrishnan, 2007).

Smoke particles can also be generated by commercially available generators which vaporise a glycerine or alcohol solution, forming a non-toxic smoke.

The helium bubble method represents a flow visualisation technique that can be used in systems with airflow speeds of up to 60 m s^{-1} and moderate levels of turbulence (Rathakrishnan, 2007). Unlike smoke particles they can still be visualised even when dispersed. Filling soap bubbles with helium allows both the size (typically 1–3 mm) and buoyancy to be controlled, making it an ideal tracing particle (Biwole et al., 2009; Klimentjew et al., 2010; Suzuki and Kasagi, 2000). However, these bubbles tend to only reflect about 5% of incident light (Mueller, 1996), resulting in increasing importance of placement of light sources. Using the maximum possible amount of light on the bubbles, while maintaining a dark background, assists in bubble visualisation (Randall and Battams, 1979).

Examples of flow visualisation to identify flow patterns in food operations include: Hellickson and Baskins (2003) and Sarkar and Singh (2004).

2.3. Non-invasive quantitative methods

Non-invasive quantitative techniques expand upon flow visualisation by quantifying particles displacement. Examples of this technique that have been used to investigate the airflow behaviour during forced-air cooling, refrigeration and drying operations are tracer gas methods, laser doppler anemometry (LDA) and particle image velocimetry (PIV). These techniques do not interfere with airflow and, in the case of LDA and PIV, can be extremely accurate.

2.3.1. Tracer gas methods

Tracer gas methods determine the air movement in a system by measuring the concentration of the gas at a specific point downstream from its release into the system. Available techniques include decay, constant injection and constant-concentration measurements (Sherman, 1990). The tracer decay technique infers the flow rate by measuring the temporal drop in tracer concentration. In constant injection a uniform concentration of tracer is continuously injected and the flow determined by measuring its concentration at specific points within the domain. In constant-concentration the amount of the injected tracer is controlled to ensure a constant concentration of the tracer at a particular location. The fluid flow rate is then calculated from the required flow rate of the tracer injected divided by the concentration of the tracer (mol tracer/mol air). The tracer (gas) itself must be safe and freely available (Smale, 2004). The most common tracer gas to fit these requirements is carbon dioxide (Yan et al., 2009). However, in situations where natural convection is likely to occur, such as the static cooling of horticultural produce, carbon monoxide becomes a better choice than carbon dioxide (Amos, 2005). The airflow pattern is then analysed from time profiles of gas concentration at different positions in the system.

The tracer gas method requires sensors with fast response times and a sufficiently small size to avoid interfering with the airflow pattern (as they need to be located in different spatial positions within the system). Tracer gases are not suitable for use in a system where measurements are required over an extended time period, due to the volume of tracer required. The errors in this technique are typically in the range of 5–10% (McWilliams, 2003).

Examples of the tracer method for measuring airflow measurements in food operations include: Amin et al. (2009, 2010, 2011, 2012), Amos (2005) and Tanner et al. (2000).

2.3.2. Laser doppler anemometry

Both LDA and PIV are based on the analysis of movement of small (neutrally buoyant) tracer particles, which are seeded in the flow. In LDA laser light of a known frequency illuminates the particles in the air flow and the scattered light is detected by a photomultiplier tube. The principle behind LDA is that when light is reflected from a moving object the frequency of the scattered light will be altered in proportion to the speed of the object under

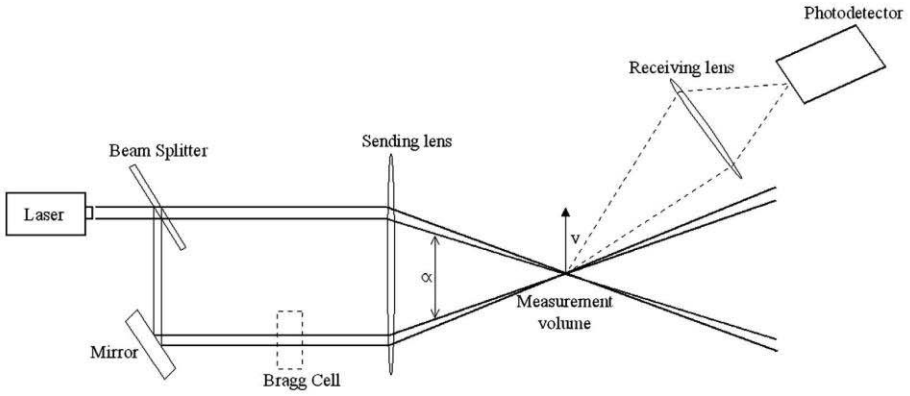

Fig. 1. Laser doppler anemometry technique for measuring fluid velocity.

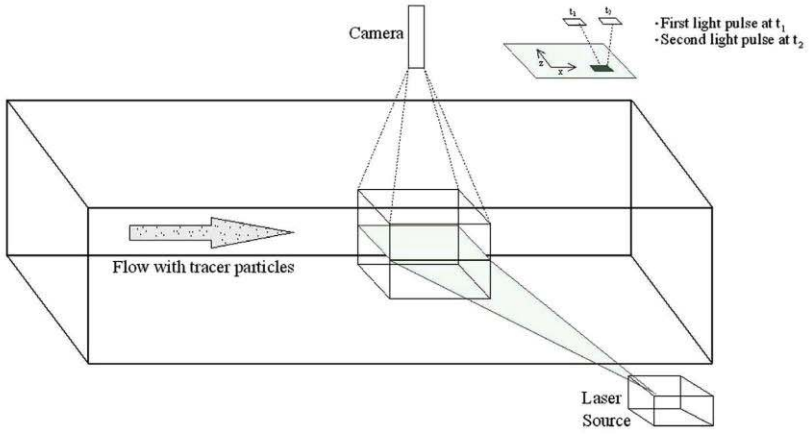

Fig. 2. Particle image velocimetry technique for measuring fluid velocity.

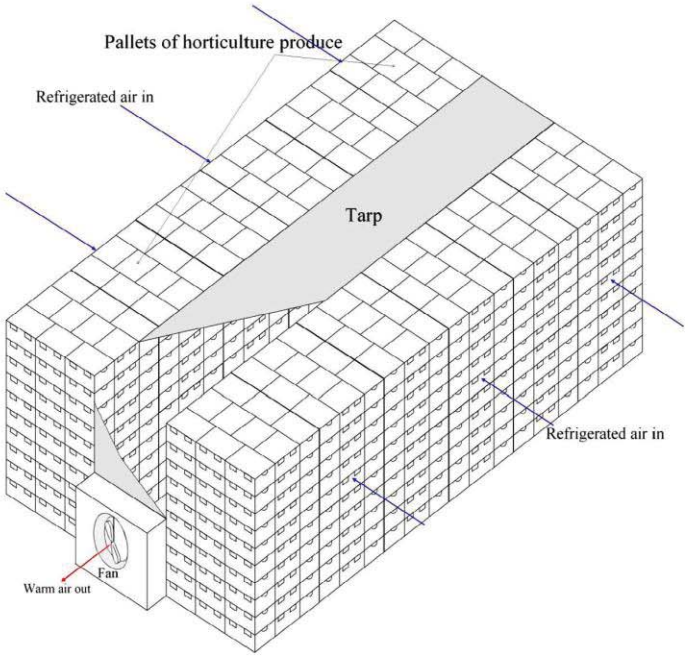

Fig. 3. Tunnel cooler, the most common forced-air cooling device. The fan creates a vacuum which draws refrigerated air through two palletized rows of horticulture produce.

investigation. By observing the frequency shift, the speed of the object can be estimated (Durst et al., 1981). This process is graphically presented in Fig. 1.

LDA measurements are linear with velocity and the device does not require external calibration (Wu et al., 2007). LDA can measure a wide range of velocities, from 10^{-4} m s^{-1} to 10^{3} m s^{-1}. It possesses a high frequency response and is insensitive to fluid temperature, density or composition. However, only a single point can be sampled at any given time.

Examples of LDA for measuring airflow measurements in food operations include: Alvarez et al. (2003), Foster et al. (2002), Marcroft et al. (1999), Marcroft and Karwe (1999), Moureh and Flick (2004) and Moureh et al. (2009a,b,c).

2.3.3. Particle image velocimetry

In PIV the flow is successively illuminated by thin layers of laser light, within a short period of time. The location of the particles is then determined within each laser pulse by measuring the light scattered by them into a CCD (Charge Coupled Device) camera. Once the location of the particles is determined for each laser pulse the particle displacement is then determined by cross-connecting their location in two successive laser pulses. From these correlations, a velocity vector can be obtained for each small region of the imaged domain, resulting in a vector field (Adrian, 1991). For a comprehensive and more detailed explanation of the PIV technique, the reader is referred to Prasad (2000). The PIV technique is illustrated in Fig. 2.

PIV has advantages compared to LDA in that it is a whole-flow-field measurement technique that provides instantaneous velocity vector measurements in an entire cross-section of the fluid flow, as opposed to the single point measurements associated with LDA. Planer flows, as well as 3D flows can be obtained and continued advances in the acquisition frequency of digital cameras have facilitated the assessment of turbulent structures in greater detail.

For LDA and PIV a clear line of sight (e.g. transparent window) must be provided to the fluid flow so the movement of the tracer particles can be recorded. Unlike the tracer gas method, LDA and PIV require an unobstructed view of the point being measured, reducing their applicability in actual food processing rooms filled with produce (Amos, 2005). This requirement has meant that although LDA and PIV have been used extensively in aerodynamics (Jeffrey et al., 2000; Raffel and Kost, 1998) and biomechanics (Gijsen et al., 1996; Lim et al., 2001) it is only recently that the techniques have been applied to complex flow systems found in food operations. LDA and PIV are also relatively expensive techniques.

Examples of PIV for measuring airflow measurements in food operations include: Laguerre et al. (2008, 2009, 2010, 2012) and Ferrua and Singh (2008, 2009a, 2009b, 2009c, 2011).

3. Design and efficiency of post-harvest cooling

3.1. Forced-air cooling

In forced-air cooling field heat is removed from freshly harvested produce by placing the produce inside palletised ventilated packages through which refrigerated air, at relatively high flow rates, is forced through by means of a fan (Fig. 3) (Brosnan and Sun, 2001). For the tunnel cooler, the most common forced-air cooling device, the fan creates a vacuum which draws refrigerated air through two palletized rows of horticulture produce.

As refrigerated air is pulled through ventilated packages preferential airflow pathway are formed, along with areas of maximum and minimum airflow velocities (Alvarez and Flick, 1999a, 1999b). This uneven distribution of the refrigerated air leads to cooling heterogeneity within the packages.

Alvarez and Flick (1999a) conducted an experimental aerodynamic study to better understand the relationship between the cooling heterogeneity during the forced-air cooling process and the behaviour of the airflow within food bins stacked in a pallet. PVC spheres were used to represent the horticultural products and a hot-wire anemometer measured the air velocity. The results showed preferential airflow pathways through the bins, along with back-mixing zones at the inlet corners. This uneven distribution of the flow was then directly related to the significant differences (up to 40%) in the heat transfer coefficients measured, resulting in non-uniform cooling of the produce.

Alvarez et al. (2003) used LDA to determine the semiempirical constants needed to numerically model the turbulent kinetic energy and the heat transfer process that develop within a porous structure of stacked spheres in vented boxes. By seeding water droplets (2×10^{-6} m mean diameter) and incense smoke in the flow field the velocities upstream, downstream and in between stacked PVC spheres representing the produce were measured. The numerical model developed then identified maximum air velocities within the centre of the vented box and decreasing velocities towards the corners of the box, which could explain the cooling heterogeneity observed within the box.

Delele et al. (2008) used hot-wire anemometry to validate a CFD model for the forced-air cooling of a box containing 32 spheres representing horticultural produce. After validation the CFD model was used to simulate various scenarios (box vent hole ratio, product size, etc.). The results showed a decay in air velocity through the box, hence cooling potential, as the distance from the box inlet increased.

Delele et al. (2013b) measured the air velocity flowing through vented packages of citrus fruit and the corresponding airflow resistance across a stack during a typical forced air cooling application. The experimental data, obtained by using a hot-wire thermal anemometer and a differential pressure transmitter, was then used to validate a 3D CFD model of the forced-air cooling process. The CFD model showed that the cooling of individual pieces of produce was dependent on their location within the package. Produce near the package vents, specifically behind the entrance vents, experienced relatively high air velocities and, consequently, experienced the fastest cooling. Airflow homogeneity was found to improve with decreasing air velocity as the air flowed from the entrance to the exit vents in the package.

Recent studies into the packaging of table grapes have shown that the airflow can be significantly affected by the presence of inner packaging, such as carry-bags and liner films. Ngcobo et al. (2012) used a pressure transducer in a wind tunnel, simulating forced-air cooling, to show that liner films inside a ventilated package caused a significant increase in pressure drop (typically over 50%) through ventilated packages of table grapes. Ngcobo et al. (2013) used a hot wire anemometer to measure the air velocity entering ventilated packages of table grapes stacked on a pallet during an experimental forced-air cooling set-up. The pressure drop through the packages was also measured using a pressure transducer device. Results showed that the inner packaging significantly restricted the airflow through the box.

Using airflow resistance measurements from previous work Delele et al. (2013a) generated a CFD model of room cooling of table grape packages. The study showed that the half cooling times were increased by 61% when a carry-bag was included in the package. Adding a liner film to the package, in addition to the carry-bag, further increased the half cooling time by 169%.

3.2. Improvements to forced-air cooling operations

Dehghannya et al. (2008, 2011, 2012) investigated the size and location of vented areas on the cooling heterogeneity. A set-up, involving a forced air tunnel to draw air through a bed of solid polymer balls, was designed to simulate postharvest cooling of spherical produce inside a ventilated package. A pitot tube recorded the air speed downstream of ventilated packages with a variety of vent areas open to incoming airflow, ranging from 2.4% to 12.1%. The same airflow was pulled through each ventilated package allowing the effect of the vent area on the cooling profile to be evaluated. Results indicated that while cooling uniformity increases with the increase in vent area the rate of cooling is more dependent on the distribution of the vent areas and may actually be lower if the vents are not distributed properly. The cooling rate can be improved, for the same overall vent area, if the vents are evenly distributed along the package wall. For example, three vents, with one vent located near both edges of the package wall and one at the centre will facilitate a faster cooling rate then if the same three vents are located beside each other in the centre of the package wall (Dehghannya et al., 2012). The evenly distributed configuration promotes a more homogeneous distribution of the airflow throughout the package, hence faster cooling.

Using a previous developed and experimentally validated CFD model Delele et al. (2013c) analysed the effect of the area, shape, number and position of package vents on the forced-air cooling of packed produce. For a given airflow rate, the cooling rate and airflow uniformity were found to improve with an increase in the vent area up to 7%. For a given pressure drop across the system, cooling rates were found to improve as the vent area increases,

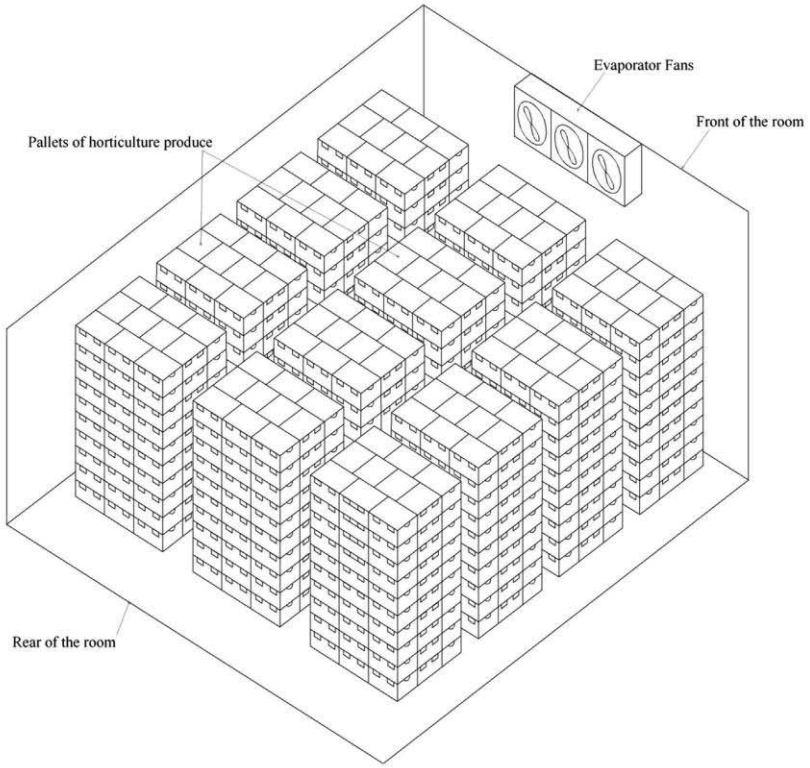

Fig. 4. Refrigerated storage room for horticulture produce. Evaporator fans circulate refrigerated air through the room.

with the highest decrease in cooling time observed for an increase in vent area from 1% to 3% and the cooling rate becoming less sensitive to increases in vent area after 7%. The airflow and cooling uniformity, but not cooling rate, could be improved by increasing the number of vents, even if the total vent area was kept constant. Changing the location of vents from the centre of the package to the top and bottom sections would change the location of the coldest sections but not cooling rate or uniformity while the cooling rate and uniformity was unaffected by the vent shape.

In order to improve upon the forced-air cooling of strawberry clamshells Ferrua and Singh (2008) developed an optically transparent model, representative of retail clamshells of strawberries to investigate the airflow behaviour. This model involved not only the use of a transparent solid material to reproduce the packaging structure (fused silica) but also a perfect refractive index matching between it and the working fluid (a mineral oil mixture). This set-up allowed the airflow behaviour within the packaging system to be measured by PIV and was then used to validate a numerical model for the forced-air cooling process of fresh strawberries in commercial packages (Ferrua and Singh, 2009a, 2009b). The authors were then able to make recommendations for a future package design, such as periodically reversing the direction is pulled through the pallet, based on guidelines formulated from the developed CFD model. In particular they found that increasing the vent area of the clamshells, hence forcing more air through the clamshells will not necessarily lead to improvements in the cooling rate of the process. Forcing more air through the clamshells causes a faster increase in the air temperature along the system which has a significant and detrimental effect on the cooling rate of the clamshells located at the end of the system (Ferrua and Singh, 2009c). It was found that the cooling rate and uniformity of the process could be improved by decreasing the temperature of the air been delivered at the warmest points within the system. This was achieved by bypassing half the airflow entering the pallet structure into the second part of the pallet, ensuring a supply of refrigerated air to the warmest clamshells located in the back half of the pallet (Ferrua and Singh, 2011). By doing this a decrease of 6% in the time taken for the warmest part of the pallet to reach seven-eighths cooling was observed.

4. Design and efficiency of refrigeration

4.1. Room cooling

Refrigerated rooms for the storage of food produce constantly circulate refrigerated air to maintain the produce at a low temperature. During storage, pallets of horticulture produce are placed within a room where an evaporator-fan circulates and cools the air within the unit (Fig. 4).

An uneven airflow distribution in refrigerated rooms (Fig. 4) can result in centrally located bins receiving very little airflow (Amos, 2005) and low air speeds towards the rear of the room (Delele et al., 2009a), effects that could be associated with the presence of warm spots and temperature heterogeneity within the produce. Within the last decade a number of studies have been done to better understand the relationship that exists between the distribution of the airflow within the system and the rate and uniformity of the refrigeration process.

Amos (2005) used the tracer gas technique to identify the airflow patterns within a cool store filled with horticulture produce stacked in bins. Carbon monoxide sensors were placed in a cool

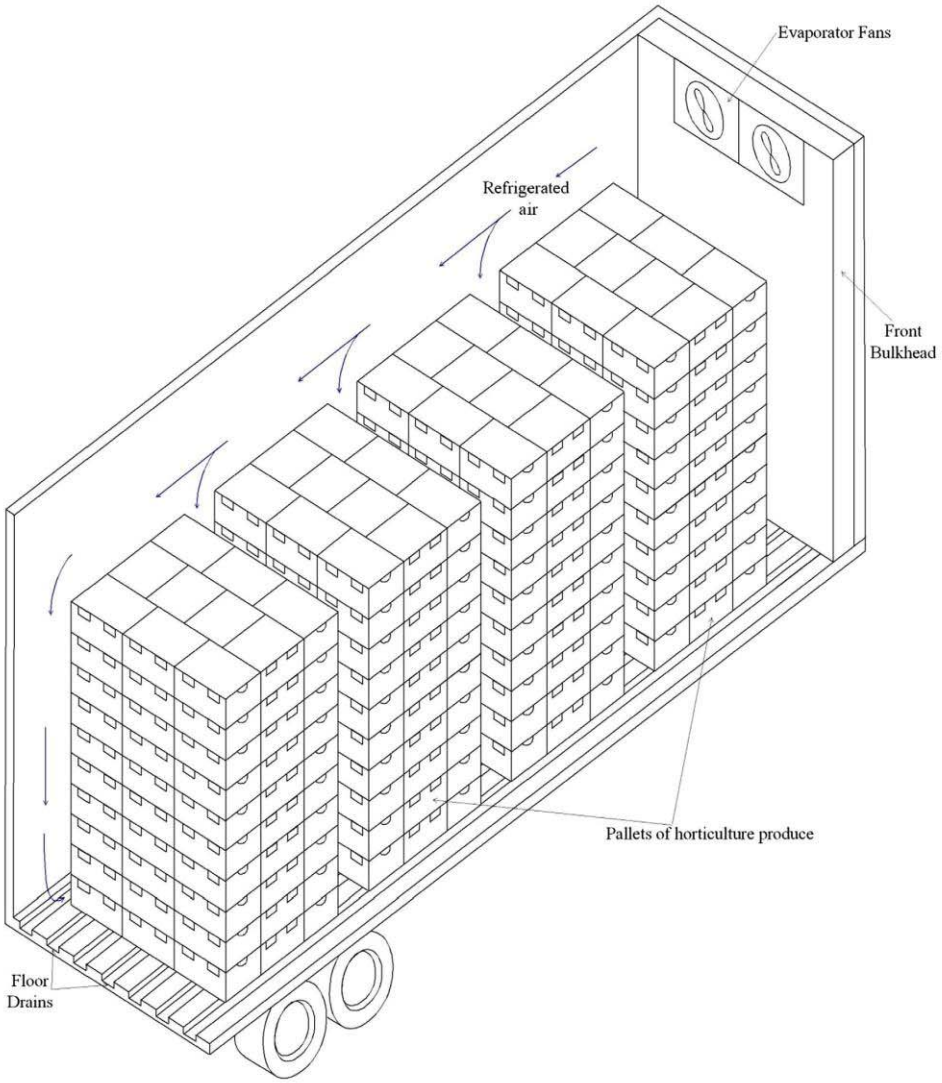

Fig. 5. Refrigerated truck with a top-air delivery system. Air is blown from the refrigeration unit at the front, over the top of the horticulture produce, down between the pallets and returns to the refrigeration unit at the front of the vehicle.

store containing 622 bins. The sensors were placed in front of the evaporator, at the rear of the cool store and within 5 sections spread uniformly between the bins where determined. Carbon monoxide was then injected into a variety of positions within the cool store and the mean velocity was calculated from the time of arrival from the injection point to each sensor. The results showed an uneven distribution of air flow within the cool store with the top layers and side columns of bins experiencing the highest air speeds while bins located centrally experienced much lower airflows. These areas of low air velocity coincided with warm spots in the cool room.

Using hot-film omni-directional anemometers Delele et al. (2009a) investigated the velocity profile around a stack of 72 boxes uniformly distributed within two rows inside a cool store. Results were used to validate a developed a multiscale CFD model of chicory root cool store to investigate how humidification intervals can reduce chicory root weight loss during cooling. The validated model clearly illustrated how the low velocity cooling towards the rear of room was unable to completely remove the heat of respiration from the produce.

4.2. Improvements to room cooling

Hellickson and Baskins (2003) used flow visualisation to study the air circulation during the postharvest cooling of apples and pears in a controlled atmosphere refrigerated storage room. Helium-filled soap bubbles where dispersed inside a commercial sized fruit storage room and the bubble motion recorded by video. The authors concluded that air-circulation and fruit cooling during this operation could be improved by ensuring a minimum space of 0.6 m between the rear walls and the bin stacks and a space of 0.2 m between the sidewalls and bin rows.

Using the developed multiscale CFD model of the chicory root cool store Delele et al. (2009b) tested potentially scenarios to improve the system. Numerical results suggested that elongating the air deflector to direct refrigerated air to the rear of the room

and reducing the stack height to increase the free air space at the top of the room, would lead to an improvement in the cooling time and overall process efficiency.

4.3. Refrigerated transport trailers

For transport vehicles of horticulture produce, such as highway trailers and trucks, a top-air delivery system is employed to continuously circulate refrigerated air (Fig. 5). Air is blown from the refrigeration unit at the front, over the top of the horticulture produce, down between the pallets and returns to the refrigeration unit at the front of the vehicle.

In refrigerated transport trailers the product temperature and homogeneity are directly controlled by the airflow patterns (Moureh et al., 2009c). Refrigerated air must be delivered to all parts of the container to compensate for heat fluxes through container walls and/or the heat of respiration of the product. To understand airflow patterns in refrigerated transport trailers Moureh and Flick (2004) constructed a reduced-scale model (1:3.3) of a refrigerated truck, containing slotted boxes filled with spheres, to validate a CFD model of the airflow within it. Atomised oil particles of 4 μm mean diameter were seeded in the airflow and LDA was used to measure the air velocity at 1110 points. Moureh et al. (2009a) used this technique when studying the airflow in slot-ventilated enclosures partially filled with vented boxes, such as refrigerated transport trucks loaded with horticultural produce. The experiments as well as numerical results showed that air circulation was found to be dependent on the porosity of the boxes. For ventilated packages the refrigerated air supply jet had an increased penetration depth along the truck length compared to non-permeable boxes. Non-permeable boxes promoted short-circuiting of the airflow in the front part of the truck. This allowed produce in the front of the truck to receive a sufficient supply of refrigerated air to maintain the produce at low temperatures and remove the heat of respiration. However, the airflow rate was inadequate to produce located at the back of the truck promoting temperature heterogeneity within the truck.

4.4. Improvements to refrigerated transport trailers

Air-ducts located at the ceiling of refrigerated trucks can improve the overall homogeneity of the airflow, and consequently temperature, in the truck (Moureh et al., 2009c). When air-ducts are included the airflow is blown into the truck at three positions (at the front, 1/3 of the truck length from the front and 2/3 of the truck length from the front). The authors combined experimental and numerical work to show that the use of air-ducts avoids the occurrence of stagnant zones and low velocities in the rear (region furthest from the evaporator fan) of the truck, while reducing the air velocities at the front. Air-ducts were shown to prevent over-chilling of produce, due to high air velocities, in the front of the trailer and overheating of the produce, due to low air velocities, at the rear of the trailer.

4.5. Refrigerated display cabinets/domestic refrigerators

In open refrigerated display cabinets (Fig. 6) and domestic refrigerators cooled air, at a low airflow rates, is circulated to the refrigerator shelves. In open refrigerated display cabinets (typically found in retail stores) warm air from outside is constantly infiltrating the cabinet, although an air curtain can reduce the amount, while in domestic refrigerators this occurs each time the door is opened.

By tracing a continuous and uniform injection of CO_2 gas Amin et al. (2009) investigated the amount of warm air infiltration into an open refrigerated display cabinet. The concentration of the tracer gas was measured at the discharge air grille, return air grille and the ambient outside environment. By finding the percentage of tracer gas that escapes to the ambient a relationship between tracer gas concentration and the amount of air infiltration can be established. Depending on the amount, this warm air infiltration can cause significant temperature heterogeneity within the cabinet resulting in temperature differences between the food products.

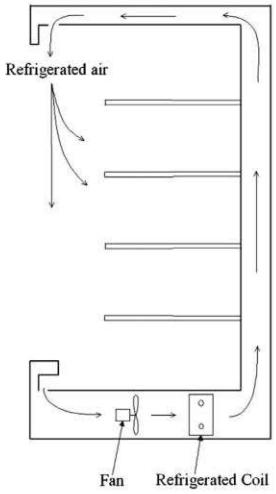

Fig. 6. Open refrigerated display cabinet.

PIV has been used to characterise the air flow behaviour that develops from natural convection within a transparent model of a domestic refrigerator and its influence on water evaporation (Laguerre et al., 2008, 2009). By analysing the dynamics of smoke particles (generated using a low-temperature water–glycol mixture to seed the airflow) the authors showed the occurrence of natural convection within the refrigerator, with warm air flowing to the top of the refrigerator and cool air flowing to the bottom. In addition, the experimental results were used to validate a CFD model that simulated the simultaneous heat and moisture transfer in the refrigerator. By using the validated model Laguerre et al. (2010) showed the dehydration of the food product near the top the refrigerator due to the higher air temperature. Likewise, as the air flowed down towards the bottom of the refrigerator its temperature decreased resulting in condensation on the food products in this region. Further work by Laguerre et al. (2012) uses PIV to measure the air velocity profiles in a vertical open refrigerated display cabinet. The results showed the highest air velocity near the air supply and return ducks. As a consequence, due to the higher heat transfer coefficients, the temperature of food products located in these areas was particularly affected by the temperature of the air flowing past compared to the food located at the top of the display cabinets.

4.6. Improvements to open refrigerated display cabinets

The infiltration rate of warm air into display cabinets can be minimised by reducing the cabinet height and adjusting the angle of the jet nozzle supplying refrigerated air (Amin et al. (2011, 2012). By tracing a continuous and uniform injection of CO_2 Amin et al. (2011, 2012) used the previously developed tracer gas approach to relate primary curtain design parameters, such as the height of the opening and flow rate ratio, and secondary variables, including space between shelves filled with food products, to the infiltration rate of open refrigerated cavities. In particular the authors found that the infiltration rate was dependent on

interacting variables. For example an extreme infiltration point could be reached by varying the height of the cabinet and the throw angle, the angle of the jet nozzle supplying refrigerated air relative to a vertical line through the cabinet.

5. Design and efficiency of drying operations

5.1. Understanding of convective drying systems

Drying operations use warm, dry air to lower the moisture content of horticulture produce. Although there are many set-up methods for drying food, in a typical forced convection dryer heated air is vertically blown across a bed of produce supported by a mesh (Fig. 7). During the drying of a bed of horticultural produce the distribution of the warm air before it encounters the product (Janjai et al., 2006) and the bed depth and porosity (Lawrence and Maier, 2011) impact upon the overall drying efficiency. For impingement jet drying technology the number of jets, airflow exiting the jets and food product location relative to the nozzle(s) impact upon the drying rate and uniformity (Marcroft and Karwe, 1999; Marcroft et al., 1999).

To understand airflow distribution in a conventional longan dryer Janjai et al. (2006) manually moved a hot-wire anemometer to different points on a predetermined grid. The results showed that the airflow distribution was not symmetric with respect to the position of the warm air inlet. Regions directly to the left and right of the air inlet were found to receive very little airflow and consequently experienced low drying rates, leading to non-uniform drying of the produce.

Lawrence and Maier (2011) used a vane anemometer to measure the air velocity at the grain surface at four locations near the centre of grain bins as well as near the periphery at four cardinal (north, south, east and west) directions. The results showed a non-uniform distribution of the air within the system and were used to validate a CFD model of the process. Results from the CFD model showed that the depth and porosity of the bed can have a major impact on the airflow distribution within the bed and the overall efficiency of the drying process. Lower porosity and greater bed depths result in a higher resistance to airflow and consequently an uneven airflow distribution, which causes non-uniform drying.

LDA was used to analyse the axial and radial air velocity components in a commercial jet impingement oven, used for conventional drying or toasting, from a single jet (Marcroft and Karwe, 1999), and multiple jets (Marcroft et al., 1999). In both cases sublimed CO_2 (dry ice fog) was used as the seeding particles. It was found that when using multiple jets the food product, on a conveyer belt would experience uneven heating rates as it passed under multiple jets. When the food product was directly under jet it experiences a high air velocity, leading to heat transfer rates 2–3 times higher than when the product is not under the any jet, and hence experience smaller air velocities. Hence, the areas of the food product receiving the higher heat transfer rates dry quicker than the other areas of the product.

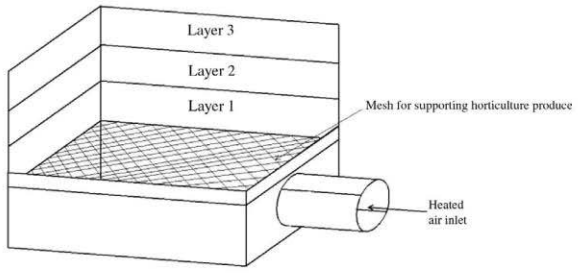

Fig. 7. Forced convection dryer. Heated air is blown under a mesh which supports the horticultural produce.

5.2. Improvements to forced convection drying systems

Nagle et al. (2010) used the portable hand held vane anemometer to record the velocity distribution at a drying facility as a way to investigate the effect of different modifications, such as a mesh to redirect the airflow, on the quality and energy performance of a hot air convection fixed-bed longan dryer. The air speed at the top of the produce bulk (25 cm depth) was determined, at 25 points in a 5×5 grid, at the beginning, middle and end of three drying operations where the inclusion of an inverted mesh evenly distributed the incoming airflow before it reached the produce. By improving the airflow distribution within the bed of products to be dried the mesh improved the uniformity of drying and overall dryer performance.

Janjai et al. (2006) increased the space under the perforated floor of a convective dryer and installed air guides after the air inlet to redirect the airflow. This improved the airflow distribution and hence drying uniformity of the process.

Sarkar and Singh (2004) used flow visualisation when investigating the relative importance of nozzle exit velocity, nozzle design and impingement equipment design on food processing, such as drying, using air impingement technology, consisting of jets emitting high-velocity air. A custom-built air impingement system allowed various nozzles sizes and equipment designs to be tested. Helium filled bubbles were introduced into the plenum and a camera was used to track the flow pattern of the jets. Experimental results showed that major improvements could be made to the air impingement systems drying performance by optimising the height to diameter ratio, in the region of 6–8, of the air jets and using fully developed jets.

6. Conclusions

For forced-air cooling, refrigeration and drying an even delivery of the airflow to each area of the system is essential to optimising the performance of the operations. In forced-air cooling preferential airflow pathways, which cause significant differences to the air speeds within ventilated packages, and an inadequate delivery of cool air to packages centrally located and at the rear of pallets result in cooling heterogeneity in the system. The cooling rate can be improved by increasing the vent area to certain percentage, specific to each package while airflow and cooling uniformity can be improved by increasing the number of vents. In room cooling and refrigerated transport trailers pallets located furthest from the evaporator fans receive a small volume of the total airflow, resulting in the presence of warm spots at these locations. In open refrigerated display cabinets localised high air speeds and warm air infiltration can result in a fluctuating air temperatures, and consequently fluctuating food product temperatures. Uneven airflow distribution causes non-uniform bed drying while the location of the food product to impingement jets can cause uneven drying rates along the width of the produce.

In order to improve these systems airflow measurements which can identify areas receiving maximum and minimum airflow rates must be identified. While on-site measurements will always remain important, non-intrusive quantitative techniques like LDA and PIV can validate numerical models which can then be used to predict the product temperature and storage life depending on the initial and environmental conditions.

Acknowledgement

This review is an output of the PhD research of Justin O'Sullivan as supported by a Zespri™ International PhD scholarship.

References

Adrian, R., 1991. Particle-imaging techniques for experimental fluid mechanics. Annu. Rev. Fluid Mech. 23, 261–304.
Alvarez, G., Flick, D., 1999a. Analysis of heterogeneous cooling of agricultural products inside bins. Part I: Aerodynamic study. J. Food Eng. 39 (3), 227–237.
Alvarez, G., Flick, D., 1999b. Analysis of heterogeneous cooling of agricultural products inside bins. Part II: Thermal study. J. Food Eng. 39 (3), 239–245.
Alvarez, G., Bournet, P.E., Flick, D., 2003. Two-dimensional simulation of turbulent flow and transfer through stacked spheres. Int. J. Heat Mass Transf. 46 (13), 2459–2469.
Amanlou, Y., Zomorodian, A., 2011. Evaluation of air flow resistance across a green fig bed for selecting an appropriate pressure drop prediction equation. Food Bioprod. Process. 89 (2), 157–162.
Amin, M., Dabiri, D., Navaz, H.K., 2009. Tracer gas technique: a new approach for steady state infiltration rate measurement of open refrigerated display cases. J. Food Eng. 92 (2), 172–181.
Amin, M., Navaz, H.K., Kehtarnavaz, N., Dabiri, D., 2010. A systematic approach for solving large-scale problems by neural network: open refrigerated display cases and droplet evaporation problems. Food Bioprocess Technol. 3 (2), 276–287.
Amin, M., Dabiri, D., Navaz, H.K., 2011. Comprehensive study on the effects of fluid dynamics of air curtain and geometry, on infiltration rate of open refrigerated cavities. Appl. Therm. Eng. 31 (14–15), 3055–3065.
Amin, M., Dabiri, D., Navaz, H.K., 2012. Effect of secondary variables on the infiltration rate of open refrigerated vertical display cases with single-band air curtain. Appl. Therm. Eng. 35, 120–126.
Amos, N.D., 2005. Characterisation of air flow in a commercial cool store using a carbon monoxide gas tracer technique. Acta Hort. 687, 305–312.
Biwole, P.H., Yen, W., Yanhui, Z., Roux, J.-J., 2009. A complete 3D particle tracking algorithm and its applications to the indoor airflow study. Meas. Sci. Technol. 20, 115403, 13pp.
Brosnan, T., Sun, D.-W., 2001. Precooling techniques and applications for horticultural products – a review. Int. J. Refrig. 24 (2), 154–170.
Cornaro, C., Fleischer, A.S., Goldstein, R.J., 1999. Flow visualization of a round jet impinging on cylindrical surfaces. Exp. Therm. Fluid Sci. 20 (2), 66–78.
Coulson, J.M., Richardson, J.F., Backhurst, J.R., Harker, J.H., 1999. Coulson & Richardson's Chemical Engineering, vol. 1: Fluid Flow, Heat Transfer & Mass Transfer, sixth ed. Oxford, pp. 232–273.
Defraeye, T., Lambrecht, R., Delele, M.A., Tsige, A.A., Opara, U.L., Cronjé, P., Verboven, P., Nicolaï, B.M., 2013. Forced-convective cooling of citrus fruit: package design. J. Food Eng. 121, 118–127.
Defraeye, T., Lambrecht, R., Delele, M.A., Tsige, A.A., Opara, U.L., Cronjé, P., Verboven, P., Nicolaï, B.M., 2014. Forced-convective cooling of citrus fruit: cooling conditions and energy consumption in relation to package design. J. Food Eng. 121, 118–127.
Dehghannya, J.M., Ngadi, M., Vigneault, C., 2008. Simultaneous aerodynamic and thermal analysis during cooling of stacked spheres inside ventilated packages. Chem. Eng. Technol. 31 (11), 1651–1659.
Dehghannya, J.M., Ngadi, M., Vigneault, C., 2011. Mathematical modeling of airflow and heat transfer during forced convection cooling of produce considering various package vent areas. Food Control 22 (8), 1393–1399.
Dehghannya, J.M., Ngadi, M., Vigneault, C., 2012. Transport phenomena modelling during produce cooling for optimal package design: thermal sensitivity analysis. Biosyst. Eng. 111 (3), 315–324.
Delele, M.A., Tijskens, E., Atalay, Y., Ho, Q., Ramon, H., Nicolaï, B.M., Verboven, P., 2008. Combined discrete element and CFD modelling of airflow through random stacking of horticultural products in vented boxes. J. Food Eng. 89 (1), 33–41.
Delele, M.A., Schenk, A., Tijskens, E., Ramon, H., Nicolai, B.M., Verboven, P., 2009a. Optimization of the humidification of cold stores by pressurized water atomizers based on a multiscale CFD model. J. Food Eng. 91 (2), 228–239.
Delele, M.A., Schenk, A., Ramon, H., Nicolai, B.M., Verboven, P., 2009b. Evaluation of a chicory root cold store humidification system using computational fluid dynamics. J. Food Eng. 94 (1), 110–121.
Delele, M.A., Ngcobo, M.E.K., Opara, U.L., Meyer, C.J., 2013a. Investigating the effects of table grape package components and stacking on airflow, heat and mass transfer using 3-D CFD modelling. Food Bioprocess Technol. 6 (9), 2571–2585.
Delele, M.A., Ngcobo, M.E.K., Getahun, S.T., Chen, L., Mellmann, J., Opara, U.L., 2013b. Studying airflow and heat transfer characteristics of horticultural produce packaging system using 3-D CFD model. Part I: Model development and validation. Postharvest Biol. Technol. 86, 536–545.
Delele, M.A., Ngcobo, M.E.K., Getahun, S.T., Chen, L., Mellmann, J., Opara, U.L., 2013c. Studying airflow and heat transfer characteristics of a horticultural produce packaging system using 3-D CFD model. Part II: Effect of package design. Postharvest Biol. Technol. 86, 546–555.
Durst, F., Melling, A., Whitelaw, J.H., 1981. Principles and Practice of Laser-Doppler Anemometry. London.
Ferrua, M.J., Singh, R.P., 2008. A nonintrusive flow measurement technique to validate the simulated laminar fluid flow in a packed container with vented walls. Int. J. Heat Fluid Flow 31 (2), 242–255.
Ferrua, M.J., Singh, R.P., 2009a. Modeling the forced-air cooling process of fresh strawberry packages, Part I: Numerical model. Int. J. Heat Fluid Flow 32 (2), 335–348.
Ferrua, M.J., Singh, R.P., 2009b. Modeling the forced-air cooling process of fresh strawberry packages, Part II: Experimental validation of the flow model. Int. J. Heat Fluid Flow 32 (2), 349–358.
Ferrua, M.J., Singh, R.P., 2009c. Design guidelines for the forced-air cooling process of strawberries. Int. J. Heat Fluid Flow 32 (8), 1932–1943.
Ferrua, M.J., Singh, R.P., 2011. Improved airflow method and packaging system for forced-air cooling of strawberry packaging. Int. J. Refrig. 34 (4), 1162–1173.
Fingerson, L.M., Freymuth, P., 1996. Fluid Mechanics Measurements, second ed. Washington, USA, pp 115–173.
Foster, A.M., Barrett, R., James, S.J., Swain, M.J., 2002. Measurement and prediction of airflow movement through doorways in refrigerated rooms. Int. J. Refrig. 25 (8), 1102–1109.
Ghisalberti, L., Kondjoyan, A., 1999. Convective heat transfer coefficients between air flow and a short cylinder. Effect of air velocity and turbulence. Effect of body shape, dimensions and position in the flow. J. Food Eng. 42 (1), 33–44.
Gijsen, F.J.H., Palmen, D.E.M., van der Beek, M.H.E., van de Vosse, F.N., van Dongen, M.E.H., Janssen, J.D., 1996. Analysis of the axial flow field in stenosed carotid artery bifurcation models – LDA experiments. J. Biomech. 29 (11), 1483–1489.
Gill, R.S., Singh, S., Singh, P.P., 2012. Design and development of desiccant seed dryer with airflow inversion and recirculation. J. Food Sci. Technol., 1–7.
Hellickson, M.L., Baskins, R.A., 2003. Visual documentation of air flow patterns in a controlled atmosphere storage. Acta Hort. 600, 173–179.
Hossain, M.A., Bala, B.K., 2007. Drying of hot chilli using solar tunnel drier. Sol. Energy 81 (1), 85–92.
Janjai, S., Intawee, P., Chaichoet, C., Mahayothee, B., Haewsungcharern, M., Muller, J., 2006. Improvement of the air flow and temperature distribution in a conventional longan dryer. International Symposium towards Sustainable Livelihoods and Ecosystems in Mountainous Regions, Chiang Mai, Thailand.
Jeffrey, D., Zhang, X., Hurst, D.W., 2000. Aerodynamics of gurney flaps on a single-element high-lift wing. J. Aircraft 37 (2), 295–301.
Jing, X., Lu, J.Y., Mioa, J.M., Hans, H., Rahman, H.A., Pan, S.S., Norford, L., 2011. An aerodynamically efficient sphere anemometer with integrated hot-film sensors for 2-D environmental airflow monitoring. In: 16th International Conference on Solid-State Sensors, Actuators and Microsystems, Beijing, China.
Jorgensen, F.E., 2002. How to measure turbulence with hot-wire anemometers – a practical guide. Dantec Dynamics.
Kadam, D.M., Nangare, D.D., Singh, R., Kumar, S., 2008. Low-cost greenhouse technology for drying onion (*Allium cepa* L.) slices. J. Food Process Eng. 34, 67–82.
Kashaninejad, M., Maghsoudlou, Y., Khomeiri, M., Tabil, L.G., 2010. Resistance to airflow through bulk pistachio nuts (Kalleghochi variety) as affected by moisture content, airflow rate, bed depth and fill method. Powder Technol. 203 (2), 359–364.
Khatchatourian, O.A., Toniazzo, N.A., Gortyshov, Y.F., 2009. Simulation of airflow in grain bulks under anisotropic conditions. Biosyst. Eng. 104 (2), 205–215.
Klimentjew, D., Flick, N.E., Bosselmann, T., Zhang, J., 2010. 3D hypergraph-oriented air flow analysis based on PTV. In: International Conference on Information and Automation, Harbin, China.
Laguerre, O., Amara, S.B., Charrier-Mojtabi, M.-C., Lartigue, B., Flick, D., 2008. Experimental study of air flow by natural convection in a closed cavity: application in a domestic refrigerator. J. Food Eng. 85 (4), 547–560.
Laguerre, O., Remy, D., Flick, D., 2009. Airflow, heat and moisture transfers by natural convection in a refrigerating cavity. J. Food Eng. 91 (2), 197–210.
Laguerre, O., Benamara, S., Flick, D., 2010. Numerical simulation of simultaneous heat and moisture transfer in a domestic refrigerator. Int. J. Refrig. 33 (7), 1425–1433.
Laguerre, O., Hoang, M.H., Osswald, V., Flick, D., 2012. Experimental study of heat transfer and air flow in a refrigerated display cabinet. J. Food Eng. 113, 310–320.
Lawrence, J., Maier, D.E., 2011. Three-dimensional airflow distribution in a maize silo with peaked, levelled and cored grain mass configurations. Biosyst. Eng. 110 (4), 321–329.
Lim, W.L., Chew, Y.T., Chew, T.C., Low, H.T., 2001. Pulsatile flow studies of a porcine bioprosthetic aortic valve in vitro: PIV measurements and shear-induced blood damage. J. Biomech. 34 (11), 1417–1427.
Lomas, C.G., 1986. Fundamentals of Hot Wire Anemometry. New York.
Maghirand, R.G., Manbeck, H.B., 1993. Modeling particle transport in slot-inlet ventilated airspaces. Trans. ASABE 36 (5), 1449–1459.
Marcroft, H.E., Karwe, M.V., 1999. Flow field in a hot air jet impingement oven – Part 1: A single impinging jet. J. Food Process. Preserv. 23 (3), 217–233.
Marcroft, H.E., Chandrasekaran, M., Karwe, M.V., 1999. Flow field in a hot air jet impingement oven – Part 2: Multiple impingement jets. J. Food Process. Preserv. 23 (3), 235–248.
McWilliams, J., 2003. Review of airflow measurement techniques, AIVC Annotated Bibliography BIB 12. www.aivc.org.
Mirade, P.S., Daudin, J.D., 1998. A new experimental method for measuring and visualising air flow in large food plants. J. Food Eng. 36, 31–49.
Mohanraj, M., Chandrasekar, P., 2008. Drying of copra in a forced convection solar dryer. J. Food Eng. 99 (4), 604–607.
Motevali, A., Younji, S., Amiri Chayjan, R., Aghilinategh, N., Banakar, A., 2013. Drying kinetics of dill leaves in a convective dryer. Int. Agrophys. 27, 39–47.
Moureh, J., Flick, D., 2004. Airflow pattern and temperature distribution in a typical refrigerated truck configuration loaded with pallets. Int. J. Refrig. 27 (5), 464–474.

Moureh, J.M., Tapsoba, M., Flick, D., 2009a. Airflow in a slot-ventilated enclosure partially filled with porous boxes: Part I – Measurements and simulations in the clear region. Comput. Fluids 38 (2), 194–205.
Moureh, J.M., Tapsoba, M., Flick, D., 2009b. Airflow in a slot-ventilated enclosure partially filled with porous boxes: Part II – Measurements and simulations within porous boxes. Comput. Fluids 38 (2), 206–220.
Moureh, J.M., Tapsoba, M., Derens, E., Flick, D., 2009c. Air velocity characteristics within vented pallets loaded in a refrigerated vehicle with and without air ducts. Int. J. Refrig. 38 (2), 220–234.
Mueller, T.J., 1996. Fluid Mechanics Measurements, second ed. Washington, USA, pp. 367–508.
Nagle, M., Carlos, J.C.A., Mahayothee, B., Haewsungcharern, M., Janjai, S., Müller, J., 2010. Improved quality and energy performance of a fixed-bed longan dryer by thermodynamic modifications. J. Food Eng. 99 (3), 392–399.
Ngcobo, M.E.K., Delele, M.A., Opara, U.L., Zietsman, C.J., Meyer, C.J., 2012. Resistance to airflow and cooling patterns through multi-scale packaging of table grapes. Int. J. Refrig. 35 (2), 445–452.
Ngcobo, M.E.K., Delele, M.A., Opara, U.L., Meyer, C.J., 2013. Performance of multi-packaging for table grapes based on airflow, cooling rates and fruit quality. J. Food Eng. 116 (2), 613–621.
O'Sullivan, J.L., Ferrua, M.J., Love, R.J., Verboven, P., Nicolaï, B.M., East, A.R., 2013. Performance of the forced-air cooling process of fruit packed in polyethylene liners as a function of pallet orientation. In: Proc. 2nd IIR International Conference on Sustainability and the Cold Chain, Paris, France.
Page, J.-F.L., Chevarin, C., Kondjoyan, A., Daudin, J.D., Mirade, J.D., 2009. Development of an approximate empirical-CFD model estimating coupled heat and water transfers of stacked food products placed in airflow. J. Food Eng. 92 (2), 208–216.
Pathare, P.B., Opara, U.L., Vigneault, C., Delele, M., Al-Said, F.A., 2012. Design of packaging vents for cooling fresh horticultural produce. Food Bioprocess Technol. 5 (6), 2031–2045.
Prasad, A.K., 2000. Particle image velocimetry. Curr. Sci. 79 (1), 51–60.
Raffel, M., Kost, F., 1998. Investigation of aerodynamic effects of coolant ejection at the trailing edge of a turbine blade model by PIV and pressure measurements. Exp. Fluids 24 (5–6), 447–461.
Randall, J.M., Battams, V.A., 1979. Stability criteria for airflow patterns in livestock buildings. J. Agric. Eng. Res. 24, 361–374.
Rathakrishnan, E., 2007. Instrumentation, Measurements, and Experiments in Fluids,, CRC Press, pp. 9–520.
Ruegg, T., Stangier, R., Stoeckli, B., Tanner, C., Dorer, V., Lommel, A., 1994. 3D airflow velocity vector sensor. Proc. of Roomvent '94, Krakow, Poland.
Santonico, M., Bellincontro, A., Di De Santis, D., Natale, C., Mencarelli, F., 2010. Electronic nose to study postharvest dehydration of wine grapes. Food Chem. 121 (3), 789–796.
Sarkar, A., Singh, R.P., 2004. Air impingement technology for food processing: visualisation studies. Food Sci. Technol. 37 (8), 873–879.
Sherman, M.H., 1990. Tracer-gas techniques for measuring ventilation in a single zone. Build. Environ. 25 (4), 365–374.
Smale, N.J., 2004. Mathematical modelling of airflow in shipping systems: model development and testing, PhD Thesis, Palmerston North, Massey University.
Smale, N.J., Moureh, J.M., Cortella, G., 2006. A review of numerical models of airflow in refrigerated food applications. Int. J. Refrig. 29 (6), 911–930.
Suzuki, Y., Kasagi, N., 2000. Turbulent air-flow measurement with the aid of 3-D particle tracking velocimetry in a curved square bend. Flow, Turbul. Combust. 63 (1), 415–442.
Tanner, D.J., Cleland, A.C., Roberston, T.R., Opara, L.U., 2000. Use of carbon dioxide as a tracer gas for determining in-package airflow distribution. J. Agric. Eng. Res. 77 (4), 409–417.
van der Sman, R.G.M., 2002. Prediction of airflow through a vented box by the Darcy-Forchheimer equation. J. Food Eng. 55 (1), 49–57.
Verboven, P., Hoang, M.L., Nicolai, B.M., 2003. Modelling turbulent air flow in cool rooms for horticultural products. Acta Hort. 599, 435–441.
Verboven, P., Tijskens, E., Ramon, H., Nicolai, B.M., 2005. Virtual filling and airflow simulation of boxes with horticultural products. Acta Hort. 687, 47–54.
Vigneault, C., Goyette, B., de Castro, L.R., 2006. Maximum slat width for cooling efficiency of horticultural produce in wooden crates. Postharvest Biol. Technol. 40 (3), 308–313.
Wang, L., Sun, D.-W., 2003. Recent developments in numerical modelling of heating and cooling processes in the food industry—a review. Trends Food Sci. Technol. 14 (10), 408–423.
Wang, A.-B., Trávníček, Z., Chia, K.-C., 2000. On the relationship of effective Reynolds number and Strouhal number for the laminar vortex shedding of a heated circular cylinder. Phys. Fluids 12 (6), 1401.
Webster, J.G., 2000. Mechanical Variables Measurement – Solid, Fluid, and Thermal. Boca Raton, Florida.
Wu, H., Lin, B., Morgan, M.N., 2007. Measurement of the air boundary layer on the periphery of a rotating grinding wheel using LDA. J. Phys.: Conf. Ser. 76 (1) (Paper No. 012059).
Yan, W., Zhang, Y., Sun, Y., Li, D., 2009. Experimental and CFD study of unsteady airborne pollutant transport within an aircraft cabin mock-up. Build. Environ. 44 (1), 34–43.

Mechanisms and performance of the forced-air cooling process of fruit packed in polyethylene liners

Justin L. O'Sullivan[1], Maria J. Ferrua[2], Richard J. Love[1], Pieter Verboven[3], Bart M. Nicolaï[3], and Andrew R. East[1]

[1]Centre for Postharvest and Refrigeration Research, Massey University, Private Bag 11-222, Palmerston North 4442, New Zealand, Ph +64 6 350 4336; Fax +64 6 350 5657

[2]Riddet Institute, Massey University, Private Bag 11-222, Palmerston North 4442, New Zealand

[3]BIOSYST-MeBioS, K.U.Leuven, Willem de Croylaan 42, Heverlee, Belgium

Written for presentation at the
2012 CIGR Section VII International Technical Symposium on

"Innovating the Food Value Chain"
Postharvest Technology and Agri-Food Processing

Stellenbosch, South Africa, 25-29 November, 2012

Abstract. A rapid and uniform forced-air cooling process immediately after harvest is essential to extend the storage life and preserve the quality of fresh produce. During this process refrigerated air is directly drawn through vented cartons of produce stacked upon pallets, with the cooling process governed by forced convection. However, to reduce the produce weight loss during extended storage, the direct contact between the refrigerated air and the horticulture product is often avoided by using polyethylene liners within the cartons. So far, little is known of how these polyethylene liners affect the performance and mechanisms governing the forced-air cooling of fresh produce. The goal of this work is to investigate the mechanisms and performance of the forced-air cooling process of a pallet (1.2 x 1.0 m) of modular polylined boxes of kiwifruit (initial temperature 20 °C). Cooling profiles of kiwifruit in individual boxes, along with the air temperature entering each monitored box and the air velocity at the inlet vents of the pallet were measured.

Results demonstrate significant temperature heterogeneity across the pallet after 8 h. Boxes located at the front cooled to 3.3 °C, while boxes at the back remained at more than 6.9 °C. Airflow through the central and lateral boxes was determined as 13.0 and 3.4 x 10^{-3} $m^3.s^{-1}$, respectively. Regardless of this difference, boxes within these two locations experienced comparable cooling profiles if the temperature of the air forced through them was similar. This work shows that, for the airflow rates commonly used by the industry, the forced-air cooling process of polylined packages is governed by the conductive and natural convective mechanisms occurring within the liners. It illustrates the need to improve the design and efficiency of this process, and the pivotal role of the temperature of the air across the pallet (rather than its distribution) on the cooling performance.

Keywords: Kiwifruit, pre-cooling, polyliner, postharvest.

1. Introduction

Proper postharvest cooling is essential to ensure that product quality is maintained from harvest to retail. To ensure maximum storage potential kiwifruit should be cooled to near 0 °C, as soon possible (Ashby 1995). Kiwifruit, kept at 0 °C and 90-95% relative humidity can have a storage period of 3-5 months (Simson and Straus 2010). However, improper cooling can lead to hot or cold spots, resulting in excessive drying or condensation during storage, and consequently quality loss in horticulture produce (Verboven, Hoang and Nicolai 2003).

Kiwifruit is typically cooled via a forced-air application. Forced-air cooling involves forcing refrigerated air through packed fresh produce stacked upon pallets. The efficiency of the forced-air cooling process is determined by the rate and uniformity that product cools in comparison to the energy input required (de Castro, Cortez and Vigneault 2004). Of the different air flow systems available the tunnel cooler is the most common (Brosnan and Sun 2001). Depending on the fruit and whether a polyliner is used to contain the fruit inside the package cooling times can vary significantly. For example, strawberries, a relatively small fruit and packed in clamshells within trays, without a polyliner can cool to near 0 °C in as little as 2 h (Ferrua and Singh 2009b). Conversely, palletized boxes of apples can take up to 12 h to cool (East, Sabarez, Tanner and Cleland 2003). Introducing a barrier between the produce and cooling air can extend the cooling period even further. For example, pears stacked in boxes and wrapped in paper can take up to 24 h to cool (Thompson and Chen 1988) .

Horticulture packaging needs to have sufficient mechanical strength to withstand the compression from overhead containers, the high humidity of cooling, transport and storage environments, the impact and vibration during transportation, and handling during loading and unloading (Ezeike and Hung 2009). In addition to these requirements, some products (such as kiwifruit) also need to be contained within a polyliner bag of high density polyethylene to retain moisture. If kiwifruit losses as much as 2.5-3 % of the total fruit weight due to water evaporation, it will begin to shrivel (Burdon and Clark 2001). This affects both its visual appearance and the selling weight at the end of the supply chain. However, polyliners significantly decrease the cooling rate as they prevent direct contact between the cool air and the kiwifruit.

The objective of this work was to investigate how the use of polyethylene liners impacts the performance and mechanisms controlling the forced-air cooling of fresh produce. As part of this study, the cooling profiles of kiwifruit modular polylined boxes as dependent on their location within the pallet were experimentally measured and related to the temperature and distribution profile of the airflow across the pallet.

2. Methodologies

2.1 Experimental Set-up

A laboratory-scale operation was designed and developed to simulate forced-air cooling of kiwifruit stacked on a pallet. This laboratory unit allowed precise control over the critical operating parameters affecting the cooling process performance during industrial applications, primarily the temperature and flow rate of the refrigerated air forced through a kiwifruit pallet. A fan draws refrigerated air through palletized kiwifruit to simulate the conditions experienced by kiwifruit modular bulk packs during forced-air cooling. The fan system consists of a fan, an orifice plate and an interface which attaches the fan system to a pallet (Figure 1).

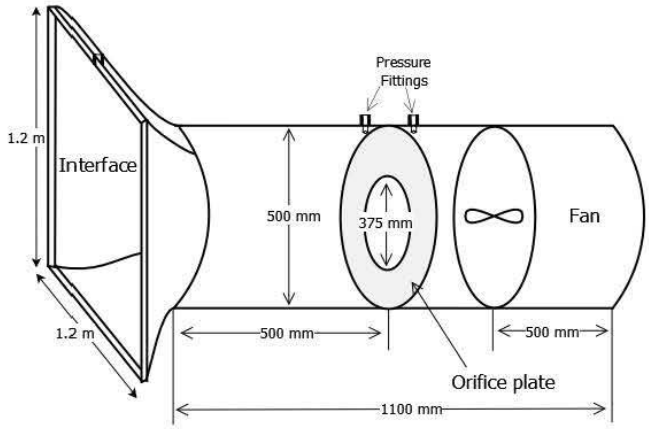

Figure 1. Laboratory scale fan system to simulate forced-air cooling

The fan has a built-in electronic variable speed drive (VSD). This allows the total airflow through the pallet to be controlled by adjusting the fan speed. The orifice plate in the fan system allows the airflow rate through the palletized structure to be measured, while a U-tube manometer measured the pressure drop across the pallet. The air velocities entering through the hand vents and side vents of the modular bulk packs were recorded by a hot-wire anemometer (TSI VelociCalc, model 8344-M-GB).

The modular bulk pack for the Hayward kiwifruit, used in these experiments is a fibreboard box (Figure 2). The box contains vents to allow for cold air to pass through the package. Two rectangular vents (hand vents) are located on the large face while one small semi-circular vent is located on the side face (side vents). Both vents are located at the top of the face. The kiwifruit are contained within a single polyliner bag, constructed of high density polyethylene and folded at the top, in order to retain moisture.

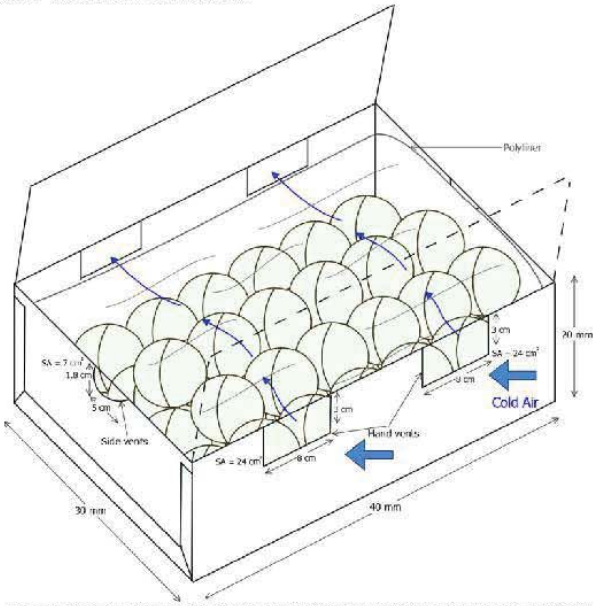

Figure 2. The modular bulk pack fibreboard for Hayward kiwifruit

2.2 Experimental data collection

A standard ISO industrial pallet (1.2 x 1.0 m) holds 100 modular polylined boxes, in 10 layers of 10 boxes. Each box holds between 10.5-11.0 kg of kiwifruit. All boxes contained count 36 size kiwifruit, resulting in 100 individual fruit per box. This gives a pallet a full height of 2 m (excluding the pallet base). The interface of the fan system is 1.2 m in height. Therefore, trials were conducted with a half pallet (a pallet consisting of 5 rows of kiwifruit) 1 m high (Figure 3). Any free space between the interface and top boxes of the pallet were sealed up with tarp to ensure that the airflow only passed through the pallet. Within these five rows only two layers were measured (rows “B” and “D”) as replicates, with the remaining three rows termed dummy layers, which provided buffering of the measured layers from edge effects. Following current industrial practice refrigerated air is drawn through the 1.0 m face. A tarp is placed over the 1.2 m lateral side walls and the free space between the interface and top boxes of the pallet, ensuring all of the airflow enters the pallet through the 1.0 m face only and hence pseudo-linear airflow occurs through the pallet, parallel to the 1.2 m face.

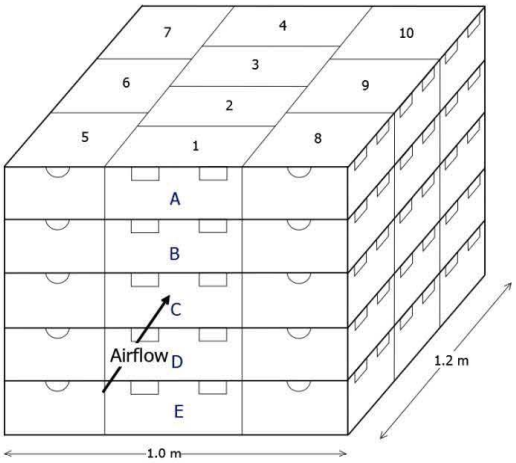

Figure 3. Half-pallet layout with rows assigned letters "A"-"B"

To ensure that airflow through each box was not influenced by fruit stacking pattern within each box kiwifruit were uniformly packed following a cubic centred distribution. A total of four layers of kiwifruits were arranged within each box, giving a total of 100 kiwifruit in each modular bulk pack (Figure 4). Type-T thermocouples were used to monitor the centre temperature of 12 kiwifruit within each monitored box (Figure 4). Temperatures were logged at one-minute intervals by 64-channel dataloggers (Squirrel, Grant Instruments, UK), over an 18 h forced-air cooling period. To promote visualization of the results the kiwifruit stacking is subdivided into individual areas termed, bottom, middle, top, inlet and outlet. For Boxes 5-7 and Boxes 8-10 air is drawn through the side vent. Therefore, due to the change in orientation to the airflow, the sides will be termed internal and external, where the internal side is in contact with Boxes 1-4 and the external side is located on the outer edge of the pallet. This enables the cooling of kiwifruit as a function of location in the modular bulk pack to be studied.

In order to gain an accurate representation of temperature change within each of the boxes a weighted average was applied to each of the temperature data points. Kiwifruit located immediately adjacent to the box walls were taken to represent all the kiwifruit beside the box walls for that kiwifruit layer, while the centre thermocouples were the average temperature of the centrally located kiwifruit.

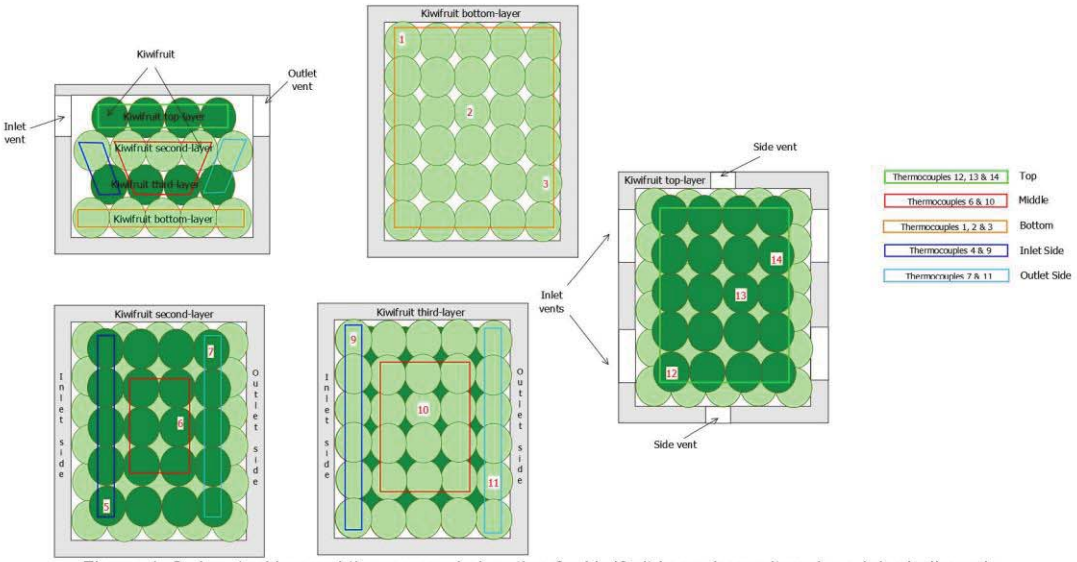

Figure 4. Order stacking and thermocouple location for kiwifruit in each monitored modular bulk pack

Velocities were recorded based on pallet layer and whether the airflow is drawn through the hand or side vents, for boxes within the entrance of the pallet. For this pallet configuration both hand vents and side vents are directly exposed to the airflow. Air passes through the side vents of Boxes 5 and 8, while been forced through the two hand vents of Box 1, resulting in four velocity measurements per pallet layer. These measurements were replicated three times for rows "B", "C" and "D", giving 36 data points.

2.3 Experimental set-up

Prior to the forced-air cooling operation kiwifruit were equilibrated to 19 °C, replicating the field heat observed in kiwifruit following harvest. The temperature control room, with the fan system placed in it, used for the trials was set and maintained at 0 °C. The instrumented pallet was rolled into the room attached to the fan system and the precooling simulation initiated, within 5 minutes of the warm kiwifruit entering the cool environment. Typically, pre-coolers operate with a volumetric airflow rate of 0.5-2.0 $L.s^{-1}.kg^{-1}$ (Thompson 2004). With approximately 10.5 kg of kiwifruit in each box, giving a pallet weight of 525 kg, the required airflow through the pallet is 0.26-1.05 $m^3.s^{-1}$. The VSD fan was set to 1500 rpm, providing an airflow through the pallet of 0.58 $m^3.s^{-1}$, with an associated pressure drop of 126 Pa across the pallet.

2.4 Data Analysis

The fractional unaccomplished temperature change, (Y), represents the amount of possible temperature change that has yet to be accomplished (Eq. 1)

$$Y = \frac{T - T_a}{T_i - T_a} \dots\dots (1)$$

where T (°C) is the average temperature of kiwifruit in the box at the defined time of cooling, T_i (°C) is the average temperature of kiwifruit in the box at the start of cooling, and T_a (°C) is the average temperature of the air entering the pallet, taken as the temperature of the cool room.

Taking the fractional unaccomplished temperature change away from one $(1-Y)$ and converting it to percentage format gives the accomplished temperature change, representing how much the kiwifruit have cooled from their initial temperatures to 0 °C. The half cooling time is defined as the time at which Y equals 0.5 or when the kiwifruit has cooled halfway from their initial temperature to that of the cooling air.

Due to the geometric nature of the pallet, a line of axial symmetry can be assumed down the centre of the pallet (through Boxes 1-4) resulting in Boxes 5 and 8, 6 and 9, and 7 and 10, representing replicas of each other. Therefore, measurements for boxes with replicas, both on separate layers and due to axial symmetry, can be averaged, leaving a reduced single layer of a pallet with Boxes numbered 1-7 (Figure 5).

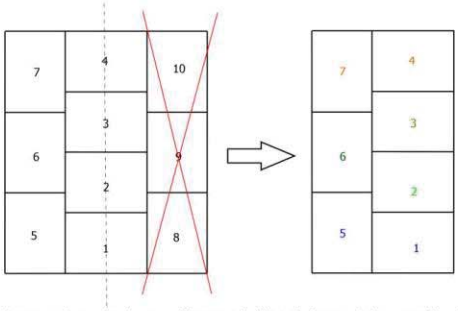

Figure 5. Reduced pallet row, for air drawn through the 1.0 m side, on the basis of axial symmetry

3. Results

Figure 6 contains the raw experimental data obtained. The change in average air temperature as it enters each Box in the pallet is shown in Figure 6(a), while the kiwifruit temperature change as dependent on location for each of the Boxes during 8 h of cooling is presented in Figure 6(b).

The kiwifruit temperature data is converted into the average fractional unaccomplished temperature change in Figure 7, with the air temperature into Box 7 taken as the average inlet temperature (°C) flowing into the pallet, over the 8 h of cooling. The average fractional unaccomplished temperature change for each of the subdivisions within Box 1 identifies which areas of the box experience the greatest degree of cooling (Figure 7(a)). Meanwhile, the average fractional unaccomplished temperature change, for the first 8 h of forced-air cooling as influenced by box position, demonstrates the impact of box location on the cooling rate (Figure 7(b)). The half cooling time is presented as a function of box position in Table 1.

Table 2 illustrates the differences in kiwifruit cooling as dependent on location within the Box after 4 h of cooling (approximated average half cooling time for all the Boxes). The air velocity and airflow through the boxes generated in the experiment is presented in Table 3.

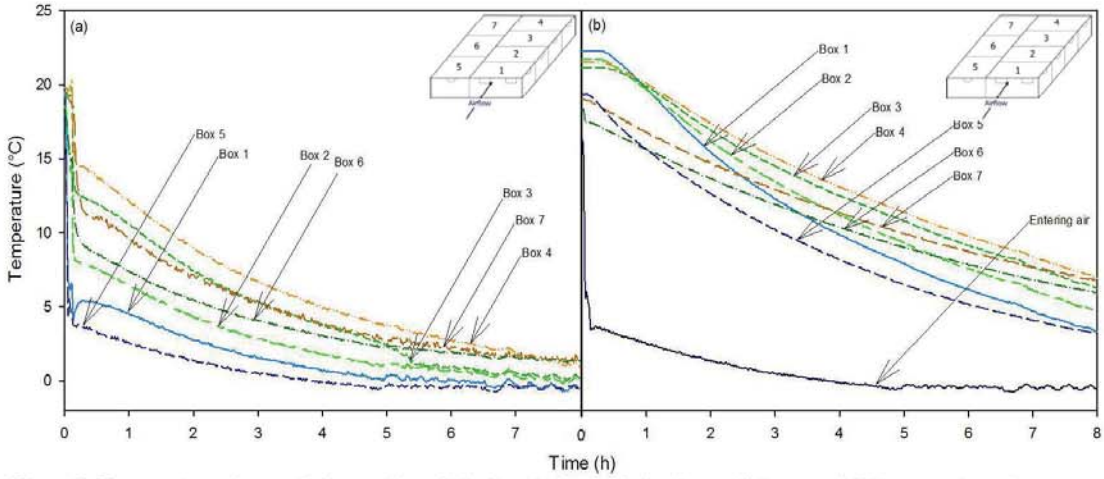

Figure 6. Temperature change during cooling of (a) air entering each box in a pallet row and (b) temperature change of each box in pallet row "B"

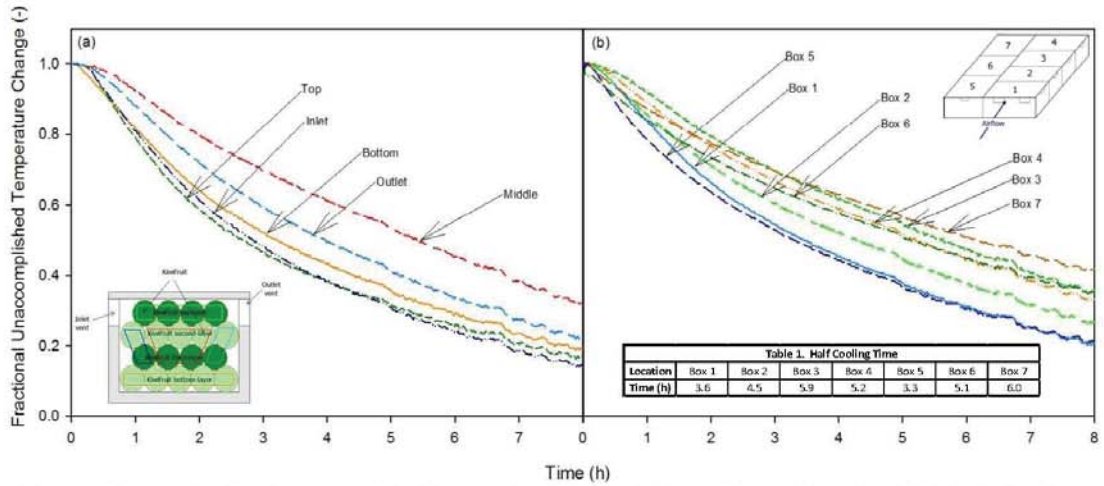

Figure 7. Average fractional unaccomplished temperature change, during cooling for (a) each subdivision in Box 1 and (b) each box in a pallet row

Table 2. Cooling of subdivisions, after 4 h of precooling, within Kiwifruit Boxes 1-7

Box No.	Bottom (%)	Middle (%)	Top (%)	Inlet (%)	Outlet (%)
1	57	39	62	62	51
2	52	28	52	56	45
3	37	21	44	41	31
4	41	20	50	47	35
Box No.	Bottom (%)	Middle (%)	Top (%)	Internal (%)	External (%)
5	54	39	66	62	53
6	47	24	50	47	38
7	39	23	47	44	34

Table 3. Airflow through the pallet

Airflow through the pallet						
Fan Speed (rpm)	Velocity through each hand vent ($m.s^{-1}$)	Airflow through both hand vents ($m^3.s^{-1}$)	Velocity through side vents ($m.s^{-1}$)	Airflow through side vents ($m^3.s^{-1}$)	Airflow through entire pallet ($m^3.s^{-1}$)	Total airflow through boxes (%)
1500	2.70	13×10^{-3}	4.84	3.4×10^{-3}	0.58	17

4. Discussion

4.1 Air Temperature

As the cooling air travels through the pallet it warms up. The air temperatures, measured inside of the Box after it has passed through the inlet vents, for Boxes 1 and 5 are 3 °C and 1 °C respectively, after approximately 2 h of cooling (Figure 6(a)). As the temperature of the air was measured inside the boxes, after the volumetric airflow has been drawn past the vents the discrepancy, between Box 1 and 5 could be explained by differences in the temperature of the fruits and the volumetric flowrates within the boxes. The air temperature which flows into Boxes 3, 4 and 7, located at the back of the pallet has considerably warmed up, situated within a temperature range of 7-9 °C.

The rise in temperature of the cooling air as it passes through the pallet is reflected in the slower cooling rates of the corresponding boxes. Box 2 has a half cooling time of 4.5 h, while Box 3 located behind Box 2 takes 5.9 h before half cooling is achieved (Table 1). This cooling rate dependence on distance from incoming refrigerated airflow was also observed by Ferrua and Singh (2009b) during the forced-air cooling of strawberry clamshells. Although the air entering Box 4 is warmer than that for Box 3 the fact that one side is exposed to the surrounding air means that an additional pathway is provided for heat transfer, resulting in a marginal improvement in the half cooling time 5.2 h.

4.2 Temperature change of subdivisions within kiwifruit boxes

Figure 7(a) shows that the bottom of the box cools faster than the middle of the box, despite being located furthest from the refrigerated airflow entering the box. This result indicates that kiwifruit are being cooled from the refrigerated air entering the box below through the cardboard packaging. The higher cooling rate of 62% for kiwifruit in the top layer (in comparison to 57% in the bottom layer) indicates that the conductive resistance to heat transfer by the polyliner is less than that of the bottom of the cardboard box (Table 2). In summary as air flows into the top of the kiwifruit box it simultaneously contributes to cooling of kiwifruit below (the fruit in the box) and above (the fruit in the above box).

The inlet side directly orientated to be exposed to the cooling air in-flow cools significantly quicker than the opposite (outlet) side, with temperature reductions of 62% and 51%, respectively, over 4 h of forced-air cooling for Box 1. Kiwifruits in the middle of the modular bulk pack experienced a relatively minor cooling (39%) after 4 h.

It can be seen that Boxes 2-4 follow the same trends as that observed in Box 1. Due to the fact that air enters through the side vents for Boxes 5-7 it might be expected that the internal and external sides would show the same degree of cooling. The discrepancy between the values implies that air is flowing through the gaps between the modular bulk packs. Hence, the inlet side, in contact with Boxes 1-4, experiences greater cooling. This is supported by the fact that only 17% of the total volumetric airflow entering the pallet flows through the openings (i.e. hand vents and side vents) of the Boxes.

4.3 Temperature change of kiwifruit boxes within pallet

As to be expected Box 1 and 5 show the greatest decrease of temperature during cooling, accomplishing 78% of the total cooling after 8 h (Figure 7(b)) with a half cooling time of 3.6 and 3.3 h, respectively. This is due to the fact that both boxes are directly exposed to the incoming refrigerated airflow and have one side, with surface areas of 8×10^{-2} m^2 and 6×10^{-2} m^2, for Box 1 and 5 respectively, orientated to this airflow. Unlike the rest of the boxes within the pallet, forced convection can occur between the box walls directly orientated to the refrigerated air and the refrigerated airflow.

Due to the orientation of Box 5, the side vent surface area for the air to enter is only 7×10^{-4} m^2. Conversely, the total surface area available for airflow through Box 1, provided by the two hand vents is 48×10^{-4} m^2 (Figure 8). As a consequence, the relatively small open area of the side vents limits the volume of air that can be pulled through Box 5 by the fan. The average velocity recorded through the side vent was found to be 4.84 $m.s^{-1}$, translating to a volumetric flowrate of 3.4×10^{-3} $m^3.s^{-1}$. Heat transfer in Box 1 has a greater potential for increased forced convection with a larger total vent area available for airflow. With the average velocity recorded through the hand vents as 2.7 $m.s^{-1}$ volumetric flowrates through the box are estimated as 13.0×10^{-3} $m^3.s^{-1}$, close to a fourfold increase over Box 5. There is lack of a prominent relationship between half cooling times and volumetric airflow, as demonstrated by the similar half cooling times for Boxes 1 and 5. Similar to previous work increasing the airflow through the horticulture produce has not led to a substantial improvement in the cooling rate. Ferrua and Singh (2009a) showed that any attempt to increase the amount of airflow through the system, consisting of strawberries packed in clamshells, by varying the vent area, will give no significant improvement to the rate or uniformity of the forced-air cooling process. Additionally, Dehghannya, Ngadi and Vigneault (2008; 2011; 2012) concluded that simply increasing the vent area, hence improving the volumetric airflow through the system, will not automatically lessen the cooling time of spheres, taken to represent horticulture produce.

A more direct relationship between airflow and heat transfer is the air velocity. Box 5 with a volumetric flowrate 3.4×10^{-3} $m^3.s^{-1}$ produces a bulk velocity of 0.38 $m.s^{-1}$, across the top of the polyliner, within the box. Conversely, Box 1 exhibits a velocity of 1.1 $m.s^{-1}$, across the top of the polyliner, almost three times the equivalent air velocity in Box 5. Usually, the convective heat transfer coefficient, for horticulture produce, is heavily influenced by the air velocity (Dincer 1995). The higher the air velocity the higher the heat transfer coefficient. Kumar, Kumar and Narayana (2008) found that changing the air velocity, in the forced-air cooling of tomatoes, from 1.2 $m.s^{-1}$ to 4.4 $m.s^{-1}$ increased the heat transfer coefficient from 16 $W.m^{-2}.K^{-1}$ to 34 $W.m^{-2}.K^{-1}$. Likewise, in this same paper, oranges witnessed a rise, from 22 $W.m^{-2}.K^{-1}$ to 38 $W.m^{-2}.K^{-1}$, in the heat transfer coefficient over the same velocity range. Tutar, Erdogdu and Toka (2009) showed through the use of numerical simulation, that increasing the air velocity will result in more rapid heat transfer from sphere surfaces, which were taken to represent horticulture produce. However, despite the increased air velocity in these cooling trials, the half cooling time for Box 1 is actually longer than that observed for Box 5. This suggests that the air velocity across the polyliner has a reduced impact on the heat transfer process of polylined kiwifruit, due to the fact that the polyliner provides a barrier to direct contact between the refrigerated airflow and produce. This has comparisons to work by Ngcobo, Opara and Thiart (2012) which identifies grapes packed in perforated liners, which allow some contact between the refrigerated airflow and produce, as possessing faster half cooling times than those in non-perforated liners which generate a complete barrier.

While the significance of increased air velocity is certainly reduced as a result of the presence of the polyliner it is still a contributing factor to heat transfer. The relatively warm air temperature,

combined with the low velocity across the polyliner, 0.38 $m.s^{-1}$ assuming that the volumetric airflow runs straight through all the boxes, results in Box 7 having the longest half cooling time of 6 h (Table 1). The fact that Box 7 has a marginally longer half cooling time than Box 4 despite receiving a refrigerated air at a cooler temperature (Figure 6(a)) indicates that the volumetric airflow and air velocity through the Boxes still has some influence on the heat transfer.

5. Conclusions

It can be concluded that the cooling rate of polylined kiwifruit in a pallet is a function of the location of the box. Not surprisingly, kiwifruit in the first column, exposed to direct airflow, with the box orientated so that the incoming refrigerated airflow can enter through the hand vents cool the fastest. The further away from the entering volumetric airflow the boxes are placed, the lower the cooling rate. One way to potentially increase the cooling rate for the boxes located in the back row would be to use an alternate pallet orientation that draws cooler air to the boxes located at the back of the pallet. For example a 90 degree change in the direction of the incoming air (i.e. air entering the pallet through boxes 5, 6 and 7) will reduce the distance and number of boxes that the cooling air must travel to pass through the pallet. As a result cooler air may be supplied to each of the Boxes within the pallet row. An alternative method to identify a potential improvement to cooling rate would be the use of numerical modeling. Numerical models could be used as an efficient screening tool to facilitate the alternative pallet structures and orientations, reducing the number of experiments needed.

Acknowledgements

The PhD research of Justin O'Sullivan is fully supported by Zespri International Ltd.

References

Ashby, B.H. (1995). Protecting perishable foods during transport by truck. *Handbook no. 669.* USDA. Washington, D.C.

Brosnan, T. & Sun, D.-W. (2001). Precooling techniques and applications for horticultural products — a review. *International Journal of Refrigeration,* 24(2): 154-170.

Burdon, J. & Clark C. (2001). Effect of postharvest water loss on 'Hayward' kiwifruit water status. *Postharvest Biology and Technology,* 22(3): 215-225.

de Castro, L.R., Vigneault, C. & Cortez, L.A.B (2004). Container opening design for horticultural produce cooling efficiency. *Food, Agriculture & Environment*, 2(1), 135-140.

Dehghannya, J.M., Ngadi, M. & Vigneault, C. (2008). Simultaneous aerodynamic and thermal analysis during cooling of stacked spheres inside ventilated packages." *Chemical Engineering & Technology,* 31(11), 1651-1659.

Dehghannya, J.M., Ngadi, M. & Vigneault, C. (2011). Mathematical modeling of airflow and heat transfer during forced convection cooling of produce considering various package vent areas, *Food Control,* 22(8), 1393-1399.

Dehghannya, J. Njadi, M. & Vigneault, C. (2012). Transport phenomena modelling during produce cooling for optimal package design: Thermal sensitivity analysis. *Biosystens Engineering*, 11(3), 315-324.

Dincer, I. (1995). Air flow precooling of individual grapes. *Journal of Food Engineering* 26(2): 243-249.

East, A.R., Jeffery, P.B. & Love, R.J. (2013). Investigating assymeterial packaging as a technique to reduce heterogeneity during pre-cooling of fresh produce, *Proc. 2nd IIR International Conference on Sustainability and the Cold Chain,* Paris, France.

Ezeike, D.G. & Hung, D.Y.-C. (2009). Refrigeration of fresh produce from field to home: refrigeration systems and logistics. In: Florkowski, W.F, Shewfelt, R.L, Brueckner, B. & Prussia, S.E. (eds.) Postharvest handling: a systems approach. 2nd ed. Elsevier's Science & Technology, Oxford, UK. pp. 513-537.

Ferrua, M.J. & Singh, R.P. (2009). Modeling the forced-air cooling process of fresh strawberry packages, Part I: Numerical model, *International Journal of Heat and Fluid Flow,* 32(2), 335-348.

Ferrua, M.J. & Singh, R.P. (2009b). Modeling the forced-air cooling process of fresh strawberry packages, Part III: Experimental validation of the energy model. *International Journal of Refrigeration* 32(2): 359-368.

Kumar, R., Kumar, A. & Murthy, U.N. (2008). Heat transfer during forced air precooling of perishable food products. *Biosystems Engineering* 99(2): 228-233.

Ngcobo, M.E.K., Opara U.L. & Thiart, G.D. (2011). Effects of Packaging Liners on Cooling Rate and Quality Attributes of Table Grape (cv. Regal Seedless), *Packag. Technol. Sci.* 25(2): 73-84

Simson, S.P. & Straus, M.C. (2010). *Post-Harvest Technolgy of Horticulture Crops*. Jaipur, India, Oxford Book company.

Thompson, J. (2004). Pre-Cooling and Storage Facilities. *The Commerical Storage of Fruits, Vegtables, and Florist and Nursery Stocks*. USDA. Washington, D.C. Agriculture Handbook no. 69.

Thompson, J. & Chen, Y. (1988). Comparative energy use of vacuum, hydro, and forced air coolers for fruits and vegetables. *ASHRAE Transactions*. 92: 1427-1433

Tutar, M., Erdogdu, F. & Toka, B. (2009). Computational modeling of airflow patterns and heat transfer prediction through stacked layers' products in a vented box during cooling. *International Journal of Refrigeration* 32(2): 295-306.

Verboven, P., Hoang, M.L. & Nicolai, B.M. (2003). Modelling turbulent air flow in cool rooms for horticultural products. *Acta Hort,* 599, 435-441.

Performance of the forced-air cooling process of fruit packed in polyethylene liners as a function of pallet orientation

O'SULLIVAN J.L.[(a)], FERRUA M.J.[(b)], LOVE R. J. [(a)], VERBOVEN P.[(c)], NICOLAÏ B. M. [(c)], and EAST A. R. [(a)]

[1]Centre for Postharvest and Refrigeration Research, Massey University, Private Bag 11-222, Palmerston North 4442, New Zealand, Ph +64 6 350 4336; Fax +64 6 350 5657

[2]Riddet Institute, Massey University, Private Bag 11-222, Palmerston North 4442, New Zealand

[3]BIOSYST-MeBioS, K.U.Leuven, Willem de Croylaan 42, Heverlee, Belgium

ABSTRACT

Following harvest, a rapid forced-air cooling application is usually required to cool fresh horticultural produce. To avoid excessive moisture loss during storage, produce such as kiwifruit needs to be wrapped in a polyliner which prevents direct contact between the fruit and the surrounding air. This work investigates the effect of pallet orientation on the performance of a standard pallet (1.2 x 1.0 m) holding 50 modular polylined boxes of kiwifruit during forced-air cooling. By forcing the cold air through the larger 1.2 m side of the pallet instead of the 1.0 m side, the airflow entering the individual Boxes doubled from 0.1 $m^3.s^{-1}$ to 0.2 $m^3.s^{-1}$ and the pressure drop across the pallet decreased by 34%. However, this did not translate into a significant improvement in cooling with the kiwifruit cooling by an average of 47% after a 4 h period, while cooling by 45% in the 1.0 m orientation.

1. INTRODUCTION

Proper postharvest cooling is essential to ensure that product quality is maintained from harvest to retail. To ensure maximum storage potential kiwifruit should be cooled to near 0 °C, as soon possible (Ashby 1995). Kiwifruit, kept at 0 °C and 90-95% relative humidity can have a storage period of 3-5 months (Simson and Straus 2010). However, improper cooling can lead to hot or cold spots, resulting in excessive drying or condensation during storage, and consequently quality loss in horticulture produce (Verboven et al. 2003).

Kiwifruit is typically cooled via a forced-air application. Forced-air cooling involves forcing refrigerated air through packed fresh produce stacked upon pallets. The efficiency of the forced-air cooling process is determined by the rate and uniformity that product cools in comparison to the energy input required (de Castro et al. 2004). Of the different air flow systems available the tunnel cooler is the most common (Brosnan and Sun 2001). Depending on the fruit and whether a polyliner is used to contain the fruit inside the package cooling times can vary significantly. For example, strawberries, a relatively small fruit and packed in clamshells within trays, without a polyliner can cool to near 0 °C in as little as 2 h (Ferrua and Singh 2009). Conversely, palletized boxes of apples can take up to 12 h to cool (East et al. 2003). Introducing a barrier between the produce and cooling air can extend the cooling period even further. For example, pears stacked in boxes and wrapped in paper can take up to 24 h to cool (Thompson and Chen 1988) .

The objective of this work was to investigate how pallet orientation impacts the performance and mechanisms controlling the forced-air cooling of fresh produce. As part of this study, the cooling profiles of kiwifruit modular polylined boxes as dependent on their location within the pallet were experimentally measured and related to the temperature and distribution profile of the airflow across the pallet.

2. METHODOLOGIES

2.1 Experimental Set-up

A laboratory-scale operation was designed and developed to simulate forced-air cooling of kiwifruit stacked on a pallet. This laboratory unit allowed precise control over the critical operating parameters affecting the cooling process performance during industrial applications, primarily the temperature and flow rate of the refrigerated air forced through a kiwifruit pallet. A fan draws refrigerated air through palletized kiwifruit to simulate the conditions experienced by kiwifruit modular bulk packs during forced-air cooling. The fan system consists of a fan, an orifice plate and an interface which attaches the fan system to a pallet (Figure 1).

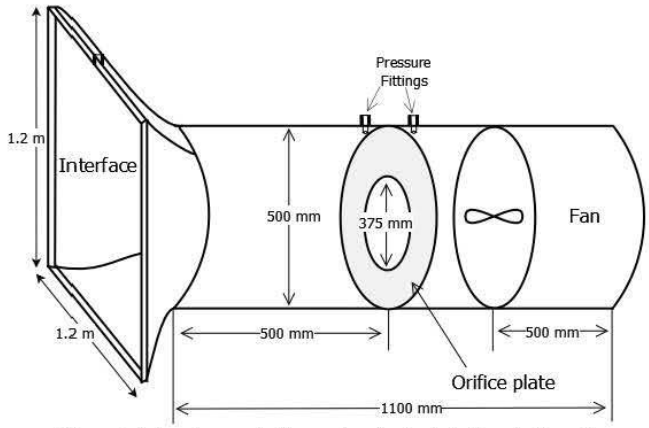

Figure 1. Laboratory scale fan system to simulate forced-air cooling

The fan has a built-in electronic variable speed drive (VSD). This allows the total airflow through the pallet to be controlled by adjusting the fan speed. The orifice plate in the fan system allows the airflow rate through the palletized structure to be measured, while a U-tube manometer measured the pressure drop across the pallet. The air velocities entering through the hand vents and side vents of the modular bulk packs were recorded by a hot-wire anemometer (Dantec, model 54-N-60).

The modular bulk pack for the Hayward kiwifruit, used in these experiments is a fibreboard box (Figure 2). The box contains vents to allow for cold air to pass through the package. Two rectangular vents (hand vents) are located on the large face while one small semi-circular vent is located on the side face (side vents). Both vents are located at the top of the face. The kiwifruit are contained within a single polyliner bag, constructed of high density polyethylene and folded at the top, in order to retain moisture.

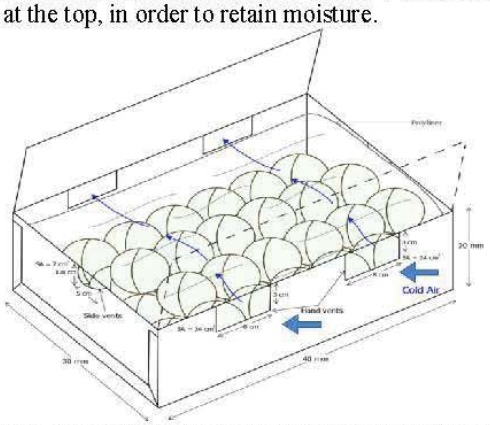

Figure 2. The modular bulk pack fibreboard for Hayward kiwifruit

2.2 Experimental data collection

Trials were conducted on a half pallet consisting of 50 modular polylined boxes, five rows high, with 100 count 36 size kiwifruit per box. Any free space between the interface and top boxes of the pallet were sealed up with tarp to ensure that the airflow only passed through the pallet. Within these five rows only two layers were measured (rows "B" and "D") as replicates, with the remaining three rows termed dummy layers, which provided buffering of the measured layers from edge effects. In order to investigate the effect of pallet orientation e refrigerated air was drawn through the 1.0 m face in Trial 1 and the 1.2 m face in Trial 2. A tarp is placed over the lateral side walls and the free space between the interface and top boxes of the pallet, ensuring all of the airflow enters the pallet through the desired face only and hence pseudo-linear airflow occurs through the pallet, parallel to the exposed face.

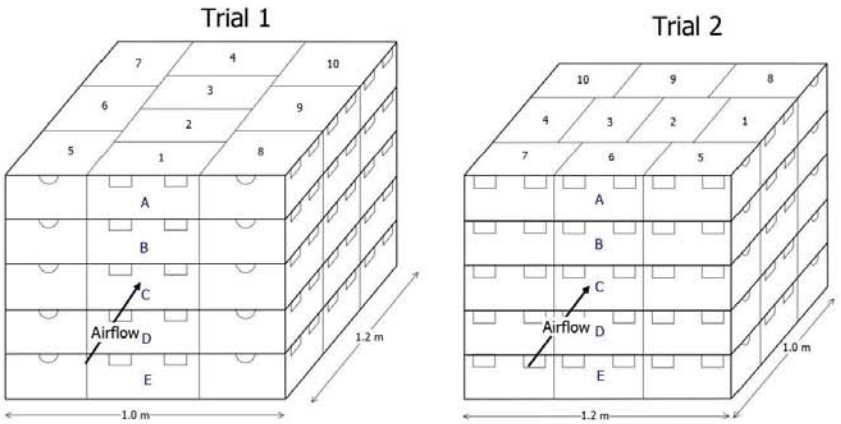

Figure 3. Half-pallet layout with rows assigned letters "A"-"B" for Trial 1 and 2

To ensure that airflow through each box was not influenced by fruit stacking pattern within each box kiwifruit were uniformly packed following a cubic centred distribution. Type-T thermocouples were used to monitor the centre temperature of 12 kiwifruit within each monitored box Temperatures were logged at one-minute intervals by 64-channel dataloggers (Squirrel, Grant Instruments, UK), over an 18 h forced-air cooling period.

In order to gain an accurate representation of temperature change within each of the boxes a weighted average was applied to each of the temperature data points. Kiwifruit located immediately adjacent to the box walls were taken to represent all the kiwifruit beside the box walls for that kiwifruit layer, while the centre thermocouples were the average temperature of the centrally located kiwifruit.

Velocities were recorded based on pallet layer and whether the airflow is drawn through the hand or side vents, for boxes within the entrance of the pallet. For Trial 1 both hand vents and side vents are directly exposed to the airflow. Air passes through the side vents of Boxes 5 and 8, while been forced through the two hand vents of Box 1, resulting in four velocity measurements per pallet layer. These measurements were replicated three times for rows "B", "C" and "D", giving 36 data points. For Trial 2 air is drawn through the hand vents of Boxes 5-7, giving six velocity measurements per pallet layer. These measurements were replicated three times for rows "B", "C" and "D", giving 44 data points.

2.3 Experimental set-up

Prior to the forced-air cooling operation kiwifruit were equilibrated to 19 °C, replicating the field heat observed in kiwifruit following harvest. The temperature control room, with the fan system placed in it, used for the trials was set and maintained at 0 °C. The instrumented pallet was rolled into the room attached to the fan system and the precooling simulation initiated, within 5 minutes of the warm kiwifruit entering the cool environment. Typically, pre-coolers operate with a volumetric airflow rate of 0.5-2.0 $L.s^{-1}.kg^{-1}$ (Thompson 2004). With approximately 10.5 kg of kiwifruit in each box, giving a pallet weight of 525 kg, the required airflow through the

pallet is 0.26-1.05 $m^3.s^{-1}$. The VSD fan was set to 1500 rpm, providing an airflow through the pallet of 0.58 $m^3.s^{-1}$, with an associated pressure drop of 126 Pa across the pallet for Trial 1 and for Trial 2 an airflow of 0.63 $m^3.s^{-1}$, with a corresponding pressure drop of 83 Pa across the pallet.

2.4 Data Analysis

In order to compare the sets of data for Trial 1 and 2 the temperature change is converted into the fractional unaccomplished temperature change (a dimensionless number). The fractional unaccomplished temperature change, (Y), represents the amount of possible temperature change that has yet to be accomplished (Eq. 1)

$$Y = \frac{T - T_a}{T_i - T_a} \dots\dots (1)$$

where T (°C) is the average temperature of kiwifruit in the box at the defined time of cooling, T_i (°C) is the average temperature of kiwifruit in the box at the start of cooling, and T_a (°C) is the average temperature of the air entering the pallet, taken as the temperature of the cool room. The half cooling time is defined as the time at which Y equals 0.5 or when the kiwifruit has cooled halfway from their initial temperature to that of the cooling air.

Due to the geometric nature of the pallet, a line of axial symmetry can be assumed down the centre of each pallet (Figure 5). Therefore, measurements for boxes with replicas, both on separate layers and due to axial symmetry, can be averaged, leaving a reduced single pallet layer.

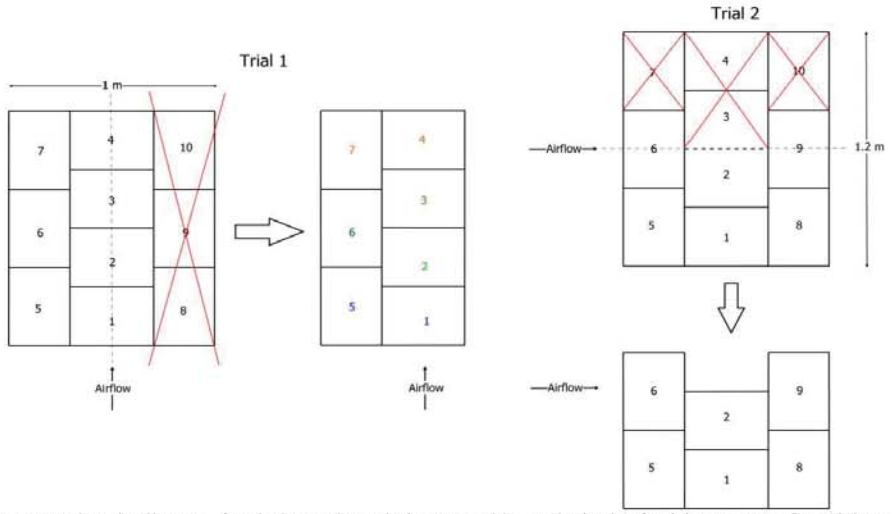

Figure 5. Reduced pallet row, for air drawn through the 1.0 m side, on the basis of axial symmetry, for Trial 1 and 2

3. RESULTS

Figure 6 shows the airflow and pressure drop across the pallet for both trials. In order to identify the relationship between airflow and pressure drop measurements were taken for a variety of fan speeds, ranging from 900 to 2400 rpm (Figure 6(a)). Figure 6(b) displays the difference in the percentage of the total airflow that enters the pallet through the Box vents due to pallet orientation. The change in average air temperature as it enters each Box in the pallet during 8 h of cooling for Trial 1 is shown in Figure 7(a), and for Trial 2 in Figure 7(b).

The average fractional unaccomplished temperature change, for the first 8 h of forced-air cooling as influenced by box position, demonstrates the impact of pallet orientation on the cooling rate for Trial 1 (Figure 8(a)), and Trial 2 (Figure 8(b)). The half cooling time is presented as a function of box position and pallet orientation in Table 1 for Trial 1 and Table 2 for Trial 2. The air velocity and airflow through the boxes and full pallet generated for a fan speed of 1500 rpm in both trials is presented in Table 3.

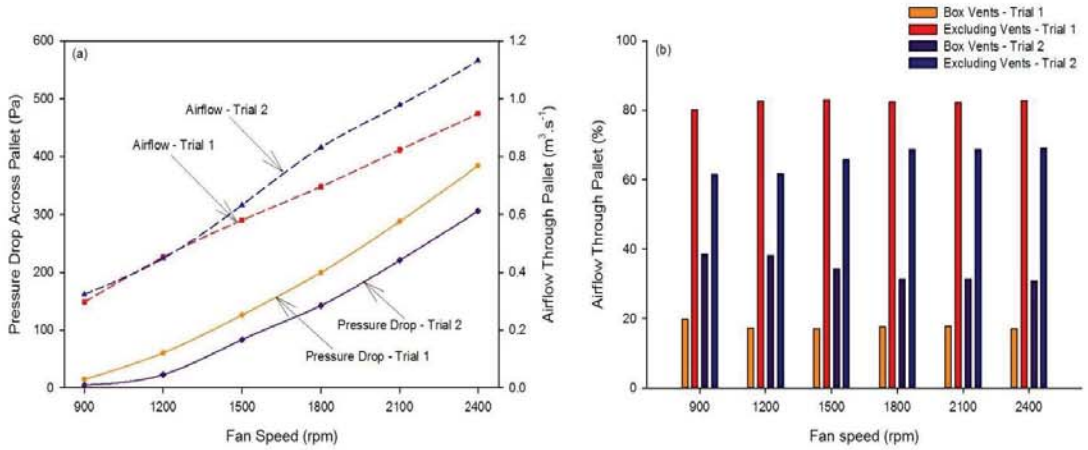

Figure 6. Airflow (a) and pressure drop across the pallet and (b) through and excluding the box vents as a function of fan speed for both Trials

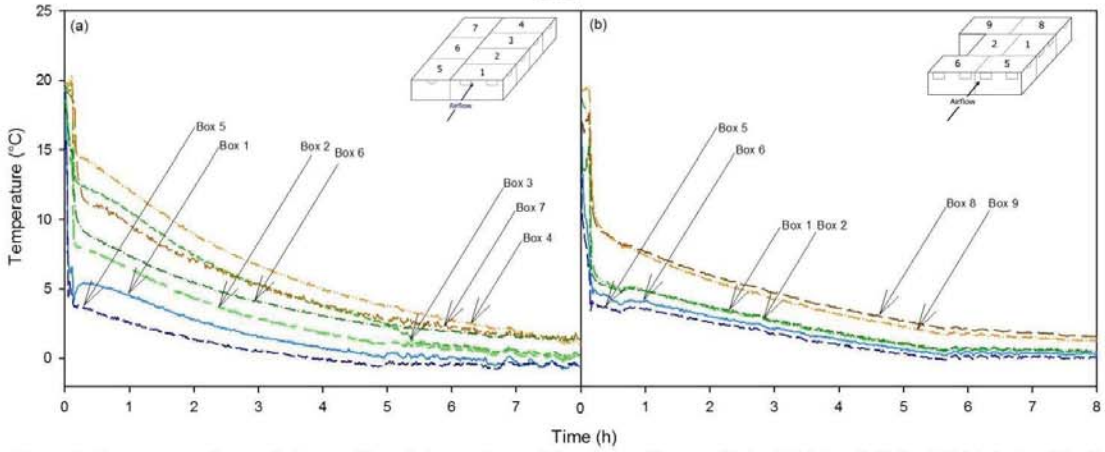

Figure 7. Temperature change during cooling of air entering each box in a pallet row (a) for Trial 1 and (b) for Trial 2 during 8 h of cooling

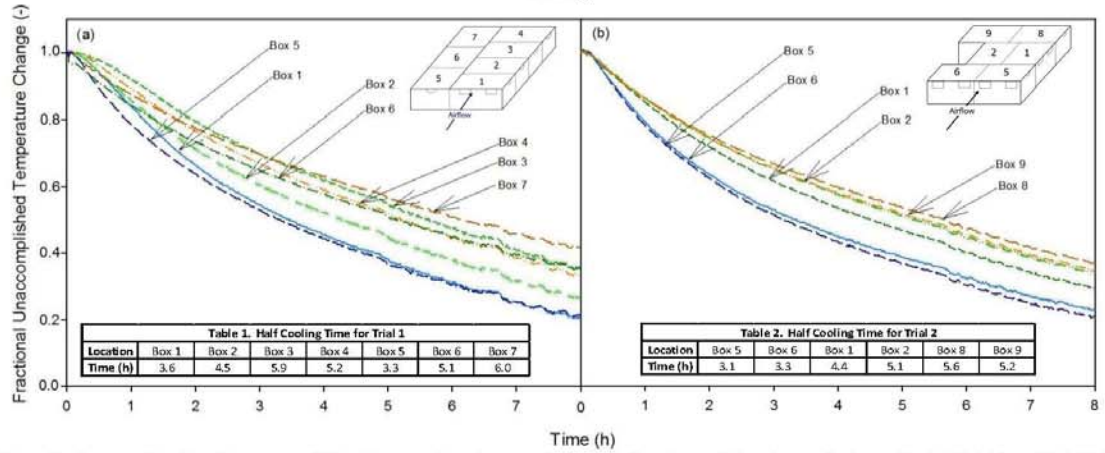

Table 1. Half Cooling Time for Trial 1

Location	Box 1	Box 2	Box 3	Box 4	Box 5	Box 6	Box 7
Time (h)	3.6	4.5	5.9	5.2	3.3	5.1	6.0

Table 2. Half Cooling Time for Trial 2

Location	Box 5	Box 6	Box 1	Box 2	Box 8	Box 9
Time (h)	3.1	3.3	4.4	5.1	5.6	5.2

Figure 8. Average fractional unaccomplished temperature change, during cooling for each box in a pallet row for (a) Trial 1 and (b) Trial 2

Table 3. Air velocity and airflow through the pallet for Trials 1 and 2 at a fan speed of 1500 rpm

Airflow through the pallet						
Trial	Vent velocity ($m.s^{-1}$)	Vent airflow (m^3s^{-1})	Channel velocity ($m.s^{-1}$)	Channel airflow ($m^3.s^{-1}$)	Airflow through entire pallet ($m^3.s^{-1}$)	Total airflow through boxes (%)
1	2.70	13×10^{-3}	4.84	3.4×10^{-3}	0.58	17
2	3.00	216×10^{-3}	-	-	0.63	34

4. DISCUSION

4.1 Pressure Drop

The higher pressure drop results in a larger resistance to airflow through the pallet (Figure 6(a)). On average the pressure drop through Trial 1 is 39% greater than that for Trial 2. As a result there is a reduction, approximately 11% across the measured fan speed range, in the amount of refrigerated air that can flow through the pallet. The higher pressure drop is a result of pallet length and orientation. In Trial 1 the refrigerated air must pass through a 1.2 m pallet length compared to the 1.0 m length in Trial 2, increasing the amount of packaging the air must be pulled through. For Trial 1 there are 6 Boxes (5-7, and 8-10) orientated so that their side-vents are exposed to the incoming airflow, compared to 4 Boxes (1-4) in Trial 2. These side-vents create higher entrance losses than the hand vents, due to their smaller area, increasing the pressure drop through the pallet. Moreover, there is a reduction in the total vent area per pallet row, orientated to the incoming airflow, available throughout the pallet (6.2×10^{-3} m^2 for Trial 1 and 14.4×10^{-3} m^2 for Trial 2). As a result a smaller amount, 17%, of total airflow through the pallet enters through the vents in Trial 1 compared to 34% in Trial 2 (Figure (6(b)). This relationship between box vent hole ratio, directly exposed to the refrigerated airflow, and resistance to airflow has been shown in numerous works (van der Sman 2002; Vigneault et al. 2006; Delele et al. 2008). In each case the pressure drop was shown to decrease when the area available for airflow was increased. However, despite the improvement in airflow through the Boxes for the Trial 2 pallet orientation, this does not translate into a significant improvement in cooling as witnessed by de Castro et al. (2005).

4.2 Air Temperature

Initially for the front and middle rows in Trial 2 the air temperate entering the Boxes is cooler than that for the equivalent Boxes in Trial 1 (Figure 7). This is due to the fact that the larger volume of airflow in Trial 2 warms up by a lesser degree than the smaller volume in Trial 1. The fact that the air temperature has warmed up significantly, in Trial 2, by the time it reaches the Boxes in the back row (8 and 9), indicates that the amount of refrigerated air been supplied to the rear of pallet is less than that for the Boxes in the middle row (1 and 2). This phenomena was observed by Tapsoba et al. (2006) and Moureh et al. (2009) when studying the supply of cool air to horticulture pallets in the back of a refrigerated truck. Warmer air was been supplied to the pallets in the rear as a result of the local air renewal rate been three times less than the overall value.

4.3 Temperature change of kiwifruit boxes within pallet

As expected the Boxes in the front rows of Trials 1 and 2 experience the greatest amount of cooling (Figure 8). Despite the fact that the total amount of airflow that enters the pallet in Trial 2 is double that of Trial 1 (Table 3) the half cooling times of Boxes 1 and 5 (Trial 1) and Boxes 5 and 6 (Trial 2) are not substantially quicker (Tables 1 and 2). On average the Boxes in Trial 2 achieve the half cooling time 21 minutes or 7% faster than their Trial 1 counterparts. This in line with conclusions by Dehghannya et al. (2008; 2011; 2012) that state that improving the volumetric airflow through a system, will not automatically lessen the cooling time of horticulture produce. The marginal improvement in cooling time for the front Boxes in Trial 2 indicates that the increased airflow across the polyliner does not significantly impact the heat transfer process of polylined kiwifruit. This is due to presence of polyliner which provides a barrier to direct contact between the refrigerated airflow and produce. This aspect of the polyliner on the heat transfer process during the forced-air cooling of horticulture produce has also been studied by Ngcobo et al. (2012). Here grapes packed in perforated liners, which allow

some contact between the refrigerated airflow and produce, are identified as possessing faster half cooling times than those in non-perforated liners which generate a complete barrier.

Similar to the air temperature through the pallet, the impact of the higher airflow in Trial 2 is limited to the Boxes in the front row as a result of the tortuous pathways through pallet. While the centrally located Boxes in Trial 2 exhibit faster half cooling times than those in Trial 1 the impact of the higher airflow rate and consequently lower air temperatures has dissipated and has little effect on the cooling for the Boxes in the back row. This leads to the pallet in Trial 2 cooling by 47% overall after 4 h, a 2% improvement in the cooling over the Trial 1 pallet orientation. For the alternate pallet orientation to improve cooling throughout the pallet the circulation of air throughout the entire pallet would have to increase, similar to that achieved by Ferrua et al. (2011) when forced-air cooling strawberry clamshells.

5. CONCLUSIONS

Pallet orientation has a major influence on the pressure drop and airflow through the pallet. In the Trial 1 orientation there is a larger resistance to airflow and as a result there is smaller volumetric airflow passing through the box vents and the pallet as a hole. In terms of cooling the increase in airflow through the Box vents, in the front of the pallet, due to the Trial 2 orientation exhibit an improved half cooling time and supply cooler air to the centrally located boxes. However, due to the tortuous pathways by the time the airflow has reached the Boxes in the back row it possesses a similar temperature to that observed in the Trial 1 orientation. Consequently, these Boxes cool by comparable amounts throughout the cooling operation. This limits the benefits of the Trial 2 pallet orientation. More importantly, with the 1.2 m face exposed to the refrigerated airflow placing 5 pallets in a row occupies the same length as 6 pallets with the 1.0 m side exposed. This could reduce the number pallets that can be cooled during multiple pallet postharvest operations. In conclusion the Trial 2 pallet orientation offers the option of a reduced pressure drop to be overcome and consequently reduced operating costs for the fan but with the disadvantage of a reduction in the amount of pallets that can be cooled at once.

ACKNOWLEDGEMENTS

The PhD research of Justin O'Sullivan is fully supported by Zespri International Ltd.

REFERENCES

Ashby, B. H. (1995). Protecting perishable foods during transport by truck. Washington, DC, USDA. **Handbook no. 669**.

Brosnan, T. and D.-W. Sun (2001). "Precooling techniques and applications for horticultural products — a review." International Journal of Refrigeration **24**(2): 154-170.

de Castro, L. A. B. Cortez, et al. (2004). "Container opening design for horticultural produce cooling efficiency." Food, Agriculture & Environment **2**(1): 135-140.

de Castro, L. R., C. Vigneault, et al. (2005). "Cooling performance of horticultural produce in containers with peripheral openings." Postharvest Biology and Technology **38**(3): 254-261.

Dehghannya, J., M. Ngadi, et al. (2008). "Simultaneous Aerodynamic and Thermal Analysis during Cooling of Stacked Spheres inside Ventilated Packages." Chemical Engineering & Technology **31**(11): 1651-1659.

Dehghannya, J., M. Ngadi, et al. (2011). "Mathematical modeling of airflow and heat transfer during forced convection cooling of produce considering various package vent areas." Food Control **22**(8): 1393-1399.

Dehghannya, J., M. Ngadi, et al. (2012). "Transport phenomena modelling during produce cooling for optimal package design: Thermal sensitivity analysis." Biosystems Engineering **111**(3): 315-324.

Delele, M. A., E. Tijskens, et al. (2008). "Combined discrete element and CFD modelling of airflow through random stacking of horticultural products in vented boxes." Journal of Food Engineering **89**(1): 33-41.

East, A. R., H. T. Sabarez, et al. (2003). Validation of a Packaging Design Tool: Case Study for Appple Packaging International Congress of Refrigeration Washington, D.C.

Ferrua, M. J. and R. P. Singh (2009). "Modeling the forced-air cooling process of fresh strawberry packages, Part III: Experimental validation of the energy model." International Journal of Refrigeration **32**(2): 359-368.

Ferrua, M. J. and R. P. Singh (2011). "Improved airflow method and packaging system for forced-air cooling of strawberries." International Journal of Refrigeration **34**(4): 1162-1173.

Moureh, J., S. Tapsoba, et al. (2009). "Air velocity characteristics within vented pallets loaded in a refrigerated vehicle with and without air ducts." International Journal of Refrigeration **32**(2): 220-234.

Ngcobo, M. E. K., U. L. Opara, et al. (2012). "Effects of Packaging Liners on Cooling Rate and Quality Attributes of Table Grape (cv. Regal Seedless)." Packaging Technology and Science **25**(2): 73-84.

Simson, S. P. and M. C. Straus (2010). Post-Harvest Technolgy of Horticulture Crops. Jaipur, India, Oxford Book company.

Tapsoba, M., J. Moureh, et al. (2006). "Airflow patterns in an enclosure loaded with slotted pallets." International Journal of Refrigeration **29**(6): 899-910.

Thompson, J. (2004). Pre-Cooling and Storage Facilities. USDA. Washington, DC. ***The Commerical Storage of Fruits, Vegtables, and Florist and Nursery Stocks;*** **Agriculture Handbook 66**.

Thompson, J. and Y. Chen (1988). "Comparative energy use of vacuum, hydro, and forced air coolers for fruits and vegetables." ASHRAE Transactions **92**: 1427-1433.

van der Sman, R. G. M. (2002). "Prediction of airflow through a vented box by the Darcy–Forchheimer equation." Journal of Food Engineering **55**(1): 49-57.

Verboven, P., M. L. Hoang, et al. (2003). Modelling turbulent air flow in cool rooms for horticultural products. Proceedings of the International Conference Postharvest Unlimited. B. E. Verlinden, B. M. Nicolai and J. DeBaerdemaeker: 435-441.

Vigneault, C., B. Goyette, et al. (2006). "Maximum slat width for cooling efficiency of horticultural produce in wooden crates." Postharvest Biology and Technology **40**(3): 308-313.

Mathematical modelling of kiwifruit packaging undergoing forced-air cooling

Justin L. O'Sullivan[a], Maria J. Ferrua[b], Richard J. Love[a], Pieter Verboven[c], Bart M. Nicolaï[c], and Andrew R. East[a]

[a]Centre for Postharvest and Refrigeration Research, Massey University, Private Bag 11-222, Palmerston North 4442, New Zealand, Ph +64 6 350 4336; email j.osullivan@massey.ac.nz

[b]Riddet Institute, Massey University, Private Bag 11-222, Palmerston North 4442, New Zealand

[c]BIOSYST-MeBioS, K.U.Leuven, Willem de Croylaan 42, Heverlee, Belgium

1.1 Abstract

A rapid and uniform forced-air cooling process immediately after harvest is essential to extend the storage life and preserve the quality of fresh produce. During this process refrigerated air is directly drawn through vented cartons of produce stacked upon pallets, with the cooling process governed by forced convection. However, to reduce the produce weight loss during subsequent extended storage, the direct contact between the refrigerated air and the product is often avoided by using polyethylene liners within the cartons. So far, little is known of how these polyethylene liners affect the performance and mechanisms governing the forced-air cooling of fresh produce. Current methods to improve the cooling process of kiwifruit involve costly trial and error experiments, and the use of numerical modelling is being increasingly used as an alternative method to efficiently identify potential improvement to the process design and efficiency.

As part of this work a computational model of a kiwifruit modular bulk pack that directly models each fruit within the package system has been developed and used to numerically predict the forced draft cooling of kiwifruit after harvest. The model demonstrates the significant temperature heterogeneity within the kiwifruit box during cooling, particularly between kiwifruit located within the middle of the box and those located to the top, bottom or sides. Furthermore, the model shows that the cooling performance of the kiwifruit box is dependent on the temperature of the air forced through it, while the volumetric airflow rate is much less significant when a polyliner is present. The numerical model developed is this study can be used as an efficient screening tool to facilitate evaluation of alternative box designs and orientations, reducing the number of experiments needed.

1.2 Introduction

Proper postharvest cooling is essential to ensure that product quality is maintained from harvest to retail. To ensure maximum storage potential kiwifruit should be cooled to near 0 °C, efficiently (Ashby, 1995). Kiwifruit, kept at 0 °C and 90-95% relative humidity can have a storage period of 6-10 months (Hewett, 1999). However, improper cooling can lead to hot or cold spots, resulting in excessive drying or condensation during storage, and consequently quality loss in horticulture produce (Verboven et al., 2003).

Kiwifruit is typically cooled via a forced-air application, where refrigerated air is forced through pallets of packed fresh produce. The efficiency of the forced-air cooling process is determined by the rate and uniformity that product cools in comparison to the energy input required (de Castro et al., 2004). Of the different air flow systems available the tunnel cooler is the most commonly used (Brosnan and Sun, 2001). The cooling of packaged horticultural produce is affected by a variety of factors. Cooling rates and heterogeneity can be influenced by package design (East et al., 2013), vent size and location (Dehghannya et al., 2010; 2012), pallet orientation (O'Sullivan et al., 2013) and the temperature and flowrate of the air forced through the pallet (van der Sman, 2002; de Castro et al., 2005a, Vigneault et al., 2006; Delele et al., 2008).

To retain moisture during cooling, storage and transportation, kiwifruit need to be contained within a polyliner bag of high density polyethylene. If kiwifruit lose as much as 2.5-3 % of the total fruit weight due to water evaporation, it will begin to shrivel, affecting its sellable weight and visual appearance (Burdon and Clark, 2001). However, what is still unclear is how the introduction of a polyliner affects the role of different operating parameters on the cooling performance of the process. By preventing fruit to air contact, the presence of the polyliner has been shown to extend the half-cooling time of grapes (Ngcobo, 2012). So far little is known about how the mechanisms governing the cooling process will be affected. With no direct contact between the refrigerated air and the fruit the assumption that forced convection is the main mechanism driving the cooling process of packaged fruit in a forced-air cooler may not apply.

The growth of computer power in recent years has led to an increased use of numerical and computational models to the predict complicated airflow patterns and cooling profile of horticultural packages during postharvest operations (Verboven et al., 2005; Delele et al., 2008; Dehghannya et al., 2008; Ferrua and Singh, 2009; Dehghannya et al., 2011 and Delele et al., 2012). However, out of these works only the research of Delele et al., (2012) involves horticultural produce (grapes) encased in a polyliner.

The objective of this work was to use computational fluid dynamics (CFD) to investigate the influence of the airflow rate and temperature of the refrigerated air on the cooling performance and mechanisms controlling the forced draft cooling of a polylined bulk pack of kiwifruit. In experimental studies it is difficult to compare sets of data due to changes in operating conditions (ambient air temperature and initial kiwifruit temperature in particular) and to gather detailed information of the temperature history within different locations of the packed structure. However, the use of CFD modelling facilitates the exact

control of different operating conditions, while also providing detailed information on the temperature profile within each individual package of the system domain. This allows the parameters that affect the cooling performance of the process to be evaluated without the need for trial and error experiments.

1.3 Materials and Methods

1.3.1 Commercial modular bulk pack

The design of the modular bulk pack for kiwifruit is based on the packaging currently specified for cv. Hayward (*Actinidia deliciosa*) kiwifruit by Zespri International (Figure 1). The box contains vents to allow for cold air to pass through the package. Two rectangular vents (hand vents) are located on the large face while one small semi-circular vent is located on the side face (side vents). Both vents are located at the top of the face. For averaged sized kiwifruit, 100 are contained within a single polyliner bag, constructed of high density polyethylene and folded at the top, in order to retain moisture. The complete modular bulk pack has an average mass of 10.5 kg.

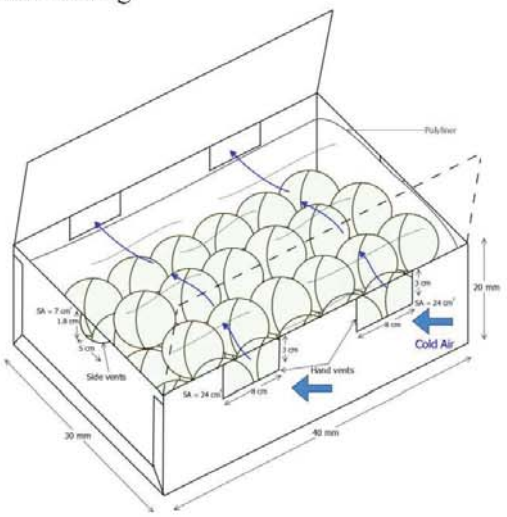

Figure 1. The modular bulk pack cardboard for Hayward kiwifruit

1.3.2 Computational design to reproduce modular bulk pack

1.3.2.1 Kiwifruit physical model

The computational domain was drawn using ANSYS DesignModeler (DesignModeler, 2010). Zespri International provided three images comprising of kiwifruit dimensions, within the relevant weight range, for the raised view, flat view and end view of Hayward green kiwifruit. Converting these dimensions to Cartesian coordinates gave values for the "xy", "xz" and "yz" axes, corresponding to the dimensions for the raised, flat and end view, respectively. Values were taken at 5 mm intervals along the x-axis. Importing the coordinates into ANSYS DesignModeler allows a 2D image of the kiwifruit, comprised of 20 individual segments, to be created on both the "xy" and "xz" axes. Connecting the xy- and yz-planes forms an outline of the three-dimensional kiwifruit, consisting of 40 individual segments.

Completing the 3D image, with coordinates from the end view, adding surfaces and merging the separate segments, as shown in Figure 2, completes the construction of an anatomically correct kiwifruit. The kiwifruit model has an area and volume of 126.1 x 10^{-4} m^2 and 98.9 x 10^{-6} m^3, respectively.

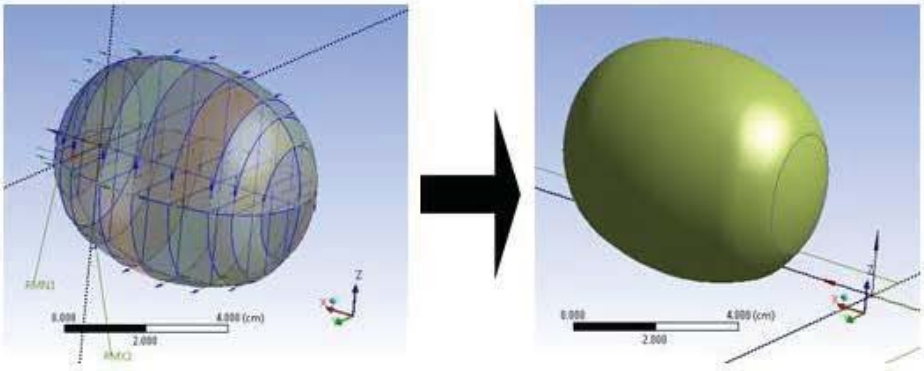

Figure 2. Completed construction of an anatomically correct Hayward green kiwifruit, formed by joining 40 individual segments

1.3.2.2 Modular bulk pack

The single kiwifruit is copied 100 times and arranged in a cubic centred distribution, as laid out in O'Sullivan et al., (2012). A total of four layers of kiwifruits were arranged within each box. The individual kiwifruit are in contact with at least one surrounding (above, below or beside) kiwifruit, to ensure heat transfer by conduction between the kiwifruit is sufficiently modeled. This one homogeneous structure of kiwifruit has an area and volume of 100.0 x 10^{-2} m^2 and 98.6 x 10^{-4} m^3, respectively. The kiwifruit is encased in a polyliner and a cardboard box, complete with hand-vent holes (and ignoring the semi-circular side vent), is then generated around the kiwifruit, forming the complete modular bulk pack for Hayward green kiwifruit (Figure 3). In a physically accurate model the kiwifruit would be in direct contact with the polyliner, however, in order to avoid high skewness of the mesh around these points, which can lead to solution inaccuracy, the kiwifruit is placed slightly (~ 0.15 cm) away from the walls. The proximity of the kiwifruit to the wall adequately replicate the heat transfer process, avoids skewness problems and reduces the overall computational time.

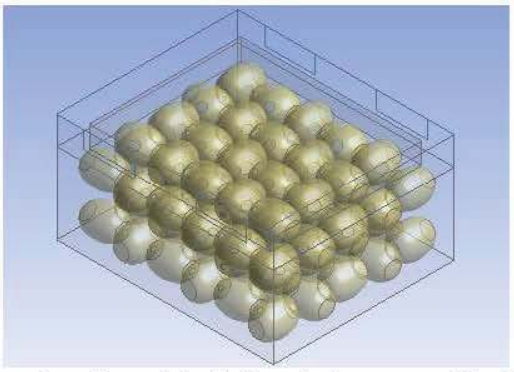

Figure 3. Model reconstruction of a modular bulk pack for Hayward kiwifruit containing 100 fruit

To allow the cooling airflow entering and exiting the box to be fully resolved, the inlet and outlet boundaries were located 100 cm upstream and 150 cm downstream of the modelled box (Figure 4). The inlet airflow region is defined as a velocity inlet while the air outlet region exit is defined as a pressure outlet boundary condition.

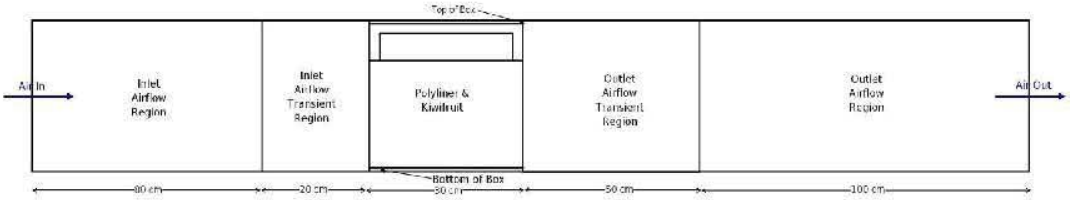

Figure 4. Cross-section view of the cross-sectional domain to simulate airflow through a modular bulk pack for Hayward kiwifruit. Features include top and bottom cardboard thicknesses, airflow and airflow transient regions

1.3.3 Mesh generation

The computation domain was meshed using the default unstructured scheme provided by ANSYS DesignModeler, with a curvature normal angle of 47° (Meshing, 2010). The transient regions are set to the patch conforming method, using tetrahedrons, allowing for mesh transition from coarser grids for the airflow regions to the fine meshes found in the modular bulk pack. Face sizing, with elements sizes of 5 mm, is applied to the hand vents, airflow inlet region face and airflow outlet region face. This ensures that these regions of interest are meshed with a sufficient number of elements to avoid discretisation errors.

The airflow behaviour within the system was modelled using the SST k-ω turbulence model, due to its expected good performance for complex configurations, such as forced-air cooling of horticulture produce stacked in a box (Defraeye et al., 2013).

The resulting mesh contains approximately 259,000 elements with a minimal orthogonal quality of 3.4×10^{-2} (above the minimal recommend value of 1.0×10^{-2}).

1.3.4 Boundary Conditions

The inlet conditions were prescribed in terms of a uniform airflow velocity across the boundary, the turbulence intensity and characteristic length, for the complete computational

volume. In order for the numerical model to simulate the conditions experienced by modular bulk packs of kiwifruit during precooling the air through the inlet vents was set to 3.0 $m.s^{-1}$. This is the average velocity recorded during laboratory experiments that replicated industrial precooling (O'Sullivan et al., 2012; 2013). Typically, pre-coolers operate with a volumetric airflow rate of 0.5-2.0 $L.s^{-1}.kg^{-1}$ (Thompson 2004). With approximately 10.5 kg of kiwifruit in each box the required airflow through the modular bulk pack is 0.0525-0.021 $m^3.s^{-1}$. As the inlet vents in the box measure 0.0048 m^2 the resulting airflow is 0.0144 $m^3.s^{-1}$, within the recommended range. For an air speed of 3.0 $m.s^{-1}$ through the inlet vents the inlet airflow region, prescribed as a velocity inlet, is set to a velocity of 0.2 $m.s^{-1}$. Intensity and Length Scale were the turbulence parameters applied to the boundary conditions of the inlet airflow. The turbulence intensity, I, at the inlet was calculated from $I = 0.16(Re_L)^{-1/8} = 5.7\ \%$ (Fluent, 2010), where Re_L is the Reynolds number for the characteristic length. Re_L is defined, for this model, as the distance between the top of the polyliner and the top of the cardboard box, 1.5 cm, as this is the area where the highest amount of turbulence occurs.

The box walls are cardboard of 3 mm thickness with shell conduction applied. It is assumed that the two side walls are completely exposed to refrigerated airflow so a free-stream air temperature of 0 °C is specified for the side walls. O'Sullivan et al. (2012) have shown that when kiwifruit are stacked in a pallet the refrigerated air that enters through the vents cools not only the kiwifruit in the box but also the kiwifruit in box directly above, through conduction across the base of the cardboard box. To account for this the cardboard thicknesses for the top and bottom of the cardboard box are included in the model, and a periodic boundary condition that links the heat transfer from the top of the box to the bottom of the box, was applied.

1.3.5 Modelling Approach

As previously mentioned, the behavior of the flow was modelled by using the SST k-ω turbulence model. A second order discretization scheme is set for the convection terms that appear in governing equations of pressure, momentum, turbulent kinetic energy, specific dissipation rate and energy.

The model assumes that no significant amount of airflow is capable of flowing into the polyliner and coming into contact with the fruit. Therefore the energy transport within the polyliner is modelled on a natural convection process. This is achieved by turning on gravity in the simulation.

The effect of radiation was included as the radiative heat flux is expected to be significant with that obtained by natural convective mechanisms. Preliminary calculations showed that under conditions likely to be encountered (cooling the fruit from 20 °C to 0 °C) the convective heat transfer coefficient between the kiwifruit and the air inside the polyliner increased from 5.85 $W.m^{-1}.K^{-1}$ to 10.07 $W.m^{-1}.K^{-1}$. The Discrete Ordinates Model, used by Laguerre et al. (2008) when conducting a CFD simulation involving overlapping spheres and close sphere proximity to the wall, is enabled.

The effect of airflow rate, temperature and natural convection, on the various heat transfer mechanisms are quantified by comparing the resulting cooling rate to that generated under a set of standard conditions. For the standard conditions the air velocity, past the inlet vents is 3.0 $m.s^{-1}$, the air temperature flowing into the box is 0 °C and gravity, hence natural convection, is included.

To assess the influence of the airflow rate on the cooling rate two simulations were run. Once at standard conditions and once with the airflow rate set 4 times lower, with a velocity past the inlet vents of 0.75 $m.s^{-1}$. All of the other standard conditions were maintained. The relative importance of the temperature of the incoming refrigerated air was assessed by changing the air temperature flowing into the box to 5 °C. By disabling gravity in the model, hence assuming that only a conductive process between the fruits and the stagnant air exists, allows the contribution of natural convection to the overall heat transfer in the model to be computed. Within each simulation study one of the three variables, air velocity, temperature, or inclusion of natural convection is changed while the other two are kept at standard conditions. All simulations are initialised with modular bulk pack (kiwifruit, polyliner and cardboard) set to 20 °C.

The simulation is initiated with the flow and energy equations coupled. To increase the simulation speed the flow and turbulence equations are disabled and the energy and discrete ordinates equations solved in one hour time intervals. After each hour the flow and turbulence is recalculated and the flow and energy equations are coupled solved together for a brief period of time. Following this the flow and turbulence equations are disabled and the process begins again. A detailed description of the flow and energy equations can be found in Fluent (2010).

1.4 Results and Discussion

Figure 5 shows experimentally collected fractional unaccomplished temperature change, for the kiwifruit, divided into subdivisions, over 4 h of forced air cooling (O'Sullivan et al., 2013). For reference purposes the experiments results for a kiwifruit box, in the front of a pallet, experiencing the same air inlet speed and temperature as the model are shown.

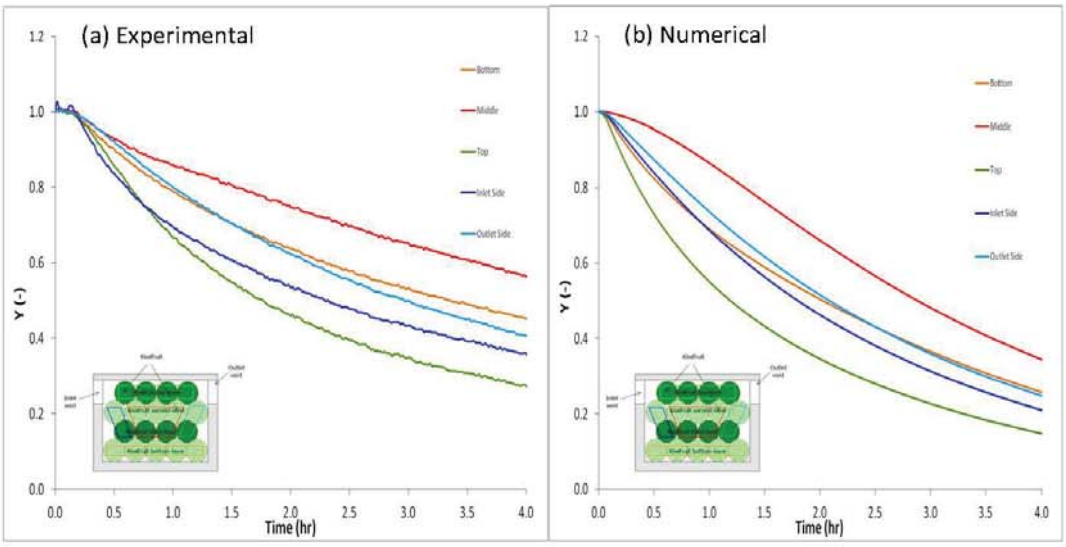

Figure 5. Average (a) experimental and (b) numerical fractional unaccomplished temperature change, during cooling for each subdivision in the modular bulk pack

Although the subdivisions predicted by Fluent do not exactly follow the experimental profiles this can be explained by the fact that the experiments were run under industrial conditions (i.e. the box was part of a pallet and not in isolation), and hence not setup for model validation. Despite efforts to have a refrigerated air temperature of 0 °C throughout the experiment in reality the temperature entering the box was initially 3.5 °C at the start of the experiment and was still 1 °C after 4 h of the cooling process. Additionally, this box is in contact with other boxes, containing warm kiwifruit, in the pallet, slowing down the cooling process. Nevertheless, the similarity in the temperature profiles obtained provided a first insight into the reliability of the developed model (in particular with regards to the natural convection process assumed to develop within the polylined box). For future simulations the air temperature entering the pallet, over time, can be set to that recorded in the precooling experiments. This should lead to a more accurate representation of the actual precooling process.

In Figure 5 the numerical model predicted that the kiwifruit in the middle of the box experience the longest cooling time, while the kiwifruit in the bottom layer were cooled faster by the refrigerated air forced along the top of the box immediately below. After 4 h kiwifruit in the middle experienced only 66% of the total temperature change, while those located at the bottom experienced 74%. The faster cooling rate of kiwifruit in the top layer, with a fractional unaccomplished temperature change of 0.15, in comparison to that in the bottom layer, 0.26, indicates that the conductive resistance to heat transfer by the polyliner is less than that of the bottom of the cardboard box. The inlet side of the box cooled down slightly faster than the outlet side (with the fruits experiencing a temperature change of 79% and 75%, respectively, over 4 h of forced-air cooling simulation). This difference could be explained by the direct exposure of the inlet side to the refrigerated air coming into the box.

Figure 6 shows the fractional unaccomplished temperature change over 4 h of forced-air cooling, under standard conditions and with one of the three variables, air velocity, temperature and natural convection changed.

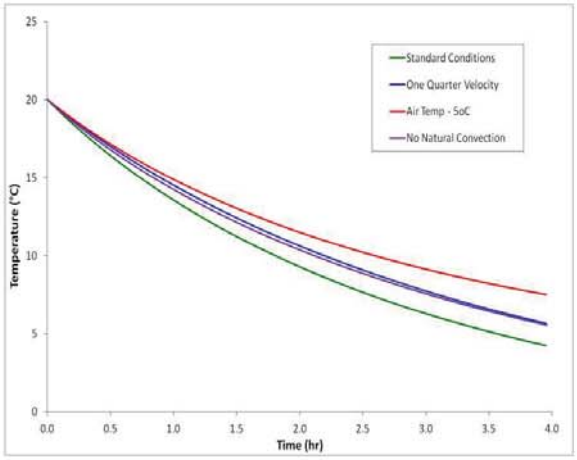

Figure 6. Effect of air speed temperature and exclusion of natural convection on the overall performance of the forced-air cooling of kiwifruit

As illustrated in Figure 6, the inclusion of natural convection in the simulation reduces the temperature of the kiwifruit after 4 h of cooling from 5.5 °C to 4.2 °C, or from 72.3% to 78.8% cooling. This shows that, during Fluent simulations, the contribution of natural convection to the heat transfer process is significant.

In horticultural produce packed without a polyliner it would be expected that the decrease in air velocity would result in a drastic reduction in the cooling percent (de Castro et al., 2004; 2005). However, in this simulation, when the air sped is reduced by 75% the kiwifruit temperature change decreases from 4.2 °C to 5.7 °C after 4 h, or by 7.1%. This suggests that the enclosure of the fruits within the polyliner has a major impact on the heat transfer process, due to the fact that the polyliner provides a barrier to direct contact between the refrigerated airflow and produce. This result supports the work of Ngcobo et al. (2012) who investigated grapes packed in perforated liners and identified that allowing some direct contact between the refrigerated airflow and produce, through the use of perforated liners, resulted in an 81 minute improvement in the seven-eighths cooling time than those in non-perforated liners which generate a complete barrier.

The major influence on the cooling efficiency of the process was found to be the temperature of the refrigerated air (Figure 6). An increase in the refrigerated air temperature to 5 °C decreased the total temperature change from 15.8 °C to 12.5 °C, over a 4 h period. This result highlights the role of natural convective mechanisms in the cooling process of kiwifruits packed within polylined cartons. In this case, the fluid motion driving the cooling performance is determined by the temperature gradients developed between the surrounding, cooler air and the warm fruits inside the polyliner.

In terms of industrial applications the model results demonstrates the importance of maintaining a low air temperature during pre-cooling and avoiding fluctuations in the air

temperature, such as those cause by the opening of doors to the temperature controlled rooms, in order to optimise cooling.

1.5 Conclusions

The results for this work show that the airflow rate forced through horticultural polylined packages is not the main parameter controlling the efficiency of the cooling process. Unlike the case of standard forced-air applications (where the refrigerated air is in direct contact with the fruit), the fluid motions promoting the cooling of the fruits inside a polylined package are the result of density differences generated by temperature gradients, instead of by the use of an external fan. The developed model could be used to streamline improvements to the forced-air cooling process of fruits packed in polyethylene liners, without the need for expensive and time consuming experimental trials. With the developed model changes to the current package design and the subsequent effect on the airflow through the package and resulting cooling profile can be assessed.

References

Ashby, B.H. (1995). Protecting perishable foods during transport by truck. *Handbook no. 669.* USDA. Washington, D.C.

Brosnan, T. & Sun, D.-W. (2001). Precooling techniques and applications for horticultural products — a review. *International Journal of Refrigeration,* 24(2): 154-170.

Burdon, J. & Clark C. (2001). Effect of postharvest water loss on 'Hayward' kiwifruit water status. *Postharvest Biology and Technology,* 22(3): 215-225.

de Castro, L.R., Vigneault, C. & Cortez, L.A.B (2004). Container opening design for horticultural produce cooling efficiency. *Food, Agriculture & Environment*, 2(1), 135-140.

de Castro, L.R., Vigneault, C. & Cortez, L.A.B (2005). Cooling performance of horticultural produce in containers with peripheral openings, *Postharvest Biology and Technology,* 38(3), 254-261.

Defraeye, T., Verboven, P. & Nicolai, B.M. (2013). CFD modelling of flow and scalar exchange of spherical food products: Turbulence and boundary-layer modelling, *Journal of Food Engineering,* 114, 495-504.

Dehghannya, J.M., Ngadi, M. & Vigneault, C. (2008). Simultaneous aerodynamic and thermal analysis during cooling of stacked spheres inside ventilated packages." *Chemical Engineering & Technology,* 31(11), 1651-1659.

Dehghannya, J. Njadi, M. & Vigneault, C. (2010). Mathematical modeling procedures for airflow, heat and mass transfer during forced convection cooling of produce: a review. *Food Engineering reviews*, 2, 227-243.

Dehghannya, J. Njadi, M. & Vigneault, C. (2012). Transport phenomena modelling during produce cooling for optimal package design: Thermal sensitivity analysis. *Biosystens Engineering*, 11(3), 315-324.

Dehghannya, J.M., Ngadi, M. & Vigneault, C. (2011). Mathematical modeling of airflow and heat transfer during forced convection cooling of produce considering various package vent areas, *Food Control,* 22(8), 1393-1399.

Delele, M.A., Ngcobo, M.E.K., Opara U.L. & Meyer, C.J. (2012). Investigating the effects of table grape package components and stacking on airflow, heat and mass transfer using 3-D CFD modelling. *Food and Bioprocess Technology,* http://dx.doi.org/10.1007/s11947-012-0895-5

DesignModeler. (2010). ANSYS DesignModeler User's Guide. Ansys Inc.

East, A.R., Jeffery, P.B. & Love, R.J. (2013) Investigating assymeterial packaging as a technique to reduce heterogeneity during pre-cooling of fresh produce, *Proc. 2nd IIR International Conference on Sustainability and the Cold Chain,* Paris, France.

Laguerre, O., Amara, S.B., Alvarez, G. & Flick, D. (2008). Transient heat transfer by free convection in a packed bed of spheres: Comparison between two modelling approaches and experimental results, *Applied Thermal Engineering,* 28(1), 14-24

Ferrua, M.J. & Singh, R.P. (2009). Modeling the forced-air cooling process of fresh strawberry packages, Part I: Numerical model, *International Journal of Heat and Fluid Flow,* 32(2), 335-348.

Hewett, E.H., Kim, H.O & Lallu, N. (1999). Postharvest physiology of kiwifruit: the challenges ahead. *Acta Hort (ISHS),* 498, 203-216

Meshing. (2010). ANSYS Meshing User's Guide. Ansys Inc.

Ngcobo, M.E.K., Opara, U.L. & Thiart, G.D. (2012). Effects of packaging liners on cooling rate and quality attributes of table grape (cv. Regal Seedless). *Packaging Technology and Science*, 25(2): 73-84.

O'Sullivan, J.L., Ferrua, M., Love, R., Verboven, P., Nicolai, B.M. & East, A. (2012). Mechanisms and performance of the forced-air cooling process of fruit packed in polyethylene liners, *CIGR Section VII International Technical Symposium on Innovating the Food Value Chain,* Stellenbosch, South Africa.

O'Sullivan, J.L., Ferrua, M.J., Love, R.J., Verboven, P., Nicolaï, B.M. & East, A.R. (2013) Performance of the forced-air cooling process of fruit packed in polyethylene liners as a function of pallet orientation, *Proc. 2nd IIR International Conference on Sustainability and the Cold Chain,* Paris, France.

Verboven, P., Hoang, M.L. & Nicolai, B.M. (2003). Modelling turbulent air flow in cool rooms for horticultural products. *Acta Hort,* 599, 435-441.

Verboven, P., Tijskens, E., Ramon, H. & Nicolai, B.M. (2005). Virtual filling and airflow simulation of boxes with horticultural products. *Acta Hort,* 687, 47-54.